

2005

Medium-Term (Months to Years) Morphodynamic Modelling of a Complex Estuarine System

Bernardes, Marcos Eduardo Cordeiro

<http://hdl.handle.net/10026.1/1813>

<http://dx.doi.org/10.24382/3553>

University of Plymouth

All content in PEARL is protected by copyright law. Author manuscripts are made available in accordance with publisher policies. Please cite only the published version using the details provided on the item record or document. In the absence of an open licence (e.g. Creative Commons), permissions for further reuse of content should be sought from the publisher or author.

Medium-Term (Months to Years) Morphodynamic Modelling of a Complex Estuarine System

by

Marcos Eduardo Cordeiro Bernardes

A thesis submitted to the University of Plymouth
in partial fulfilment for the degree of

Doctor of Philosophy

School of Earth, Ocean and Environmental Sciences
Faculty of Science

March 2005

LIBRARY STORE

University of Plymouth Library	
Item No.	900 6634627
Shelfmark	THESIS SS1.470724 BGL

REFERENCE ONLY

*To all individuals acting to make this world
more peaceful, tolerant and positive.*

Abstract

Medium-term (months to years) morphodynamic modelling of a complex estuarine system

Marcos Eduardo Cordeiro Bernardes

This contribution focuses on the medium-term (months to years) morphodynamic modelling of natural estuaries. A 2D morphodynamic model based on the Telemac system was calibrated and validated using extensive field measurements¹ at Teignmouth (UK).

Statistical tools indicate that the model is capable of predicting the observed hydrodynamics with 'good' accuracy, given that measurement noise is removed. Despite some qualitative agreement, morphological predictions show a more limited skill; consistent with the current 'state of the art' in this area of scientific research. The typical long simulation times associated with process-based morphodynamic models are optimised through the successful implementation of an input reduction approach, adapted from Latteux (1995). The technique is shown to reduce the model run times by up to 85% without a significant loss in accuracy.

Bathymetric surveys spanning 2 years (December 2002 to November 2004) at Teignmouth have clearly demonstrated a seasonal variability in the sediment volumes within the estuary, with accretion in the relatively energetic winter periods and erosion during the quiescent summer months. The net longer-term trend over this period is accretionary with average seabed accumulation rates of 20 cm.year⁻¹. It is demonstrated that if the wave stirring effect is neglected, the predictions carried out with a single grain size do not replicate the observed sediment import to the estuary from the neighbouring coastal region, due to the ebb dominated tidal regime found at Teignmouth. The importance of the combined effects of wave stirring and mixed grain sizes on reproducing the sediment import processes is confirmed by the Brier skill scores. Model predictions show a high influx of suspended sediment into the estuary in the presence of wave stirring effects at the coastal region. These sediments are advected into the estuary during the flood phase and are rapidly deposited at the outer estuary, since lag effects are neglected. The sediment input is predicted to be dominated by the finer sediment fractions (primarily silts and clays) although in very energetic conditions even granule-sized sediments can enter the estuary. Starting from an isotropic sediment distribution, a realistic spatial redistribution of sediment grain sizes is predicted, with sediments generally fining towards the shallower and upper regions of the estuary, whilst coarser grains were concentrated seawards.

¹ COAST3D Project (Whitehouse, 2004) and CoastView Project (Davidson et al., submitted).

Contents

Abstract	iv
List of Figures	ix
List of Tables	xvi
List of Symbols	xviii
Acknowledgements	xxi
 Chapter 1 - Introduction.....	1
1.1. General introduction.....	1
1.2. Specific objectives.....	2
1.3. Thesis outline.....	3
 Chapter 2 - Literature Review.....	5
2.1. Introduction.....	5
2.2. Estuaries: definitions and general aspects.....	5
2.3. Coastal morphodynamics.....	9
2.4. Modelling morphodynamic processes.....	12
 Chapter 3 - Study Area and Available Data.....	21
3.1. Study area.....	21
3.1.1. <i>Geomorphology and sediment distribution</i>	21
3.1.2. <i>Hydrodynamic processes</i>	29
3.2. Available data.....	31
3.2.1. <i>Water levels</i>	34
3.2.2. <i>River discharges</i>	35
3.2.3. <i>Currents</i>	35
3.2.4. <i>Meteorological conditions</i>	35
3.2.5. <i>Sediment samples</i>	36
3.2.6. <i>Bathymetric surveys</i>	37
3.3. Conclusions.....	46

Chapter 4 - Numerical Modelling.....	47
4.1. Introduction.....	47
4.2. Hydrodynamic set-up.....	50
4.2.1. <i>Bottom settings</i>	50
4.2.2. <i>Mesh resolution</i>	51
4.2.3. <i>Boundary conditions</i>	54
4.3. Hydrodynamic calibration	55
4.3.1. <i>Statistical tools in hydrodynamic modelling</i>	56
4.3.2. <i>Hydrodynamic calibration set-up</i>	59
4.3.3. <i>Hydrodynamic validation</i>	67
4.4. Morphodynamic calibration.....	72
4.4.1. <i>Statistical tools in morphodynamic modelling</i>	74
4.4.2. <i>Morphodynamic calibration set-up</i>	78
4.5. Conclusions.....	86
 Chapter 5 - Ensemble Technique.....	 87
5.1. Introduction.....	87
5.2. Short-term (hours to days) application of the ensemble technique.....	89
5.3. Medium-term (weeks to months) application of the ensemble technique	97
5.4. Conclusions.....	99
 Chapter 6 - Model Predictions.....	 101
6.1. Introduction.....	101
6.2. Short-term (hours to days) morphodynamic processes.....	102
6.2.1. <i>Water level distribution on short-term scales</i>	102
6.2.2. <i>Instantaneous velocities on short-term scales</i>	106
6.2.3. <i>Morphological changes on short-term scales</i>	109
6.3. Seasonal modulations in mophodynamic processes over the medium-term (months to years).....	114
6.3.1. <i>Water level distribution on medium-term scales</i>	114
6.3.2. <i>Residual velocities on medium-term scales</i>	117
6.3.3. <i>Morphological changes on medium-term scales</i>	122

6.4. Inclusion of mixed grain sizes and wave effects on medium-term (months to years) morphodynamic processes	128
6.4.1. <i>The implementation of mixed grain sizes and stirring wave effects</i>	128
6.4.2. <i>Residual current patterns under the influence of mixed grain sizes and wave effects</i>	130
6.4.3. <i>Residual total sediment transport patterns under the influence of mixed grain sizes and wave effects</i>	132
6.4.4. <i>The fate of sediment fractions under the influence of mixed grain sizes and wave effects</i>	143
6.4.5. <i>The effects of isotropy on the sediment distribution patterns</i>	149
6.5. Conclusions.....	153
Chapter 7 - General Conclusions and Further Research.....	157
7.1. General conclusions	157
7.2. Further research	164
Appendix 1 - Model Description.....	167
A1.1. Introduction.....	167
A1.2. Telemac-2D.....	168
A1.2.1. <i>Overview</i>	168
A1.2.2. <i>Numerical methods of Telemac-2D</i>	169
A1.2.3. <i>Bottom friction of Telemac-2D</i>	170
A1.2.4. <i>Boundary conditions of Telemac-2D</i>	172
A1.2.5. <i>Turbulence modelling</i>	172
A1.2.6. <i>Wetting and drying modelling</i>	173
A1.2.7. <i>Global parameters of Telemac-2D</i>	174
A1.3. Sisyphe.....	175
A1.3.1. <i>Overview</i>	175
A1.3.2. <i>Bed evolution</i>	177
A1.3.3. <i>Bed-load and suspended-load</i>	177
A1.3.4. <i>Bottom friction of Sisyphe</i>	178
A1.3.5. <i>Wave effects</i>	178
A1.3.6. <i>Sediment transport formulae</i>	179
A1.3.7. <i>Treatment of non-erodable areas</i>	185

<i>A1.3.8. Multiple grain sizes, bed stratification and hiding effects.....</i>	<i>186</i>
<i>A1.3.9. Numerical methods of Sisyphé.....</i>	<i>187</i>
<i>A1.3.10. Numerical solution of the bed evolution equation.....</i>	<i>187</i>
<i>A1.3.11. Global parameters of Sisyphé.....</i>	<i>189</i>
References.....	190

List of Figures

Chapter 2

2.1. Energy variation along the axis of a wave-dominated estuary (A); plan view of the estuary with main morphological features highlighted (B) and plot C shows a side view of the stratigraphy along the estuary axis (after Dalrymple et al., 1992).	6
2.2. Residual sediment transport patterns at a tidal inlet and its adjacent flood and ebb tidal deltas (after Dyer, 1994).	8
2.3. Schematic description of a coastal morphodynamic system.	9
2.4. Morphological features (bold) and the main forcing processes (<i>italic</i>) as a function of time and space (after de Vriend, 1991).	10
2.5. Residual 'primary' tidal transport (after de Vriend, 1993).	11
2.6. Morphological model concepts (after de Vriend et al., 1993).	16

Chapter 3

3.1. Location map of the Teign estuary and its main physiographic features: The Salty (A); Estuarine flood tidal channel (B); Main channel (C); The Ness (D); Ness sandbar (E); Submerged sandbar (F); Ebb shoals (G); Coastal flood tidal channel (H); Spratt sand (I); Sandy spit (J); Teignmouth beach (K); Shaldon bridge (L). As depicted in the picture (arrow), dredging activities take place at the outer ebb-delta to date (Photo courtesy of South West Water). For further information on classification of coasts and associated features, refer to Dyer and Huntley (1999) and Finkl (2004).	22
3.2. Estuary subdivision proposed by Wells (2002a), with likely sediment pathways and their sources and sinks ($\text{tonnes}\cdot\text{year}^{-1}$). The 0 m (ODN) isobath is depicted in grey. Prominent locations are shown in <i>italic</i> . The inclusion of the 'Coast' section is proposed in this thesis.	23
3.3. Photographic records of the Teign estuary and adjacent coast: upper estuary finer sediments and associated tidal flats (A); coarser sediments distributed in "bands".	24
3.4. Diagrammatic representation of the cyclic changes in bank positions (Siegle, 2003 after Robinson, 1975).	26
3.5. Schematic sediment transport pathways, sources and sinks on a regional scale for Holcombe to Torquay (Carter and Bray, 2003).	28
3.6. Instruments location for COAST3D main experiment relative to Admiralty Chart Datum (ACD; Sutherland et al., 2001b). Sites used for model calibration and validation are shown in squares.	33
3.7. Average grain size distribution of the Teign estuary (data from ABPMer) and adjacent coastal area (data from COAST3D project). The grain-size fractions are	36

classified according to Wentworth's (1922) classical diagram: Silts and clays (squares); Very fine and fine sands (diamonds); Medium sands (circles); Coarse and very coarse sands (stars); Granules (triangles) and Gravels (inverted triangles). Missing data are represented by grey diagonal crosses.

- 3.8. Bathymetric surveys of the Teign estuary and adjacent coastal area: example of COAST3D coverage area (1); Nunny (1980) depth-contour levels (2) and COAST3D data interpolated from Admiralty Chart 3155 and LIDAR data (3); ABPMer bathymetric survey carried out in November 2001 (4); ABPMer bathymetric survey of April and May 2002 (5) and the red line delimits an example of the CoastView surveys of the outer estuary and adjacent coastal area (6). Grey area corresponds to survey gap in November 2003 CoastView survey. 38
- 3.9. Morphological changes at the Teign estuary between 1979 (Nunny, 1980) and 2002 (ABPMer). Erosion features are associated to green and blue areas. Reddish patterns correspond to sediment deposition in the period. Main deposition sites are represented by a dashed line. 39
- 3.10. Field conditions during CoastView surveys 2 to 6. Water level (m-ODN) is shown on plot A; river discharge ($\text{m}^3.\text{s}^{-1}$) on plot B; rms of wave height (m-ODN) on plot C and wave period rms (s) on plot D. Periods of 'no measurements' are shown as null values. 41
- 3.11. Morphological changes at the Teign estuary between CoastView surveys during the following periods: from December 2002 to May 2003 (A); May 2003 to November 2003 (B); November 2003 to June 2004 (C); June 2004 to November 2004 (D). Erosion features are associated to green and blue areas. Yellow and red patterns correspond to sediment deposition in the period. Isobaths (m ODN) correspond to bottom properties at the beginning of the respective period. 43
- 3.12. Sediment volume changes for CoastView bathymetric surveys: whole surveyed area (A) and outer estuary area only (B). Linear regression segments are represented by dotted lines. Vertical bars correspond to measurement errors, which are within the range of ± 2.5 cm (Ganderton, pers. comm.). 45

Chapter 4

- 4.1. Schematic description of the morphodynamic loop within Telemac system. 48
- 4.2. Generated meshes with varying grid resolution and offshore coverage area. The insets represent areas of further mesh refinement due to channel meandering and complex bathymetry. Mesh 'A' has 1721 nodes; mesh 'B' 2037; mesh 'C' 4355 and 5009 nodes in mesh 'D'. 52
- 4.3. Bed evolution between COAST3D surveys 2 and 4 and how different meshes reproduce the observed conditions. The letters 'A' to 'D' correspond to the mesh definition used in Figure 4.2. Contour bed level intervals are of 1 m (ODN) and correspond to COAST3D bathymetric survey 2. 53
- 4.4. Water level (A), river discharge (B) and wave height (C) for hydrodynamic calibration period. Although waves are not considered in these simulations, they are shown for illustrative purposes. Dashed vertical lines delimit periods of wave heights = 0.5 m (ODN). 60

4.5. Observed and predicted water levels and currents during the calibration period. Field data are represented by black crosses, while red dotted line corresponds to model output. Dashed vertical lines delimit periods of wave heights = 0.5 m (ODN). For more information on the location of the sites, the reader is referred to Figure 3.6.	65 and 66
4.6. Water level (A), river discharge (B) and wave height (C) for hydrodynamic validation period. Although waves are not considered in these simulations, they are shown for illustrative purposes. Dashed vertical lines delimit periods of wave heights = 0.5 m (ODN).	68
4.7. Observed and predicted water levels and currents during the validation period. Field data are represented by black crosses, while red dotted line corresponds to model output. Dashed vertical lines delimit periods of wave heights = 0.5 m (ODN). For more information on the location of the sites, the reader is referred to Figure 3.6.	70 and 71
4.8. Bed evolution between COAST3D surveys 2 and 4. Observed bed evolution (A); Model result considering single-grain-size of 0.3 mm and no waves (B; BSS= -0.33); Multiple grain-sizes without waves as a stirring agent (C; BSS= -0.11) and multiple grain-sizes with stirring effect of waves (D; BSS= -0.11). Contour bed level intervals are of 1 m (ODN) and correspond to COAST3D bathymetric survey 2.	84

Chapter 5

5.1. Input reduction of observed tides for a 17-day period. Original water level variation at the Pier (A); all 33 tidal cycles of the period (B) and the selected average tides according to the respective tidal range classification (C; bottom part of Table 5.2).	90
5.2. BSS distribution of different average tides in reproducing the morphodynamic result of the reference run for the short-term period of 17 days (08/11/99 to 25/11/99).	92
5.3. Average tides based on different tidal classes and the tidal ranges associated. In order to use them as a continuous record, some schematisation must be carried out either by distorting the average tide (A) or by the creation of hydraulic jumps between two average tides of different tidal range (B).	93
5.4. Morphodynamic outcome of the reference run for the period between COAST3D surveys 2 and 4 (A). The sum of the bed evolution of all average tides (based on different tidal ranges) multiplied by the respective frequency of occurrence is given in plot B (BSS= -1.24). The use of the average tides as a continuous record and also by the application of the scaling factor in descending order and in ascending order (full ensemble technique) is shown in plots C (BSS= 0.86) and D (BSS= 0.91), respectively. Insets correspond to tidal conditions used to force each set of runs.	95
5.5. Water level (A) and freshwater discharge (B) for medium-term application of ensemble technique. These conditions are used to compute the morphodynamic evolution of the reference run.	97

5.6. Boundary conditions for medium-term application of ensemble technique. Bed evolution depicted in plot 'A' corresponds to the reference run, while the outcome of the application of the ensemble technique is shown in plot 'B'. Insets represent tidal conditions used to force each set of runs. The 'Salty' sandbank is also shown. 99

Chapter 6

- 6.1. Instantaneous water level differences (relative to the pier level) during peak EBB currents at the estuary entrance. The following conditions are considered: 'NL' (A); 'NH' (B); 'SL' (C) and 'SH' (D). Points 'Inner' (and 'Outer') are used to define the water level differences between the inner (and outer) estuary and the pier. In plot E, a zoom into the case 'NL' (cross-section E.1 to E.2 to be used in Figure 6.5) and the water level patterns of the test 'SH' (F). The 0 m (ODN) isobath is indicated as a continuous line. 104
- 6.2. Instantaneous water level differences (relative to the pier level) during peak FLOOD currents at the estuary entrance. The following conditions are considered: 'NL' (A); 'NH' (B); 'SL' (C) and 'SH' (D). Zoomed water level differences for the cases 'NL' (E) and 'SH' (F). The 0 m (ODN) isobath is indicated as a continuous line. 105
- 6.3. Instantaneous currents during peak EBB currents at the estuary entrance. The following conditions are considered: 'NL' (A); 'NH' (B); 'SL' (C) and 'SH' (D). Zoomed areas of cases 'NL' (E) and 'SH' (F). The 0 m (ODN) isobath is indicated by the inner continuous line. Squares indicate the areas of peak resultant current magnitudes. Vectors under 0.01 m.s^{-1} are omitted. 107
- 6.4. Instantaneous currents during peak FLOOD currents at the estuary entrance. The following conditions are considered: 'NL' (A); 'NH' (B); 'SL' (C) and 'SH' (D). Zoomed areas of cases 'NL' (E) and 'SH' (F). The 0 m (ODN) isobath is indicated by the inner continuous line. Squares indicate the areas of peak resultant current magnitudes. Vectors under 0.01 m.s^{-1} are omitted. 108
- 6.5. Instantaneous sediment transport during the following conditions: total sediment transport for peak EBB currents (A and C) and for peak FLOOD currents (B and D) of cases 'SL' (A and B) and 'SH' (C and D). The inner continuous lines correspond to 0 m (ODN) isobath. Vectors under $1 \times 10^{-6} \text{ m}^2.\text{s}^{-1}$ are omitted. The largest vectors emanate from the estuary entrance. 111
- 6.6. Peak resultant water level difference, current magnitudes and total sediment transport across the estuary entrance (profile E.1 to E.2, defined in Figure 6.1.E) during ebbing phase (A, B and C) and flooding phase (D, E and F): case 'NL' (continuous black line); case 'NH' (dashed orange line); case 'SL' (continuous blue line with solid squares) and 'SH' (continuous red line with crosses). 113
- 6.7. Time-averaged water level differences at the Teign estuary relative to the pier, under the following conditions: neap tides of winter-spring 2002/2003 (A) and summer-autumn 2003 (B); spring tides of winter-spring 2002/2003 (C) and summer-autumn 2003 (D). The inner continuous lines correspond to 0 m (ODN) isobath. 115
- 6.8. Time-averaged water level differences at the outer estuary and adjacent coast 116

relative to the pier, under the following conditions: neap tides of winter-spring 2002/2003 (A) and summer-autumn 2003 (B); spring tides of winter-spring 2002/2003 (C) and summer-autumn 2003 (D). The inner continuous lines correspond to 0 m (ODN) isobath.

6.9. Residual currents at the Teign estuary under the following conditions: neap tides of winter-spring 2002/2003 (A) and summer-autumn 2003 (B); spring tides of winter-spring 2002/2003 (C) and summer-autumn 2003 (D). The inner continuous lines correspond to 0 m (ODN) isobath. Vectors under 0.01 m.s^{-1} are omitted. 118

6.10. Residual velocity at outer estuary and adjacent coast associated with the tidal range for the winter-spring 2002/2003. $TR = 1.5 \text{ m}$ (A); $1.5 \text{ m} < TR = 2 \text{ m}$ (B); $2 \text{ m} < TR = 2.5 \text{ m}$ (C); $2.5 \text{ m} < TR = 3 \text{ m}$ (D); $3 \text{ m} < TR = 3.5 \text{ m}$ (E); $3.5 \text{ m} < TR = 4 \text{ m}$ (F); $4 \text{ m} < TR = 4.5 \text{ m}$ (G) and $TR > 4.5 \text{ m}$ (H). The inner continuous line corresponds to 0 m (ODN) isobath. Vectors under 0.01 m.s^{-1} are omitted. 119

6.11. Residual currents at the outer estuary and adjacent coastal area under the following conditions: neap tides of winter-spring 2002/2003 (A) and summer-autumn 2003 (B); spring tides of winter-spring 2002/2003 (C) and summer-autumn 2003 (D). The inner continuous lines correspond to 0 m (ODN) isobath. Vectors under 0.01 m.s^{-1} are omitted. 120

6.12. Residual currents at the estuary entrance under the following conditions: neap tides of winter-spring 2002/2003 (A) and summer-autumn 2003 (B); spring tides of winter-spring 2002/2003 (C) and summer-autumn 2003 (D). The inner continuous lines correspond to 0 m (ODN) isobath, while the red ellipsoidal element represents the -8 m (ODN) isobath. Vectors under 0.01 m.s^{-1} are omitted. 121

6.13. Residual total sediment transport volume per unit width at the whole estuary for spring tides of winter-spring 2002/2003 (A) and summer-autumn 2003 (B). The inner continuous line corresponds to 0 m (ODN) isobath. Vectors under $1 \times 10^{-6} \text{ m}^2.\text{s}^{-1}$ are omitted. 123

6.14. Residual total sediment transport volume per unit width at the outer estuary and adjacent coast associated with the tidal range for the winter-spring 2002/2003. $TR = 1.5 \text{ m}$ (A); $1.5 \text{ m} < TR = 2 \text{ m}$ (B); $2 \text{ m} < TR = 2.5 \text{ m}$ (C); $2.5 \text{ m} < TR = 3 \text{ m}$ (D); $3 \text{ m} < TR = 3.5 \text{ m}$ (E); $3.5 \text{ m} < TR = 4 \text{ m}$ (F); $4 \text{ m} < TR = 4.5 \text{ m}$ (G) and $TR > 4.5 \text{ m}$ (H). A single-grain size (0.3 mm) and the formulation of Engelund-Hansen (1967), modified by Cholley and Cunge (1979) are used. The inner continuous line corresponds to 0 m (ODN) isobath. Vectors under $1 \times 10^{-6} \text{ m}^2.\text{s}^{-1}$ are omitted. 124

6.15. Residual total sediment transport volume per unit width at the outer estuary and adjacent coast for spring tides of winter-spring 2002/2003 (A and zoomed in C) and summer-autumn 2003 (B and zoomed in D). The inner continuous line corresponds to 0 m (ODN) isobath, while the red ellipsoidal element in plots 'C' and 'D' represents the -8 m (ODN) isobath. Vectors under $1 \times 10^{-6} \text{ m}^2.\text{s}^{-1}$ are omitted. 126

6.16. Morphological changes at the Teign estuary between December 2002 to May 2003 (A: observed data and C: model results) and May 2003 to November 2003 (B: observed data and D: model results). Erosion features are associated to green and blue areas. Yellow and red patterns correspond to sediment deposition in the period. Isobaths (m ODN) correspond to bottom properties at the beginning of the respective period. 127

6.17. Mesh used for the simulation of mixed grain sizes and the wave-induced 129

stirring effects (4234 nodes). The inset represents the area of further mesh refinement due to channel meandering and complex bathymetry.

- 6.18. Residual velocity at outer estuary and adjacent coast for the winter-spring 2002/2003 under the joint effects of wave stirring and mixed grain sizes. TR = 1.5 m (A); 1.5 m < TR = 2 m (B); 2 m < TR = 2.5 m (C); 2.5 m < TR = 3 m (D); 3 m < TR = 3.5 m (E); 3.5 m < TR = 4 m (F); 4 m < TR = 4.5 m (G) and TR > 4.5 m (H). The inner continuous line corresponds to 0 m (ODN) isobath. Vectors under 0.01 m.s⁻¹ are omitted. 131
- 6.19. Residual total sediment transport volume per unit width at outer estuary and adjacent coast for the winter-spring 2002/2003 2003 under the joint effects of wave stirring and mixed grain sizes. TR = 1.5 m (A); 1.5 m < TR = 2 m (B); 2 m < TR = 2.5 m (C); 2.5 m < TR = 3 m (D); 3 m < TR = 3.5 m (E); 3.5 m < TR = 4 m (F); 4 m < TR = 4.5 m (G) and TR > 4.5 m (H). The inner continuous line corresponds to 0 m (ODN) isobath. Vectors under 1x10⁻⁶ m².s⁻¹ are omitted. 133
- 6.20. Partitioned total sediment transport for TR = 1.5 m. Silt and clay fraction (A); Very fine and fine sands (B); medium sands (C); coarse and very coarse sands (D); granules (E) and gravels (F). The inner line corresponds to 0 m (ODN) isobath. 136
- 6.21. Partitioned total sediment transport for 2 m < TR = 2.5 m. Silt and clay fraction (A); Very fine and fine sands (B); medium sands (C); coarse and very coarse sands (D); granules (E) and gravels (F). The inner line corresponds to 0 m (ODN) isobath. 137
- 6.22. Partitioned total sediment transport for 3 m < TR = 3.5 m. Silt and clay fraction (A); Very fine and fine sands (B); medium sands (C); coarse and very coarse sands (D); granules (E) and gravels (F). The inner line corresponds to 0 m (ODN) isobath. 138
- 6.23. Partitioned total sediment transport for 4 m < TR = 4.5 m. Silt and clay fraction (A); Very fine and fine sands (B); medium sands (C); coarse and very coarse sands (D); granules (E) and gravels (F). The inner black line corresponds to 0 m (ODN) isobath. 139
- 6.24. Schematic residual sediment transport patterns for the silt and clay fraction under tides, river discharge and a single grain size. Normal river discharge conditions (under 15 m³.s⁻¹) are considered throughout. Tidally-induced residual sediment transport is indicated by red shaded arrows; thinner blue arrows are related to the net sediment transport. 140
- 6.25. Schematic residual sediment transport patterns for the silt and clay fraction under mixed grain sizes and considering the wave stirring effect. Normal river discharge conditions (under 15 m³.s⁻¹) are considered throughout. Tidally-induced residual sediment transport is indicated by red shaded arrows; the net effect of the wave stirring is given by black arrows and thinner blue arrows are related to the net sediment transport. The sediment availability as a function of the wave stirring is represented by black dots. 141
- 6.26. Initial grain size concentration for the tests with mixed sediments. Red and yellow patterns are associated with concentrations higher than 50%, while the areas with purple and blue colours are related to grain concentrations smaller than around 30%. Silt and clay fraction (A); Very fine and fine sands (B); medium sands (C); coarse and very coarse sands (D); granules (E) and gravels (F). 144

6.27. Differences in the grain size concentration at the end of simulation of the winter-spring 2002/2003 period relative to the initial conditions. Red and yellow patterns are associated with the accumulation of sediments, while the reduction of a given grain fraction is shown in green and blue tones. Silt and clay fraction (A); Very fine and fine sands (B); medium sands (C); coarse and very coarse sands (D); granules (E) and gravels (F).	146
6.28. Morphological changes at the Teign estuary between December 2002 to May 2003: observed data (A) and model results (B). Erosion features are associated to green and blue areas. Yellow and red patterns correspond to sediment deposition in the period. Isobaths (m ODN) correspond to bottom properties at the beginning of the respective period.	149
6.29. Differences in the grain size concentration at the end of the first tide (TR= 1.5 m) for the winter-spring 2002/2003 period relative to an isotropic initial distribution. Red and yellow patterns are associated with the accumulation of sediments, while the reduction of a given grain fraction is shown in green and blue tones. Silt and clay fraction (A); Very fine and fine sands (B); medium sands (C); coarse and very coarse sands (D); granules (E) and gravels (F).	150
6.30. Differences in the grain size concentration at the end of simulation of the winter-spring 2002/2003 period relative to an isotropic initial distribution. Red and yellow patterns are associated with the accumulation of sediments, while the reduction of a given grain fraction is shown in green and blue tones. Silt and clay fraction (A); Very fine and fine sands (B); medium sands (C); coarse and very coarse sands (D); granules (E) and gravels (F).	151

List of Tables

Chapter 2

2.1. Effect of wave stirring on residual currents and net sediment transport (modified from de Vriend, 1993).	12
---	----

Chapter 3

3.1. Tides, river states and role on sediment transport in inner estuary (Nunny, 1980, after Wells, 2002a).	31
3.2. Field data properties considered in this study. No direct wave data observations are taken into account.	32
3.3. COAST3D main experiment sites used for model calibration and validation. Site 5 was serviced and slightly moved during the main experiment.	34
3.4. COAST3D main experiment bathymetric surveys on the coastal area adjacent to the Teign estuary.	37
3.5. CoastView bathymetric surveys on the outer estuary and adjacent coast. Average wave conditions are based on the root mean square (rms) of these parameters.	40
3.6. Sediment volume changes during CoastView surveys. Positive and negative values mean sediment deposition and erosion, respectively.	44

Chapter 4

4.1. Boundary conditions applied to hydrodynamic tests.	54
4.2. Qualification of RMAE error ranges for wave height and velocity (van Rijn et al., 2003) and for ARMAE error estimates (Sutherland et al., 2004a).	58
4.3. Model sensitivity to key parameters during hydrodynamic calibration period. Simulations are compared against observed U and V velocity components (averaged values). The model performance is expressed in terms of the average RMAE and ARMAE estimated from 5 different site locations. Values in bold are the selected ones for the model calibration.	61
4.4. Calibration parameters for hydrodynamic simulation between 08/11/99 07:00 to 22/11/99 07:00 (GMT).	62
4.5. RMAE for hydrodynamic calibration period.	67
4.6. Model performance for hydrodynamic validation period. Statistical errors below are calculated based on the average RMAE and ARMAE of corresponding U and V velocity components. RMAE qualification ranges are based on van Rijn et al. (2003) while ARMAE categorisation is based on Sutherland et al. (2004a).	69
4.7. Qualification of BSS error ranges for morphodynamic studies (van Rijn et al.,	78

2003).

4.8. Sediment transport module sensitivity to key parameters during a period of 2 days of COAST3D project. Values in bold are the selected ones for the calibration of the morphological module. 80

Chapter 5

5.1. Model set-up used for the studying the ensemble technique. 89

5.2. Classification of tides based on respective tidal range observed in the 17-day period and frequency of occurrence of each average tide. 91

5.3. BSS decomposition for the tests shown in Figure 5.4. The initial condition is COAST3D survey 2 and final condition corresponds to bed evolution modelled from the reference run. 96

5.4. Classification of tides based on respective tidal range observed in the 6-month period and frequency of occurrence of each average tide. The parameters S_C and N_{TIDES} are explained in Equation 5.1. 98

Chapter 6

6.1. Forcing conditions for short-term hydrodynamic tests in the Teign estuary and adjacent coast. 102

List of Symbols

(variations in symbols are stated in the text next to derivation)

α	direction of solid transport in relation to the flow direction
a_b	slope angle of the bottom
θ_w	direction of wave propagation (degrees)
Δt	time step
κ	van Karman's constant
β_i	hiding factor for the i -th sediment fraction
μ	ripple-correction factor for skin friction
F_b	non-dimensional bedload transport rate
F_s	non-dimensional current-induced transport rate
ω	wave frequency (s^{-1})
β	slope effect
$\zeta(x,y,t)$	surface elevation (m)
τ_b	dimensionless bottom friction or Shields parameter
θ_p	dimensionless skin friction shear stress
$\tau_{c,c}$	critical Shields parameter
τ_{cw}	non-dimensional shear stress due to wave-current interaction
f	sediment friction angle
ν_w	water viscosity ($m^2.s^{-1}$)
e_c, e_s	Bailard's empirical factors
ρ	density of water ($kg.m^{-3}$)
ρ_s	density of the sediment ($kg.m^{-3}$)
τ	vectorial bed shear stress ($kg.m^{-1}.s^{-2}$)
τ_0	scalar bed shear stress
τ_c	bed shear stress induced by currents
τ_{cw}	combined shear stress due to the effects of waves and currents
τ_w	wave-derived shear stress
K_t	momentum diffusion coefficient ($m^2.s^{-1}$)
K_T	tracer diffusion coefficient ($m^2.s^{-1}$)
A_S	total-load coefficient associated with Soulsby-van Rijn formulation

A_w	wave orbital amplitude on the bed
b	dimensionless coefficient for bedload transport (Bijker)
$C(x,y)$	Chézy friction coefficient ($m^{1/2}.s^{-1}$)
C_d	dimensionless friction coefficient
C_h	Chézy coefficient associated to total friction
C_{hp}	Chézy coefficient due to skin friction
D	sediment grain diameter (mm)
D_{50}	median grain size (mm)
D_{90}	sediment size for which 90% of the bed material is finer (mm)
D_*	non-dimensional grain diameter
D_i	average grain size of the i -th sediment fraction
D_m	average grain size of all sediments found in the active layer
E	eddy viscosity coefficient ($m^2.s^{-1}$)
f_w	wave friction coefficient
F_{oc}	frequency of occurrence of a given average tide
F_X and F_Y	source terms of the momentum equations in u and v , respectively
g	acceleration due to gravity ($m.s^{-2}$)
$h(x,y,t)$	water depth (m)
H_s	significant wave height (m)
I	Einstein's integrals
k	wave number
k_s	Nikuradse friction coefficient (mm)
k_{sp}	skin friction roughness
L	wave length (m)
m	Manning friction coefficient ($m^{1/3}.s^{-1}$)
n	number of samples
n_b	bed porosity
N_{TIDES}	random number of times the respective average tide will be used in the modelling run in question
p	porosity
P_C	coefficient function of porosity
Q_{bed}	bedload sediment transport volume per unit width ($m^2.s^{-1}.m^{-1}$)
Q_s	solid sediment volume transport per unit width ($m^2.s^{-1}$)
$Q_{s,i}$	corrected sediment transport rate for the i -th sediment fraction

Q_{susp}	suspended-load sediment transport volume per unit width ($m^2.s^{-1}.m^{-1}$)
$Q_{s,i}^*$	uncorrected sediment transport rate for the i -th sediment fraction
r	bed roughness
s	relative density of the sediment
s_c	current direction coordinate
S_C	scaling factor
S_h	source or sink of fluid ($m.s^{-1}$)
S_L	bed slope effect
S_T	tracer source or sink ($g.l^{-1}.s^{-1}$)
S_x and S_y	source or sink terms in dynamic equations (e.g. wind, Coriolis force, bottom friction), expressed in $m.s^{-2}$
t	time (s)
T	non-buoyant tracer ($g.l^{-1}$ or $^{\circ}C$)
T_p	wave period (s)
U, V	depth-averaged velocity components in the x- and y-directions ($m.s^{-1}$)
u, v	velocities in the x- and y-directions ($m.s^{-1}$)
U_{cr}	critical entrainment velocity ($m.s^{-1}$)
U_w	wave orbital velocity ($m.s^{-1}$)
u_{cw}	friction velocity derived from the wave-current interaction ($m.s^{-1}$)
w_s	grain settling velocity ($m.s^{-1}$)
x, y	space coordinates (m)
x_f	forecast value of the parameter in question
x_v	corresponding verifying value
z	vertical elevation (m)
$Z(x,y,t)$	free surface elevation (m)
Z_f	bed elevation (m)
Z_f^n	bottom depth at the time $n^{\circ} t$

Acknowledgements

To the Brazilian National Research Council (*Conselho Nacional de Desenvolvimento Científico e Tecnológico* – CNPq) for sponsoring this unique experience at the University of Plymouth.

To my supervisor, Mark A. Davidson. His constant support and enthusiasm have always been fundamental to me. I hope we can carry on working together in the future.

I am also very grateful to Prof. Keith R. Dyer for helping turning this dream into reality. His expertise and kindness are greatly appreciated. I would like to express my gratitude to Dr. Ken J. George for helping me with the various aspects of numerical modelling. The collaboration of Prof. David A. Huntley during this PhD is also acknowledged.

My big thanks to the people who provided the means and the assistance with Telemac system: Dr. Alan Cooper and Mr. John Baugh (HR Wallingford); Mr. Pierre Lang (SOGREAH) and Dr. Catherine Villaret, Dr. Jean Michel Hervouet and Dr. Cecile Machet (Electricité de France). Dr. Bernard Latteux is acknowledged for the important contribution on the improvement of the ensemble technique. Dr. Ian Townend (ABP Mer) and Dr. Tim Wells are also thanked for providing field data.

To our great friends: Edu and Claudinha (get the bbq ready and the beer ice cold!); Claudinha (sogrinha); James, Kevin and Linda; Elisa and Gilberto; Adrian; the superb family Cecilia, Ismael, Ale and Gise; the great French guys (Tophe, Lolo, Bastien and David); the Angolan squad (Boto, Luaty, Kadao, Kimy and Pedro); Muxa; Cesar and Ena; Conde; Paulo; Peter Figueiredo; Marcelo and Fernanda; Hector and Laura; Nigel; Ken; Peter; Debbie; Henry and Helen; Asha, Clare; Lu, Nico and Artur; Manu; Garga and Gre; Steve; SEOES office staff. A very special thank you to the people who first welcomed us to Plymouth: Vanessinha and family; Mags; Jojo; and the greatest landlords: Ed, Chris, Amy, Martin and Emily. Jam Samba and all its members (Joff, Tom, Percy, Andy, Debbie, Heather, Michelle, Noel, Janes, Al, and so many others) will be always in our very best memories of Plymouth. To Bezerra da Silva, thanks for singing 'Brasil' in its most pure and sincere form.

To our families and friends in Brazil. Finally to Painho, Mainha, Negao, Menna and Ninha... To my wife Carolina, the most wonderful partner I could ever have wished for... Your perseverance, love and positive energy are (and will be) part of my true happiness!!!!

Author's Declaration

At no time during the registration for the Degree of Doctor of Philosophy has the author been registered for any other University award without prior agreement of the Graduate Committee.

This study was financed with the aid of a studentship from the Brazilian National Research Council (CNPq).

Relevant scientific seminars and conferences were regularly attended at which work was often presented; external institutions were visited for consultation purposes.

Presentations and Conferences Attended:

Coastal Dynamics, 04-08 April 2005. Barcelona, Spain.

Oral presentation: Waves and grain-size effects on the morphodynamic evolution of the Teign estuary (UK) (Bernardes, MEC, Davidson, MA, Huntley, DA, Dyer, KR and George, KJ).

Visit and presentation at the Katholieke Universiteit Leuven of the main findings of the thesis. 22 March 2005. Leuven, Belgium.

Physics of Estuaries and Coastal Seas, 18-22 October 2004. Merida, Mexico.

Oral presentation: Towards Medium-Term (order of months) Morphodynamic Modeling of the Teign Estuary, UK (Bernardes, MEC, Davidson, MA, Dyer, KR and George, KJ).

XI Telemac Users Club, 07-08 October 2004. Toulouse, France.

Oral presentation: Waves and grain-size effects on the morphodynamic evolution of the Teign estuary (UK) (Bernardes, MEC, Davidson, MA, Huntley, DA, Dyer, KR and George, KJ).

X Telemac Users Club, 17-18 October 2003. Chamrousse, France.

Oral presentation: Coupling Telemac-2D and Sisyphe: A case study (Bernardes, MEC, Davidson, MA, Dyer, KR and George, KJ).

3rd IAHR Symposium on River, Coastal and Estuarine Morphodynamics, 01-05 September 2003. Barcelona, Spain.

Physics of Estuaries and Coastal Seas, 17-20 September 2002. Hamburg, Germany.

VIII Telemac Users Club 2001, 15-16 November 2001. Paris, France.

One oral presentation in the Institute of Marine Studies, University of Plymouth (UoP), Research Seminar Series 2001 and another in the joint seminar series of Coastal Group (SEOES-UoP) and School of Engineering (UoP).

External Contacts:

Electricité de France R&D (Paris, France)

SOGREAH (Grenoble, France)

HR Wallingford (Wallingford, UK)

Word count of main body of thesis: 46569

➤ **The contribution to this project from collaborators is as follows:**

Bernard Latteux contributed towards the development of the ensemble technique.

Amended the code of the morphological module to allow the input of the multiple grain sizes on a node-by-node basis.

Date 18/05/05

Chapter 1 - Introduction

1.1. General introduction

Coastal areas have an important effect on economic, social and ecological issues worldwide. Being at strategic locations - the interface between land and sea - estuaries have been subject to multiple uses. These range from providing shelter to many organisms to providing favourable conditions for the construction of harbours; from being a source of water and destination of sewage to supporting leisure activities, among many other uses. In the UK, around 84% of imports and exports pass through ports located in estuaries (Townend, 1995); some 76% of the area of estuaries has some form of European nature conservation designation (Townend, 1997). Thus, understanding the environmental behaviour of estuaries is crucial to estimate their response to a variety of impacts; among them, the effects of the sea level rise, natural catastrophes (notably hurricanes and tsunamis) and engineering works (dredging and land reclamation).

Until recently, the study of estuaries was based mainly on descriptive observations and on empirical relationships between physical properties. Although these tools are still valid and in use, the development of informatics has accelerated the conditions towards one of the main challenges of coastal science: predicting future changes with a reasonable level of accuracy. Nowadays, the combination of field data with numerical models provides useful insights about the underlying mechanisms driving the hydrodynamics of estuaries. In order to fulfil the predictive goal aforementioned, the current challenge of estuarine science is to be able to replicate the effects of flow properties on sediment transport, water quality and biota.

This thesis aims to contribute to a better understanding of the interactions and feedback mechanisms between hydrodynamics, sediment transport and consequent bed evolution in estuaries. These processes are simulated and coupled within time scales of hours to months through the use of Telemac-2D (developed by Laboratoire National d'Hydraulique - LNH and Electricité de France - EDF/DER), a vertically averaged numerical model. The Teign estuary, Teignmouth, Devon, UK was selected as the study area due to two main factors: i)

its dynamic properties and ii) the abundance of field data at the adjacent coastal area. In order to complement the current knowledge on the coastal processes off the Teign estuary, this thesis aims at contributing to the understanding of morphodynamic processes in meso- to macrotidal estuaries, such as the Teign. Extensive field data campaigns were conducted mainly in the adjacent coastal area, especially by the EU-funded projects COAST3D^{1.1} and CoastView^{1.2}. Although not considered in this study, the area around the estuary entrance is also monitored by the Argus system of cameras (Holman, 1994). Based on the COAST3D and CoastView measurements and other data sets (Table 3.2), the main estuarine processes are simulated in short-term (order of tidal cycles) time scales. A new input reduction technique (so-called ensemble technique) is devised in order to allow for longer-term morphodynamic simulations. When compared against the model output of a complete simulation, simulation results based on the ensemble technique are shown to accurately reproduce the modelled bed evolution patterns, with the added benefit of significantly reducing (i.e. order of 80% faster) the simulation time. Special attention is given to the combined effects of mixed sediment grain sizes and waves, allowing for the reproduction of seasonal patterns, and insights on the sediment pathways within the area are considered. This work was carried out with the collaboration of HR Wallingford, who kindly supplied the numerical model Telemac-2D and its accompanying modules.

1.2. Specific objectives

In order to achieve a better understanding of the morphodynamics of estuarine systems, and of the Teign estuary in particular, the following specific goals are proposed:

- Implement, calibrate and validate a hydrodynamic model based on Telemac-2D for the Teign estuary and adjacent coastal area;
- Enhance the current knowledge of morphodynamic processes in coastal systems through the implementation of a morphodynamic model to the Teign estuary and adjacent coastal area;

^{1.1} For further details, visit <http://www.hrwallingford.co.uk/projects/COAST3D>.

^{1.2} For further details, visit: <http://www.thecoastviewproject.org>

- Develop and validate an accurate and computationally efficient method for longer-term morphodynamic simulations;
- Identify the main mechanisms and their interactions responsible for the short-term (order of hours to days) morphodynamic evolution of the area;
- Understand the effects of residual patterns on the seasonal morphodynamic evolution of the area;
- Explore the role of waves and multiple grain sizes on the evolution of the area;
- Assess the main sediment transport pathways on medium-term scales (order of weeks to months).

1.3. Thesis outline

This thesis is structured on the following way: a literature review on estuaries and the main methods of studying these systems is presented in **Chapter 2**. It is seen from this chapter that many gaps in the knowledge of estuarine (and coastal) systems have been filled by the combination of field data with numerical models.

In **Chapter 3**, the Teign estuary and its adjacent coastal area are described in terms of their principal hydrodynamic and morphological features, followed by a summary of the field data previously gathered for the area. A unique bathymetric data set is shown to illustrate the morphodynamic response of the estuary and adjacent coastal area to seasonal conditions.

The hydrodynamic module is described, calibrated and validated successfully in **Chapter 4**. Despite some model limitations, the morphological module is implemented and tested with encouraging results towards a comprehensive description and reproduction of the rather complex morphodynamic features of the Teign estuary. Robust statistical techniques are used to determine quantitatively the model ability in describing field processes.

The development and validation of an ensemble technique to allow longer-term simulations is discussed in **Chapter 5**. Tides are treated as the main forcing mechanism on the morphodynamic processes within the Teign estuary. The technique is shown to describe accurately the outcome of complete model simulations, with the added benefit of a time efficient performance.

In **Chapter 6** the main model predictions are described. Short-term morphodynamic features are explored and linked to the residual patterns and their effects on the seasonal evolution of the area. Based on the use of the ensemble technique, the importance of the stirring effect of waves and the inclusion of mixed grain sizes in the model configuration is highlighted as crucial to replicating medium-term patterns. Also, the likely sediment transport pathways between the estuary and the adjacent coastal area are assessed.

Finally, **Chapter 7** is devoted to the main conclusions and considerations highlighted in this thesis, along with the recommendations on further research.

Chapter 2 - Literature Review

2.1. Introduction

As stated in Section 1.1, the main goal of this thesis is to assess and understand the principal morphodynamic processes within estuaries in general, and those acting on the Teign estuary in particular. This chapter is aimed at providing background information on relevant issues, ranging from the different definitions of estuaries to the most suitable techniques to predict their longer-term evolution.

2.2. Estuaries: definitions and general aspects

In general terms, estuaries are the interface zone between fresh and seawater. Moreover, these systems are influenced by strong gradients, such as in fluid density, suspended sediment concentration, chemical and biological factors (Dyer, 1994). A universal definition that encompasses the wide range of different processes - which occur in several time and spatial scales - is virtually impossible. However, one of the most accepted definitions was proposed by Cameron and Pritchard (1963): "An estuary is a semi-enclosed coastal body of water which has free connection to the open sea and within which seawater is measurable diluted with freshwater derived from land drainage". According to Dyer (1997), this definition is valid only if average tidal conditions are considered.

Estuaries can also be classified under a wide range of parameters. i) Tidal range, e.g. the classification of Davies (1964) using microtidal, mesotidal, macrotidal and hypertidal ranges; ii) Convergence of lateral topography against friction, e.g. the classification of Nichols and Biggs (1985) on hypersynchronous (where lateral topography convergence exceeds the friction effects, resulting in larger tidal ranges and higher tidal currents towards the head of the estuary), synchronous and hyposynchronous estuaries (where friction effects dominate over the convergence; thus tidal range and respective currents decrease up-estuary); iii) Salinity stratification classification by Pritchard (1955) and

Cameron and Pritchard (1963), with estuaries of different types: salt wedge; fjords, partially mixed and vertically homogeneous; iv) Topography, proposed by Pritchard (1952), where estuaries are divided in three groups: coastal plain, fjords and bar-built and v) Morphology, the classification postulated by Dalrymple et al. (1992), whereby an estuary is divided into an inner, central and outer zones. In this classification, these authors inter-relate the effects of morphology, sediment type and energy distribution to define the three zones. While riverine-dominated processes would prevail on the inner zone, tides and waves (at the seaward limit of the estuary) would be dominant on the outer zone, with mixed influences at the central zone.

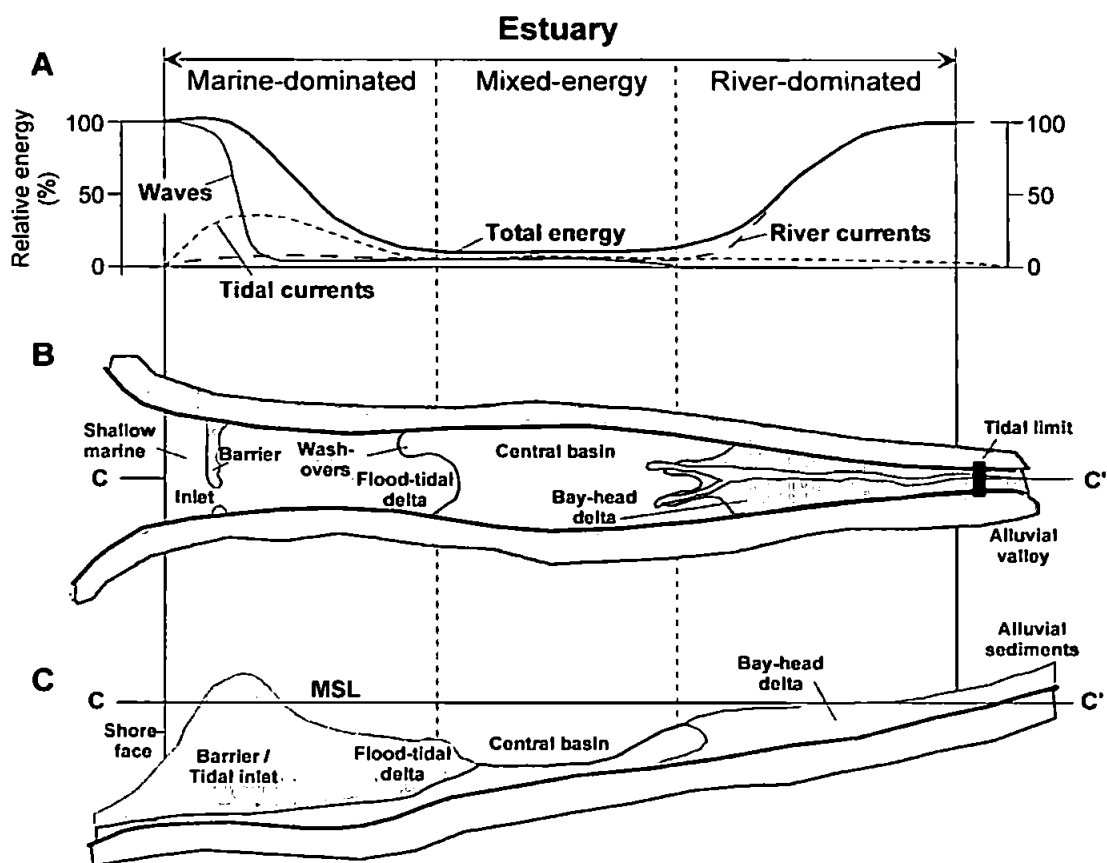


Figure 2.1: Energy variation along the axis of a wave-dominated estuary (A); plan view of the estuary with main morphological features highlighted (B) and plot C shows a side view of the stratigraphy along the estuary axis (after Dalrymple et al., 1992).

An example of the interactions between these forcing conditions is shown in Figure 2.1. The two extreme zones would be subject to more dynamic conditions (and more likely to consist of coarser grain sizes), while the central zone would behave as a sedimentary sink, with finer grain sizes (Dalrymple et al., 1992). Anderson (1983) added that intertidal areas

would be one of the main sources and sinks of suspended sediment within an estuary. In a long-term evolution perspective, Masselink and Hughes (2003) differentiate estuaries from deltas by associating the former to a net landward transport of sediments, while a seaward sediment transport would prevail in deltas.

Owing to several reasons (e.g. high ratios between the intertidal area and that of the whole estuary), the velocity distribution along an estuary can vary significantly, according to the tidal phase, i.e. flooding or ebbing. Thus, asymmetries in both the duration of the tidal phase and in the velocity field are observed and may vary spatially within the estuary. If the currents during the rising tide are more intense (shorter period) than those at the falling tide, then the estuary or channel are said to be flood-dominant. Conversely, ebb-dominated estuaries present stronger ebbing currents relative to the velocities during the flooding phase. For more information, the reader is referred to Walton (2002).

Given the non-linear dependence of the sediment transport on the velocity distribution, tidal asymmetries have a considerable effect on the ultimate morphodynamic behaviour of estuaries - especially those where non-cohesive sediments predominate. Therefore, estuaries which are classified as ebb-dominated will tend to export sediment to the adjacent coastal area (approaching the classical definition on deltas, given earlier in this section), whilst flood-dominated estuaries will be subject to sediment infilling. Exceptions to this general rule, induced by phenomena like tidal asymmetry, secondary effects (e.g. inertia, Coriolis and lateral curvature) are highlighted by de Vriend (1993) and illustrated in Figure 2.5 and Table 2.1. Although not mentioned by this author, different types of lag effects can also be important in the overall morphodynamic characteristics of estuarine systems (Dyer, 1994).

The presence of spits is relatively common at the entrance of many estuarine systems. These features are formed mainly by littoral drift and interactions between hydrodynamic forces and the local morphology, along with the availability of sediment. As a result of the flow constriction, tidal deltas are formed (Oertel, 1972; Hayes, 1975; Boothroyd, 1978). According to Dyer (1994), the residual flow at these areas will be characterised by a divergence zone at the estuary entrance, with opposite direction at the sides of the inlet (Figure 2.2).

Wave effects will affect the extent of the ebb tidal delta, and its form will depend on the local residual currents and on the sediment transport properties (Sha, 1989). By studying a micro-tidal estuary, Green and MacDonald (2001) observed that wave-driven currents were the main mechanism of initiation of sediment transport, which was conducted into the estuary mainly by bedload processes. Wave-driven flows can also play a role on the inner areas of estuaries, given some favourable conditions of wind speed, direction and duration, estuarine morphology, etc. (Figure 2.1). The influence of waves might also be dependent on the local tidal range, especially in areas subject to meso- to macro-tidal ranges, with intertidal areas being the most likely influenced by wave-driven currents.

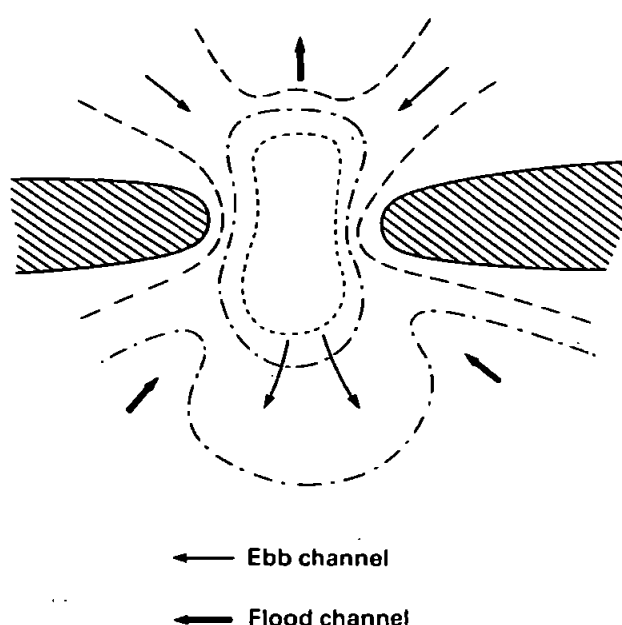


Figure 2.2: Residual sediment transport patterns at a tidal inlet and its adjacent flood and ebb tidal deltas (after Dyer, 1994).

If constant wind conditions are assumed, locally generated waves would tend to have a larger fetch and consequently bigger heights during high tide periods. Conversely, waves will be smaller under low tides due to restricted fetch. By studying a meso- to macro-tidal estuary in New Zealand, Green et al. (1997) observed during high tides that wave-related friction on the bottom layer were minimised due to the generation of rather short period waves, resulting in wave-orbital motions not big enough to reach the bed (and hence disturb the sediments). During the ebbing phase, the fetch was reduced and the wave heights decreased, but the wave orbital motions were enhanced at the bottom and peaked

around low water. Oldman et al. (2002) argued that wave-driven effects can play an important role in the longer-term sedimentation patterns within an estuary.

2.3. Coastal morphodynamics

Wright and Thom (1977) founded the concept of coastal morphodynamics. As demonstrated by Figure 2.1, the understanding of the behaviour and evolution of coastal systems, such as estuaries, is intimately linked to the three-dimensional interactions between currents, sediment transport processes and the resulting bed changes (Figure 2.3)^{2.1}. The feedback between these processes are defined as morphodynamics, whereby currents forced by several physical mechanisms (e.g. tides and waves), along with the bathymetric features, influence the sediment transport. Since these interactions are variable in space and time (Figure 2.4), gradients in the sediment transport patterns will trigger erosion and sedimentation features, ultimately changing the bed morphology. The altered morphology will then have a feedback effect on the behaviour (enhancement or inhibition) of the effect of the forcing conditions on generating currents and on altering the local morphology.

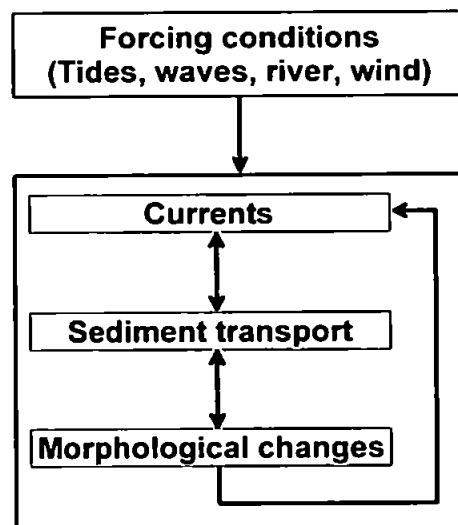


Figure 2.3: Schematic description of a coastal morphodynamic system.

^{2.1} For online information on estuarine morphodynamic interactions, visit <http://www.estuary-guide.net/>.

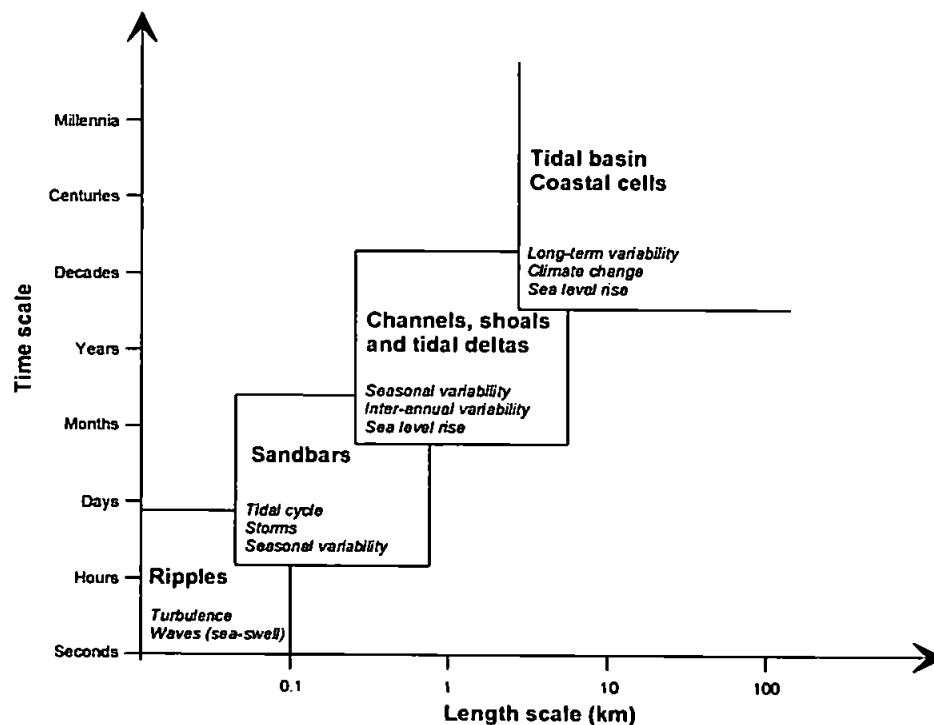


Figure 2.4: Morphological features (bold) and the main forcing processes (italic) as a function of time and space (after de Vriend, 1991).

In order to understand longer-term morphodynamic evolution of a coastal system, a few realisations of the interactions between currents, sediment transport and bed evolution may not suffice. Hence, residual patterns at similar time scales of the process of interest are needed. De Vriend (1993) argued that although the morphological time scale of tidally driven currents are much longer than the tidal period itself, tides play a fundamental role in determining large-scale morphodynamic patterns. He also established various causes for residual sediment transports generated by tidal action:

- 'primary', i.e. due to tidal asymmetries and residual currents. These processes are generally included in current coastal and estuarine numerical models (Figure 2.5);
- 'secondary', caused by accelerations (e.g. inertia, Coriolis and estuary curvature) or depth-dependent processes (e.g. wind, waves, density effects), which tend to influence the residual flow patterns. These processes are rarely included in recent models, but may be important in some coastal systems;
- the relationship between the tidal currents and the wave stirring effect, which can result in the net residual current being opposed to the net sediment transport (Table 2.1). This

effect can have a major impact on an estuarine morphodynamic evolution, as it will be shown in Chapter 6.

As described by Dyer (1994), residual currents can also be in opposite direction to the net residual sediment transport if lag effects - which are especially important for the interaction between the fluid and cohesive sediments - play a major role in the morphodynamic processes of the system considered. As lag effects are not considered in this thesis, their relative importance in the bed evolution of the Teign estuary cannot be assessed (more details in Section 4.4).

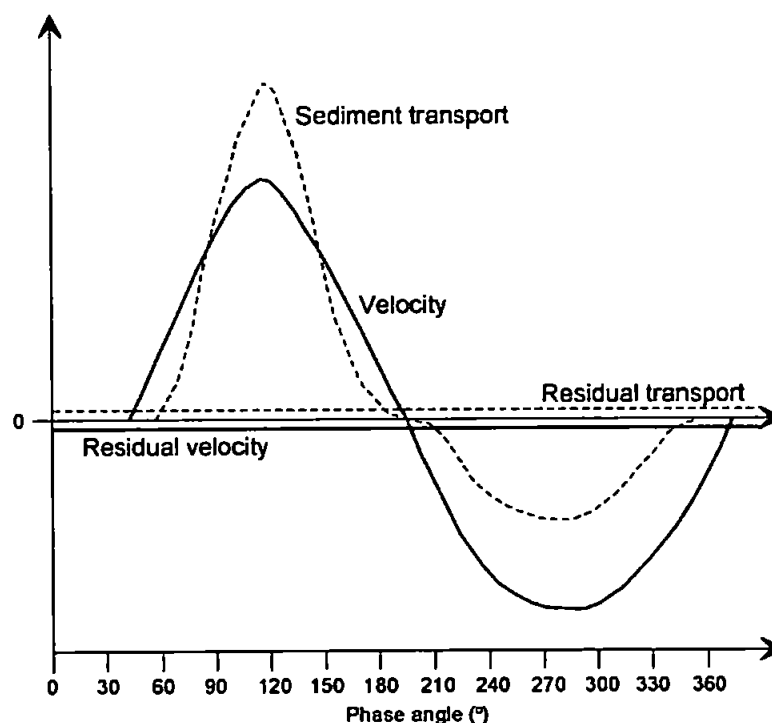










Figure 2.5: Residual 'primary' tidal transport (after de Vriend, 1993).

Apart from daily tides, other factors can also be important on the longer-term response of coastal and estuarine systems, such as: i) the spring-neap modulation, where spring tides can be much more morphodynamically important than neap tides, ultimately dominating the residual currents; ii) storm surges, which can alter the morphodynamic features, despite their low frequency of occurrence; iii) heterogeneity of wave climate, with chronology effects, i.e. two consecutive storms having a different effect compared to two storms separated by a calm period and iv) seasonal variation of conditions, as the water temperature (de Vriend, 1993). Green et al. (1997) added that in order to describe estuarine

morphodynamics processes, the concepts of 'sediment availability' (Black, 1987 and Black et al., 1989), sediment transporting capacity and settlement time scales are also crucial to the comprehension of the sediment transport patterns within estuaries. The assessment of observed medium-term (order of months to years) morphodynamic processes is illustrated in Chapter 3, while a technique to assist longer-term morphodynamic predictions is developed and validated in Chapter 5.

Table 2.1: Effect of wave stirring on residual currents and net sediment transport (modified from de Vriend, 1993).

	<i>Current</i>	<i>Wave stirring</i>	<i>Sediment transport</i>
Ebb total			
Flood total			
Residual		N/A	

2.4. Modelling morphodynamic processes

With the fast developments of computational resources in recent years, the application of numerical models to coastal-related issues has been intensified. Although morphodynamic processes are essentially three-dimensional, the successful application of 3D models in coastal areas is still limited. For recent developments on this approach, the reader is referred to Lesser et al. (2004). Hence, two-dimensional (depth-averaged) models are the most commonly used numerical tools in coastal issues, and estuaries are no exception. Alternative model approaches such as neural networks (e.g. Westra et al., 2002 and Huang, 2003), self-organisation concepts (e.g. Coco, et al., 2000) and genetic programming (e.g. Babovic and Keijzer, 2000) are also proving very useful tools for modelling coastal morphodynamics processes. However they are beyond the scope of this thesis and will not be discussed in further detail.

The accuracy and performance of numerical models have been improved in line with advances in scientific knowledge on coastal processes. Yet, many scientific gaps remain, such as a thorough comprehension on the non-linear interactions between currents,

sediment transport processes and the effects on the bed evolution; or the rather variable sediment transport rates especially under the joint effect of waves and tides on irregular bathymetric features (Komar, 1996 and van de Kreeke, 1996). These days, state-of-the-art numerical models are able to reproduce fairly well short-term (order of seconds to days) hydrodynamic features of a coastal system, although it is not necessarily true on longer-term scales. It should also be stressed that a successful model application will be dependent on the use of reliable field data to calibrate - and validate - the model performance (further details in Chapter 4).

Given the wide range of temporal and spatial scales which are characteristic of coastal systems (Figure 2.4), it is crucial that a sound choice is made in selecting the appropriate tools and methods. Reviews of the suitability of different methods to model the morphodynamic behaviour of coastal systems are given by de Vriend (1993), de Vriend et al. (1993), Hanson et al. (2003) and Stive and Wang (2003), among others. De Vriend (1996) categorised different types of model based on the inherent scales of the morphodynamic processes under study:

- *Data-based models*

Consist of the application of measured data to the comprehension of the phenomena under scrutiny, through regression analysis techniques, empirical orthogonal functions (EOF), etc. (e.g. application of EOF to predict sea surface temperatures, by Davis, 1976);

- *Empirical relationships*

Also considers observed data through a relationship between measured parameters (e.g. relationships between the cross-section area and the tidal prism, such as the one proposed by O'Brien, 1969);

- *Process-based or bottom-up models*

First physical principles (e.g. conservation of mass, momentum, energy, etc.) are used as a basis for the description of tides, waves, sediment transport and bathymetric changes through a set of mathematical equations. These models are mainly subdivided into coastal

profile and coastal area models, operating in time scales of up to 5 years and spatial scales of around a few kilometres square (van Rijn et al., 2003). The former are intended for studies of cross-shore processes, with the assumption of longshore uniformity (further details in Roelvink and Broker, 1993 and van Rijn et al., 2003), whilst the latter deal with two- or three-dimensional processes (for a review on these models, see de Vriend, 1993). Examples of process-based model applications are given in Wang (1991), Wang et al. (1995), Cayocca (2001), Mason and Garg (2001). A comparison between process-based models and long-term models is given in Hibma et al. (2003a);

- *Formally integrated, long-term or top-down models*

These models are also based on first physical principles (e.g. conservation of mass, momentum, energy, etc.), but assume idealised conditions such as a constant width of the system considered. The processes - which are based on scales smaller than those of the phenomena of interest - are formally integrated over time and space, according to empirical or parametric closure relationships. Contrary to process-based models, the predicted morphological patterns of long-term models are compared against a hypothetical equilibrium condition. According to Hibma et al. (2004a), an advantage of using idealised models is that the simplifications assumed would enhance the physical insight by the isolation of individual processes, whereas some drawbacks would be related to limited geometries and, for two-dimensional models, the use of initial linear growth of channels-shoal patterns (though efforts by the use of finite-amplitudes approach is shown in Schramkowski et al., 2004). The application of idealised models is given by Schuttelaars and de Swart (1999), Seminara and Tubino (2001), Schramkowski et al. (2002), van Leeuwen and de Swart (2002), Hibma et al. (2004a, b) and Kragtwijk et al. (2004).

Like the one applied in this work, process-based numerical models are usually made of a series of independent modules which deal with the constituent physical processes (e.g. waves, tides, sediment transport) separately. In order to predict morphological changes, they can be linked to each other through the application of a bed evolution equation, which is based on sediment conservation. In this study, the selection of a 2D implicit process-based modelling is justified by two main factors: i) the possibility of including/removing different processes from the model frame (e.g. understanding the effects of including mixed grain sizes in the overall bed evolution) and ii) the use of actual properties of the

system (e.g. the observed water level variation and the observed bathymetry) as opposed to idealised conditions, which is assumed in formally integrated models. It is also important to bear in mind that for all methodologies discussed in this section, there will always be limitations and shortcomings in the techniques proposed.

De Vriend et al. (1993) proposed the following classification for process-based models (Figure 2.6):

- *"Initial sediment/erosion" (ISE) models*

The modelled information is exchanged between the different modules only once. Thus, the model result is given in terms of the rate of sedimentation and erosion, based on an invariant bed topography. These models demand less computational power, are relatively 'simple' and 'easy' to implement. Since no feedback morphodynamic mechanisms are considered, they are suitable for assessing only those processes which have a much smaller scale than the morphological one. In other words, this approach is unable to embed the dynamic behaviour of the system under study, describing the initial morphological adjustment after a strong impact to the system (e.g. effects of a man-made structure on an estuary entrance). In order to assess residual patterns on sediment transport estimates, ISE models can also be applied to test the influence of separate sets of conditions (low to high river discharge, calm to storm wave periods, neap to spring tides, etc.). Examples of applications of such approach can be found in Walker et al. (1991); Steijn et al. (1992); Villaret and Latteux (1992); Siegle et al. (2004);

- *"Medium-term morphodynamic" (MTM) models*

These models do take in account the time-varying bed evolution, which is fed back into the hydrodynamic and sediment transport modules. Thus, the combination of such modules yields a new dynamic system, with added complexity relative to the application of each module separately. These models are unlikely to be able to predict morphodynamic changes on time scales larger than those of the target morphological processes. On the other hand, the processes with shortest time scales to be considered in the model will determine the maximum morphological time step, resulting in large simulation times for the reproduction of the largest time scale processes. De Vriend et al. (1993) suggested that

although bed slope effects may have a small contribution to the sediment transport, they are very important for the model stability. As seen in Section 4.4.2, slope effects are taken into account within the MTM model used in this thesis. However, MTM models are prone to numerical instabilities, which can be generated from boundary conditions. Boundary-related disturbances associated with errors or inconsistencies tend to migrate into the model domain through bed evolution features, sometimes leading to the instability in the model (de Vriend and Ribberink, 1996). Further reference to these models is given in Shimizu et al. (1990), Andersen et al. (1988, 1991), Watanabe et al. (1991), Negen (1994) and Idier and Astruc (2003);

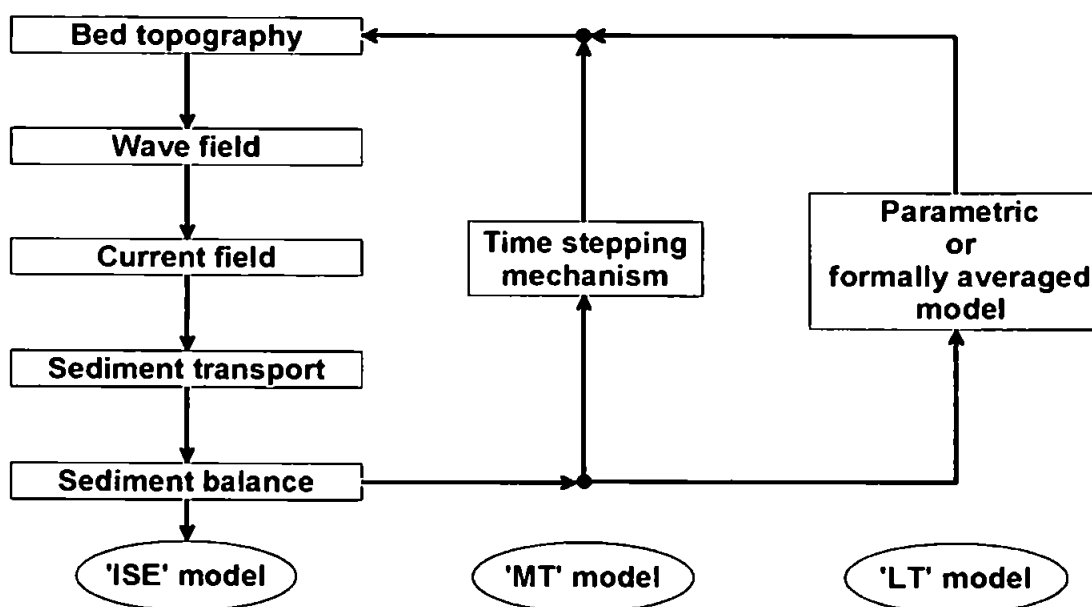


Figure 2.6: Morphological model concepts (after de Vriend et al., 1993).

- *"Long-term morphological" (LTM) models*

The constituent equations represent integrated processes at a macro scale rather than as an individual process, normally associated with the concept of dynamic equilibrium (de Vriend, 1993). This "higher level of aggregation", as proposed by de Vriend et al. (1993), can be achieved by the formal integration of the physical processes with time and spatial scales smaller than those of interest. Since this approach involves non-linear processes, closure terms (e.g. Reynolds-stress terms in turbulent flow models or the radiation-stress terms in wave-driven current models) must be considered, according to de Vriend and Ribberink (1996). These authors highlight the importance of LTM as very useful for the

understanding of the morphodynamic behaviour (e.g. channel pattern formation and stability of channel/shoal features) of a coastal system and to what extent such models can deal with non-linear processes. Applications of this concept can be found in Schutelaars and de Swart (1999), Seminara and Tubino (2001), Schramkowski et al. (2002) and Hibma et al. (2004a, b).

If the coastal process of interest occurs in long time scales (order of more than years), then the reduction of information is a crucial issue on the modelling exercise. According to de Vriend et al. (1993), there are several approaches to address this matter: i) input reduction, where representative conditions of the original data are searched for in order to ensemble the same initial information in a more compact format; ii) model reduction: smaller-scale processes are disregarded and the model itself is reformulated based on analysis and integration methods; the resulting models tend to reproduce site-specific conditions, as a result of selecting only the main processes in the formulation of the model and iii) behaviour-oriented modelling, where the phenomena of interest are assessed without detailing the underlying processes.

The application of the input reduction approach is commonly applied to tides and waves. Despite the deterministic nature of tides, they are modulated in many different time scales (e.g. from spring-neap periods to nodal cycles), posing a problem for realistic simulations in longer-term time scales due to the associated demanding computational power. Hence, representative conditions - which can reproduce accurately not only the average tidally-driven currents, but the net sediment transport - are required. Latteux (1987, 1990a, 1990b and 1993) used the concept of 'representative tides' for the study of tidal action on the modelling of coastal processes. It was found that a single representative tide would exist for relatively simple coastal geometries, and the magnitude of this tide would be about 7 to 20% larger than that of the mean tide, depending on the choice of sediment transport formula and on the threshold of sediment motion. As an example, Latteux (1995) reported an underestimation of the annual sediment transport of about 50% if a mean tide is considered as the representative tide along with the application of the sediment transport formula of Einstein-Brown. For areas of irregular bottom properties, more than one representative tide would be necessary in order to encapsulate the tidal action effects on the local morphological bed evolution. In the absence of feedback mechanisms between the hydrodynamics, sediment transport and bed evolution (similar to the concept of ISE

models), Latteux (1995) found that the representative tide which best described the transport rates was not necessarily the most accurate in forcing the correct morphological bed patterns. As shown in Section 4.4, this problem is likely to be reduced in this work due to the inclusion of feedback mechanisms between the fluid and the morphological evolution (MTM concept) in the modelling exercise.

Due to the random properties of waves in coastal systems, their longer-term simulation is more complex than under the sole effect of tides. De Vriend et al. (1993) categorised two different methodologies: the multiple and the single representative wave approach (MRW and SRW), respectively. The first one was developed by Steijn (1989, 1992), based on the reduction of wave (or wind) field data into a limited number of combinations between wave heights and their directions. Each of the representative conditions would be used to force the numerical model separately and the final bed evolution outcome would be the sum of all the realisations scaled by the respective weighting factor (which depends on the bulk longshore drift and the sediment stirring). This approach seems to be suitable to rather simple situations, where few sediment transport mechanisms predominate (de Vriend et al., 1993).

In the SRW approach, proposed by Chesher and Miles (1992) the currents generated by the various representative waves are simulated and combined into a single set of representative wave parameters, which will be then used to predict the hydrodynamics and the sediment transport field. According to de Vriend et al. (1993), this method tends to be more time efficient, since only one run of the hydrodynamic and sediment transport modules is required; on the other hand, the choice of the appropriate weighting factor is not always straightforward. They added that comparisons between both methods for an open coastal area have shown that both methods have their own limitations, being recommended that separate schematisations are applied for mean conditions and storm events.

In order to represent field conditions more realistically, it is desirable that both tidal and wave effects are taken into account simultaneously, which was pioneered by Steijn (1989, 1992). A number of interactions is expected (e.g. the effect of water level on the stirring effect generated by waves), along with the spatial variability of both wave and tidal effects, potentially leading to complex residual effects (de Vriend et al., 1993). Steijn and Hartsuiker (1992) and van Overeem et al. (1992) compared the performance of the SRW

and MRW approaches for the Wadden Sea area. They found that the presence of storms and calmer periods was fundamental in determining the sediment circulation patterns at study site.

Alternatively to the application of input reduction techniques, Latteux (1995) also successfully tested several approaches to increase the morphological time step, what de Vriend et al. (1993) termed as "model reduction" technique. Some examples of empirical methods (i.e. not derived from mathematical sets of equations 'per se') are straightforward extrapolation; time-centered extrapolation; lengthening of the tide and expansion of sediment transport as a function of bed evolution. Formally derived methods were used by Huthnance (1982), Krol (1990) and Fokkink (1992).

According to de Vriend et al. (1993), behaviour-oriented models are much simpler than the process-based ones, since the former mainly take into account the processes observed by field data (or even by simulations from a process-based model). According to EMPHASYS (2000), behaviour-oriented models can be based on data analysis (e.g. accommodation space, regression techniques, sediment budget analysis, etc.) or on equilibrium assumptions (regime relationship, intertidal form analysis, estuary rollover, etc.). For further information on these models, the reader is referred to Di Silvio (1989, 1991), O'Connor et al. (1990), de Vriend et al. (1994), Stive et al. (1998) and EMPHASYS (2000).

More recently, the combination of process-based and behaviour-oriented models has given rise to a new concept: the hybrid approach. It is based on making use of the relatively well represented short-term phenomena by the process-based models to feed a longer-term, behaviour-oriented model. To date, these types of model tend to focus on representing estuaries in one-dimension (EMPHASYS, 2000). The work of Walstra et al. (1997) illustrates the usefulness of such approach, which is expected to have a definite contribution towards the longer-term modelling of coastal areas.

In summary, this chapter illustrated the diversity of estuarine and coastal systems: from their multiple definitions and complex interactions to a wide range of approaches to study their evolution processes. Based on the principal goals of this thesis, the main morphodynamic mechanisms of the Teign estuary and adjacent coast are assessed through the application of the two-dimensional version of the TELEMAC system (release 5.3).

This system is classified as a process-based, coastal area model, which is arranged to allow medium-term morphodynamic (MTM) simulations. The description of the Teign estuary and available field data are given in Chapter 3, followed by an overview of the model, its limitations and its performance against observations in Chapter 4.

Chapter 3 - Study Area and Available Data

3.1. Study area

The Teign estuary is located in south Devon, in the southwest of the United Kingdom (Figure 3.1). It is around 6 to 7 km long and up to 800 m wide, with tidal flats especially in its upper reaches. Its entrance, which links the system to Lyme Bay (English Channel), is constrained to the north by a sandy spit and to the south by a rocky headland (The Ness). Flood and ebb-deltas are also found landward and seaward of the inlet, respectively. A complex system of mobile ebb-delta bars border the entrance channel to the estuary and have historically altered its alignment (Wells, 2002a). As shown in Figure 3.1, the area is characterised by irregular bottom features, especially close to the estuary mouth. Shaldon bridge marks a rapid transition in the depth of the main channel (from about -5.5 m to -6.5 m ODN^{3.1} down-estuary to about -3 m ODN up-estuary), after which the bottom attains a gentler slope over the next 4 km to about -1 m ODN (Wells, 2002a). An extensive bank made mainly of gravel and sand (The Salty) is found at the outer area of the estuary, close to its mouth. Apart from the recreational and associated fishing activities, a harbour is also located in the estuary. For the purposes of maintaining the navigability of vessels of up to 110 m long and 5 m of draught and to minimise the effects of the cyclic movement of the sandbanks, the approach channel is regularly dredged, as illustrated in Figure 3.1.

3.1.1. Geomorphology and sediment distribution

The coastline around the estuary has been largely conditioned by Holocene sea-level rise (Carter and Bray, 2003). The estuary is a drowned river valley (ria-like), with its hard geology consisting of Permian red sandstone bedrock (Wells, 2002a). In the most extensive study about the Teign estuary, Nunny (1980) subdivides the estuary into three distinct portions, based on the distribution of sediment types and on transport mechanisms: upper (Hackney Marshes to Flow Point/Arch Brook), middle (from there to Broadmeadow/Ringmore) and lower (from there to the mouth). In a similar classification,

Wells (2002a) proposes a change in nomenclature, which is shown in Figure 3.2 and is applied hereafter.

Relative to the surface, the depth of the bedrock varies from 4 m in the inner (or upper) estuary to 10 m in the region of the outer (or lower) estuary (Environmental Resources Ltd., 1990), where an exposed area of bedrock is found close to the estuary mouth. Regarding the 'holocenic' sediments, Nunny (1980) estimates the thickness of these sediments to be up to 30 m above the New Red Sandstone bedrock in the inner estuary. He also highlights a sediment infilling at the inner parts of the estuary during the last 3000 years, without concluding whether this trend is still happening to date. Through the assessment of several geomorphological parameters, Dyer (2002) considers the Teign estuary to have achieved a satisfactory sedimentary balance, due to its low ratio between the cross-sectional area and the tidal prism.



Figure 3.1: Location map of the Teign estuary and its main physiographic features: The Salty (A); Estuarine flood tidal channel (B); Main channel (C); The Ness (D); Ness sandbar (E); Submerged sandbar (F); Ebb shoals (G); Coastal flood tidal channel (H); Spratt sand (I); Sandy spit (J); Teignmouth beach (K); Shaldon bridge (L). As depicted in the picture (arrow), dredging activities take place at the outer ebb-delta to date (Photo courtesy of South West Water). For further information on classification of coasts and associated features, refer to Dyer and Huntley (1999) and Finkl (2004).

^{3.1} Ordnance Datum Newlyn (ODN).

The grain size distribution is highly variable at the Teign estuary and its adjacent coast (Figure 3.3). The upper reaches of the estuary are characterised by finer sediments- especially its intertidal flats - while sand and coarser particles dominate in the channels, closer to the mouth of the estuary and to the adjacent coast. By assessing the suspended sediment concentration under conditions of i) high river discharge (riverine suspended sediment concentrations of 100 to 200 mg.l⁻¹) and ii) presence of waves (30 to 60 cm high and around 3 seconds period), Nunny (1980) reports suspended sediment concentrations varying between 70 and 1000 mg.l⁻¹ throughout complete tidal cycles.

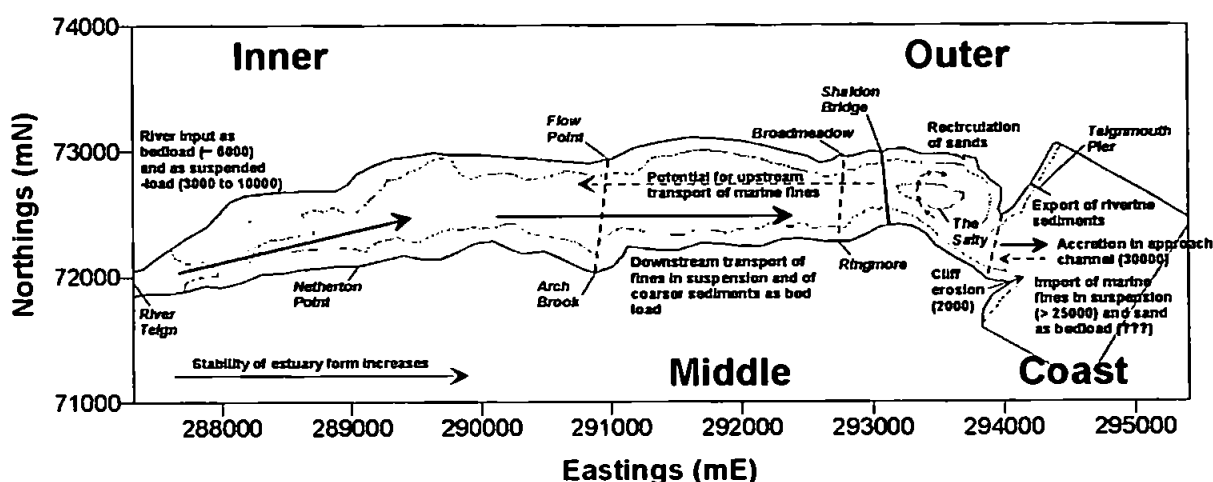


Figure 3.2: Estuary subdivision proposed by Wells (2002a), with likely sediment pathways and their sources and sinks (tonnes.year⁻¹). The 0 m (ODN) isobath is depicted in grey. Prominent locations are shown in *italic*. The inclusion of the 'Coast' section is proposed in this thesis.

Relative to the coastal sediment budget, the Teign estuary is likely to serve as "a strong source of fine sediment, and a weak sink for coarse sediment" (Dyer, 2002). Based on sediment analysis, Nunny (1980) described the likely pathways and the respective magnitudes of the sediment transport within the estuary. Several patterns are corroborated by the results obtained by Wells (2002a) through the application of the Delft3D numerical model (Figure 3.2).

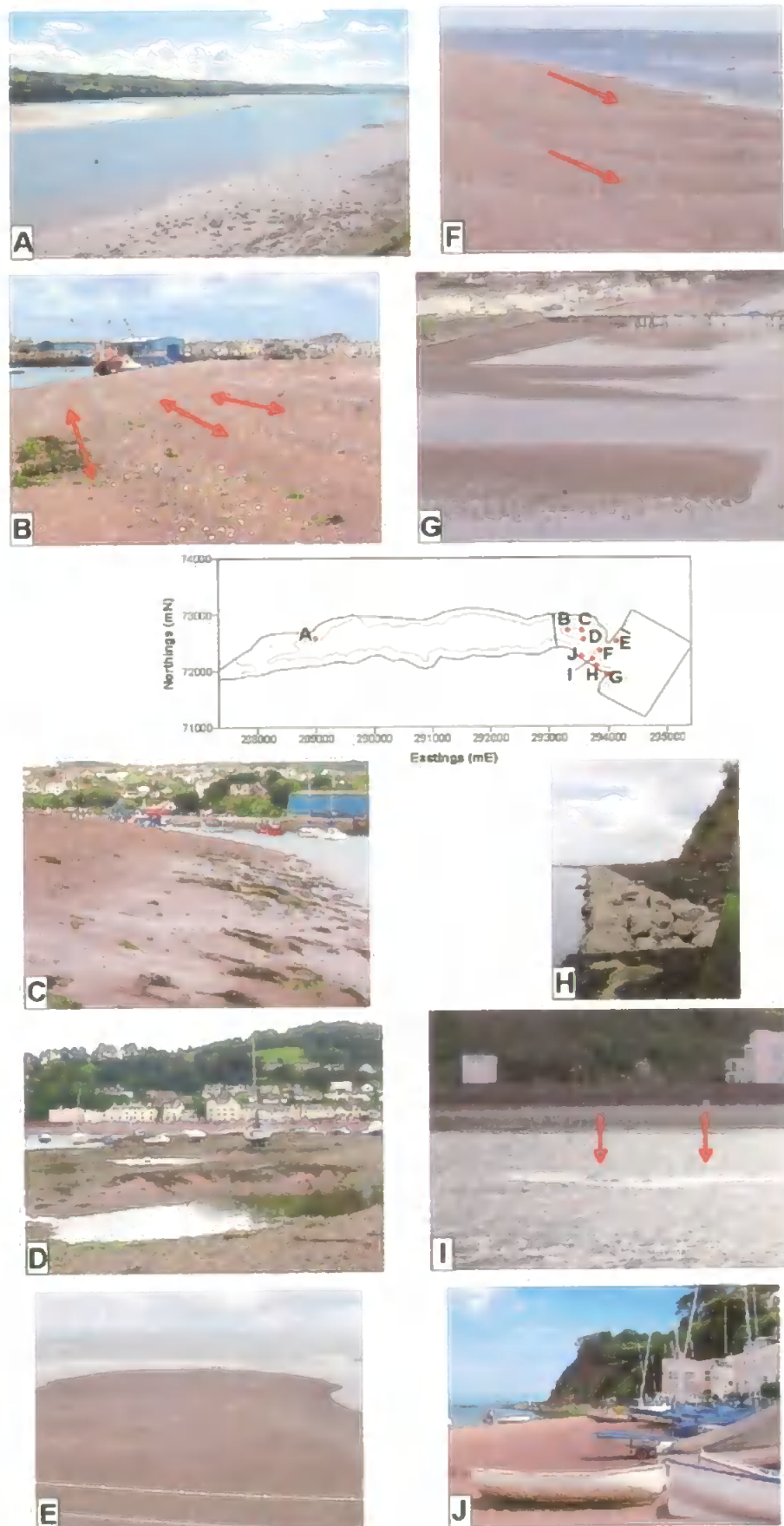


Figure 3.3: Photographic records of the Teign estuary and adjacent coast: upper estuary finer sediments and associated tidal flats (A); coarser sediments distributed in "bands"

Continued from Figure 3.3: along the northwestern edge of the Salty (B); relatively finer and better sorted grain size towards the northern border of the Salty (C); irregular bottom patterns at the eastern edge of the Salty (D); sandbar attachment to Teignmouth beach (E); influence of the flood dominated channel at the offshore side of the sandy spit (F); Teignmouth beach and the pier (G); wall protection along the southern reaches of the estuary mouth (H); evidence of lateral shear stress (front) along the channel at the estuary mouth (I); Shaldon beach, on the southern side of the Teign estuary (J). Pictures E to I were taken in May 2004, where the remaining were taken on June 2004 during CoastView survey 5 (Table 3.5).

Under average tidal and river discharge conditions, Wells (2002b) argues that a slow build-up of muds and fine sediments (predominantly marine) would take place in the intertidal areas of the estuary. Meanwhile the main channel would be subject to an intermittent downstream bedload transport (Nunny, 1980). In this context, fine sands would be mainly from a marine source, since no direct relationship between high-river discharge events and an influx of fine sand could be found. The outer estuary would, therefore, act as a "reservoir" for this sediment fraction, with the most likely up-estuary dispersion being associated with suspension effects during flooding periods of spring tides.

According to Nunny (1980), extensive deposits of medium sand of riverine source are found at the inner portions of the system. The net transport of this sediment fraction is always down-estuary, due to the ebb-dominance, especially at the outer areas, where a clockwise movement of sediments around the Salty area takes place (Figure 3.2). Based on model results, Wells (2002b) highlights that while the presence of sands on the estuary entrance would not be a stable feature, the approach channel would be subject to processes of deposition. The comparison between two scenarios with and without wave effects (wave-driven currents included) indicates that although sand is mobile at the coastal area, the sediment transport towards the estuary entrance was not enhanced under the presence of waves (Wells, 2002b). It is also concluded from these tests that coastal sediment availability and the presence of waves may be responsible for deposition patterns at the approach channel, but it is unlikely that these processes would be significant in providing sediment for the estuary. Further analysis on these aspects is given on Chapter 6.

By studying the mineralogy of medium sands in this area, Nunny (1980) found they are mainly derived from the New Red Sandstones, which would come from the eroding coastal cliffs (such as The Ness) at the southern limit of the estuary entrance. This author also

described the presence of medium sands lying on the resistant substrate of the Salty and channels of the outer estuary, favouring a constant exchange between this area and the adjacent coastline mainly through bedload transport processes. By comparing the bathymetric records at that time with Spratt (1856) data, Nunny (1980) claims the form of the outer estuary to be very stable over the period, where the main changes are found at the spit at the mouth of the estuary and at the quay areas along Teignmouth waterfront.

Suspended sediment concentrations would vary according to the main hydrodynamic forcings and also to the sediment availability. Field data collected by Nunny (1980) for the estuary show conditions of waves ranging from 30 to 60 cm in height (period of 3 seconds) and under high river discharge (with a suspended solids content of 100 to 200 mg.l⁻¹ to the estuary) for complete tidal cycles. The estuary is constrained by a steeply rising topography at its mouth, while sea defences and a railway embankment limit some areas along the estuary (Wells, 2002a). According to this author, the influence of Shaldon bridge as a system constraint is still unclear, given that it is located immediately downstream of a rapid shallowing of the estuary bathymetry. Wells (2002b) claims that under "normal" conditions, the annual deposition rates were of about 1 cm.year⁻¹, being increased to 5 cm.year⁻¹ by the inclusion of waves and river discharge effects.

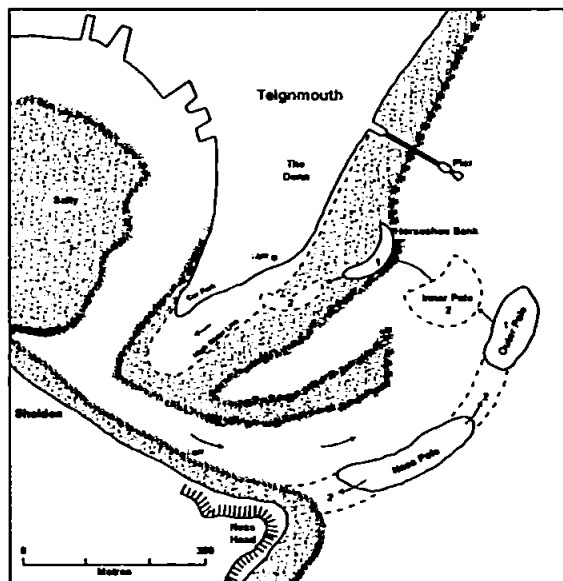


Figure 3.4: Diagrammatic representation of the cyclic changes in bank positions (Siegle, 2003 after Robinson, 1975).

The first formal study of the area, however, was focussed outside the estuary, on the ebb-tidal delta. Spratt (1856) documented the cyclic movement of the sandbars. Based on sporadic observations and some surveys of the area, he concluded the bars migration was not "wholly fortuitous". Robinson (1975) also described a cyclic evolution of the sandbar system at the area, based on the analysis of hydrodynamic data, tracer experiments and morphological maps over a period of 10 years (1964 to 1974). According to him, an anticlockwise three-stage cycle takes place in the area, with a periodicity of 3 to 7 years, which depends on the frequency of severe storms in the area (Figure 3.4). Therefore, the coupled effect of tidal currents and waves would be fundamental for the nearshore morphodynamic evolution.

More recently, van Lancker et al. (2004) discuss the highly dynamic changes in bedforms and sediment mobility, based on side-scan sonar imagery and sediment trend analysis technique. They argue that fair-weather and storm-dominated processes are needed to explain the textural and morphological differentiation at this site and also that the influence of waves and associated longshore currents cannot be neglected when assessing the morphodynamic processes of the area. Siegle et al. (2004) added that sediment accumulation to the system occurs only during higher wave energy periods, while a small but constant net loss of sediment takes place under calm conditions.

Hoekstra et al. (2004) discuss the time-dependent character of bedform dimensions and associate an increase of bedload transport by a factor of 2 under the presence of waves, which would also reduce the hiding effect between sediment grains of different sizes. Suspension processes also rely on wave presence, since the observed suspended sediment distribution is small under the sole presence of even considerable tidal currents (order of 1 m.s^{-1} ; Hoekstra et al., 2004). They argue the likely cause of this phenomenon is the hiding effect (where smaller grains tend to be deposited between bigger grains), which tends to be important in such a poorly sorted sediment distribution area. They also highlight the difficulties of describing and modelling the role of the bedload transport processes and the effect of mixed grain sizes. A relationship is established between the presence of storms and a greater thickness of the sediment layer close to the estuary mouth (Spratt sand; Hoekstra et al., 2004), which could be due to an onshore sediment transport at this area under the presence of storms.

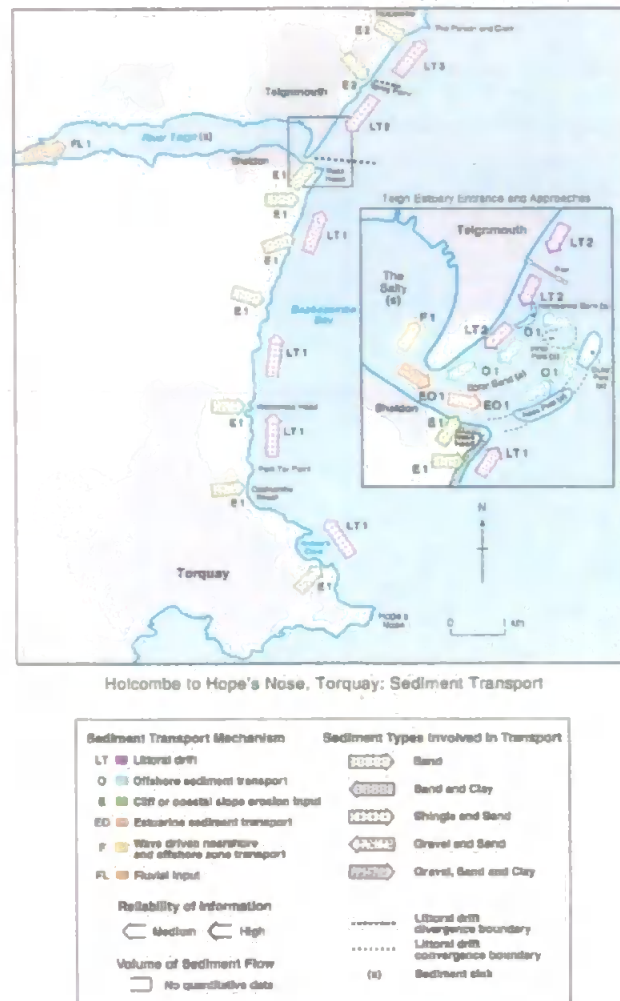


Figure 3.5: Schematic sediment transport pathways, sources and sinks on a regional scale for Holcombe to Torquay (Carter and Bray, 2003).

At a regional level, the assessment of the main sediment transport pathways in Babbacombe Bay is qualitatively described by Carter and Bray (2003), based on geomorphological observations and comparison to previous studies (Figure 3.5). They suggest, like the proposals of Nunny (1980) and Wells (2002a) for the Teign estuary, the main source of sediment input for the adjacent coastal area is riverine-borne (mainly fine sediment) and from the cliffs' erosion. Moreover, since Hope's Nose peninsula to the south, and the Holcombe promontory to the north appear to be absolute boundaries to bedload transport, this coastline is characterised by a quasi-independent transport and budgetary system, where the mouth of the Teign estuary would be at a zone of convergence in terms

of littoral drift (Carter and Bray, 2003). The coastal area around the Teign estuary is classified by Eurosion (2004)^{3.2} as of accretional characteristics.

3.1.2. Hydrodynamic processes

The Teign estuary is subject to a mesotidal to macrotidal regime, semi-diurnal tides with a range varying from around 1.7 m at neaps to 4.2 m at springs. The tidal range reduces in an upstream direction by about 0.5 m to 1.5 m on neap and spring tides, respectively, due to a change in the low water level (Wells, 2002a). During the rising and falling tide the water level gradient between the upper estuary and the coastal area commonly differ in height by up to 0.5 m, with the steepest variations occurring in the vicinity of the harbour (Nunny, 1980). During a period of the COAST3D main experiment, Siegle (2003) observed the water level in the estuary channel being as much as 0.9 m higher than in the adjacent coastal area, while a difference in excess of 0.4 m was predicted by the application of numerical modelling for the same period.

Typical currents off the estuary mouth are around 0.2 to 0.5 m.s⁻¹ but could reach values in excess of 1.5 m.s⁻¹ close to the estuary entrance. Residual current data suggest a complex flow structure, with an overall ebb-domination at the estuary mouth and marginal flood-dominated areas, such as the features *B* and *H* in Figure 3.1. The highest maximum bed shear stresses clearly occur within the main channel areas where the main flow of water takes place, attaining values of 1 N.m⁻² to 5 N.m⁻², on neap and spring tides respectively (Wells, 2002a). Also according to this author, the energy distribution is approximately linear up to 2 km from the estuary mouth and may be dominated by the spit across the mouth, which imposes a geomorphological constraint. The remaining portions of the estuary tends towards an exponential distribution, with a more idealised estuary form (Wells, 2002a).

For approximately 90% of the year wind speeds are less than 10 m.s⁻¹ whilst for about 5% of the year gale force (> 17 m.s⁻¹) winds occur (Wells, 2002a). The site is relatively protected from the swell of the Atlantic Ocean, being subject to significant heights greater

^{3.2} For further details, visit: <http://www.eurosion.org/>.

than 0.5 m for less than 10% of the year (Miles et al., 1997). Between 1998 and 1999, Sutherland et al. (2001a) found significant wave heights (in the high frequency domain, 0.05 - 0.33 Hz) of 0.83 m at the coast and 0.25 m at the estuary entrance, for a 10% probability of exceedance; the significant wave periods associated were in the range of 6 to 7 s. The predominant wave direction is from the easterly and southeasterly quadrant.

The estuary is sheltered from offshore waves due to its narrow entrance and to the complicated system of bars around the mouth (Nunny, 1980). By the use of numerical modelling, this hypothesis is tested by Wells (2002a), who found little energy propagating through the estuary mouth even when the area was submitted to offshore waves as high as 2 m. However, Wells (2002b) modelled the effect of storm conditions (westerly gale at high tide) and concluded that small waves of about 1 m high and periods of 3 seconds could be generated inside the estuary in "restricted areas", being sufficiently large to alter the sediment transport at the intertidal areas. Thus, fine sediments at the intertidal banks could be re-suspended, eventually being deposited in sheltered areas and even at the estuary entrance reaches. Based on simultaneous wind speed and wave height data, Nunny (1980) estimated that wind speeds within the range 2 to 5 m.s⁻¹ are required to produce small wavelets (2 cm high and period of 0.5 s) inside the estuary, while waves of up to 60 cm (3 s period) are formed in this area if the wind speed attains values of 10 to 20 m.s⁻¹.

The total catchment area of the river Teign basin is around 380 km² with additional inputs from rivers Lemon and Bovey. Typical river discharge rates are around 10 m³.s⁻¹ during summer periods (about 4-9% of the spring and neap tidal prism respectively) and in the range of 10 to 30 m³.s⁻¹ during winter periods (Wells, 2002a), while during freshets the discharge can be over 150 m³.s⁻¹. Under these circumstances, during ebbing phase periods, it is likely that a plume of sediments will be formed at the adjacent coast (Dyer, 2002). River discharges of less than 5 m³.s⁻¹ persist, on average, for 55% of the year, while a 200 m³.s⁻¹ river discharge has a recurrence interval of 6-7 years (Nunny, 1980).

When compared to the tidal prism, which is of the order of $4.8 \times 10^6 \text{ m}^3$ on neaps and around $10 \times 10^6 \text{ m}^3$ on spring tides (Wells, 2002b), the flow ratio (river discharge fraction) can vary from 2.5% on spring tides under low river discharge to values higher than 90% on neap conditions associated with high river discharge. Thus, well-mixed conditions prevail for the majority of the time. Using water level and bathymetry data, Nunny (1980)

calculated that no salt water penetrates further upstream than Netherton Point (Figure 3.2) on spring tides if the river discharge exceeds $50 \text{ m}^3.\text{s}^{-1}$, or on neap tides if the river discharge exceeds $20 \text{ m}^3.\text{s}^{-1}$. Table 3.1 gives an overall view of the interactions between some of the morphodynamic agents in the inner estuary.

Table 3.1: Tides, river states and role on sediment transport in inner estuary (Nunny, 1980, after Wells, 2002a).

<i>Category (% of time)</i>	<i>River</i>		<i>Tidal</i>	<i>Sediment transport</i>
	<i>Discharge ($\text{m}^3.\text{s}^{-1}$)</i>	<i>SSC (mg.l^{-1})</i>		
Normal (75%)	< 5	-	All	Accumulation of marine muds
	5 - 15	-	Mean spring	
	5 - 15	Low (< 30)	Low/mean neap	
Flooding (20%)	5 - 75	High	Neaps	Accumulation of fluvial muds
	25 - 100	(up to 300)	Springs	
Extreme flooding (1:3 year event)	> 100	High (up to 300)	All	Erosion of intertidal areas
Gale force winds (5%)	Any	-	All	Scouring and erosion of intertidal areas

3.2. Available data

The data used in this study have multiple sources, which are detailed in Table 3.2: main experiment of Nunny (1980; bathymetric surveys), COAST3D Project (velocity, sediment samples, bathymetric surveys), Environment Agency (freshwater discharge and LIDAR bathymetric/topographic data), University of Plymouth (water level), ABPMer (sediment samples, bathymetric surveys), and CoastView Project (bathymetric surveys). A brief overview of COAST3D and Coastview projects is given prior to the description of the data available.

The COAST3D (Coastal Study of Three-dimensional Sand Transport Processes and Morphodynamics) project, a consortium of 11 partners from 5 different state members of the European Union, was run from October 1997 to March 2001. The adjacent coastal area off the Teign estuary was one of the selected sites in order to achieve the main objectives

of the project: i) to improve understanding of the physics of coastal sand transport and morphodynamics; ii) to remedy present lack of validation data of sand transport and morphology suitable for testing numerical models of coastal processes and iii) to deliver validated modelling tools, and methodologies for their use, in a form suitable for coastal zone management (Soulsby, 2001). The calibration and validation of the model to be applied in this study (more details in Chapter 4) is based on some of COAST3D data, which are shown in Figure 3.6 and detailed in Table 3.3. For more details regarding COAST3D data set, refer to Whitehouse and Sutherland (2001).

Table 3.2: Field data properties considered in this study. No direct wave data observations are taken into account.

<i>Parameter</i>	<i>Sampling site</i>	<i>Sampling frequency</i>	<i>Coverage period</i>	<i>Source</i>
Water levels	Pier and Quay	10 minutes	Oct and Nov 1999	COAST3D
	Pier	10 minutes	2000 to Nov 2004	University of Plymouth
River discharges	Preston	15 minutes	Continuous	Environment Agency
Currents	Coastal area	Various	Oct and Nov 1999	COAST3D
Meteorological conditions	Pier	15 minutes	18 to 26/11/1999	COAST3D
	Portland Station	Hourly	Continuous	UK Met Office
Sediment samples	Coastal area	N/A	Oct and Nov 1999	COAST3D
	Estuary	N/A	April 2002	ABPMer
	Estuary	N/A	March 1979	Nunny (1980)
	Estuary	N/A	1998	Environment Agency
Bathymetric surveys	Coastal area and channel of outer estuary	Weekly	25/10/1999 to 22/11/1999	COAST3D
	Estuary	N/A	Nov 2001 and April 2002	ABPMer
	Outer estuary and coastal area	6-monthly	Dec 2002 to Nov 2004	CoastView

A series of studies focussed on the calibration and validation of numerical models based on COAST3D data set. Among them, the University of Liverpool 2DH hydrodynamic and morphodynamic model (Pan et al., 2001), DELFT3D-MOR (Walstra et al., 2001), TELEMAC and PISCES (Sutherland et al., 2001b; Walstra et al., 2001 and Sutherland et

al., 2004a), CIIRC with LIMOS wave model (Sierra et al., 2001), DELFT3D-FLOW with the "online" (simultaneous) extension to account for the sediment transport (Wells, 2002b), MIKE-21 (Siegle, 2003 and Siegle et al., 2004) and DELFT3D (Sutherland et al., 2004a).

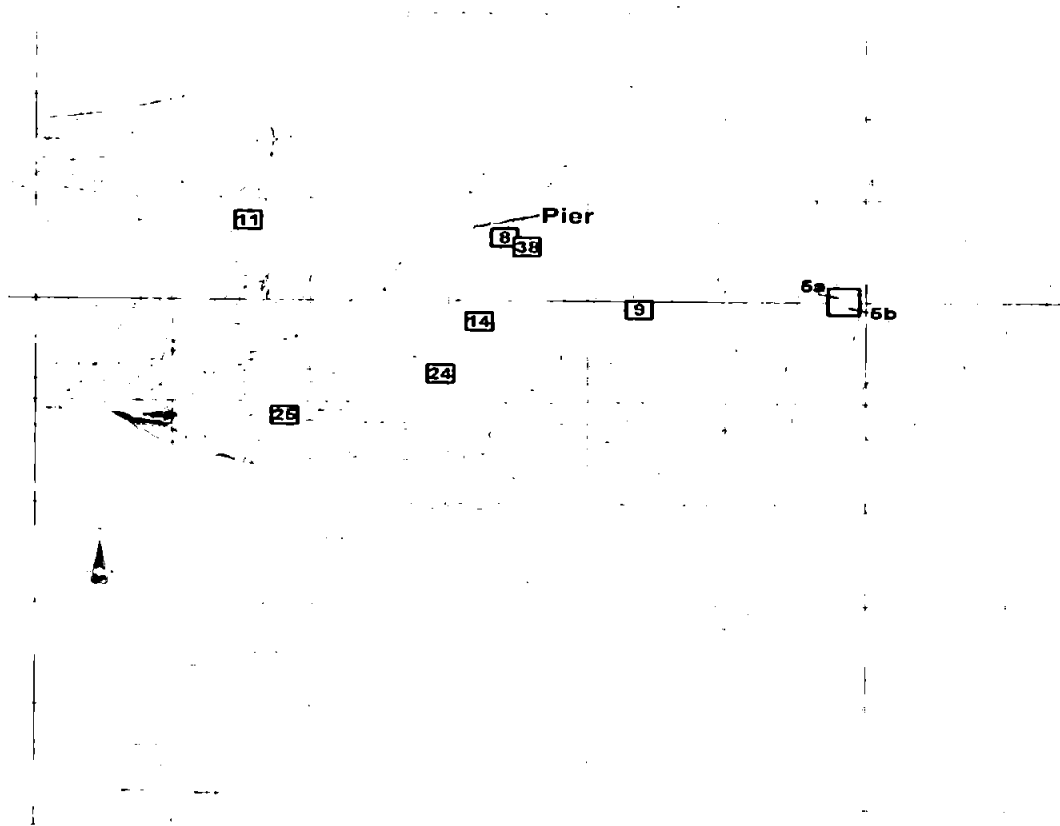


Figure 3.6: Instruments location for COAST3D main experiment relative to Admiralty Chart Datum (ACD; Sutherland et al., 2001b). Sites used for model calibration and validation are shown in squares.

The general aim of the CoastView project is to develop coastal video monitoring systems in support of coastal zone management. Research groups from 5 different European countries compose the project, which started in 2002 and is planned to finish in 2005. Teignmouth is one of the 4 sites selected for the project. Bathymetric surveys of both the adjacent coastal area and of the outer estuary are collected every 6 months in order to support the video-based data. CoastView bathymetric surveys are used in this thesis to enhance the comprehension of the morphological changes in the area and to serve as boundary conditions on the modelling of the morphodynamic processes of the Teign estuary.

Table 3.3: COAST3D main experiment sites used for model calibration and validation. Site 5 was serviced and slightly moved during the main experiment.

<i>Site</i>	<i>Equipment description</i>	<i>Date deployed (GMT)</i>	<i>Date recovered (GMT)</i>	<i>Eastings (mE - OSGB)</i>	<i>Northings (mN - OSGB)</i>	<i>Elevation above bed (m - ACD)</i>
5a	S4	25/10/99 15:30	16/11/99 09:43	294955	72515	0.65
5b	S4	16/11/99 09:46	22/11/99 08:55	294962	72491	0.65
8	Tide gauge	25/10/99 12:00	26/11/99 11:20	294347	72656	N/A
9	Frame	26/10/99 08:06	22/11/99 17:54	294593	72481	1.09
11	Tide gauge	21/10/99 11:00	26/11/99 14:30	293885	72696	N/A
14	S4	25/10/99 15:41	22/11/99 13:23	294304	72447	0.65
24	S4	25/10/99 17:19	22/11/99 13:33	294234	72319	0.65
25	Frame	26/10/99 07:14	22/11/99 17:30	293952	72218	1.12

3.2.1. Water levels

The water level data used in this work derive from two main sources: COAST3D project (sites 8 and 11 of Figure 3.6 and Table 3.3) and pressure transducer installed by the University of Plymouth at the offshore end of the pier on Teignmouth beach, also shown in Figure 3.6. All instruments described in this section had sampling frequencies of 10 minutes.

Regarding the COAST3D data, as site 8 was exposed to swell and waves, it was set to average field data over 180 seconds. Site 11, located inside the estuary, averaged field data every 20 seconds. All averages were corrected and time stamped at the centre time of the sample. Both systems were levelled by land survey closed looped traverse to the same two nearby Ordnance Survey Benchmarks. The typical resolution was in the range of 1 or 2 mm, with accuracy around 5 mm or better (Whitehouse and Sutherland, 2001).

The pressure transducer installed by the University of Plymouth at the seaward end of the pier has been collecting data since 2000 to November 2004, when a major storm caused the collapsing of the pier legs where the instrument was attached. The field data are averaged over a period of 10 minutes, based on water level sampling bins of 1 second.

3.2.2. River discharges

The Environment Agency collects continuous flow meter data at the river Teign at sampling frequencies of 15 minutes. River discharge data used in this study spans the period from October 1999 to November 2004.

3.2.3. Currents

In this study, only the COAST3D current data are used to calibrate and validate the model. The flow velocity measurements were carried out by electromagnetic velocity meters: for sites 9 and 25 (Figure 3.6), the data collection was performed with EMF sensors (manufactured by Delft Hydraulics), while for sites 5, 14 and 24 sensors S4 (from InterOceans Systems Inc.) were employed. Field data were collected every 10 minutes, but most sensors had some periods of longer sampling frequency or operational problems (e.g. Figures 4.6 and 4.8). The respective heights of the instruments in relation to the bed are shown in Table 3.3. According to van Rijn et al. (2000), error measurements within the COAST3D data are estimated to be on average around 0.05 m.s^{-1} , with sampling inaccuracies being inversely proportional to the time-averaged velocities (values under 0.05 m.s^{-1} , in the range of 0.15 to 0.3 m.s^{-1} and bigger than 0.5 m.s^{-1} having inaccuracies of 100%, 30% and 15%, respectively).

3.2.4. Meteorological conditions

The meteorological station installed at the Pier for the COAST3D project (Site 38; Figure 3.6) had operational problems and collected data for a few days only. In order to fill the

measurement gap, the data gathered by the UK Met Office meteorological stations at Portland Isle (around 75 km to the east of Teignmouth and 52 m above sea-level) was used instead. Three-day comparisons between the two data sets show good agreement of barometric pressure, wind direction and air temperature, whilst wind speeds were on average 3 m.s^{-1} higher at the Isle of Portland data set (Siegle, 2003).

3.2.5. Sediment samples

Three data sets are merged in order to define the multiple grain-size distribution at the Teign estuary and adjacent coastal area (Figure 3.7). This distribution is then used as boundary condition for the morphodynamic modelling of the area (Chapters 4 and 6). From the COAST3D pilot experiment (March 1999), 9 grab samples of the adjacent coastal area sea bed are used to determine the grain-size parameters and the respective sediment fractions, according to Wentworth's (1922) classification (Figure 3.7). Other 23 grab samples from COAST3D main experiment (October and November 1999) also from the coastal area, are taken into account.

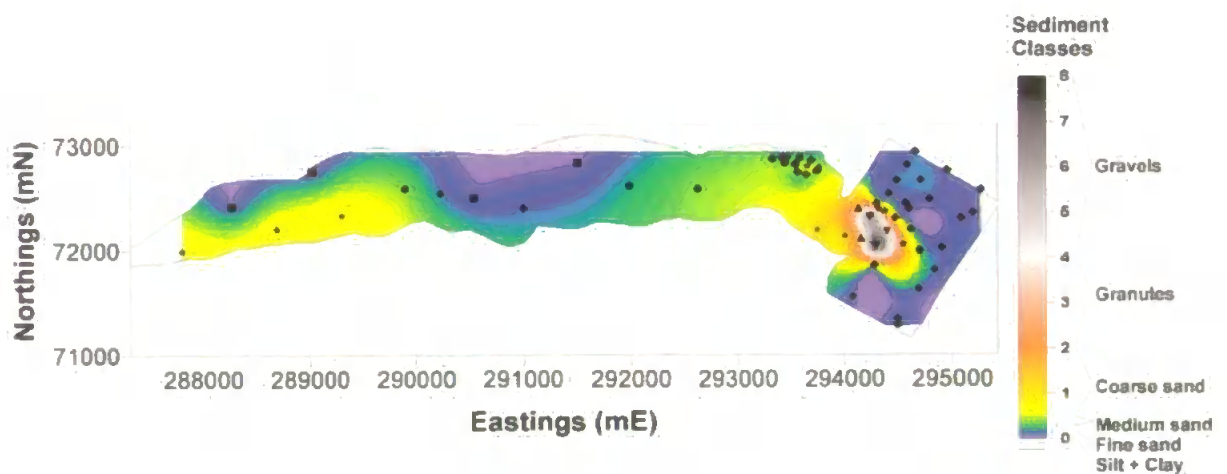


Figure 3.7: Average grain size distribution of the Teign estuary (data from ABPMer) and adjacent coastal area (data from COAST3D project). The grain-size fractions are classified according to Wentworth's (1922) classical diagram: Silts and clays (squares); Very fine and fine sands (diamonds); Medium sands (circles); Coarse and very coarse sands (stars); Granules (triangles) and Gravels (inverted triangles). Missing data are represented by grey diagonal crosses.

In April 2002 ABPMer collected other 28 grab samples from the estuarine area, with emphasis on the harbour surroundings (Wells, pers. comm.). The presence of finer sediments is observed to concentrate mainly on the intertidal areas of the estuary, its middle reaches (Figure 3.2) and the areas offshore of the ebb-delta banks. Assuming this offshore trend of fine sediments is observed, the vicinities outside the sampling area are also considered to be composed predominantly of fine sediments. Medium sands are mainly found in the inner estuary and close to its mouth. Coarser sediments are abundant in the area between the estuary mouth and the ebb-delta. In order to cover the sampling gaps shown in Figure 3.7, the observed grain-size characteristics are extrapolated to the adjacent areas, such as the northern intertidal banks and the head of the estuary.

3.2.6. Bathymetric surveys

As shown in Table 3.2, several data sets are taken into account to represent as accurately as possible the topographic and bathymetric features around the Teign estuary and its vicinities. The bathymetric data collected by Nunny (1980) consisted of 20 cross-section transects using echo-sounding techniques covering most of the estuary. These data were then digitised within the frame of the COAST3D project as isobathymetric contour levels (Figure 3.8). In 1998, the Environment Agency commissioned a LIDAR survey of the area around the Teign estuary. Nearly all the estuary was covered by this survey. Within the COAST3D project, the bathymetry of area '3' in Figure 3.8 has been derived from the aforementioned LIDAR data and by the Admiralty Chart 3155.

Table 3.4: COAST3D main experiment bathymetric surveys on the coastal area adjacent to the Teign estuary.

<i>Survey</i>	<i>Dates</i>	<i>Wave conditions (height and period)</i>
1	27-28 October 1999	0.2 to 0.3 m; 3 to 6 s
2	6-8 November 1999	0.1 to 0.4 m; 3 to 10 s
3	16,17 and 19 November 1999	0.1 to 0.3 m; 3 to 7 s
4	24-25 November 1999	0.3 to 0.75 m; 5 to 7 s

During COAST3D experiments, four bathymetric surveys were carried out mainly in the coastal area adjacent to the estuary (Table 3.4). The surveys were conducted by DGPS

positioning techniques onboard a vessel for the deeper areas, whereas the intertidal reaches were surveyed with the use of a quad bike, upon which the surveying kit was mounted. The data were geo-referenced to the Ordnance Survey National Grid of Great Britain (OSGB), in a Transverse Mercator Projection, spheroid OSGB 36. Water depths were measured in metres relative to Admiralty Chart Datum (ACD), which is 2.65 m below ODN. The data were then reduced to the latter reference level for standardisation purposes. The error measurements in the surveys of intertidal areas (with the quad bike) were around 0.05 m for relatively flat areas and 0.1 m for steep slope bar faces (van Rijn et al., 2000). For the vessel surveys, these authors estimate the error measurements can reach up to 0.25 m in shallow reaches, due to ship-induced motions.

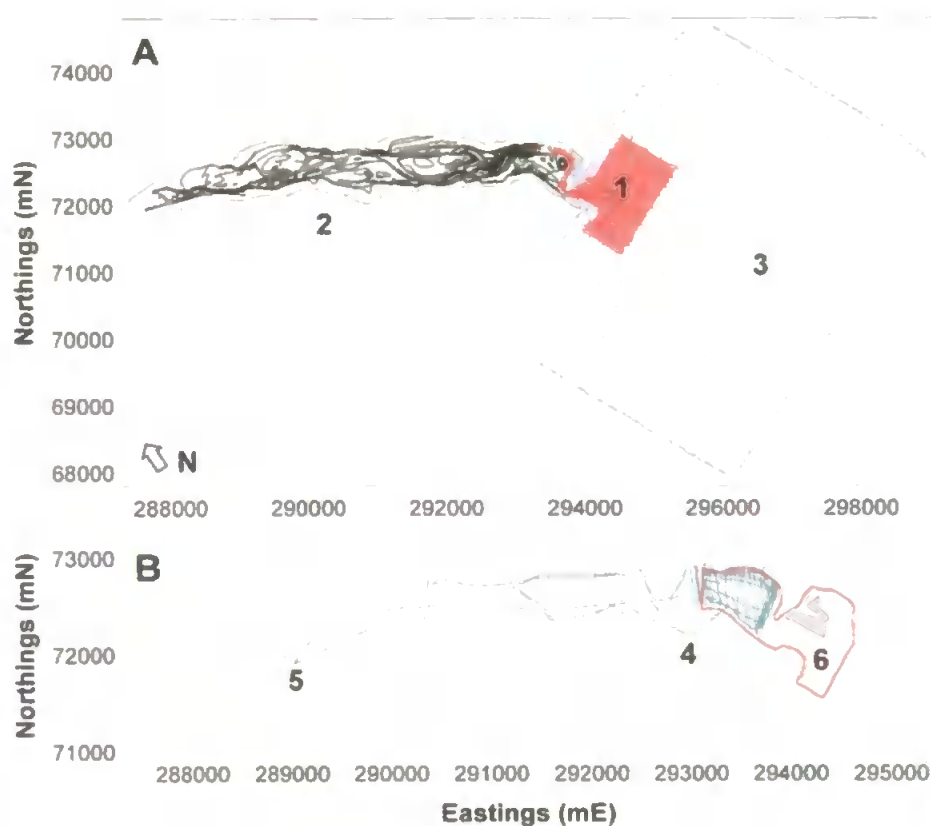


Figure 3.8: Bathymetric surveys of the Teign estuary and adjacent coastal area: example of COAST3D coverage area (1); Nunny (1980) depth-contour levels (2) and COAST3D data interpolated from Admiralty Chart 3155 and LIDAR data (3); ABPMer bathymetric survey carried out in November 2001 (4); ABPMer bathymetric survey of April and May 2002 (5) and the red line delimits an example of the CoastView surveys of the outer estuary and adjacent coastal area (6). Grey area corresponds to survey gap in November 2003 CoastView survey.

ABPMer carried out two bathymetric surveys in the Teign estuary: one in November 2001 and another between April and May 2002 (Wells, 2002b), shown in Figure 3.8.B. When

combined, these data are useful for estimating the morphological evolution of the deeper areas of the estuary (i.e. excluding most of the intertidal banks) in a scale of over 20 years (between 1979 and 2001/2002), against the information gathered by Nunny (1980). By estimating the volume difference between these two data sets - only for the coloured area shown in Figure 3.9 - results suggest a net erosion of the order of $1.3 \times 10^6 \text{ m}^3$ or around $6 \times 10^4 \text{ m}^3 \cdot \text{year}^{-1}$, what indicates that the deeper areas of the estuary have not changed much between 1980 and 2000. Despite the overall erosion trend, areas of sediment deposition are found at both ends of the estuary: on its inner part and especially towards the outer estuary.

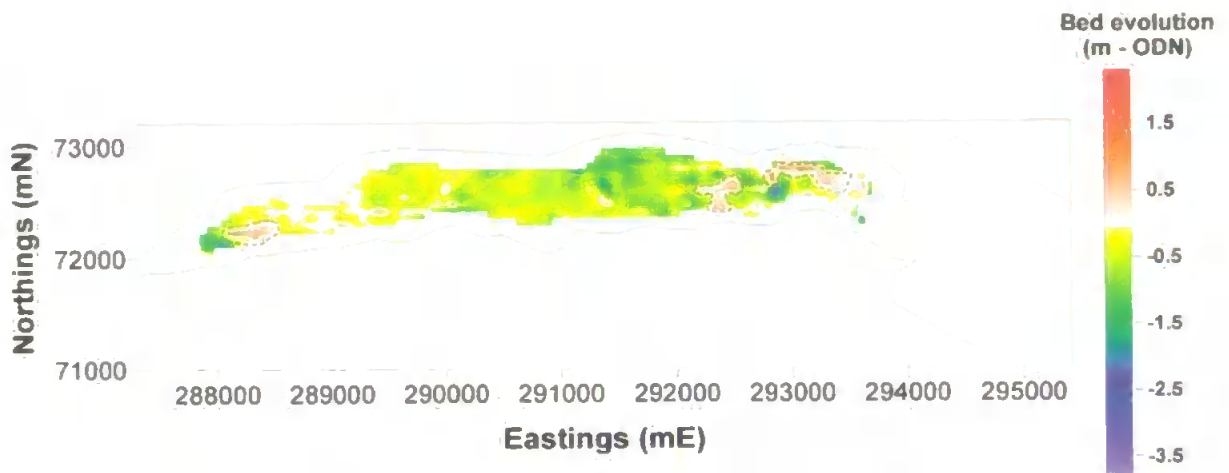


Figure 3.9: Morphological changes at the Teign estuary between 1979 (Nunny, 1980) and 2002 (ABPMer). Erosion features are associated to green and blue areas. Reddish patterns correspond to sediment deposition in the period. Main deposition sites are represented by a dashed line.

Bathymetric surveys have been carried out within the CoastView project (Table 3.5). Apart from the campaign of August 2002 - with a coverage area limited to the adjacent coast and part of the estuarine main channel- all other surveys also included the outer estuary reaches, up to the vicinities of the Shaldon bridge. Kinematic DGPS systems were installed in a small vessel (for deeper areas) and on a quad bike for the surveys on intertidal areas on Teignmouth beach and on the Salty. Error measurements of the surveying technique are estimated to be $\pm 2.5 \text{ cm}$ on the land survey and around $\pm 5 \text{ cm}$ for the vessel-based measurements (Ganderton, pers. comm.^{3.3}). Field conditions from CoastView survey 2 to survey 6 are shown in Figure 3.10.

^{3.3} Peter Ganderton, School of Earth, Ocean and Environmental Sciences (SEOES), University of Plymouth.

From the field conditions, the period between CoastView surveys 3 and 4 (summer-autumn of 2003, from May 2003 to November 2003) was characterised by relatively lower river discharges when compared to the other periods. Regarding the wave distribution, all periods were subject to at least one storm of wave heights in excess of 1 metre and wave periods over 12 seconds. The wave direction, a key parameter in defining the sediment availability at the Teign estuary mouth, was not systematically measured at the area. Virtually all surveys depicted in Figures 3.10.C and D were carried out after storm events at the adjacent coastal area. Despite the absence of wave data for the periods prior to CoastView surveys 5 and 6, the latter one was preceded by a major storm, which caused the collapse of the pier legs where the pressure transducer was installed.

Table 3.5: CoastView bathymetric surveys on the outer estuary and adjacent coast. Average wave conditions are based on the root mean square (rms) of these parameters.

<i>Survey</i>	<i>Dates</i>	<i>Average wave conditions (height and period)</i>
1	29-30 August 2002	0.07 m; 6.7 s
2	02-03 December 2002	0.12 m; 9.3 s
3	18-19 May 2003	0.12 m; 6.5 s
4	25-26 November 2003*	0.16 m; 6.7 s
5	03-04 June 2004	0.08 m; 6.6 s
6	13-14 November 2004	Not available due to collapse of sensor supporting structure

* During this campaign, there is a survey gap of about 5% of the surveyed area (Figure 3.8) due to depth limitations.

In order to estimate the bed evolution between the 5 surveys (from December 2002 to November 2004) which covered the outer estuary and the adjacent coast surveys, only the common area between them is taken into account. SURFER[®] software (Golden Software, 1995) is used for the handling of bathymetric data and for estimating volume changes. Before assessing the morphological changes in further detail, it is important to highlight the survey gap in November 2003 CoastView campaign (Figure 3.8), which was filled by interpolating the neighbouring data.

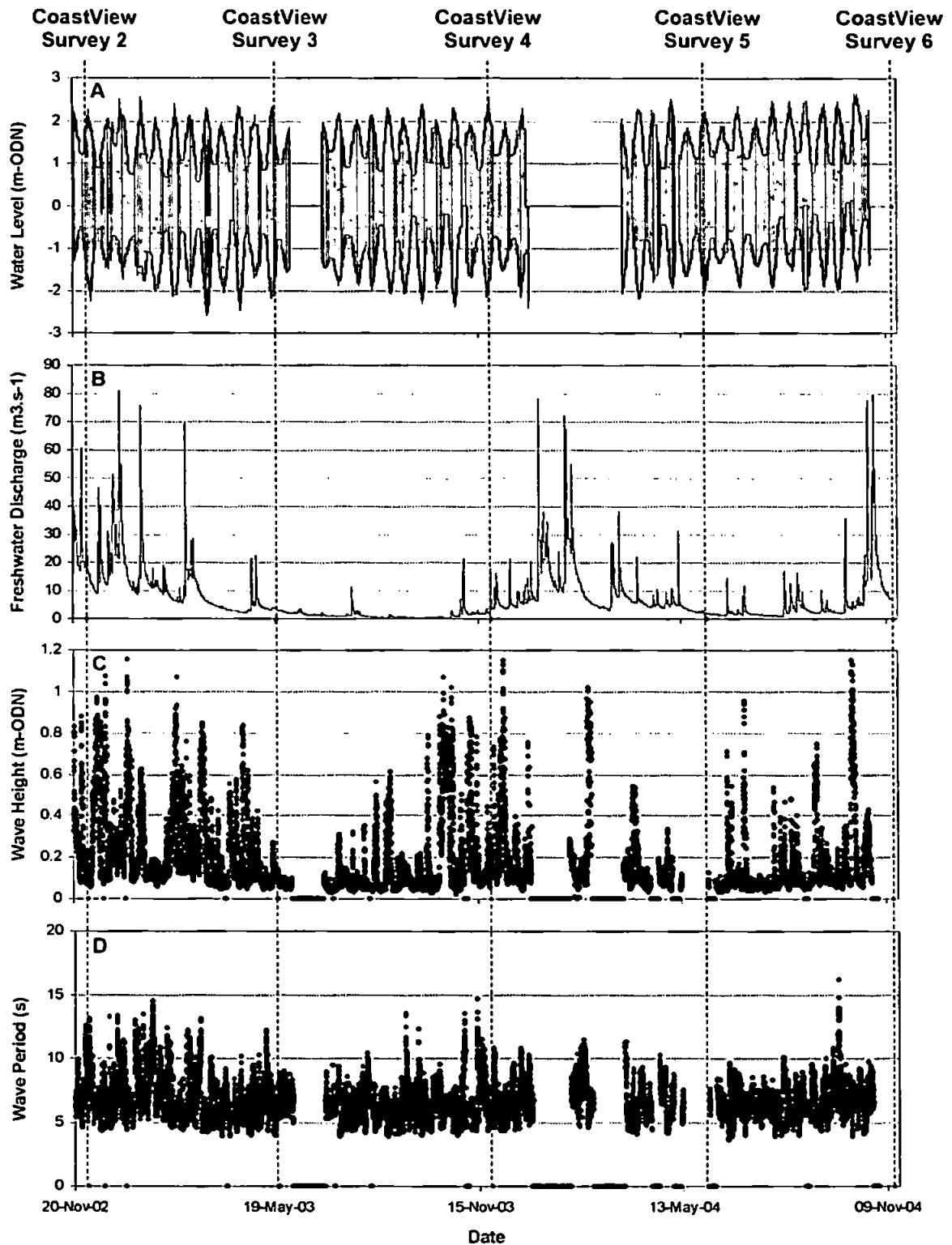


Figure 3.10: Field conditions during CoastView surveys 2 to 6. Water level (m-ODN) is shown on plot A; river discharge ($\text{m}^3 \cdot \text{s}^{-1}$) on plot B; rms of wave height (m-ODN) on plot C and wave period rms (s) on plot D. Periods of 'no measurements' are shown as null values.

The missing area, which corresponds to around 5% (47,783 m²) of the whole surveyed area, is likely to have a minor influence on the volume estimations for the summer-autumn of 2003 and that of winter-spring of 2003/2004 (November 2003 to June 2004).

As shown in Figure 3.11, a seasonal trend is observed on the resulting morphological changes. Analyses carried out within the framework of this thesis indicated that the winter-spring periods 2002/2003 and 2003/2004 were characterised by a net sediment deposition, with a relatively homogeneous widespread thin layer (order of tens of centimetres) almost over the entire surveyed area (Figures 3.11.A and C)^{3,4}. On the other hand, overall sediment erosion was observed during 2003 and 2004 summer-autumn periods (Figure 3.11.B and D).

When assessed through the underlying hydrodynamic processes at the area, morphological changes on summer-autumn periods are mainly driven by tidally generated currents, which tend to predominate in the relatively smaller frequency of storms and lower river discharge. Hence, the ebb-domination pattern at the mouth of the estuary described by several authors (e.g. Nunny, 1980; Wells, 2002b) is likely to be responsible for flushing sediments out of the estuary towards the adjacent coastal area. During winter-spring months, although a higher river discharge will tend to enhance the export of sediment out of the estuary, the residual balance might be defined by the sediment transport generated by wave-driven currents, increasing the sediment availability close to the shore.

Hoekstra et al. (2004) observed landward bedform migration and sediment accumulation close to the Teign estuary mouth under the presence of storms. These authors attributed the presence of suspended sediment to the wave-generated flows. Despite the unlikely presence of swell waves inside the estuary (Section 3.1.2), the stirring effect of waves could be a key mechanism in entraining sediment in suspension, thus causing the widespread deposition patterns during winter-spring months. Further tests on this issue are described in Chapter 6. Siegle et al. (2004) also found an increase of sediment availability during higher wave energy periods and a small but constant sediment loss during calm conditions. They added that this balance controls the overall sediment budget of the system.

^{3,4} Unfortunately, no sediment samples were collected during CoastView surveys.

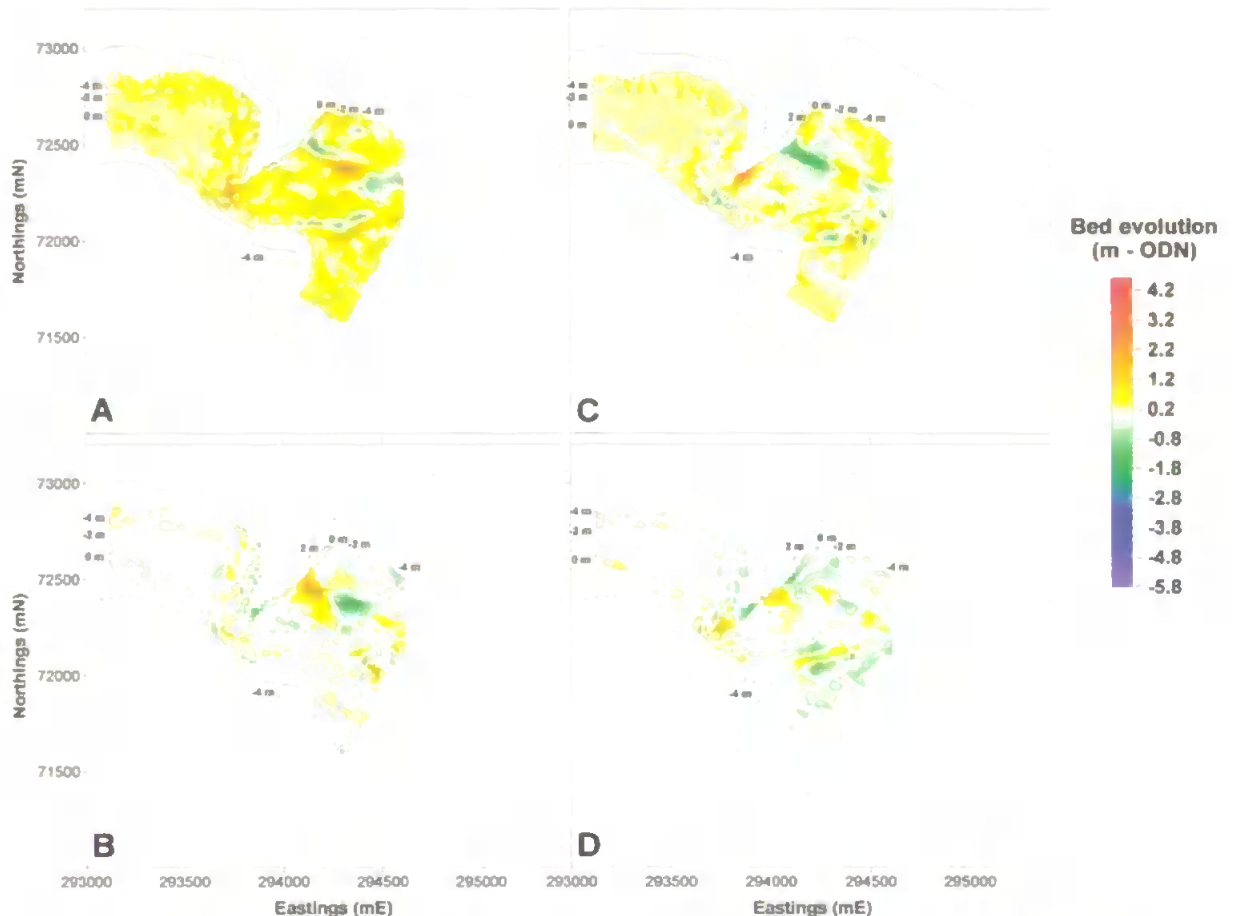


Figure 3.11: Morphological changes at the Teign estuary between CoastView surveys during the following periods: from December 2002 to May 2003 (A); May 2003 to November 2003 (B); November 2003 to June 2004 (C); June 2004 to November 2004 (D). Erosion features are associated to green and blue areas. Yellow and red patterns correspond to sediment deposition in the period. Isobaths (m ODN) correspond to bottom properties at the beginning of the respective period.

During the two winter-spring periods analysed, the sediment accumulation at the outer area is between 30% and 40% of the sediment accumulation of the whole area surveyed (Table 3.6). However, a greater variability is observed by comparing the eroded sediment volume during the summer-autumn periods. During the 2003 summer-autumn, most of the erosion processes took place in the outer estuary (around 68%), while the relative sediment volume eroded in the outer estuary was significantly lower (around 27%) during the summer-autumn of 2004, despite the relatively higher river discharge during the latter period (Figure 3.10.C). In this case, the presence of a major storm a few days prior to the CoastView survey 6 may have played a fundamental role in offsetting the net erosion trends normally forced by tidally-driven flows during summer-autumn periods. A more comprehensive analysis on the morphodynamic processes of the area is limited by the lack

of wave direction data, which would indicate whether the observed storms were driving sediments towards the estuary mouth or away from it (i.e. to the north of Teignmouth beach).

Table 3.6: Sediment volume changes during CoastView surveys. Positive and negative values mean sediment deposition and erosion, respectively.

<i>Season/Year</i>	<i>Sediment volume changes (m³) in the period</i>		<i>Relative volume changes.(%)</i>
	<i>Outer estuary only</i>	<i>Whole survey area</i>	
Winter-spring 2002/2003 (Nov 02 to May 03)	110,855	358,300	30.9
Summer-autumn 2003 (May 03 to Nov 03)	-35,630	-52,577	67.8
Winter-spring 2003/2004 (Nov 03 to Jun 04)	70,417	185,628	37.9
Summer-autumn 2004 (Jun 04 to Nov 04)	-21,288	-77,663	27.4

The cumulative effect of the bed evolution between December 2002 and November 2004 suggests sediment infilling for the whole surveyed area, despite the seasonal erosion/sedimentation patterns (Figure 3.12). Considering the observed sediment accumulation to be equally distributed throughout the surveyed area, the net deposition rate based on linear regression analysis indicates average values of about 21 cm.year⁻¹ (and 19 cm.year⁻¹ if only the outer estuary is considered) compared to the 5 cm.year⁻¹ estimated for the estuary as a whole by Wells (2002b), under the presence of waves and river discharge effects (Section 3.1.1).

However, a deposition rate of the magnitude measured during CoastView surveys is unlikely to be sustained in longer-time scales (order of several years to decades). Within the concept of a morphodynamic equilibrium, processes such as tidal currents and the intermittence of freshets would enhance the export of sediment, pushing the estuary back to its equilibrium conditions. Another scenario would be the landward migration of the estuary, as long as the system could cope with such a considerable deposition rate without silting up. However, given the presence of urban areas at the head of the estuary (town of

Newton Abbott) and some training walls along its way, this alternative also seems unlikely.

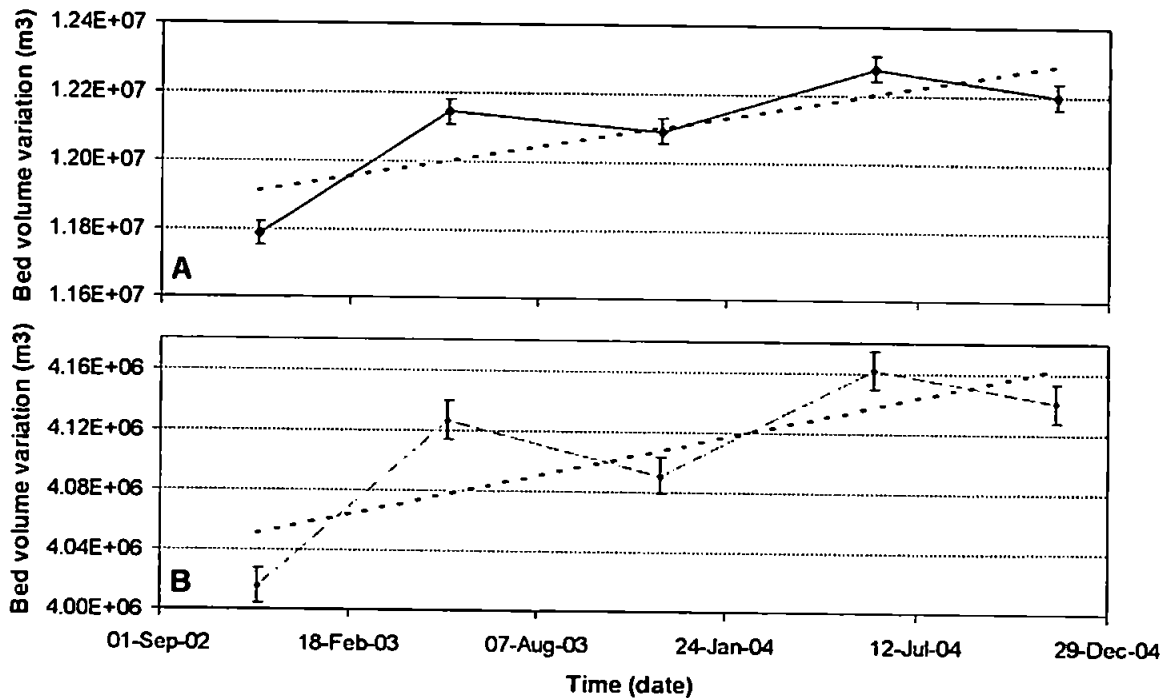


Figure 3.12: Sediment volume changes for CoastView bathymetric surveys: whole surveyed area (A) and outer estuary area only (B). Linear regression segments are represented by dotted lines. Vertical bars correspond to measurement errors, which are within the range of ± 2.5 cm (Ganderton, pers. comm.).

The outer estuary also follows the overall trend, showing a considerable coupling between the morphodynamic processes at the adjacent coastal area and at the outer estuary. Although there seems to be no direct effect of offshore waves inside the estuary (Wells 2002a), the agreement between the bed evolution of the outer estuary and that of the surveyed coastal area seems to reinforce the hypothesis that waves do play a role in the morphodynamics of the estuary, through an increase of the suspended sediment concentration. It is suggested that, once in suspension, these sediments would be taken (and eventually deposited) into the estuary by tidally-dominated residual flood currents, which are found mainly at the southern reaches of the Salty sandbank (Figure 3.2 and Sections 6.2.2 and 6.3.2). Under storms, these residual flood currents would be enhanced close to the estuary approaches, increasing the sediment availability in the area. Finally, the infilling trend would fit with the 23-year comparison between the data collected by Nunny

in 1979 and the ABPMer surveys 2001 and 2002 (Figure 3.9), where a long-term deposition area towards the outer estuary is observed.

3.3. Conclusions

In this chapter, the Teign estuary and adjacent coastal area were defined. The extensive data set available for the area is used in several stages of the calibration and validation of the model (Chapters 4 and 5) and its application to understand the morphodynamic processes at the system (Chapter 6).

The analysis of the 6-monthly CoastView surveys for a period of 2 years (from December 2002 to November 2004) indicated a net infilling trend for the whole surveyed area, at an average deposition rate of around $20 \text{ cm} \cdot \text{year}^{-1}$. This trend is unlikely to be sustained in longer-term scales, since the estuary would probably be forced into a phase of sediment export, in order to maintain its morphodynamic equilibrium. A seasonal signal on morphological changes was also found, with sediment accumulation during winter-spring periods (usually associated with higher wave energy), and sediment erosion during summer-autumn periods, normally characterised by a smaller storm frequency. A direct relationship between the bed evolution at the outer estuary and the overall evolutionary trend of the adjacent coastal area was also observed. Although offshore waves may not penetrate into the estuarine domain, they do seem to influence the morphodynamic evolution of the estuary through the enhancement of suspended sediment concentration especially under stormy periods.

Chapter 4 - Numerical Modelling

4.1. Introduction

Coastal systems are morphodynamic systems consisting of a number of interrelated elements and possessing a series of inherent properties (Cowell and Thom, 1995). Although coastal evolution processes tend to be three-dimensional, important aspects of the coastal behaviour can be understood and predicted with modelling concepts based on fewer dimensions, because coastal systems often behave at different length and time scales in the vertical, cross-shore and longshore directions (de Vriend et al., 1993). Moreover, three-dimensional flow modules are much more computationally intensive, so are less commonly used for the modelling of large coastal areas (Sutherland et al., 2004b). Tides, waves, river discharge and wind are among the most important processes to drive the sediment transport and the bed morphology patterns, ultimately changing the characteristics of these regions.

Modelling these processes and their interactions is also very complex and demanding. Although many coastal processes are not well understood to date, much progress has been made in this field by the use of several tools, among them numerical modelling. Through the development, refinement and application of such numerical methods, the two-dimensional depth-averaged hydrodynamics of coastal areas are fairly well described and reproduced. While there is room for further advances in hydrodynamic modelling, the greatest effort has been devoted to understanding the morphodynamic processes, the sediment transport and their feedback mechanisms on the bed evolution. For a review on morphodynamic modelling of two-dimensional depth-averaged models, the reader is referred to de Vriend (1993; 1996). The important task of intercomparing the predictive skills of different models has been carried out by several authors, such as de Vriend et al. (1993), Nicholson et al. (1997), Péchon et al. (1997), Davies et al. (1997), Walstra et al. (2001), Davies et al. (2002), Davies and Villaret (2002) and Sutherland et al. (2004) among others.

For the sake of computational efficiency and for the reasons exposed above, the two-dimensional version of the numerical model Telemac (release 5.3), is used in this study. The model is developed by Laboratoire National d'Hydraulique - LNH and Electricité de France - EDF/DER. Further details on its development can be found in Hervouet (1994) and Hervouet et al. (1994).

Telemac is a finite element model, composed of independent modules, each of which is applied to model specific environmental processes, ranging from the hydrodynamics of water bodies to groundwater flows; from wave-generated currents to sediment transport within aquatic systems. In order to adapt the modelling to their specific objectives, users have access to most of the model formulation through its Fortran 90-based algorithms. More details about the modules applied are available in Appendix 1, where a thorough description of the parameters used in this work is given: Table A1.1 for the hydrodynamic tests and Table A1.2 for the morphological tests. Further applications of Telemac-2D in coastal systems can be found in Hervouet et al. (1995), Marcos and Benoit (1999), Malcherek (2000), Sauvaget et al. (2000), Fernandes (2001), Fernandes et al. (2002; 2004), Bastos et al. (2003), Tyrrell (in prep.), among others.

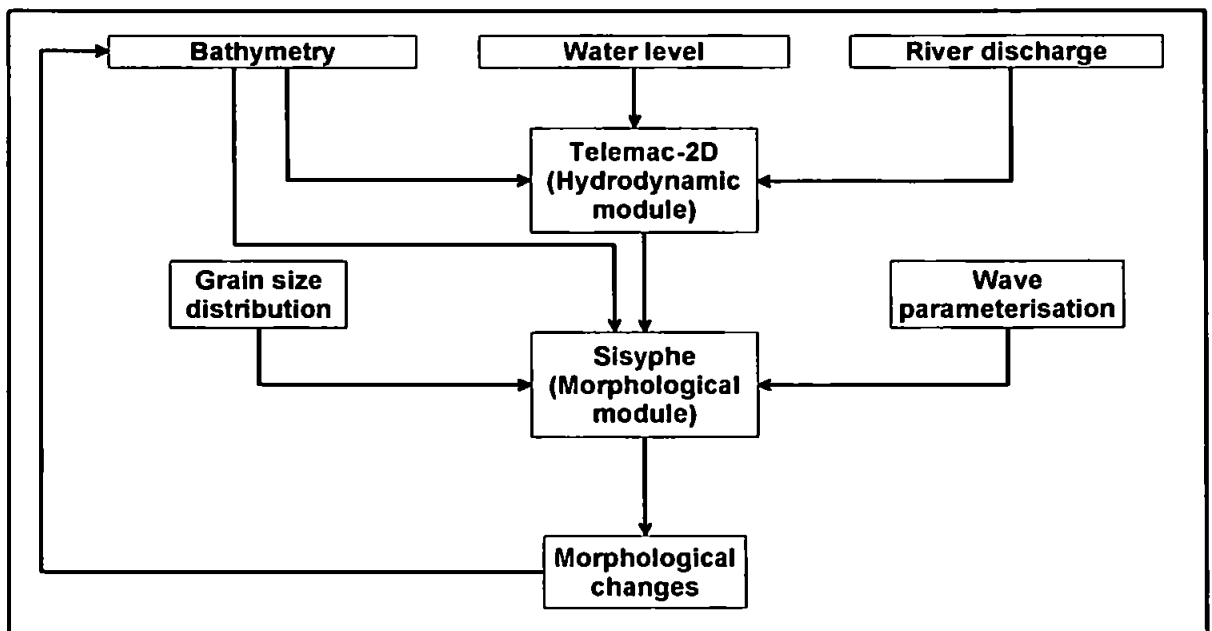


Figure 4.1: Schematic description of the morphodynamic loop within Telemac system.

The morphodynamics of the Teign estuary are then modelled through the coupling between the hydrodynamic module, Telemac-2D and the so-called morphological module, Sisyph

(Masson and Machet, 2002; Villaret, 2004). According to Wu (2004), coupling the hydrodynamics to the sediment transport enhances the stability of the model, relative to an uncoupled version of the model considered. Sisyphé is the module of Telemac system for estimating the sediment transport of non-cohesive grains and the evolution of the bed (Figure 4.1). On the other hand, the cohesive fraction of sediment, although observed especially at the middle reaches of the estuary (Section 3.2.5), is not formally modelled (i.e. cohesive sediments are assumed to behave as passive tracers) in this work due to the lack of a module within Telemac system capable of dealing with the whole spectrum of sediment grain-sizes - and their inherent and complex interactions - at the same time.

While wave effects on the hydrodynamics are neglected, they are modelled as a stirring agent in the sediment transport module, induced by the wave influence on the bottom friction. This is due to the fact that coupling is operational between only the hydrodynamics and the sediment transport modules, and not currently possible between the wave and the hydrodynamic modules. Keeping the model set-up as simple as possible will help the understanding of the basic morphodynamic processes in this estuary. Nevertheless, it is important to highlight that despite the limitations discussed above, the use of TELEMAC system in this thesis can be regarded as innovative, since it takes into account the behaviour of mixed grain sizes, an option not yet available in other state-of-the-art process-based models. It is also seen that when compared to better understood systems, such as rivers, the modelling framework proposed in this study is similar to those used by Wu et al. (2004) and Wu (2004).

According to Villaret (2004), the accuracy of Sisyphé - and ultimately of the morphodynamic predictions - will be dependent on several factors:

- the accuracy of the empirical sediment transport formulae;
- the sensitivity of sediment transport rates to important hydrodynamic forces, namely the current velocity and the bottom friction;
- the residual tidally-driven sediment transport, which is dependent on antagonistic elementary transports (flooding and ebbing phases of tide) that are normally equivalent to each other;
- the bottom evolution results from the spatial gradient of the sediment transport, which is lower in accuracy relative to the instantaneous transport;

- the empirical assumptions on the implementation of multiple grain sizes and hiding/exposure effects.

The calibration and validation of the hydrodynamics is based on COAST3D project (Soulsby, 1998, 2001). Inter comparison with the hydrodynamic results described in Siegle (2003) and Sutherland et al. (2004a) for Teignmouth is also carried out. The sediment transport is also calibrated against COAST3D data set. The performance of the modules is assessed not only by visual analysis, but also through the application of statistical tests specifically adapted to environmental applications.

In this chapter, the calibration of the model through key hydrodynamic parameters is discussed, followed by the validation tests. Then, the sediment transport and bed evolution issues are coupled to the hydrodynamics as a means of assessing the performance of the resultant morphodynamic loop. In general terms, the results in morphodynamic modelling are still far from accurate when compared to observations due to many remaining gaps in current knowledge about coastal and estuarine processes.

4.2. Hydrodynamic set-up

4.2.1. Bottom settings

According to Cheng et al. (1991), an accurate bathymetric representation of a coastal area is one of the most important and fundamental requirements in successful modelling. These authors also argue that this is particularly true for estuarine models because bathymetric variations in estuaries are usually very complex, such as at the outer portion of the Teign estuary. As shown in Section 3.2.6, several data sets are used for building up the bathymetric charts of the Teign estuary and the adjacent coast. For the purposes of hydrodynamic calibration and validation, which are based on COAST3D period (November, 1999), the following data are considered:

1. COAST3D hydrographic surveys of the estuary mouth and adjacent coastal area;

2. Hydrographic survey of nearly the entire estuary (Nunny, 1980);
3. COAST3D bathymetric mosaic for coastal area and deeper reaches (based on LIDAR data from the Environment Agency and Admiralty Chart 3155, respectively).

Where an overlapping of data from different sources take place, the most recent data collected are applied. Therefore, the bathymetric data '1' has priority upon the data sets '2' and '3' (Figure 3.8). In order to standardise this information to a common reference bed level, all data are reduced relative to ODN. By using the Telemac mesh generator ('Matisse'), the next step is to generate the meshes and test them according to the resultant resolution.

4.2.2. Mesh resolution

The quality of the model output will be directly dependent on the chosen mesh resolution. Creating a mesh which resolves well the bottom features and proportionate a time efficient model performance is crucial, especially when taking into account that morphodynamic modelling is a time-demanding process.

A great advantage of using finite element-based models such as Telemac-2D is the possibility of having irregular grids. Shallow areas and complex bathymetric features can be resolved with greater detail whereas deeper areas can be represented through coarser grids. Thus, the model performance is enhanced by increased resolution only where it is required. Another advantage of finite element based models is the fact that the boundary conditions are embedded in the equations themselves as opposed to finite differences schemes, where they are a separate feature (Dyke, 2001).

Some consideration must also be given to the quality and resolution of the original bathymetric and topographic data. On one hand, important information may be lost if the mesh resolution is much coarser than the original field data, whereas a much finer ('over specified') mesh - when compared to the original data - could generate inconsistent information, numerical instability due to higher Courant numbers and therefore unrealistic outcomes.

By considering the factors above, four meshes are generated based on the same original information described in Figure 3.8. Not only the mesh resolution, but also the offshore extent of the mesh is varied in order to define the most suitable grid (Figure 4.2), which will depend on the calibration tests (Section 4.3). The meshes 'A' and 'C' extend around 4 km offshore, with northern (top cross-shore limit) and southern boundaries about 3 km and 2.5 km away, respectively. Meshes 'B' and 'D' have much shorter offshore limits: 1 km on the offshore direction; 900 m to the north and about 650 m to the south.

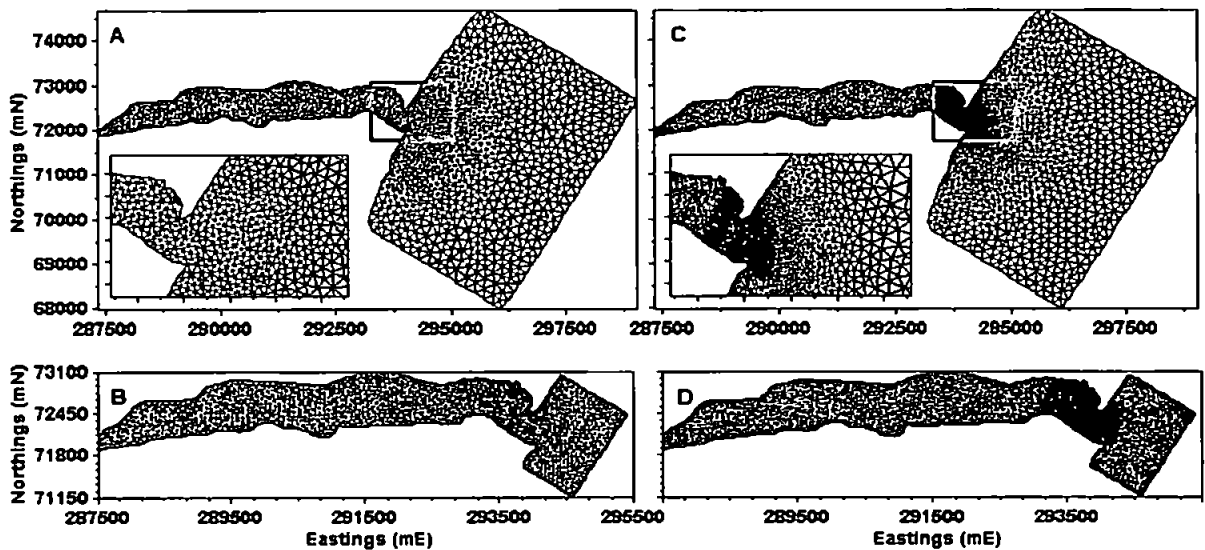


Figure 4.2: Generated meshes with varying grid resolution and offshore coverage area. The insets represent areas of further mesh refinement due to channel meandering and complex bathymetry. Mesh 'A' has 1721 nodes; mesh 'B' 2037; mesh 'C' 4355 and 5009 nodes in mesh 'D'.

Another way of assessing the mesh resolution is by interpolating the observed data into the different meshes considered and then using visual comparison and statistical tools to determine the most suitable mesh. At this stage no modelling results are considered whatsoever. In Figure 4.3, the bed evolution observed between COAST3D surveys 2 and 4 is compared to the schematised bed evolution of meshes 'A' to 'D' (Figure 4.2). Only meshes 'C' and 'D' qualitatively resolve the observed bed evolution features.

Quantitatively, the estimation of the Brier Skill Score (BSS, introduced in morphodynamic studies by Brady and Sutherland, 2001 and Sutherland et al., 2001b; more details in Section 4.4.1) shows the bed representation for survey 4 of the mesh 'A' is very poor

(BSS= -3.36). Mesh 'B' has improved representations of the bed features (BSS= -0.26), while the most accurate representation of observed bed features come from meshes 'C' and 'D', with respective BSS of 0.54 and 0.46. Since the closer to 1 the BSS is, the better the match between the target bathymetry and the bathymetry of interest, it can be said from the application of the BSS that only meshes 'C' and 'D' replicate reasonably well the field data. The relative decrease in the BSS for the mesh 'D' in comparison to mesh 'C' seems to reinforce the hypothesis of over specification mentioned earlier in this section, as a greater resolution of the mesh did not necessarily improve the representation of observed features.

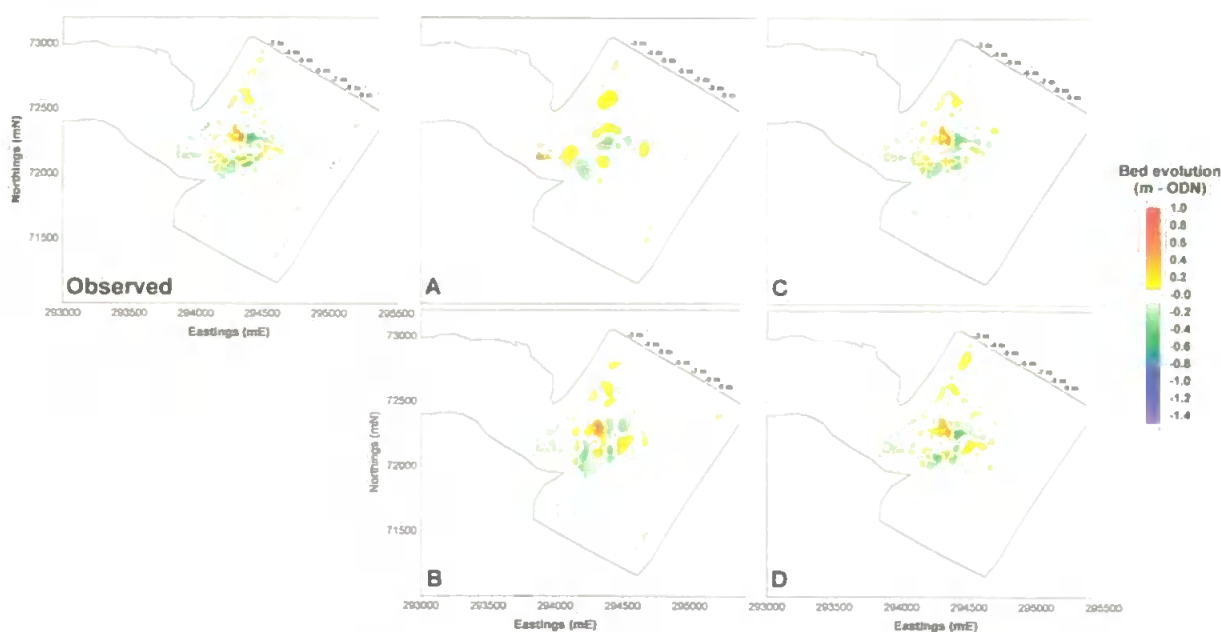


Figure 4.3: Bed evolution between COAST3D surveys 2 and 4 and how different meshes reproduce the observed conditions. The letters 'A' to 'D' correspond to the mesh definition used in Figure 4.2. Contour bed level intervals are of 1 m (ODN) and correspond to COAST3D bathymetric survey 2.

Although the bed evolution estimated from the meshes 'C' and 'D' compares well with the observed features in Figure 4.3, the resultant BSS are classified in the 'reasonable/fair' range of the qualifications of BSS (Table 4.7). As it will be shown later in Section 4.4.1, if the observed conditions do not change significantly during the period considered, BSS values will be very sensitive to small changes in the bathymetry data. This seems to be the case here, as for the period between December 2002 and May 2003 (CoastView surveys 2 and 4, respectively) - subject to major bathymetric changes in the area - the BSS calculated with mesh 'C' (not shown) is of 0.86, in the 'excellent' range of Table 4.7. Thus, through the

application of the BSS, mesh 'C' is shown to represent very well the measured bottom conditions.

4.2.3. Boundary conditions

As mentioned in Chapter 3, the Teign estuary hydrodynamics are forced mainly by tides and river discharge. At this stage, the effects of wave-driven and wind-driven currents are regarded as of secondary importance.

Table 4.1: Boundary conditions applied to hydrodynamic tests.

<i>Boundary</i>	<i>Type</i>	<i>Interval</i>	<i>Source</i>
Sea - Alongshore Only	Water Level (m-ODN)	10 minutes	Pier Pressure Transducer
River	Discharge rate (m ³ .s ⁻¹)	15 minutes	EA Flow Gauge at River Teign
Coastline, Northeast and Southwest Oceanic Limits	Closed	N/A	N/A

Two options are available for the prescription of the oceanic boundary water level: a simulation carried out in COAST3D project with DELFT3D regional scale model (Sutherland et al., 2004a) or the use of measured water level at the Pier station (Chapter 3). A brief comparison between these two data sets for a month period shows little difference, with the root-mean-square error (RMSE) around 0.01. The RMSE is defined as

$$RMSE = \sqrt{\frac{1}{n} \sum (x_f - x_v)^2} \quad (4.1)$$

where n is the number of verifying points (grid points or observations) in the verification area; x_f is the forecast value of the parameter in question and x_v is the corresponding verifying value (analysed or observed).

Thus, for being an actual measure of the observed water level and for allowing the modelling of periods outside the COAST3D project, the pressure transducer data at the pier

at 10-minute intervals are used to impose a spatially uniform water level along the offshore boundary (Table 4.1). In other words, although time-dependent (based on the pier data), the water level at the whole boundary will be assumed as constant at a given time. It is also important to mention that by applying the measured data as boundary condition, the wind and wave-generated disturbances on the water level will be also taken into account. After some sensitivity tests, it was found that the Southwest and the Northeast oceanic limits can be assumed as closed boundaries, since it makes little difference to the model results if these boundaries are also tide-dependent or not. Finally, measured river flow rates collected by the Environment Agency every 15 minutes are prescribed as the upstream boundary.

4.3. Hydrodynamic calibration

For the purpose of scientific and commercial applications, numerical models must first be calibrated, tuned and validated^{4.1} against field data in order to serve as reliable practical tools. Great advances have been observed on computational power lately, but even nowadays there are no standard methods to calibrate and validate numerical models (Cheng et al., 1991). The validation of a model is the comparison between a calibrated model output and observations (Dyke, 2001). The relationship between the range of values for a parameter and the model agreement is known as the calibration curve for that parameter (Mulligan and Wainwright, 2004). They also argue that if a parameter shows a significant change in error with a change in its value is known as a sensitive parameter.

According to Sutherland et al. (2001a), statistical analysis methods have not been used in the validation of coastal engineering models. There is not much argument that it is preferable to have quantitative methodologies of assessing the quality of a model output than subjective and qualitative judgement upon the performance of a model. However, according to Sutherland et al. (2001a), it is not possible to make any objective conclusions

^{4.1} Terms such as 'calibration' and 'validation' can have similar meanings. In this study, 'calibration' will be the initial comparison between model output and observations. 'Validation' will be the comparison between modelling and measurements without any further adjustment to the previously calibrated model parameters.

without a discussion of the measurements and their inherent errors. These authors also discuss the likely origin of measurement errors, while Brady and Sutherland (2001) analyse the drawbacks of the 'traditional' statistical analysis techniques (e.g. effect of outliers in final statistical results). Other methods than statistical tools to assess model's performance are suggested by Cheng et al. (1991), such as the comparison of the amplitudes and phases of the tides and tidal currents.

In this section, key parameters are tested in order to define the calibration curves mentioned above against the consistent data set gathered during the COAST3D project. Then, inter comparisons with the results of Siegle (2003) and Sutherland et al. (2004a) follows. Finally, the hydrodynamic validation is done also with COAST3D data, with what Mulligan and Wainwright (2004) call 'split sample' approach, in which the available data is separated into a calibration set and a separate validation set.

4.3.1. Statistical tools in hydrodynamic modelling

As shown, the use of statistical tools is fundamental in assessing present day's model performance. For this purpose, the relative mean absolute error (RMAE) described in Sutherland et al. (2001b); van Rijn et al. (2003) and Sutherland et al. (2004a) is used in this study. Some advantages of this methodology are that it can be applied to either scalars (e.g. water level or wave height) or vectors (currents) and includes errors of magnitude and direction in a single statistic (Sutherland et al., 2004a). As with any other statistic tool the inherent variability reduces as the number of samples increases. Therefore, it is advisable that 100 samples or more are used whenever possible (Sutherland et al, 2001). This condition has been ensured in all tests to follow in the next section.

Let X be a set of N observed values (x_1, \dots, x_N) and let Y be a set of N predicted values (y_1, \dots, y_N) with the n th value ($n=1, \dots, N$) of each being at the same position in space and time. The mean absolute values of the observed data (set X) and the predicted values (set Y) are given by:

$$\langle |X| \rangle = \frac{1}{N} \sum_{n=1}^N |x_n| \quad (4.2)$$

$$\langle |Y| \rangle = \frac{1}{N} \sum_{n=1}^N |y_n| \quad (4.3)$$

where the angular brackets denotes an average and $|x|$ is the modulus of x . As suggested in Sutherland et al. (2004a), the resulting average could be replaced by a weighted average for points that are not evenly distributed in space or time, which is the case of finite element-based models such as Telemac. In this study, however, the arithmetic mean described in Equations 4.2 and 4.3 was applied throughout.

The mean absolute error (MAE) is given by:

$$MAE = \langle |Y - X| \rangle \quad (4.4)$$

Sutherland et al. (2004a) also comment the use of modulus makes the statistic non-analytic and thus more difficult to work with than using a RMSE. The MAE, however, has the benefit of not being as heavily influenced by outliers as the RMSE (Sutherland et al., 2001b). They also make the point that $RMSE \geq MAE$, therefore defining RMSE as a conservative error predictor. The quality of the modelled results are assessed from the value of relative mean absolute error (RMAE):

$$RMAE = \frac{\langle |Y - X| \rangle}{\langle |X| \rangle} = \frac{MAE}{\langle |X| \rangle} \quad (4.5)$$

where $RMAE=0$ would in theory mean a perfect match between modelling and measurements. This, however, is never achieved since the RMAE includes contributions from the measurement errors (Sutherland et al., 2004a). Van Rijn et al. (2000) discuss the error measurements made in COAST3D field campaigns. Measurement error estimations were made for different velocities and combined to give an average observed error (OE) of 0.05 m.s^{-1} . These observational errors are related to various sources: i) the physical size of the instruments; ii) the measurement principle and iii) the conversion principle including

assumptions of applied theories. In order to remove the OE factor from the analysis, the adjusted relative mean absolute error (ARMAE) is given by:

$$\text{ARMAE} = \frac{\langle |Y - X| - OE \rangle}{\langle |X| \rangle} \quad (4.6)$$

with negative values of the numerator set to zero before averaging. If negative values are found, then it means the computed value is within the error band range of the measured value (van Rijn et al., 2003). As the ARMAE is derived from the ratio of two quantities it is unbounded at the upper limit and is highly sensitive to small changes in the numerator when the denominator is small (Sutherland et al., 2001b). Finally, the relative error will be relatively large if the average value is close to zero, such as for a tidal current varying around zero, according to van Rijn et al. (2003). They also propose an objective ranking of the modelling performance (Table 4.2).

Table 4.2: Qualification of RMAE error ranges for wave height and velocity (van Rijn et al., 2003) and for ARMAE error estimates (Sutherland et al., 2004a).

<i>Qualification</i>	<i>RMAE Wave height</i>	<i>RMAE Velocity</i>	<i>ARMAE Velocity</i>
Excellent	< 0.05	< 0.1	< 0.2
Good	0.05 - 0.1	0.1 - 0.3	0.2 - 0.4
Reasonable / Fair	0.1 - 0.2	0.3 - 0.5	0.4 - 0.7
Poor	0.2 - 0.3	0.5 - 0.7	0.7 - 1.0
Bad	> 0.3	> 0.7	> 1.0

Some comments must also be made on the comparison of observed current data at a single point location (such as with current meters) with depth-averaged models. Sutherland et al. (2001b) comment that altering observed current data to make them representative of a depth-averaged profile would be done through assuming a depth-profile and converting from the measured value at a depth to the depth-averaged value, although this method would tamper with the observations. Alternatively, they suggest that modelled depth averaged currents to be converted into a point value at the measurement height. Since neither of the methods would completely eliminate the errors (Sutherland et al., 2001b) - and perhaps even introducing other spurious information - the only treatment carried out in this study with the field data was to vertically average the measured currents when there

was more than one current meter device at the same location (e.g. several current meters at different depths; $u(z)=\text{constant}$). It is important to bear in mind the COAST3D current meters are, on average, about 1/5 up the water column relative to the seabed and are likely to record lower velocities than the depth-averaged velocities produced by the numerical models (Sutherland et al., 2004a). For current measurements to be representative of the whole water column (i.e. a depth-averaged velocity), the instrument must be located at around 1/3 of the local depth (Soulsby, 1997). When using the velocity data for estimating the morphological changes to the bed, it is important to bear in mind the likelihood of lag effects between the observed currents and the resulting sediment transport.

4.3.2. Hydrodynamic calibration set-up

In order to match the hydrodynamic tests with the morphological ones (to be discussed later in this chapter), a spring-neap cycle from 08/11/1999 to 22/11/1999 within the COAST3D main experiment (between surveys 2 and 4) is chosen for the model calibration. Measured tides and river discharge data (Table 4.1) are used as boundary conditions (Figure 4.4). A sensitivity test is carried out by comparing the effect of tuning several key model parameters to data sampled at 5 different locations (sites 5, 9, 14, 24 and 25, see Figure 3.6) during COAST3D project. For the calculation of RMAE and ARMAE, around 7650 samples were used.

The limits of the various parameters to be tested in this section were chosen based on realistic values found in the literature. The spatially constant Chézy bed friction coefficient of $65 \text{ m}^{1/2} \cdot \text{s}^{-1}$ used by Sutherland et al. (2001b) for modelling the coastal area adjacent to the Teign estuary with the PISCES system appears to be a suitable value (Table 4.3). When comparing this bed friction coefficient against depth-dependent values - which are assumed to vary around $65 \text{ m}^{1/2} \cdot \text{s}^{-1}$ - (Table 4.4), no significant statistical differences are observed (RMAE=0.78 for both tests). However, the choice of a depth-dependent bed friction coefficient is closer to reality and is kept in the following tests. The model sensitivity to eddy viscosity indicates that for values higher than $0.5 \text{ m}^2 \cdot \text{s}^{-1}$, many modelled hydrodynamic features are smoothed when compared to observations. This is due to an increase in the modelled turbulence, hence a more efficient mixing, resulting in a decrease

in the model skill (higher RMAE) in reproducing observed currents. The model sensitivity to the eddy viscosity seems to suggest that unless high values of this parameter (e.g. greater than $5 \text{ m}^2.\text{s}^{-1}$) are used, turbulence will play a secondary role in determining the observed hydrodynamic patterns. Since Sutherland et al. (2001b) applied a constant eddy viscosity of $0.5 \text{ m}^2.\text{s}^{-1}$, this value is also kept in this study.

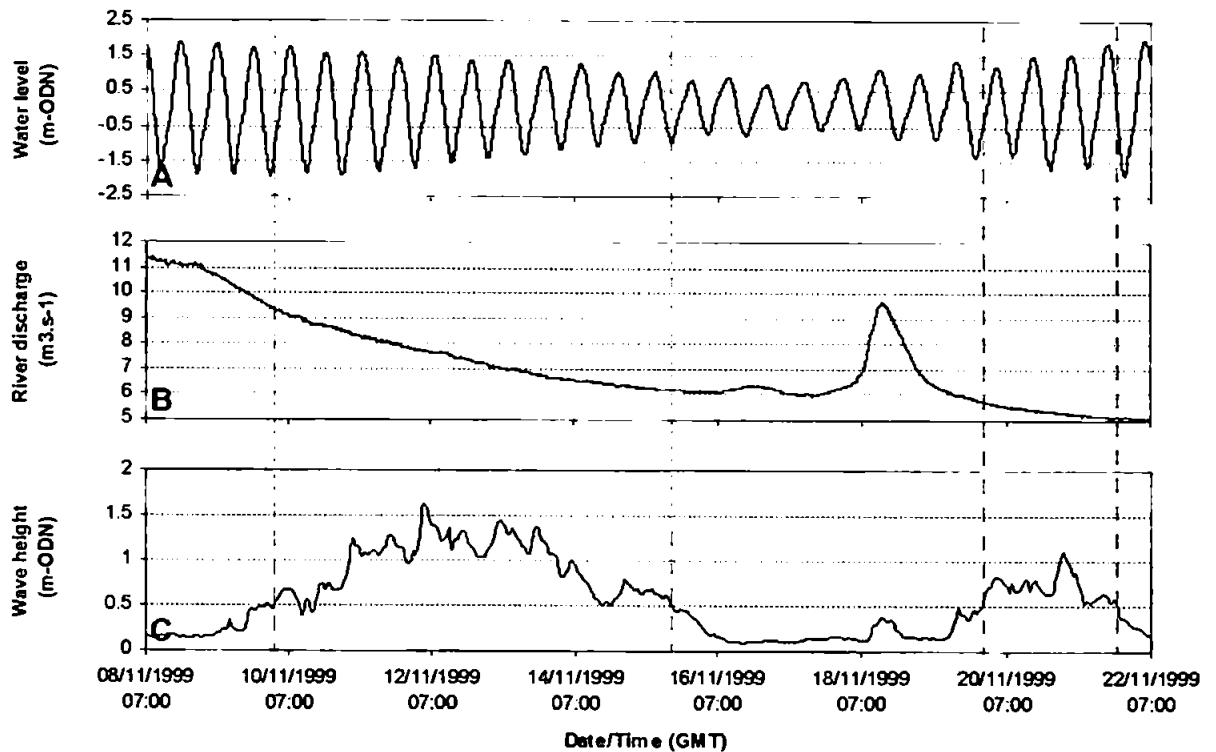


Figure 4.4: Water level (A), river discharge (B) and wave height (C) for hydrodynamic calibration period. Although waves are not considered in these simulations, they are shown for illustrative purposes. Dashed vertical lines delimit periods of wave heights $\geq 0.5 \text{ m}$ (ODN).

The mesh resolution test illustrates the model exercise is affected by the number and distribution of the nodes within a grid. The use of a more refined mesh close to the estuary mouth (Figure 4.2.B) - even with a restricted oceanic area - delivers better results (RMAE=0.77) than that of a mesh with an extended coastal coverage area (Figure 4.2.A), and coarser grid resolution (RMAE=0.98). This may be reinforced by the fact that observed data used in this test originate mainly from the area close to the estuary mouth. In the next hydrodynamic tests, mesh 'C' (Figure 4.2.C) is chosen for combining reasonable description of bathymetry to affordable computational time. Moreover, an extended offshore area helps keeping boundary effects away from the area of interest.

The model sensitivity to wind effects suggests that observed data may not always improve the model outcome. This is because the wind data were collected some 75 km (Portland meteorological station) away from the Teign estuary. There is a general decrease (higher RMAE) in the model skill by introducing the wind effect. Further adjustments would also be required for the modelling of the observed conditions, since the observed wind is input into the model as being constant throughout the domain. Due to physiographic features (Chapter 3), which shelter the estuary from the direct effect of winds of most directions, this effect is regarded as of secondary importance for the scope of this study.

Table 4.3: Model sensitivity to key parameters during hydrodynamic calibration period. Simulations are compared against observed U and V velocity components (averaged values). The model performance is expressed in terms of the average RMAE and ARMAE estimated from 5 different site locations. Values in bold are the selected ones for the model calibration.

<i>Parameter</i>	<i>Values tested</i>	<i>Average RMAE</i>	<i>Average ARMAE</i>
Bed friction in terms of Chézy coefficient ($\text{m}^{1/2}.\text{s}^{-1}$)	35	0.86	0.37
	60	0.78	0.33
	65	0.78	0.33
	70	0.78	0.33
	95	0.79	0.34
	Depth- dependent	0.78	0.33
Eddy viscosity ($\text{m}^2.\text{s}^{-1}$)	0.005	0.78	0.33
	0.05	0.78	0.33
	0.5	0.78	0.33
	5	0.90	0.40
Mesh resolution	A	0.98	0.46
	B	0.77	0.33
	C	0.78	0.33
	D	0.76	0.31
Wind effect	None	0.78	0.33
	Portland Wind Station	0.91	0.40

The numerical modelling of tidal flats, or wetting and drying processes - within Telemac system is treated either by the correction of the free surface gradient (i.e. by assuming a thin layer of water is found above the areas which should be "dry") or by the masking and consequent removal of the "dry" areas from the modelling domain. Sensitivity analysis and calibration tests (not shown) carried out in this study have demonstrated that only the free

surface gradient correction option was sufficiently robust to satisfactorily simulate the meso-macrotidal characteristics of the Teign estuary and surroundings, while numerical instabilities were found when applying the "masking" option.

Once the model parameters are adjusted, the runs for the hydrodynamic calibration period are set up and compared to the results obtained by Siegle (pers. comm.)^{4.2} and Sutherland et al. (2001b) and shown in Table 4.4. The model performance is compared against observed water level (sites 8 and 11) and current data at 5 different locations (sites 5, 9, 14, 24 and 25). Then, the model ability is assessed through plots (Figure 4.5) and statistical analysis of RMAE and ARMAE (Table 4.5), where the results from the studies cited above are also given.

Table 4.4: Calibration parameters for hydrodynamic simulation between 08/11/99 07:00 to 22/11/99 07:00 (GMT).

<i>Parameter</i>	<i>This study</i>	<i>Siegle (pers. comm.)</i>	<i>Sutherland et al. (2001b)</i>
Hydrodynamic numerical model	Telemac-2D	MIKE21	Telemac-2D
Mesh discretisation	Finite elements	Finite differences	Finite elements
Number of nodes in mesh	4355	180000	16790
Forcings considered	Tides and river discharge	Tides and river discharge	Tides, waves, wind and river discharge
Other modules used	None	None	FDWAVE
Hydrodynamic time step (seconds)	5	10	5
Bed friction in terms of Chézy coefficient ($m^{1/2}.s^{-1}$)	Depth-dependent (m-ODN)	Depth-dependent (m-ODN)	Constant 65
	$H < -3 = 68$	$H < -3 = 38$	
	$-3 < H < -1 = 64$	$-3 < H < -1 = 34$	
	$-1 < H < 1 = 62$	$-1 < H < 1 = 32$	
	$H > 1 = 60$	$H > 1 = 30$	
Eddy viscosity ($m^2.s^{-1}$)	0.5	0.16 at estuary and 0.5 at coastal area	0.5
Wetting and drying	Yes	Yes	Yes

As expected, since the observed water level at the pier is used as the tidal boundary condition, the agreement between the modelled and the observed water level at the pier is virtually perfect, with no visible differences between them (RMAE=0.01). For the harbour

^{4.2} For 'full' numerical experiments including tides, waves, river discharge and wind effects with MIKE21 for Teignmouth, the reader is referred to Siegle (2003).

station, which is inside the estuary, the residual water level (observations minus model output) follows a tidal signal, where the residuals tend to be minimal at low tide periods up to around 14/11/99. In this period, the presence of a storm off the estuary also contributed to increasing the residuals. Then, what seems to be a correction in the tide gauge sensor causes a general decrease on the residual signal (RMAE=0.07).

When comparing the modelled velocities against field data, however, the same degree of accuracy is not achieved when compared to that of water level data. This difference is also expressed in the qualification table for RMAE proposed by van Rijn et al. (2003), where the classification ranges for wave height estimation (such as the water level) and velocities is different (Table 4.2). There are several reasons for this decrease in the model skill: i) the velocity field is a by-product of several hydrodynamic agents, therefore dependent on a more complex set of physical variables than the water level; ii) a likely under-resolution of bathymetric schematisation in the mesh chosen for certain complex areas, especially close to the estuary mouth (however, one must bear in mind the balance between mesh resolution and simulation time consumption); iii) experimental errors described in van Rijn et al. (2002).

There is an overall improvement of agreement between modelled and observed current fields especially closer to the estuary mouth (item 25), where tidal currents are more pronounced (Figure 4.5 and Table 4.5). However, some specific features such as current direction and magnitude are sometimes not well represented by the model. As suggested by Sutherland et al. (2001b), many of the deviations between predictions and observations are caused by inaccuracies in modelling meandering features and vortices, where small errors in predicting their position can lead to large errors in the velocities at a point. Clearly, the absence of wave and wind-driven currents in the calibration period is also a limiting factor of the model performance, as two periods of wave heights ≥ 0.5 m ODN (hereafter named as 'storm' periods) took place in the area for the modelled period.

Observed current velocities at site 5, the most seaward instrument used for the calibration, were mainly alongshore-directed (negative values of north velocity component) during the passage of the two main storms of the period, with a RMAE of 0.94. As expected, these features are not captured by the tidally driven currents in the offshore area. At site 9, the storm effects are also noticed through southward velocities. Modelled velocities are

slightly worse than the ones for site 5, with a RMAE of 0.97. Closer to the shore, the current data of site 14 seem to indicate a tidal signal throughout the spring-neap cycle, which is enhanced by the storm presence mainly in the seaward cross-shore direction. Due to the stronger tidal influence, the model performance is improved (RMAE=0.80). With a RMAE of 0.79, the model performance at site 24 is similar to the one at site 14. At these two sites, a consistent northward current is observed, it is interesting to observe the contrasting behaviour of the cross-shore velocity component. While the storm presence enhances the observed offshore current at site 14, at site 24 the opposite happens and an onshore current appears. Since they seem to be storm-related, neither of these features is replicated by the model. At site 25, the closest to the estuary mouth used in this analysis, storm effects are nearly non existent and the tidal influence seems to dominate the current structure, since the freshwater discharge is also small, within 5 to 10 $\text{m}^3.\text{s}^{-1}$ (Figure 4.4). The best model performance is achieved in this area, with a RMAE of 0.39. Sparse observations with site 25 suggest currents leaving the estuary attained velocities close to 1 m.s^{-1} , while the model predicts velocities of up to 1.5 m.s^{-1} (note change in scale).

It is common practice to present the model performance through averaged RMAE of U and V velocity components, instead of presenting the results for RMAE for U and V separately. By doing that, the model skill in predicting the observed current direction is preserved. However, it is found for the results of this study that if the resultant current magnitude and the correspondent RMAE (here called $\text{RMAE}_{\text{speed}}$) are calculated instead of averaging the error for both U and V , an 'artificial' improvement of model performance - of around 25% - is achieved (Table 4.5). This finding is linked to the fact that - by estimating the resultant velocities - only the current intensity is preserved, while its directional information is lost.

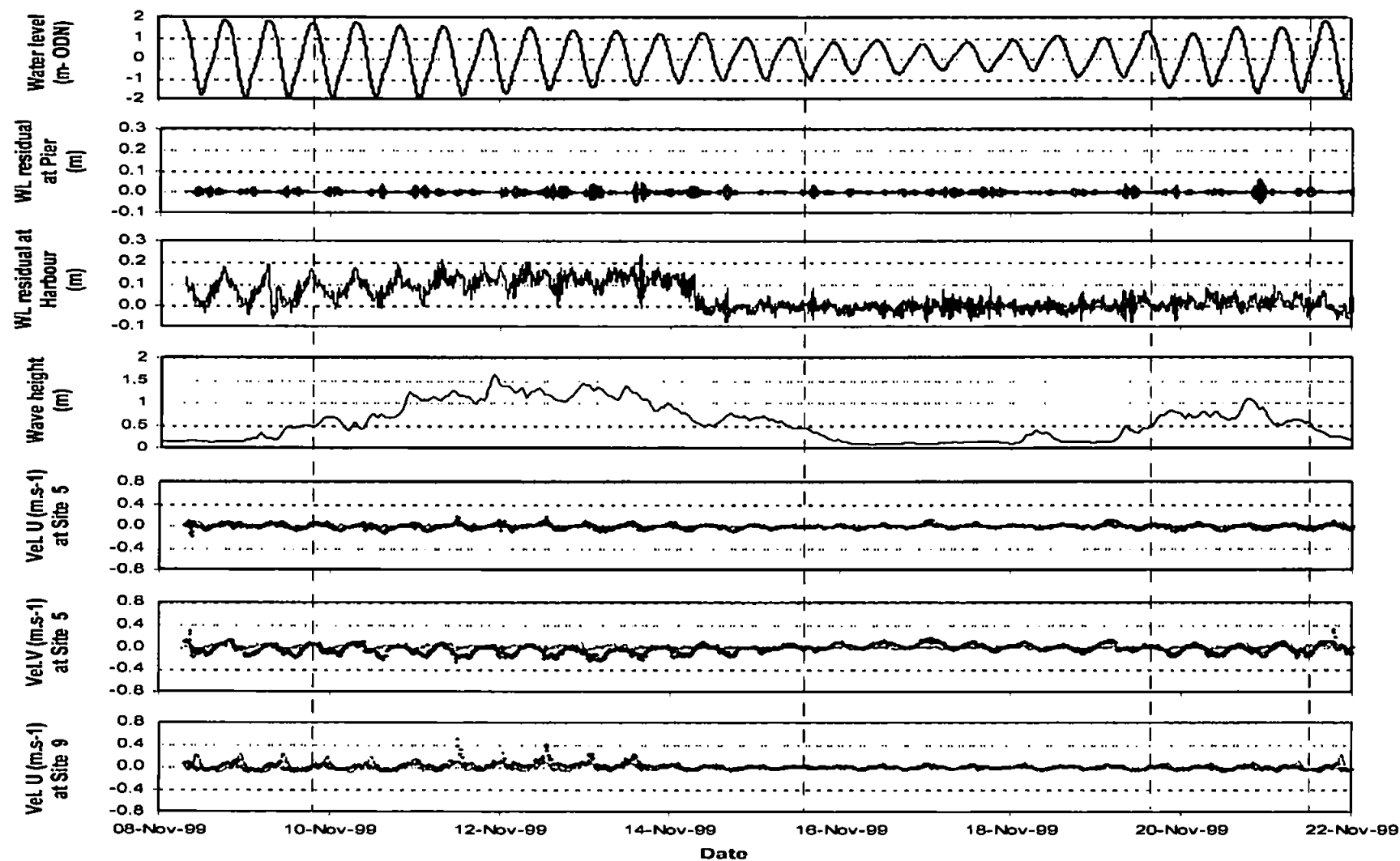


Figure 4.5: Observed and predicted water levels and currents during the calibration period. Field data are represented by black crosses, while red dotted line corresponds to model output. Dashed vertical lines delimit periods of wave heights ≥ 0.5 m (ODN). For more information on the location of the sites, the reader is referred to Figure 3.6.

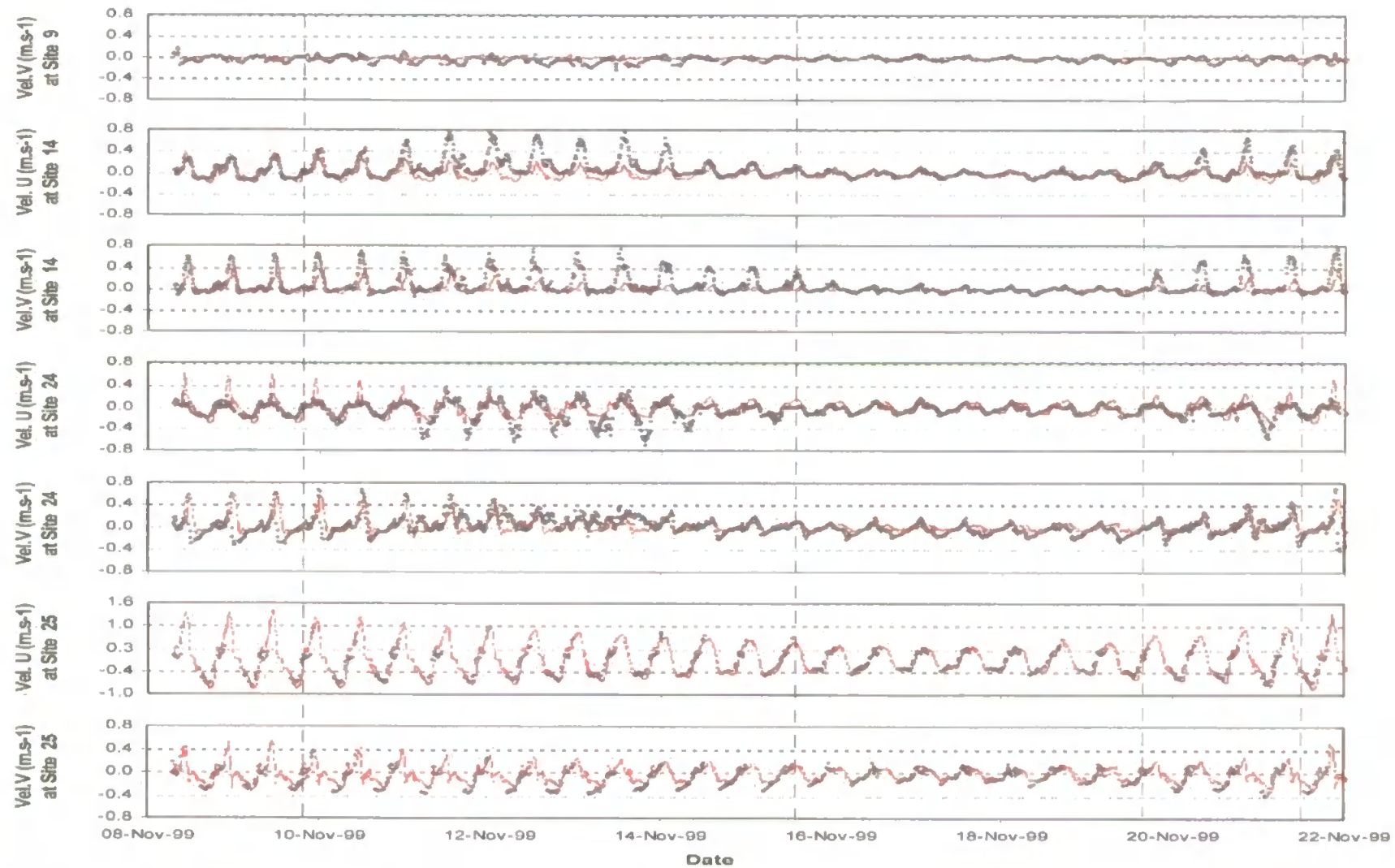


Figure 4.5, *Continued*: Observed and predicted currents during the calibration period. Field data are represented by black crosses, while red dotted line corresponds to model output. Dashed vertical lines delimit periods of wave heights ≥ 0.5 m (ODN). For more information on the location of the sites, the reader is referred to Figure 3.6.

It can be seen in Table 4.5 that where the flow is important both in the cross-shore and longshore directions, the reductions by using $RMAE_{speed}$ are much bigger than at areas where the flow is basically along a single direction, such as the case for site 5 (close to the estuary mouth), where velocity is mainly cross-shore and the difference between $RMAE$ and $RMAE_{speed}$ is relatively smaller.

In this study, model results compared well with other modelling exercises applied to the area, given that two boundary conditions were considered, with only an offshore tidal-dependent boundary and a freshwater flow limit. The relatively low number of nodes (due to the finite element mesh structure and mesh resolution tests) was a key element in optimising the computational time - about 15 hours to simulate 14 days in a 1 GHz Pentium III PC.

Table 4.5: $RMAE$ for hydrodynamic calibration period.

<i>Parameter/ Location</i>	<i>This study ($RMAE_{speed}$)</i>	<i>This study (Average velocity-based $RMAE$)</i>	<i>Siegle (pers. comm.)</i>	<i>Sutherland et al. (2001b)</i>
Water Level				
Pier	0.01	0.01	0.01	N/A
Harbour	0.07	0.07	0.07	N/A
Currents				
Site 5	0.69	0.94	0.66	0.85
Site 9	0.62	0.97	0.97	1.05
Site 14	0.67	0.80	0.74	1.00
Site 24	0.55	0.79	0.86	0.76
Site 25	0.33	0.39	0.42	0.47
Average	0.57	0.78	0.73	0.83

4.3.3. Hydrodynamic validation

Given the data richness of the COAST3D project, the validation period is also based on this data set. It extends for 14 days, from 25/10/99 to 08/11/99, with an overlap with the calibration period of about 12 hours (Figure 4.6). Separating the data into a calibration set and a separate validation set is what Mulligan and Wainwright (2004) call 'split sample' approach. During this spring-neap cycle, two main periods of wave heights higher than 0.5

m were observed, with the last one coinciding with a five-fold increase in the river discharge, within a couple of hours (from the average $10 \text{ m}^3 \cdot \text{s}^{-1}$ up to around $50 \text{ m}^3 \cdot \text{s}^{-1}$). The effects of the storm period can be observed on the tidal record at the pier, where a distortion on the tidal curve is recorded. As for the calibration period, the number of samples for estimating the error statistics is much higher than 100 samples, as recommended by Sutherland et al. (2001b).

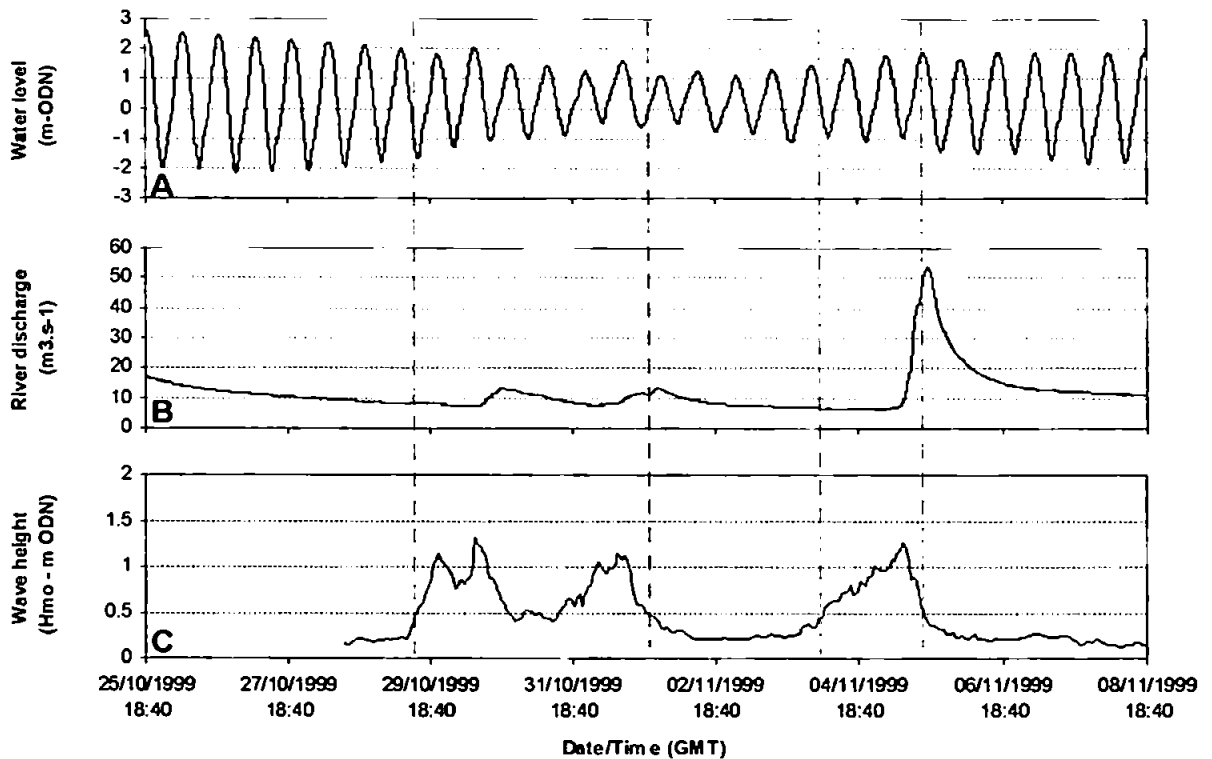


Figure 4.6: Water level (A), river discharge (B) and wave height (C) for hydrodynamic validation period. Although waves are not considered in these simulations, they are shown for illustrative purposes. Dashed vertical lines delimit periods of wave heights $\geq 0.5 \text{ m}$ (ODN).

The overall model performance during the validation tests ($\text{RMAE}=0.72$ and $\text{ARMAE}=0.27$, Table 4.6) is slightly better than the error estimates for the calibration period. ($\text{RMAE}=0.78$ and $\text{ARMAE}=0.33$, Table 4.5). Since waves are not modelled in these tests either, this decrease in the model skill may be due to the passage of the biggest storm of the main COAST3D field campaign in Teignmouth during the calibration period. In general terms, modelling is more accurate closer to the areas of tidal dominance, i.e. the estuary mouth.

It is also seen that the modelled output is classified as having a 'poor' quality (Table 4.6), according to the classification of van Rijn et al. (2003), if the instrument errors are not taken out of the statistics (by the use of RMAE). If these errors - which were estimated by van Rijn et al. (2000) to be on average 0.05 m.s^{-1} - are removed by the application of the ARMAE, then the model performance is considerably improved. The overall model skill is then considered as 'good' by the classification proposed by Sutherland et al. (2004a).

Table 4.6: Model performance for hydrodynamic validation period. Statistical errors below are calculated based on the average RMAE and ARMAE of corresponding U and V velocity components. RMAE qualification ranges are based on van Rijn et al. (2003) while ARMAE categorisation is based on Sutherland et al. (2004a).

	$\langle X \rangle$ (m.s^{-1})	$\langle Y \rangle$ (m.s^{-1})	MAE (m.s^{-1})	RMAE	RMAE qualification	ARMAE	ARMAE qualification
Water level							
Pier	0.978	0.978	0.011	0.01	Excellent	0.0001	N/A
Harbour	0.947	0.929	0.059	0.06	Good	0.02	N/A
Average	0.963	0.953	0.035	0.04	Good	0.01	N/A
Current							
Site 5	0.058	0.022	0.052	0.90	Poor	0.27	Good
Site 9	0.051	0.030	0.045	0.90	Poor	0.25	Good
Site 14	0.098	0.068	0.071	0.73	Poor	0.35	Good
Site 24	0.094	0.096	0.069	0.73	Poor	0.32	Good
Site 25	0.261	0.286	0.092	0.36	Good	0.18	Excellent
Average	0.112	0.100	0.066	0.72	Poor	0.27	Good

As expected, there is close agreement between the modelled and observed water level at the pier, since the observed data at this site are applied as the offshore boundary (Figure 4.7). For the harbour, the residuals (observations minus model output) in water level are very variable throughout the validation period, attaining differences larger than 10 cm at certain periods. After the storm of 01/11/99, the average water level residue increases to around 15 cm. Nevertheless, the resultant RMAE is classified as 'good' by categorisation proposed by van Rijn et al. (2003).

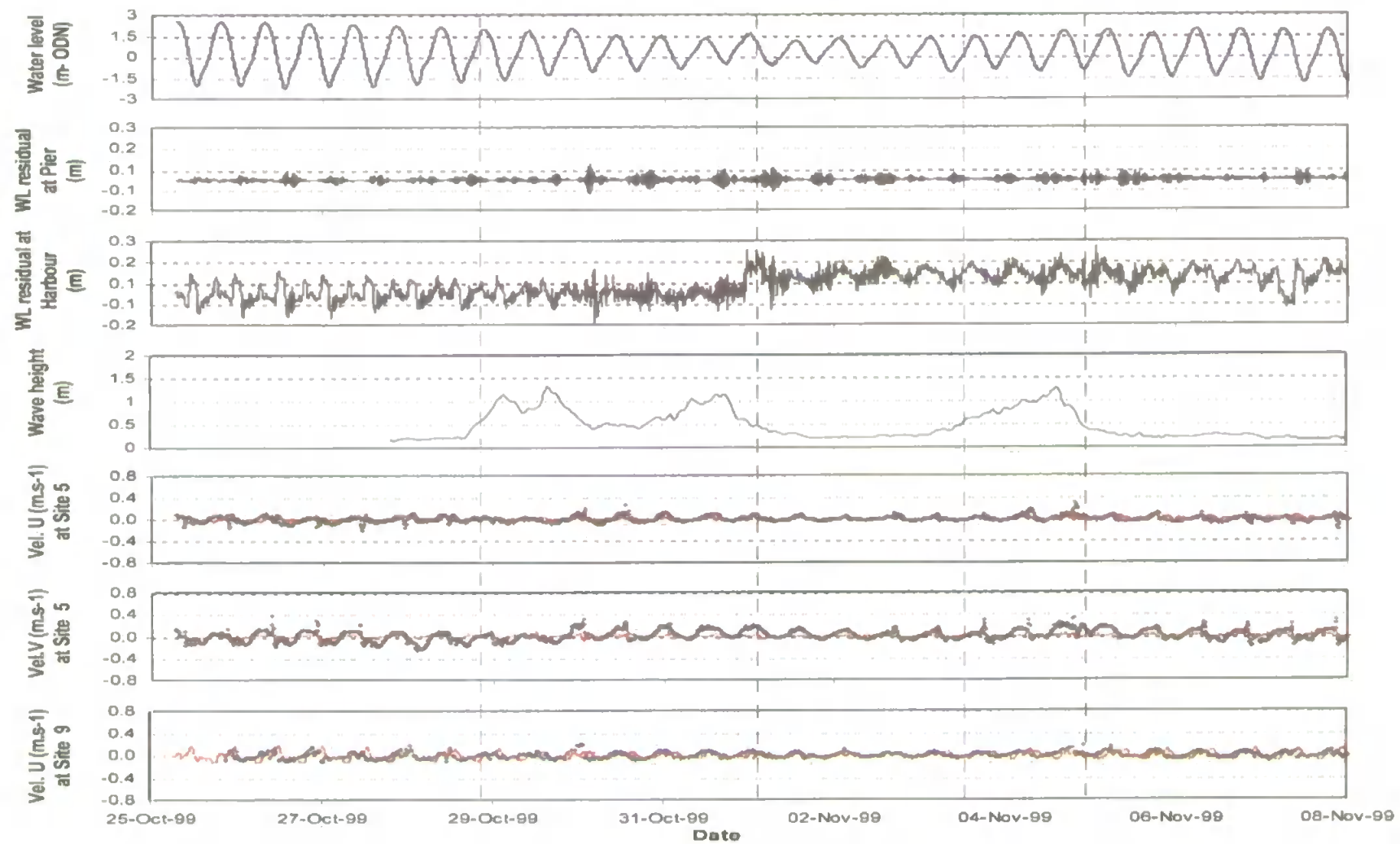


Figure 4.7: Observed and predicted water levels and currents during the validation period. Field data are represented by black crosses, while red dotted line corresponds to model output. Dashed vertical lines delimit periods of wave heights ≥ 0.5 m (ODN). For more information on the location of the sites, the reader is referred to Figure 3.6.

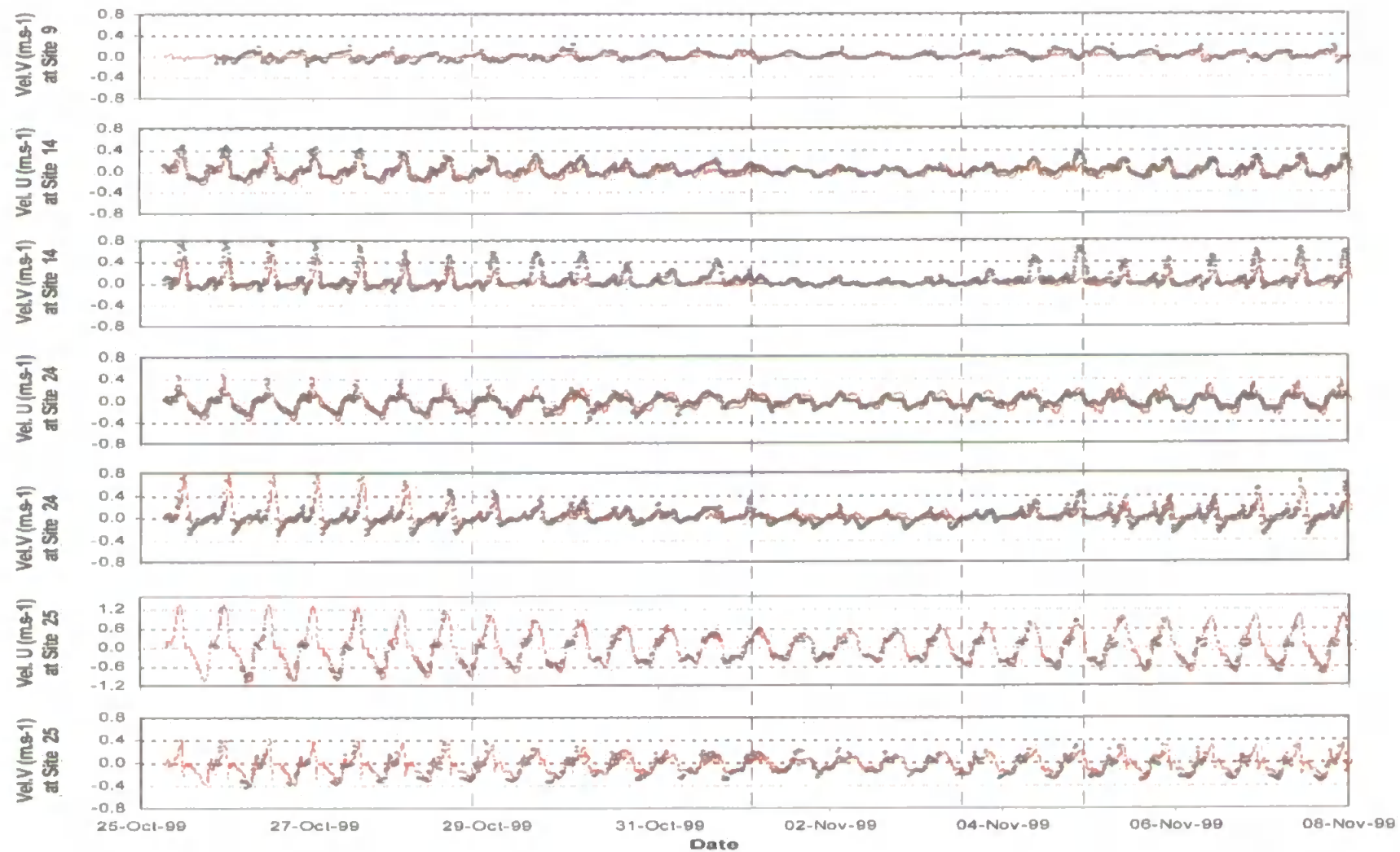


Figure 4.7, *Continued*: Observed and predicted currents during the validation period. Field data are represented by black crosses, while red dotted line corresponds to model output. Dashed vertical lines delimit periods of wave heights ≥ 0.5 m (ODN). For more information on the location of the sites, the reader is referred to Figure 3.6.

Regarding the current structure, the effects of the storms observed during this period are observed at the longshore velocity component at site 5, where prior to the storm presence, a northward longshore current was recorded. The current then turns to the south during the storm. Neither of these flow shifts is captured by the model, presumably due to the absence of longshore currents (lateral offshore boundaries are closed; Section 4.2.3) and of wave-driven currents in the model set-up. While the cross-shore flow structure at sites 14 and 24 are relatively well reproduced by the model, the observed longshore currents are underestimated by the model. In the case of site 14, northward currents are modelled, but not with the observed intensity. At site 24, the model is unable to predict the flood currents approaching the estuary. These southward features in the observed data seem to be offset by the storm fronts. Although based on sparser data measurements, the model skill to predict the flow structure at site 25 is shown to be 'good' to 'excellent', both in terms of direction and magnitude (note change in scale).

4.4. Morphodynamic calibration

In recent years, the use of morphodynamic models to study coastal processes has served as a very important tool in developing this research field, despite the limitations still involved, such as the lack of: i) high-resolution field data sets for calibrating and validating such models and ii) comprehensive understanding of coastal processes and their inherent interactions. As mentioned in section 4.1, in this study the morphological module (Sisyphe) is applied in a coupled mode to Telemac-2D in order to provide morphodynamic insights into the bed evolution of the Teign estuary.

Depending on the selected sediment transport formulation, Sisyphe computes either bed-load transport (Meyer-Peter and Muller, 1948; Einstein, 1950; Engelund and Hansen, 1967) or total transport (Bijker, 1968; van Rijn, 1984a,b, adapted by Soulsby, 1997; Bailard, 1981; Dibajnia and Watanabe, 1992) induced by current-borne and by wave-borne flows (Masson and Machet, 2002). Given that these transport functions were conceived to represent specific processes in aquatic systems (e.g. Bailard approach was designed to

represent cross-shore wave-induced sediment transport), the formulae of Meyer-Peter and Muller (1948), Einstein (1950), Engelund and Hansen (1967), Bijker (1968), van Rijn (1984a,b), adapted by Soulsby (1997) were considered in this study. More details are given in Section 4.4.2.

If wave-driven flows are to be considered, the coupling between Telemac-2D and Sisyphe is not possible. Equilibrium conditions for the sediment transport are assumed; thus response lag effects^{4.3} - such as on the suspended-load transport - are neglected due to operational limitations in the model release (5.3; Appendix 1) considered in this study. On the cutting edge of the modelling of mixed grain sizes in coastal systems, Sisyphe deals with up to 10 different grain-size classes in the range of 0.1 to 4 mm, with vertical stratification of the bed. The mixed grain size treatment is later shown to be important in understanding the morphodynamics of the complex grain-size patterns of the Teign estuary.

The instantaneous sediment flow rate is highly dependent on the current velocity. Therefore, errors in the flow field modelling will be amplified on the estimates of the residual currents (which are also very sensitive to offsets and bias in the velocity field), in the sediment transport rates and - ultimately - in the resulting bed evolution. As an example, Masson and Machet (2002) mention thus for the bed-load formulae an increase of about 10% on the current field would result in an increase of 30% in the transport rate for the Meyer-Peter and Muller formula, 60% for the Engelund-Hansen's and almost 80% for the formulation of Einstein. They also state the average transport will be highly influenced by the stronger currents and will not be directly related to the mean current. Soulsby (1997) estimates the accuracy of total load sediment transport as being larger than a factor of 5 in 70% of coastal applications.

The coupling is then run up to a point where a critical evolution ratio, the ratio between the bed evolution at a point and the respective water depth, as proposed in Villaret (2004) is reached, where the flow field is no longer valid. Under these conditions, the simulation is stopped and restarted with an updated bathymetry. The critical evolution ratio of 0.1 is the recommended value (Villaret, 2004), as it means the flow description at a given point

^{4.3} For further reference on lag effects, the reader is referred to Dyer (1994).

would still be valid until the local bed evolution is equivalent to 10% of the local water depth. For the Teign estuary, the areas which more frequently achieved the critical evolution ratio are located at very shallow water depths (order of a few centimetres). In order to avoid too many frequent stops to the simulation process, a critical evolution ratio of 1 is assumed hereafter.

The choice on the morphological boundary condition - especially the offshore one - is essential in determining the morphodynamic response of estuaries (Hibma et al., 2003a). In this study, the following time-invariant conditions are implemented throughout: at the river boundary, a fixed bottom depth is imposed, whereas for the oceanic boundary a free evolution boundary is allowed.

In a similar way to the hydrodynamic calibration, statistical methods to assess the performance of the morphodynamic model predictions are considered in this section. The description of these tools is followed by the calibration period (which includes a sensitivity analysis of the main parameters of the morphological module), where the difficulties and drawbacks of adjusting and validating the model to reality are highlighted.

4.4.1. Statistical tools in morphodynamic modelling

The result of a morphodynamic modelling, by definition, is the result of complex hydrodynamic and morphological interactions. Thus, its performance depends on the accuracy of several steps: i) well-estimated water level distribution; ii) a consistent hydrodynamic pattern determination; iii) a reliable sediment transport rates modelling; iv) a robust description of the feedback mechanisms between hydrodynamic and morphological processes and v) arriving at an accurate morphodynamic features observed in the field.

In order to assess a model behaviour under such conditions, Brady and Sutherland (2001) and Sutherland et al. (2001b) adapted from meteorology the use of the Brier Skill Score (BSS), where the skill is a measure of the accuracy of a prediction relative to the accuracy of a baseline prediction. Since then, many authors (e.g. van Rijn et al., 2002; van Rijn et

al., 2003; Siegle, 2003; Sutherland and Soulsby, 2003 and Sutherland et al., 2004a and 2004b) have estimated the performance of morphodynamic models through the application of BSS. The description that follows is based on Sutherland et al. (2001b) and Sutherland et al. (2004a).

Let X and Y be sets of N bed levels respectively observed and predicted at the end of the period to be modelled. Let B be a set of N bed levels that serve as a baseline prediction of the bed level at the end of the period to be modelled. The n th points in sets X , Y and B must occur at the same position. A model's performance can be judged by calculating its BSS:

$$BSS = 1 - \frac{\langle (Y - X)^2 \rangle}{\langle (B - X)^2 \rangle} \quad (4.7)$$

Higher values of the BSS indicate improved predictions (opposite to the interpretation of the RMAE and ARMAE). Modelling the baseline condition gives a BSS=0, and perfect agreement gives a value of 1. If the model is further away from the final measured condition than the baseline prediction, the skill score is negative. The BSS is unbounded at its lower limits. An advantage of the BSS is that, in principle, it is not altered by the inclusion of an inactive area in the model. If such a region is included, neither the measured or model results change in this region, then the BSS remains unaltered. This would not be the case of simple correlation coefficients between predicted and measured final bathymetries (such as linear or rank order correlation), which would increase due to the inclusion of an inactive area. Their value would depend on how large an inactive area is included in the modelling domain.

However, if measurement errors are taken into account, then the BSS will be dependent on them, regardless of being or not being in an inactive area. Taking the example of the COAST3D bathymetric surveys, the estimated observational error was 0.1 m (for depths shallower than 10 m) under wave heights up to 0.2 m (van Rijn et al., 2000). That implies that, even in an inactive area, where no bed level changes take place, measurement errors will be associated with bed differences between two consecutive surveys. Although Sutherland et al. (2001b) propose a methodology for removing the effects of measurement errors, it is not applied in this study due to difficulties in determining their values. The BSS

can be very sensitive to small changes when the denominator is low, which is a problem found in other non-dimensional skill scores derived from the ratio of two numbers.

This skill score was reduced by Murphy and Epstein (1989) for errors in the prediction of amplitude, phase and mean (Sutherland et al., 2001b). Further details on this technique are found in Livezey et al. (1996). The BSS can be decomposed in terms of anomalies in the prediction ($Y' = Y - B$) and in the measurements ($X' = X - B$). The variance in predicted and observed anomalies are given by $\sigma^2_{X'} = \langle X'^2 \rangle - \langle X' \rangle^2$ and $\sigma^2_{Y'} = \langle Y'^2 \rangle - \langle Y' \rangle^2$ and the covariance between the anomalies is $S_{Y',X'} = \langle Y' X' \rangle - \langle Y' \rangle \langle X' \rangle$. The linear correlation between the anomalies in predicted and observed sets is the anomaly correlation coefficient ($r_{X'Y'}$) given by:

$$r_{X'Y'} = \frac{S_{X'Y'}}{\sigma_{X'} \sigma_{Y'}} \quad (4.8)$$

Then Murphy and Epstein (1989) decomposition shows that it can be written as:

$$BSS = \frac{A - B - C + D}{1 + D} \quad (4.9)$$

where:

$$A = r^2_{Y'X'} \quad (4.10)$$

$$B = \left(r_{Y'X'} - \frac{\sigma_{Y'}}{\sigma_{X'}} \right)^2 \quad (4.11)$$

$$C = \left(\frac{\langle Y' \rangle - \langle X' \rangle}{\sigma_{X'}} \right)^2 \quad (4.12)$$

$$D = \left(\frac{\langle X' \rangle}{\sigma_{X'}} \right)^2 \quad (4.13)$$

with:

A = a measure of the phase error, i.e., when the sediment is moved to the wrong position;

B = measure of amplitude error, i.e., when the wrong volume of sediment is moved;

C = a measure of the map mean error, i.e., when the predicted average bed level is different from the measured;

D = normalisation term.

The higher A and D are, the better the final BSS will be, whereas higher values of B and C will mean a decrease in the overall model skill. Regarding the qualification of BSS results, Sutherland et al. (2001b) suggest as a first approach that a BSS bigger than 0.2 would represent a useful forecast. However, they highlight this value may be inappropriate and a suitable level may eventually emerge from experience. Van Rijn et al. (2003) propose a table for error qualification when using the BSS (Table 4.7) and point out that one of the limitations of the BSS is that it cannot account for the migration direction of a bar. However, there are many advantages of the BSS over other accuracy measures and even relative to other skill scores (Sutherland et al., 2004b). As shown in section 4.2.2, the BSS can also be used to determine the skill of a given mesh in representing observed bed features.

Table 4.7: Qualification of BSS error ranges for morphodynamic studies (van Rijn et al., 2003).

<i>Qualification</i>	<i>BSS</i>
Excellent	1.0 - 0.8
Good	0.8 - 0.6
Reasonable / Fair	0.6 - 0.3
Poor	0.3 - 0
Bad	< 0

4.4.2. Morphodynamic calibration set-up

The complexity of using a morphodynamic model is proportional to its simulation time. To simulate the same 14 days, the purely hydrodynamic run takes about 15 hours (section 4.3.2). With the inclusion of the sediment transport and bed evolution module, time is an issue: the simulation takes about 6 or 7 times^{4.4} longer to estimate the morphodynamic result, due to the file exchange between the two modules. Thus, the sensitivity analysis for the key parameters in the morphological module is presented in Table 4.8 for a period of two days under spring tides: from 25/10/99 to 27/10/99. The initial conditions are detailed in Figure 4.6, while the hydrodynamic parameters follow the calibration period set-up (Table 4.3).

For the sake of calculating the BSS, the baseline condition is the COAST3D survey 1 (i.e. the simulation is initialised with the bathymetry measured during COAST3D survey 1), carried out around 25/10/99. The final or target condition corresponds to COAST3D survey 2, which took place around 08/11/99. Thus, the closer the predicted bed evolution is to the bathymetry data gathered during survey 2, the higher the BSS. Since the estimation of BSS requires the points to be compared at the same position, both the initial and final conditions and the modelled bathymetry are interpolated into a regular grid. As seen in Table 4.8, all the results present a negative BSS, meaning the modelled bathymetry is further away from the baseline condition (COAST3D survey 1). As the objective of the

^{4.4} Not considering the fact the simulation could reach the critical evolution ratio and stop while the user is away from the laboratory (e.g. night periods), which would increase the simulation time even further.

sensitivity analysis is to assess the model response to different parameters, the model performance against observed features is formally assessed in the calibration period, later in this section.

Two parameters in Table 4.8 are explained in further detail: the slope bed effect and the porosity influence. Taking into account the effects of the bed slope increases the sediment transport in the downslope direction. Its effect is similar to adding a diffusion term in the bed-evolution equation, as it tends to smooth the results and reduce instabilities (Villaret, 2004). Also, it does not include the effect of friction angle and is only applicable to gentle slopes. A correction factor to both magnitude and direction of the solid transport rate is applied before solving the bed-evolution equation. The formulation is based on Koch and Flokstra (1981):

$$S_L = \left(1 - \beta \frac{\partial Z_f}{\partial s_c} \right) \quad (4.14)$$

where Z_f is the bed elevation, s_c is the current direction coordinate and β is an empirical factor ($\beta=1.3$). In the sensitivity analysis below, the value of β is tested. The change in direction of solid transport is given by:

$$\tan \alpha = \tan \delta - \beta \frac{\partial Z_f}{\partial n_f} \quad (4.15)$$

where α is the direction of solid transport in relation to the flow direction, δ is the direction of bottom stress in relation to the flow direction and n_f is the coordinate along the axis perpendicular to the flow.

The coefficient function of porosity (P_c) also influences the sediment transport rate through the following formulation:

$$P_c = \frac{1}{1 - p} \quad (4.16)$$

where p is the porosity and the default value for P_C is 1 (no porosity effects).

The analysis on Table 4.8 shows that, if the van Rijn et al. (2003) classification for the BSS is taken into account, then all the results in the sensitivity runs are 'bad'. However, for the moment, the use of the BSS will help understand the relative influence of different parameters in the model sensitivity. The model skill to reproduce realistic patterns will be discussed in the morphodynamic calibration section. Bearing this in mind, the biggest model sensitivity is due to the choice of the grain size and to the sediment transport formula. Regarding the grain size, the finer the sediment, the more intensive the morphodynamic activity will be. However, the choice of the grain size is relatively simpler, since it can be based on observed data, which is not the case for selecting the most appropriate sediment transport formula.

Table 4.8: Sediment transport module sensitivity to key parameters during a period of 2 days of COAST3D project. Values in bold are the selected ones for the calibration of the morphological module.

<i>Parameter</i>	<i>Values tested</i>	<i>BSS</i>
Sediment transport formula	Meyer-Peter and Muller (1948)	-0.29
	Einstein (1950)	-0.43
	Engelund and Hansen (1967)	-1.05
	Bijker (1968; b=2)	-0.27
	Soulsby (1997)	-0.31
Grain size (mm)	Single size: 0.25	-2.97
	Single size: 0.6	-1.29
	Single size: 1.2	-0.44
	Single size: 2.5	-0.29
	Multiple sizes: from 0.0335 to 34 mm	-0.03
Slope effect (β)	0	-0.27
	0.6	-0.27
	1.3	-0.29
	2.4	-0.28
Coefficient function of porosity (P_C)	1	-0.27
	1.6	-0.29
	2.5	-0.28
Shields parameter	0.02	-0.29
	0.047	-0.29
	0.08	-0.27
Inclusion of waves (stirring effect only)	Yes	-0.28
	No	-0.29

As mentioned earlier in the section 4.4, the sediment transport rate will be very dependent on the flow field. It is also true that for similar hydrodynamic conditions (such as the one used for this sensitivity analysis), the morphological outcome can be quite different - especially on the volume of sediment moved around - depending on the sediment transport formulation chosen. For the period modelled, as expected, the morphodynamic evolution is dependent on the sediment transport formulation. Among some of the most used sediment transport functions for estimating either bed-load transport or total transport, the best performances (i.e. highest BSS) come from the formulae of Meyer-Peter and Muller (1948), Bijker (1968) and the adapted version of van Rijn's formula (1984a and b) by Soulsby (1997).

It has long been acknowledged there is no 'perfect' sediment transport formulation, with each of them being applicable to a limited range of conditions, especially under the combined effects of waves and tides and on irregular bottom features (Komar, 1996 and van de Kreeke, 1996). Wu et al. (2004) claim that sediment transport formulation based on the median grain size distribution (such as Engelund-Hansen's) will tend to underestimate the sediment transport rates. As a first approach to the morphodynamics of the Teign estuary, Bijker's (1968) formula is selected for the following tests based on the advantages of taking into account the stirring effect of waves (i.e. enhancement of the bed shear stress due to the wave influence) and not being limited to coarser grains, such as Meyer-Peter and Muller (1948) set of equations (which is limited to grains coarser than 1 mm). On the other hand, Camenen and Larroude (2003) point out that Bijker's formulation overestimates the sediment flux of finer sediments and that it should not be applied to grains coarser than 1 mm. The reasons for not choosing Soulsby's (1997) formulation are due to its greater sensitivity to variations in the current field (which indirectly increases the computational time through more frequent flow updates) and to the fact that wave-driven currents are not taken into account in the morphodynamic set of models used in this study.

In order to standardise the bed friction coefficients between the hydrodynamic and the morphological modules, the same values applied for the depth-dependent bottom friction (Table 4.4) are also used in this section. If a single grain size (until recently the only option within the morphological module) is to be assumed for the whole domain in such a variable grain-size site, a medium sand ($D_{50}=0.3$ mm) seems to be a reasonable choice especially for studying the outer estuary and adjacent coastal area. With the

implementation of a multiple grain size approach in the morphological module, much more realistic patterns of sediment distribution can be defined (Figure 3.7). Areas outside the sampling zone are defined to have a spatially constant distribution, where the fine sands fraction predominates (95%). The remaining concentration of 5% is composed of silts and clays. It is shown in Table 4.8 the considerable improvement in the modelling performance (BSS= -0.03) when taking into account a multiple grain-size approach, being the single most important factor in improving the BSS. Under conditions of heterogeneous grain sizes, a hiding factor is applied, since bigger particles are more exposed to the flow than smaller particles, which will tend to be accommodated at the void space. This effect is considered in Sisyphé by the formulation of Karim and Kennedy (1982), which directly modifies the sediment transport rate. Wu (2004) added that hiding effects have a significant effect on the bed material sorting and armouring processes.

As described at the beginning of Section 4.4, the morphological module accounts for up to 10 different grain-size classes in the range of 0.1 to 4 mm. However, as seen in Chapter 3 and in Table 4.8, the observed grain-size distribution is broader than these limits, with the *silts + clays* ($D_{50}= 0.0335$ mm) and the *gravels* ($D_{50}= 34$ mm) classes lying outside the recommended grain size range of the morphological module. Although some care must be taken especially when interpreting the results of very fine sediments such as silts and clays, the model results can serve as a first approach to the modelling of such sediments, since many inherent processes are not accounted for (e.g. cohesion properties). Thus, this limitation must be born in mind when assessing the morphodynamic results of multiple grain-sizes.

In a very complex bathymetry such as for the Teign estuary and coastal area, the slope effect might be very important. Since the model sensitivity to a range of these parameters is not pronounced, the value of 1.3 is selected for further tests, based on de Vriend (1981). The effects of varying the coefficient function of bed porosity were very small. Considering the heterogeneity of grain sizes in the area, porosity might play a role in the sediment dynamics. Thus, a coefficient function of porosity of 1.6 is considered in the next tests. The Shields parameter is used to determine the critical bed shear stress, i.e. the threshold of sediment transport under a given set of conditions. During these tests, the variation of the Shields parameter did not cause major changes in the modelled result. Finally, since the effect of waves is known to be important on the morphodynamics of the

adjacent coastal area, a recently introduced parameterisation of wave effects on the sediment transport rates is also included in the following tests. Under these circumstances, the stirring wave effect is estimated to act on the same direction of the mean current (Villaret, 2004).

The calibration period for the morphodynamic runs is 3 days longer than the one used for the hydrodynamic calibration (Figure 4.4). It starts at 08/11/1999, coinciding with the end of COAST3D bathymetric survey 2, and finishes at 25/11/1999, after the completion the COAST3D survey 4. Due to the complexities involved in the morphodynamic modelling, three different set-ups are tested for the calibration period: i) single grain-size of 0.3 mm without waves as a stirring agent; ii) multiple grain sizes without stirring effects from waves and iii) multiple grain sizes with waves as a stirring agent. Results are shown in Figure 4.8.

The observed bed evolution patterns (Figure 4.8.A) illustrate the mobility of bedforms during the spring-neap cycle considered. The most distinctive patterns are the sediment deposition at the Ness sandbar (physiographic features defined in Figure 3.1) between -3 m and -4 m (ODN) and the onshore migration of the ebb shoal (Figure 4.8.A). At least this latter feature was probably influenced by wave action, due to the two storms (with significant wave heights of up to 1 m) observed for the period (Figure 4.6.C).

The absence of wave-driven currents in all three modelling exercises seems to be the main reason for the rather poor (visual disagreement and negative BSS) model skill to predict observed bed evolution. The inclusion of mixed grain-sizes, however, triggers considerable differences in the morphodynamic output. For the single-grain size case ($D_{50} = 0.3$ mm; Figure 4.8.B), the modelled tidal currents are responsible for flushing sediment out of the estuary, with major erosion spots on both sides of the main channel, while the depositional areas have a widespread distribution and higher concentrations at the end of the Ness sandbar. Meanwhile, the ebb shoal is predicted to erode slightly on its upper areas, while some marginal deposition is modelled.

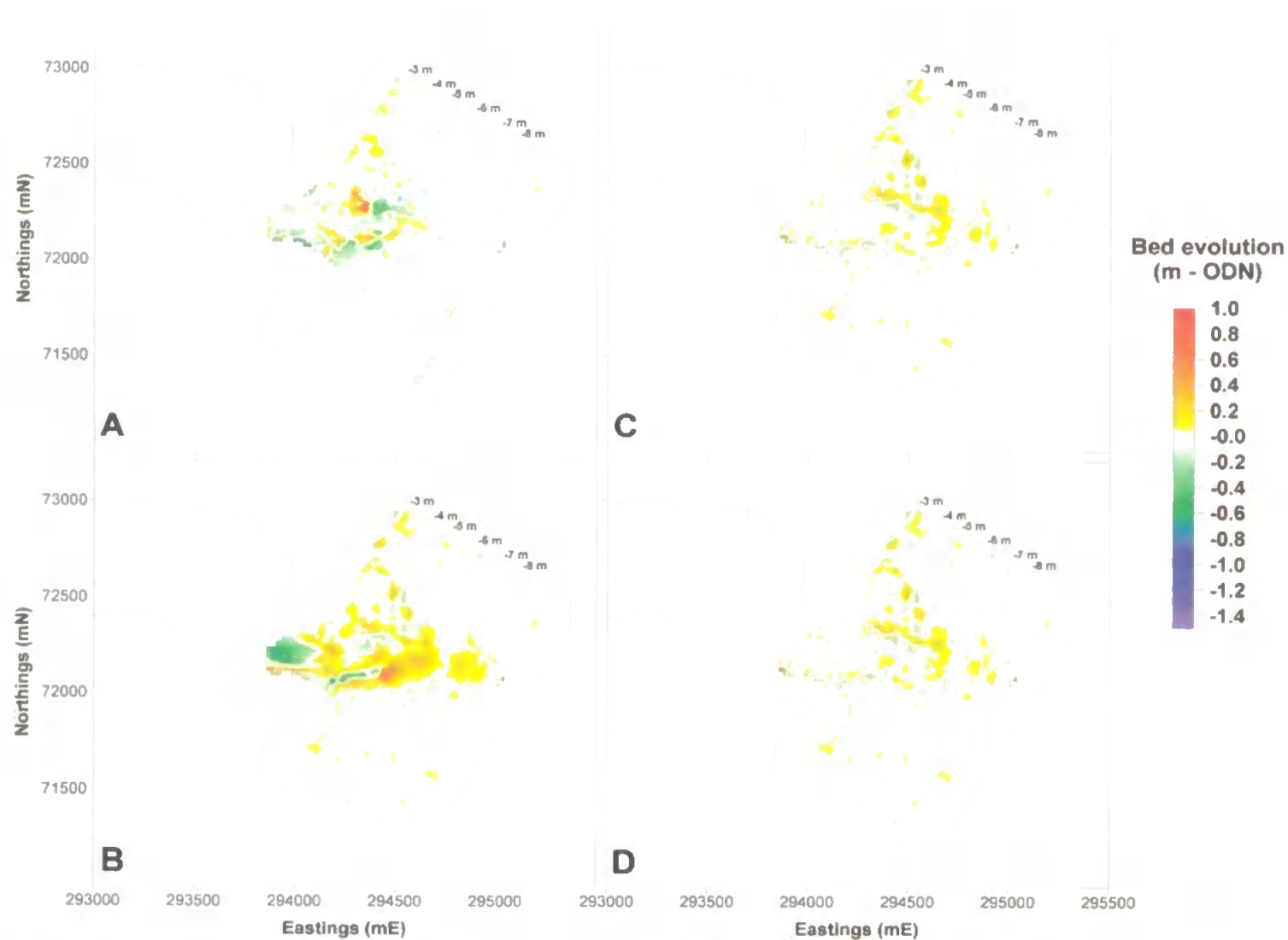


Figure 4.8: Bed evolution between COAST3D surveys 2 and 4. Observed bed evolution (A); Model result considering single-grain-size of 0.3 mm and no waves (B; BSS= -0.33); Multiple grain-sizes without waves as a stirring agent (C; BSS= -0.11) and multiple grain-sizes with stirring effect of waves (D; BSS= -0.11). Contour bed level intervals are of 1 m (ODN) and correspond to COAST3D bathymetric survey 2.

Although a net deposition is predicted, the inclusion of the multiple grain-size distribution is responsible for considerably decreasing the amount of sediment transported (Figures 4.8.C and D). This is mainly due to the fact the outer estuary and the adjacent coastal area are basically composed of sediments coarser than 0.3 mm, hence decreasing the efficiency of sediment transport mechanisms and the correspondent bed evolution. Under only the effects of tidal actions, the ebb shoal is again predicted to have its higher areas eroded, with some deposition along its northern flank. The effect of waves as a stirring agent is not very evident, given the qualitative and quantitative similarity between the cases with and without the stirring effect (Figures 4.8.C and D). The main bed evolution differences between these two runs are found in the estuary mouth (not shown due to absence of observed data in the area). The overall sediment balance for the case without wave effects corresponds to an export of sediment of the order of 230 m^3 of sediment, while a sediment import an order of magnitude higher (around 2400 m^3) is predicted for the case with the stirring effect of waves. Since the imported grains are mainly made of fine sediments, their effects on the bed morphology are minimised. This preliminary finding might corroborate the hypotheses of Nunny (1980) and Wells (2002a) regarding the importance of suspension effects in the import of fine sediments into the estuary.

Given the operational conditions to date, whereby the inclusion of wave generated currents is not yet available to the coupling between Telemac-2D and Sisyphe, the modelling exercise is unable to satisfactorily predict the complex bed morphology patterns observed at the adjacent coastal area to the Teign estuary. The extension of bathymetric surveys to the outer estuary area within the frame of the CoastView project might help exploring in more detail the model skill to encapsulate the main morphodynamic processes in this area, which, according to Nunny (1980) and Wells (2002a), is sheltered from direct offshore wave action. In order to improve the understanding of longer-term morphodynamic evolution of estuaries, one of the main objectives of this study, and to apply the 6-month frequency bathymetric surveys of the CoastView project, ways of decreasing the simulation times for such periods are required. This is because modelling longer-term morphodynamic evolution with process-based models (such as the one proposed in this study) is a very time consuming task. The accumulation of errors generated in shorter time scales is another problem of such approach. In Chapter 5, some methodologies to minimise

these drawbacks are discussed. The model skill in reproducing longer-term morphodynamic evolution is then assessed.

4.5. Conclusions

The application of the numerical model Telemac-2D, coupled to the sediment transport and bed evolution module Sisyphe, is carried out for the Teign estuary and adjacent coastal area. The COAST3D project database is used to calibrate and validate the model, especially at the adjacent coastal area, the main focus of that project.

Robust statistical tools are also considered for assessing the model ability. For the hydrodynamics results, the Relative Mean Absolute Error (RMAE; Sutherland et al., 2001b; van Rijn et al., 2003 and Sutherland et al., 2004a among others) is applied. For the morphodynamic evolution, the Brier Skill Score (BSS; Brady and Sutherland, 2001 and Sutherland et al., 2001b among others) is chosen.

The hydrodynamic calibration and validation are carried out with a reasonable performance. When compared to similar studies in the Teignmouth area using the COAST3D data, the model ability in reproducing the main hydrodynamic results are in the same quality range. Wave generated currents are not taken into account in the modelling exercise due to an operational limitation of the model. Hence, the modelling of nearshore processes in the area is limited and has a direct effect on the predictability of the morphodynamic evolution.

Given the non-linear dependence of the sediment transport estimates on the underlying hydrodynamic processes, the modelled bed evolution patterns are very limited in reproducing observed features at the coastal area. The inclusion of the multiple grain size distribution has an impact on the morphodynamic modelling of the complex and variable grain sorting characteristics at the Teign estuary and adjacencies. The application of a schematised stirring effect of waves to the morphodynamic calibration period is seen to act as a trigger for the import of fine sediments into the estuary, corroborating the findings of Nunny (1980) and Wells (2002a). Further investigation is required in order to determine the transport mechanisms responsible for such a result.

Chapter 5 - Ensemble Technique

5.1. Introduction

The prediction of medium and long-term coastal morphodynamic behaviour is an increasingly important issue in coastal engineering (Southgate, 1995). Compared to the morphodynamic behaviour of uninterrupted coastlines and rivers, the morphodynamic behaviour of tidal basins, such as estuaries and tidal lagoons, is a degree more complex and less well understood (Stive and Wang, 2003). The interaction between morphodynamic processes of different time and spatial scales often leads to non-linear relations (e.g. the non-linear dependence of sediment transport formulae on hydrodynamics), which can be unpredictable. Thus, in order to simulate a longer-term trend in a coastal system, a process-based model is usually driven by short-term (seconds to days) hydrodynamic events. Even if the computation time is not an issue, the final outcome may not be representative of realistic conditions, since processes which are negligible at the smaller scale can have significant long-term effects and vice-versa (de Vriend et al., 1993).

As discussed in Section 2.4, despite the difficulties in understanding the relative importance of coastal processes in different time scales, many advances in this field have been made in recent years (for examples, see Steijn et al., 1992; Villaret and Latteux, 1992; de Vriend et al., 1993; Latteux, 1995; Southgate, 1995; Cayocca, 2001; Roelvink et al., 2001; Fortunato and Oliveira, 2002; Lanzoni and Seminara, 2002; Hibma et al., 2003b; Stive and Wang, 2003; Hibma et al., 2004a). One of the most used approaches to longer-term simulations is through schematising the forcing conditions, either by the concept of input reduction, i.e. selecting a representative set of observed conditions or through 'process filtering', where short and medium time scale processes are averaged out, according to Southgate (1995). This author also observes the scarcity of suitable longer-term data in order to test and verify models. Villaret and Latteux (1992) add that modelling processes which are strongly dependent on chronology, such as the deposition processes of cohesive sediments, adds further complexity to morphodynamic predictions.

Since the principal purpose of this thesis is to study the morphodynamic evolution of the Teign estuary, the main forcing to have its input reduced is the tides. Contrary to other hydrodynamic forcings, which have a stochastic behaviour such as waves and wind, the astronomical tides are purely deterministic (Latteux, 1995). However, they are modulated by various cycles: spring-neap, yearly and nodal time scales, which makes a real-time representation of the tides computationally demanding; requiring some sort of input reduction (de Vriend et al., 1993).

An input reduction is considered to perform well if its final outcome is similar to the one based on the original data. Taking tides as an example, an input reduction approach must reproduce not only the mean hydrodynamics properties, but also the morphodynamic patterns of the original data set. Therefore, Latteux (1995) highlights several factors which must be considered in the input reduction technique: i) due to the strong non-linearities involved, the mean effect of the various input forcings is quite different from the effect of the mean value of these inputs; ii) chronology may play an important role, especially for stochastic events such as waves (Southgate, 1995) or when the system variability is more frequent than the period modelled and iii) long-term trends of the inputs have to be taken into account, although the magnitude of their variation is far weaker than the shorter term processes.

By studying tidal flows and techniques to model them in longer-term temporal scales, Latteux (1995) concludes that a single representative tide is only capable of adequately representing the residual patterns if the bed and coast topography are rather simple. On the other hand, if the bottom has strong 3D features - such as in Teignmouth - capable of distorting the flow field, then the tidal cycle has to be discretised under several tidal classes. When a single representative tide is sufficiently accurate to represent the original input, Latteux (1995) has found - by studying tidal inputs only - the idealised tide has to have a tidal range of 7% to 20% bigger than that of the mean tide. Likewise, Steijn (1992) reached similar conclusions by studying the input reduction of tides and waves. The percentage will be proportional to the threshold of motion selected and, above all, to the choice on the sediment transport equation (Latteux, 1995). Conversely, if the transport rates estimated for a given averaged tide is close to those of the original tidal data, then this tide is called a 'morphological tide'.

In this chapter an input reduction - called 'ensemble technique' hereafter - based on the findings of Latteux (1995) for tidal areas is developed. A period of 17 days and one of 6 months are modelled in order to test the technique performance. It is shown that some key factors must be taken into account in order to reduce associated errors.

5.2. Short-term (hours to days) application of the ensemble technique

The morphodynamic response from the coupling between Telemac-2D and Sisyphe to an input reduction technique is assessed based on observed data from COAST3D project. It spans the same period used for the morphodynamic calibration in Chapter 4; from 08/11/1999 to 25/11/1999 (Figure 4.5). The model set-up used in this chapter is shown in Table 5.1. Before assessing the model performance in predicting observed features, the spring-neap cycle is reduced through the ensemble technique. The modelled morphodynamic outcome is then compared against what is called the reference run, i.e. a complete simulation of the same period.

Table 5.1: Model set-up used for the studying the ensemble technique.

	<i>Parameter value</i>
Mesh used	C (Figure 4.3)
Hydrodynamic time step	5 seconds
Hydrodynamic coupling period	180 seconds
Hydrodynamic friction coefficient	Depth-dependent (Table 4.4)
Sediment transport time step	120 seconds
Sediment transport coupling period	1440 seconds (24 minutes)
Sediment transport friction coefficient	Depth-dependent (same values applied for hydrodynamic runs)
Sediment transport formula	Engelund and Hansen (1967)
Medium grain size	0.3 mm
Wetting and drying	Yes

From the observed data set (Figure 5.1.A), the continuous record is split at each consecutive high tide (Figure 5.1.B). Although some phase differences can be noted, this rather simple approach seems to be sufficiently robust. With all tides of the original record positioned at the same time frame, then average tides can be calculated through simple

arithmetic means (Figure 5.1.C). Hence, based on the input reduction concept, the goal is to encapsulate the properties of the observed tides as close to the original conditions as possible, such as their energy and their capacity of influencing the morphodynamic evolution of the area. Since the modelled results are output every 30 minutes, the resultant tidal period is then standardised to 12 hours and 30 minutes. The river discharge data is treated under the same procedure described above. Although not shown, it is likely that the morphodynamic effects of freshets will be smoothed in the averaging process. All runs described in this section are based on the same set-up parameters. The only difference between them relies on the method of computing the boundary conditions. Up to this point, no numerical simulation is used for defining the average tides.

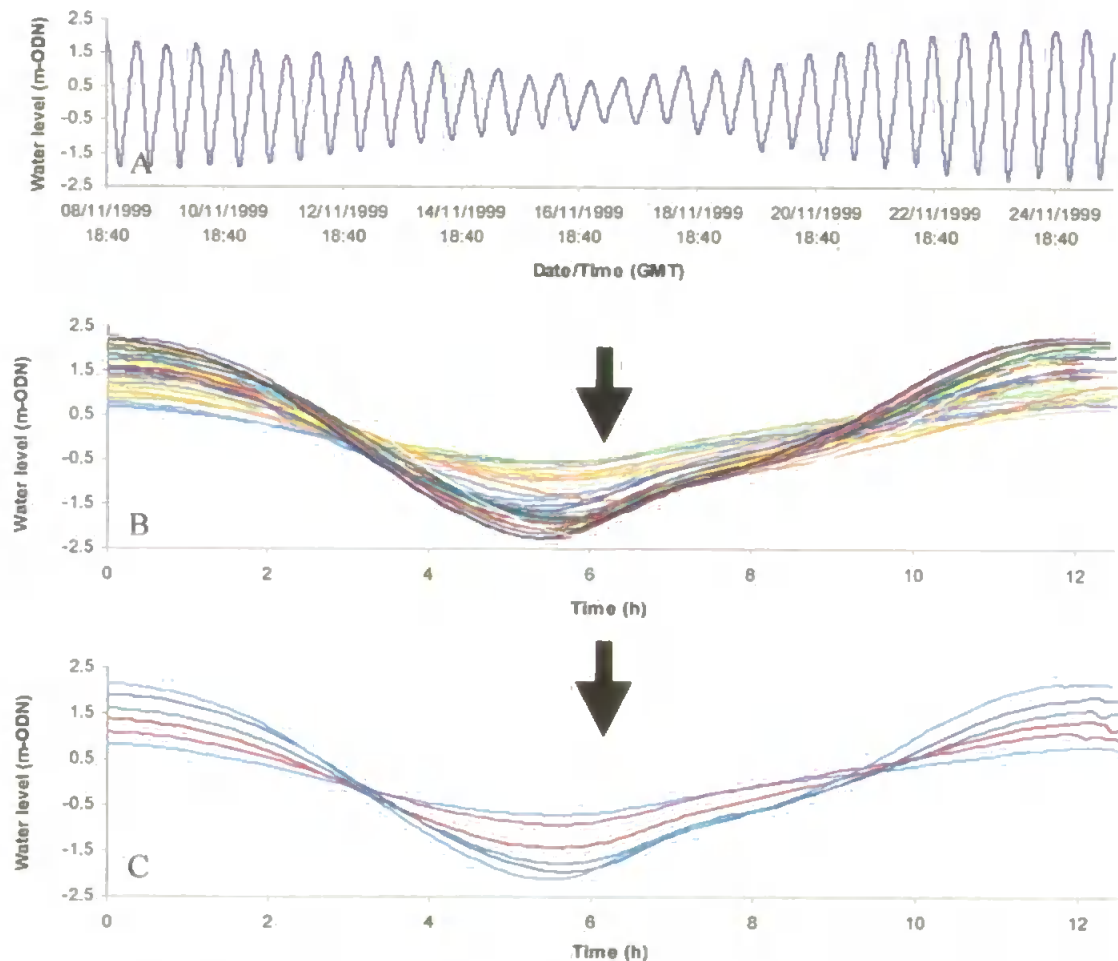


Figure 5.1: Input reduction of observed tides for a 17-day period. Original water level variation at the Pier (A); all 33 tidal cycles of the period (B) and the selected average tides according to the respective tidal range classification (C; bottom part of Table 5.2).

The following tests were conducted in order to investigate whether the spring-neap cycle morphodynamic evolution of the area can be encapsulated by a single representative tide. Thus, average tides are then created by two different criteria: i) by estimating an average neap tide, an average tide and an average spring tide or ii) by calculating average tides based on their tidal range (TR; Table 5.2). The respective frequency of occurrence of each average tide is also given in Table 5.2. Then, the model is run for a single tidal period, forced by each of the average tides and the respective average river discharge. The bed evolution at the end of each of these tests is then weighted by multiples of 4 between 1 and 32, as there are 33 tides altogether in the 17-day period. These values are chosen to determine the best (highest) BSS (Section 4.4.1) of each average tide. Hence, to check whether the product of the bed evolution of any of the average tides multiplied by a factor is able to represent satisfactorily the bed evolution estimated from the reference run.

Table 5.2: Classification of tides based on respective tidal range observed in the 17-day period and frequency of occurrence of each average tide.

<i>Frequency of occurrence (Number of tides considered in averaging process)</i>	
3 tidal ranges (TRs)	
Average neap tide (TR \leq 2.5 m)	11
Average tide	33
Average spring tide (TR \geq 2.5 m)	11
6 TRs	
TR \leq 2 m	5
2 m < TR \leq 2.5 m	6
2.5 m < TR \leq 3 m	6
3 m < TR \leq 3.5 m	5
3.5 m < TR \leq 4 m	5
TR > 4 m	6
Total number of tides	33

Figure 5.2 shows the model skill to reproduce the morphodynamic patterns of the reference run is directly proportional to the tidal range. For each average tide, the highest BSS were achieved by multiplying the corresponding bed evolution by a factor of 8. The exception is the TR > 4 m, where multiplying the respective bed evolution by a factor of 8 would mean an overestimation of the morphodynamic evolution and, thus, a decrease in the BSS. By taking into account the classification proposed by van Rijn et al. (2003), for whom a

reasonable BSS must be bigger than 0.3, then only tidal ranges above the "Average tide" (Figure 5.2) must be used as a single representative tide. The maximum BSS achieved by this method is given by the average spring tide, with a BSS of 0.39. Though, if an accurate longer-term methodology is to be proposed, these values of BSS are still rather low.

Nevertheless, as pointed out by Latteux (1995), in areas of irregular bottom such as the Teign estuary and its adjacent coast, a single representative tide may not be sufficient to accurately describe the local morphodynamic evolution. The combination of 2 representative tides (average spring tide + average tide) gives a BSS of 0.40, while the use of 3 average tides (average neap tide + average tide + average spring tide) results in a BSS of 0.39. Thus, it can be concluded the upper limit of this approach is reached, where not even the combination of more than one average tide is sufficient to improve the morphodynamic outcome any further, in disagreement with the findings of Latteux (1995). The sum of the morphodynamic evolution of all representative tides (starting from the same initial bathymetry) is also insufficient to deliver quantitatively reasonable results (BSS= -1.24; Figure 5.4.B).

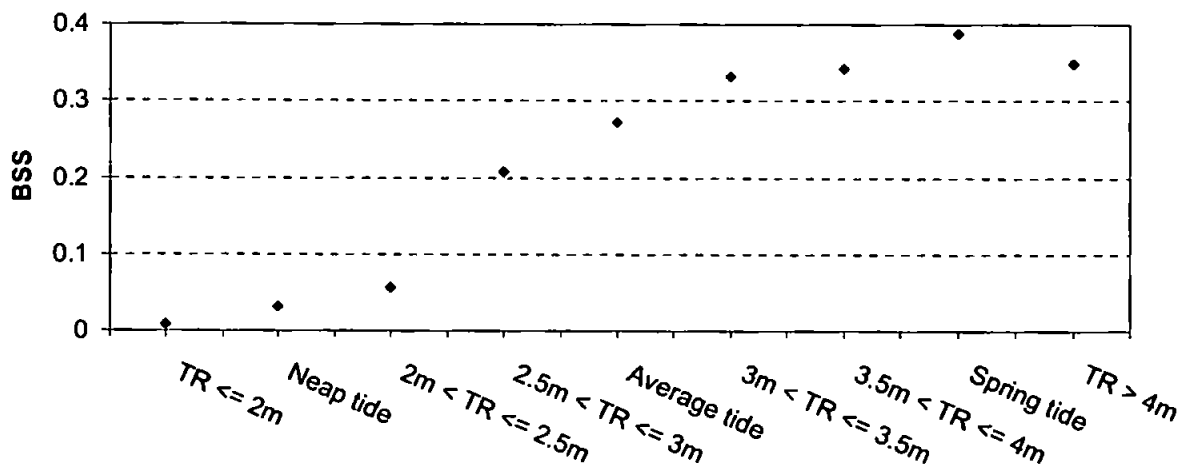


Figure 5.2: BSS distribution of different average tides in reproducing the morphodynamic result of the reference run for the short-term period of 17 days (08/11/99 to 25/11/99).

A second approach is considered by implying a cumulative effect, i.e. the bed evolution of a given average tide is considered as the initial condition for the modelling of the next average tide. In order to do that, all the average tides based on classes of different tidal ranges must be connected to each other as if it were a continuous record. However, some

sort of schematisation must be assumed, where the average input data (tides and river discharge) is treated in different ways: i) by linking the different average tides through the still water level; ii) by interpolating between the end of one average period and the next one, which causes distortion of the tidal signal (and thus maybe altering the hydrodynamic and morphodynamic results; Figure 5.3.A) and iii) by creating artificial 'hydraulic jumps' between tides of different tidal ranges (Figure 5.3.B). In the latter case, no interpolation of the average input data is carried out and all the instabilities generated by the sudden change mainly in the average tidal record are concentrated on a specific time of the simulation. Since each of these methods has its own limitations, the one depicted in Figure 5.3.B is selected for its simplicity. At this stage the effects of chronology (i.e. the order of the average tides) remains undetermined. This issue is assessed by taking into account the scaling factor, which is described below.

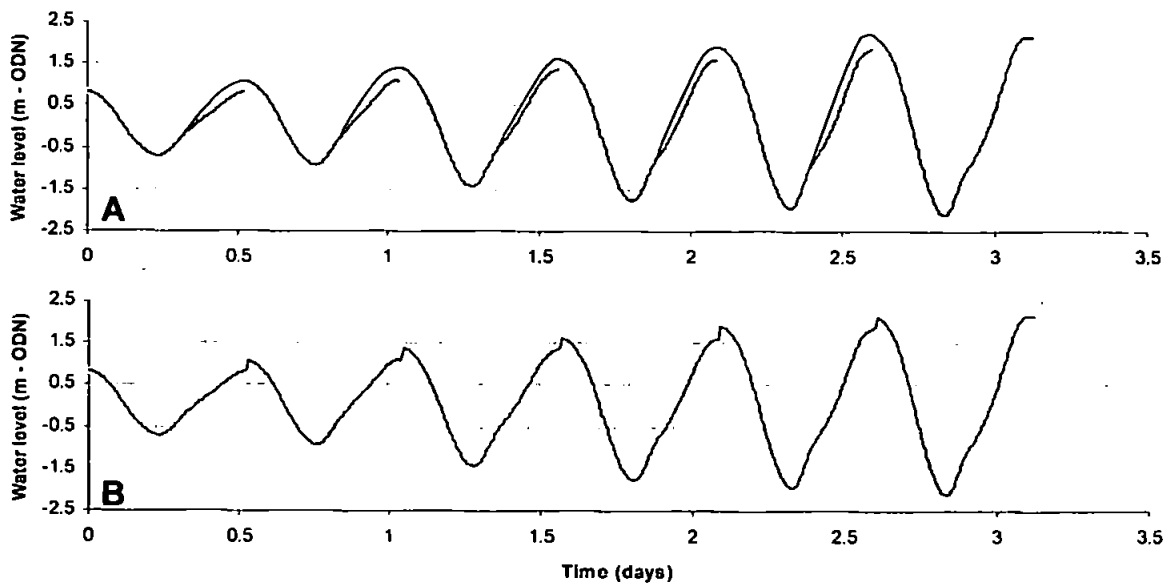


Figure 5.3: Average tides based on different tidal classes and the tidal ranges associated. In order to use them as a continuous record, some schematisation must be carried out either by distorting the average tide (A) or by the creation of hydraulic jumps between two average tides of different tidal range (B).

According to Latteux (pers. comm.) another way of both improving the bed evolution accuracy and reducing the simulation time is by applying a scaling factor (S_C , given by Equation 5.1) to the sediment transport in the modelling exercise. As an example, a given representative tide, such as the $TR \leq 2$ m, which occurs 5 times in the 17-day period is considered. In order to avoid the time-consuming task of running this tide 5 times, a

representative condition can be achieved by running that tide only twice, for example, given the sediment transport formula is multiplied by the scaling factor of 2.5 (i.e. 5/2). Alternatively, the TR \leq 2 m could be run four times, if the sediment transport is weighted by a scaling factor of 1.25 (i.e. 5/4) and so on. The scaling factor (S_C) is given by:

$$S_C = \frac{F_{oc}}{N_{TIDES}} \quad (5.1)$$

where F_{oc} corresponds to the frequency of occurrence of a given average tide during the original period (such as in Table 5.2). N_{TIDES} is the user-defined number of times the respective average tide will be used in the modelling run in question. An empirical balance between the S_C and N_{TIDES} must be found. If the values of the S_C are too high (thus reducing the N_{TIDES}), then the increased weighting factor on the sediment transport formula will force the model to stop more frequently due to reaching the critical evolution ratio (Section 4.4). The overall simulation time is likely to be increased. Conversely, if S_C is too small, N_{TIDES} will be relatively higher, thus not significantly reducing the overall simulation time, one of the goals of applying an ensemble technique. In this study, appropriate values for the S_C in this study were not bigger than 10.

The inclusion of the cumulative effect and of the S_C does improve the morphodynamic outcome. As shown in Figure 5.4, the bed evolution estimated by the reference run is qualitatively reproduced by all methods tested. To calculate the BSS, the observed data from COAST3D survey 2 is used as initial or baseline condition, whereas the modelled bed evolution through the reference run is considered the final condition. The usefulness and sensitivity of the BSS is demonstrated by quantitatively differentiating the bed evolution of average tides run separately (Figure 5.4.B; BSS= -1.24) from the ones based on the 'continuous record' concept (Figures 5.4.C and 5.4.D; BSS= 0.86 and 0.91, respectively). The breakdown of the BSS for these tests is shown in Table 5.3. Also, the high values of BSS confirm that the creation of hydraulic jumps between average tides of different tidal ranges does not substantially affect the final bed evolution when compared to the one modelled with the reference run.

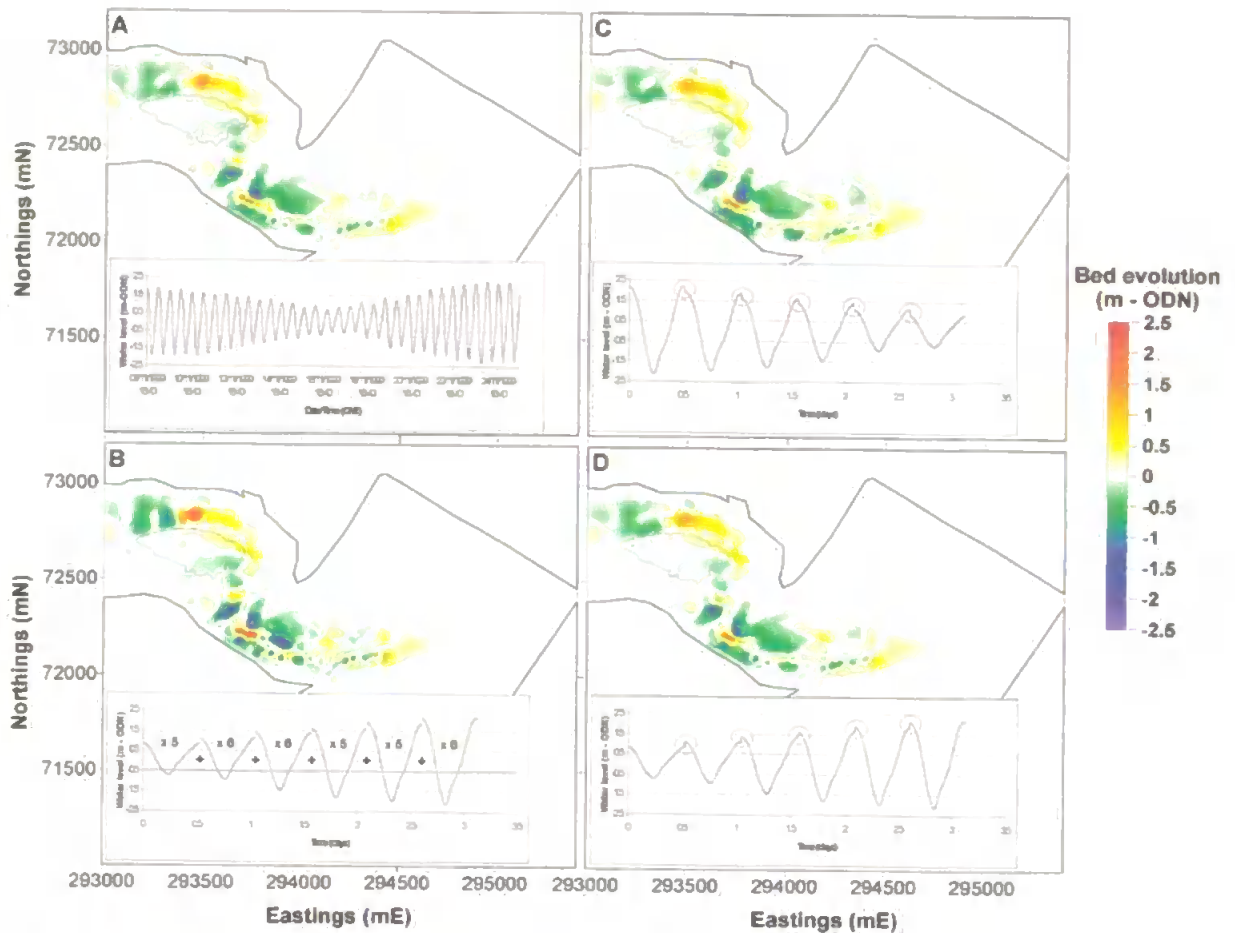


Figure 5.4: Morphodynamic outcome of the reference run for the period between COAST3D surveys 2 and 4 (A). The sum of the bed evolution of all average tides (based on different tidal ranges) multiplied by the respective frequency of occurrence is given in plot B (BSS= -1.24). The use of the average tides as a continuous record and also by the application of the scaling factor in descending order and in ascending order (full ensemble technique) is shown in plots C (BSS= 0.86) and D (BSS= 0.91), respectively. Insets correspond to tidal conditions used to force each set of runs.

Once 'excellent' (Table 4.7) values of BSS are found, before proceeding to longer-term runs, the chronology effects are assessed, i.e. whether the order of average tides affects the overall morphodynamic result. Although slight, a difference exists and is of the order of 5% (difference between BSS of 0.86 and 0.91). This residue may be due to two factors: i) the match between the 'ascending order-case' and the original record, since both periods finish at increasing tidal ranges (insets of Figures 5.4.A and 5.4.D) and ii) the position of the hydraulic jumps: when in an descending order of tidal range, the jumps of water level between successive average tides of different tidal ranges take place at the ebb flow, whereas in an ascending order, the hydraulic jumps are at the late stages of the flooding phase. Since the Teign estuary is ebb-dominated, this asymmetry is captured by the model and velocity peaks (and thus the most intensive sediment transport rates) take place at

ebbing periods. When the hydraulic jumps are positioned at the early stages of the ebbing period (case of descending tidal ranges), the instabilities generated by the hydraulic jumps affect the estimate of the ebb velocities, therefore increasing the errors in the final bed evolution outcome (decreasing the BSS). Ordering the average tides, so as to replicate the spring-neap cycle, does not deliver satisfactory results, since the hydraulic jumps generated are considerable, bringing too much instability to the modelling exercise.

Table 5.3: BSS decomposition for the tests shown in Figure 5.4. The initial condition is COAST3D survey 2 and final condition corresponds to bed evolution modelled from the reference run.

<i>Run</i>	<i>A</i>	<i>B</i>	<i>C</i>	<i>D</i>	<i>Total BSS</i>
Sum of bed evolutions multiplied by frequency of occurrence	0.38	1.62	0	0	-1.24
Full ensemble technique in descending order	0.89	0.02	0	0	0.86
Full ensemble technique in ascending order	0.92	0.01	0	0	0.91

The decomposition of the BSS (explained in section 4.4.1) improves the interpretation of the applied input reduction strategies. The three runs estimate the correct average bed level ($C=0$). When using the sum of the bed evolution of separate average tides and multiplying them by the respective frequency of occurrence, the wrong volume of sediment (given by the high B factor) causes the negative BSS (further away from the initial condition). By using the full ensemble technique, it is seen both accurately predict the position of the main bed features (high values of A), while estimating a virtually perfect change in the bed volume (low values of B).

Whilst it has been proved the efficiency of the technique proposed in reproducing the patterns of the reference run, the simulation time is also reduced. For a 1 GHz Pentium III PC of 512 Mb of RAM running Windows NT, the computation time for the reference run is around 5 days, 15 hours and 30 minutes, while for the most accurate approach using the ensemble technique (Figure 5.4.D), around 20% of that time is required (1 day and 3 hours). The bed evolution modelled by the ensemble technique is around 7% above that estimated for the reference run.

5.3. Medium-term (weeks to months) application of the ensemble technique

Since a greater influence of non-linear terms in the final morphodynamic patterns is expected, the use of the ensemble technique for longer periods, on the order of weeks to months, is also challenging. The correct migration of bed features is of fundamental importance in assessing whether the ensemble technique is suitable for runs in the time scale considered. In order to test the validity of the assumptions made in the previous section, a period of 6 months is considered: from 01/12/02 to 20/05/03. Observed boundary conditions - which are used for modelling the reference run - are presented in Figure 5.5. The initial and final periods coincide with two bathymetric surveys of the Teign estuary and adjacent coastal area carried out as part of the CoastView project. The model set-up parameters are the same as described for the previous section (Table 5.1).

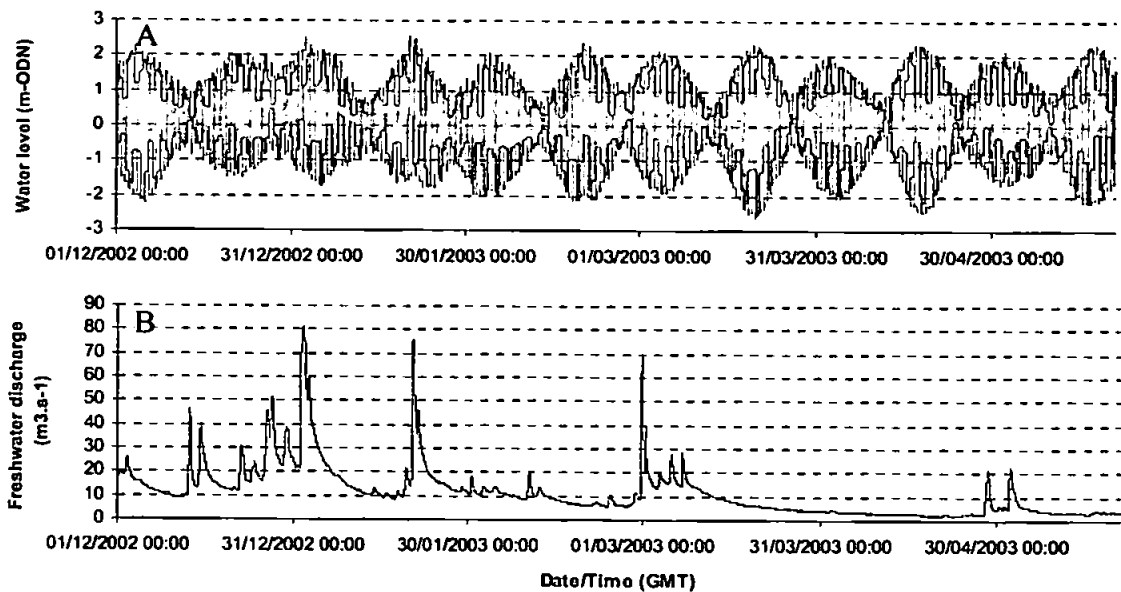


Figure 5.5: Water level (A) and freshwater discharge (B) for medium-term application of ensemble technique. These conditions are used to compute the morphodynamic evolution of the reference run.

The simulation time of the reference run (330 tides) is 61 days and 13 hours (Figure 5.6.A). The ensemble technique applied to this data set consider the steps described in the previous section, with the average tides ordered in an ascending order (inset of Figure 5.6.B). The average boundary conditions are used as a continuous record, where the number of times each average tide is repeated is given by N_{TIDES} (Equation 5.1) and the

sediment transport formula is then multiplied by the scaling factor (S_C ; Table 5.4). As for the 17-day period, the random choice on the values of S_C and N_{TIDES} relies on the compromise of maximising the ensemble technique by reducing the simulation time and avoiding too many model stops, due to high values of S_C .

Table 5.4: Classification of tides based on respective tidal range observed in the 6-month period and frequency of occurrence of each average tide. The parameters S_C and N_{TIDES} are explained in Equation 5.1.

<i>Classes of different tidal ranges (TR)</i>	<i>Frequency of occurrence (Number of tides considered in averaging process)</i>	<i>Number of tides (N_{TIDES})</i>	<i>Scaling factor (S_C)</i>
TR \leq 1.5 m	16	3	5.33
1.5 m < TR \leq 2 m	42	6	7
2 m < TR \leq 2.5 m	44	6	6.29
2.5 m < TR \leq 3 m	52	6	8.67
3 m < TR \leq 3.5 m	58	7	8.29
3.5 m < TR \leq 4 m	71	10	7.1
4 m < TR \leq 4.5 m	34	5	6.8
TR > 4.5 m	13	4	3.25
Total number of tides	330	47	

Based on 47 average tides, the results of the application of the ensemble technique are very good when compared against the modelled bed evolution of the reference run, since the simulation time is much smaller (9 days and 13 hours, around 15% of the time to compute the reference run) and the bed evolution is accurately predicted (BSS= 0.92). An overall underestimation of the total bed evolution by the ensemble technique is around 9% of that modelled based on the reference run. The averaging process carried out for the riverine data will smooth the morphodynamic effects of freshet events (as observed at least three times in Figure 5.5.B), being a likely error source when applying the ensemble technique.

Therefore, in this study the use of the ensemble technique is proved to be a very time-efficient and reliable tool in replicating the model results of a complete simulation (reference run). Considering its relatively simple approach, there is still opportunity for further improvements to the ensemble technique, such as the treatment given to the linking of average tides of different tidal ranges (another likely error source).

Nevertheless, it is important to bear in mind that the predictions expected from the ensemble technique will be as good as the assumptions (and limitations) made in the model

framework. This means that field conditions will only be well replicated if the model takes into account the most important morphodynamic processes at the area considered. When compared to observed bed evolution features (Figure 3.11), it is seen that the model estimates (Figure 5.6) is still unable to satisfactorily represent field conditions. In Chapter 6, the relative importance of including wave stirring effects and mixed grain sizes in the morphodynamic evolution of the Teign estuary are assessed.

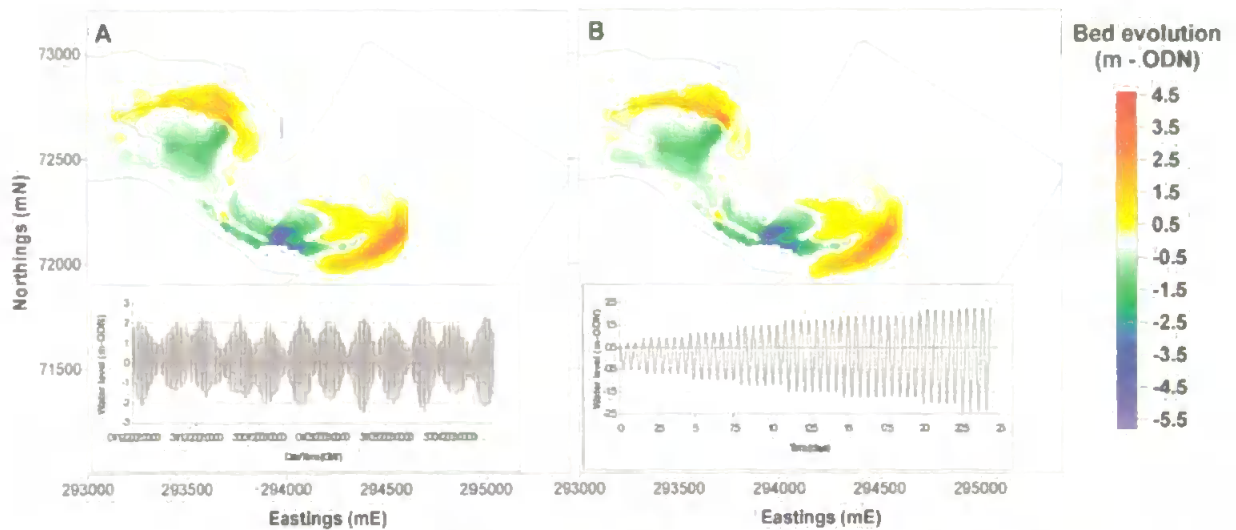


Figure 5.6: Boundary conditions for medium-term application of ensemble technique. Bed evolution depicted in plot 'A' corresponds to the reference run, while the outcome of the application of the ensemble technique is shown in plot 'B'. Insets represent tidal conditions used to force each set of runs. The 'Salty' sandbank is also shown.

5.4. Conclusions

In this study an input reduction approach based on the work carried out by Latteux (1995) was successfully applied to tidal and riverine data within time scales spanning hours to months. When comparing the bed evolution of the so-called ensemble technique to the one of the reference run, very high values of the BSS (around 0.91) were found, corresponding to the correct prediction of the modelled morphodynamic evolution. Not only the accuracy of the results was ensured: the simulation time was significantly reduced. This reduction will be proportional to the number of average tides (N_{TIDES}) used. For the tests shown in

this chapter, the simulation time was reduced to around 17% of the original time. The ensemble technique encompasses several steps, which are described below:

- All average tides (based on classes of different tidal ranges) must be included in the modelling process as a continuous record, i.e., for the Teign estuary not a single representative tide is found to satisfactorily encapsulate the morphodynamic evolution of the reference run;
- A cumulative bed evolution change must be ensured by the use of the bed evolution of a given average tide to be used as initial conditions for the modelling of the next average tide;
- As suggested by Latteux (pers. comm.), a scaling factor (S_C) can be used in the sediment transport formula to ensure simultaneously a time- and quality-effective result;
- For the 17-day analysis, a chronology effect was observed to play a role in the bed evolution predicted for the ensemble technique runs. The water level of both the reference run and the ensemble technique with an ascending order of tidal ranges increased at the end of the simulation period. This is the most likely reason for the differences in the final bed evolution patterns (and BSS) found between the ascending and descending order runs.

Based on this relatively simple approach to tidal flows, the ensemble technique is applied in next chapters in order to develop a model for the medium-term (weeks to months) morphodynamic evolution of the Teign estuary and adjacent areas.

Chapter 6 - Model Predictions

6.1. Introduction

Based on the data sets (Chapter 3) and calibration tests (Chapter 4) described so far, some of the most important aspects of the morphodynamic evolution of the Teign estuary and adjacent coastal region - like the influence of tides, waves and multiple sediment grain sizes - are discussed in this chapter. In order to provide a general description on the effects of river and tidally driven processes for the whole estuary and adjacent coastal area in the short-term scale (tidal cycles), four simulations ranging from "low" to "high" river discharges and from neap to spring tides are presented (Section 6.2).

Nevertheless, since one of the main goals of this thesis is to explore longer-term processes within the area considered, emphasis is given to longer time scales, through the analysis of residual currents - and resulting morphodynamic changes - generated by tides and river discharge (Section 6.3). Mean tidal and river discharge properties considered in this chapter are based on a period of 1 year: from December 2002 (CoastView survey 2) to May 2003 (CoastView survey 3) representing winter-spring conditions and the summer-autumn period spanning from May 2003 to November 2003 (CoastView survey 4). The sediment transport properties and the resulting morphology are then assessed in Section 6.4 through the inclusion of wave stirring effects and the consideration of mixed grain sizes.

The following results were calculated through the application of the ensemble technique, which is described in Chapter 5. Since the freshets are smoothed during the averaging process (based on data shown in Figure 3.10), the river discharge considered in the results to follow is classified as 'normal', below $15 \text{ m}^3 \cdot \text{s}^{-1}$ for both periods. According to Table 3.1, under this magnitude of river influence, the inner estuary can be subject to the accumulation of marine sands during potentially all tidal ranges, even in the absence of wave-related effects. Therefore, the influence of river discharge peak events (e.g. flooding periods) on morphodynamic processes inside the estuary is neglected in this thesis.

6.2. Short-term (hours to days) morphodynamic processes

6.2.1. Water level distribution on short-term scales

Since stratification effects are assumed to be insignificant most of the time inside the Teign estuary and at the adjacent coastal area (Section 3.1.2), general flow processes are likely to be mainly dependent on the barotropic component of the motion equations. If this is the case for the Teign estuary, the assessment of the water surface topography in the area is fundamental for a sound understanding of the hydro- and morphodynamic processes associated. Thus, the distribution of instantaneous water levels, currents and sediment transport on short-term (hours to days) scales is discussed hereafter, like it is done in Section 6.3.1 for time scales of weeks to months. The short-term analyses carried out in this section (6.2) are based on the flood and ebb peak currents at the estuary entrance and are relative to the same timeframe for the water levels, currents and sediment transport.

Four different tidal and river discharge conditions (Table 6.1) are simulated during two tidal cycles, based on average tides calculated for the period between CoastView surveys 2 (December 2002) and 3 (May 2003). Neap tides are represented by tidal ranges (TR) = 1.5 m, while spring tides tests are based on TR > 4.5 m (Table 5.4). River discharge values are based on observed data (Section 3.1.2). Since a single grain size ($D_{50} = 0.3$ mm) is considered, the assessment of the behaviour of finer grains under different tidal ranges and river discharge conditions is carried out only from Section 6.4.

Table 6.1: Forcing conditions for short-term hydrodynamic tests in the Teign estuary and adjacent coast.

<i>Case description</i>	<i>Tidal range (m)</i>	<i>River discharge ($m^3.s^{-1}$)</i>
Neap tides + 'Low' river discharge (NL)	= 1.5	5
Neap tides + 'High' river discharge (NH)	= 1.5	100
Spring tides + 'Low' river discharge (SL)	> 4.5	5
Spring tides + 'High' river discharge (SH)	> 4.5	100

Plots of the peak water level differences between the estuary and the pier are displayed (Figures 6.1 and 6.2), followed by the respective resultant current magnitude plots (Figures 6.3 and 6.4) and by the resulting total sediment transport patterns (Figures 6.5 and 6.6). The distribution of the parameters above is also given for a cross-section of the estuary entrance (Figure 6.7).

As described in Section 4.3.2, the approach chosen for the modelling of wetting and drying processes considers 'dry' areas to be non-existent, since a thin layer of water above the whole domain is assumed. Hence, the water level differences predicted between the upper areas of the domain and the pier (e.g. Figures 6.1 and 6.2) are expected to follow the bottom features, which attain values in excess of 2 m. In order to illustrate whether the water level difference is artificially induced by bottom features or not, the 0 m (ODN) isobath serves as a reference to indicate the channel limits inside the estuary. Since the water surface topography in the following figures is calculated relative to the water level at the pier, direct comparisons between neap and spring conditions require further attention. The variation of the reference level (i.e. pier water level) with the tidal range will, for example, result in differences on the water level of 'dry' areas between neap and spring tides.

The maximum water level differences relative to the offshore end of the pier are shown in Figures 6.1 and 6.2, during ebb and flood respectively. During the falling tide, the water level difference for the 'NL' case (Figure 6.1.A) are predicted to be around 0.2 m higher in the inner estuary than at the pier, whereas differences between the outer estuary and the coastal area are on the order of a few centimetres.

During relatively high discharge periods and neap tides (case 'NH' - Figure 6.1.B), the effect of the induced freshet on the ebbing phase at the inner estuary is seen to increase the water level difference to 0.45 m higher than at the pier. Further down the estuary, the freshet effects on the water level distribution are slight, with a water level difference of 0.05 m.

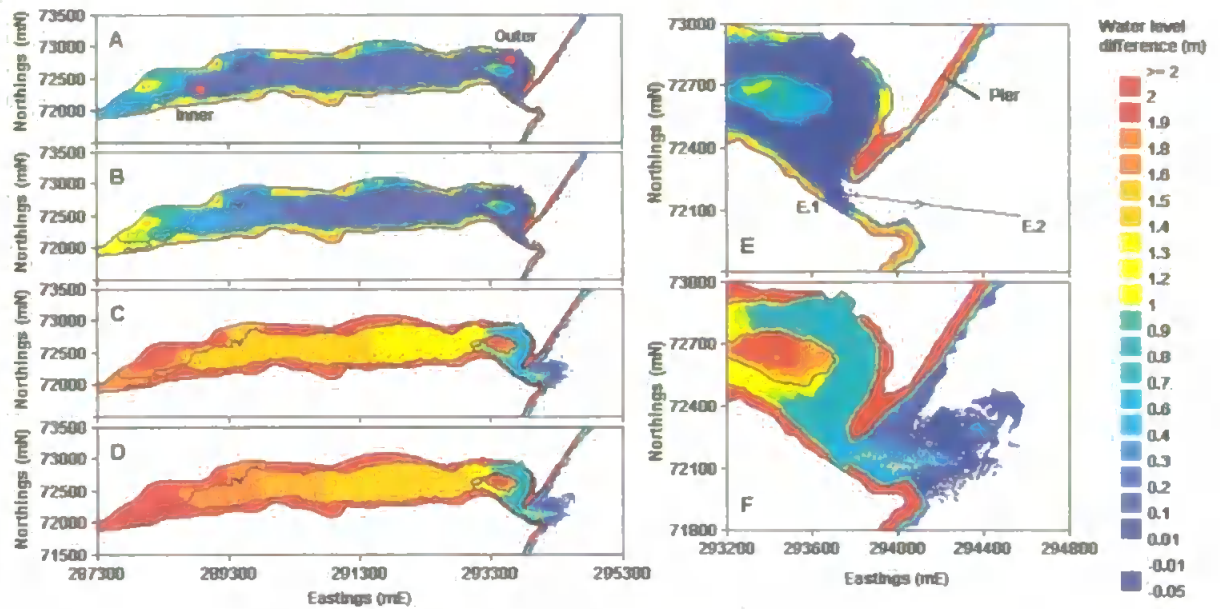


Figure 6.1: Instantaneous water level differences (relative to the pier level) during peak EBB currents at the estuary entrance. The following conditions are considered: 'NL' (A); 'NH' (B); 'SL' (C) and 'SH' (D). Points 'Inner' (and 'Outer') are used to define the water level differences between the inner (and outer) estuary and the pier. In plot E, a zoom into the case 'NL' (cross-section E.1 to E.2 to be used in Figure 6.5) and the water level patterns of the test 'SH' (F). The 0 m (ODN) isobath is indicated as a continuous line.

Considerable changes in the water level differences are modelled during spring tides. For the case with low-river discharge ('SL'), the water level differences increased to 1.6 m (0.7 m), between the inner (outer) estuary and the pier (Figure 6.1.C). For the most dynamic condition, the case 'SH', the freshet presence increased the differences described for the previous case to 1.8 m and 0.85 m for the inner and outer estuary, respectively, suggesting that freshets may have an increasing impact on the morphodynamics of the area towards higher tidal ranges. However, this model prediction still requires validation from field data. Further details on the hydrodynamic patterns of the cross-section E.1 to E.2 (across the estuary mouth, defined in Figure 6.1.E) are shown in Figure 6.3.

During the flooding phase, the water levels at the estuary tend to be lower than at the adjacent coast, creating a 'negative' balance (i.e. a positive balance is given by the water levels at the estuary being higher than those at the pier; Figure 6.2). Under neap tides and in the absence of freshet events, this difference is predicted to be of a few centimetres, with the water levels at the inner (outer) estuary being around 0.03 m (0.01 m) lower than that of the pier (Figures 6.2.A and E).

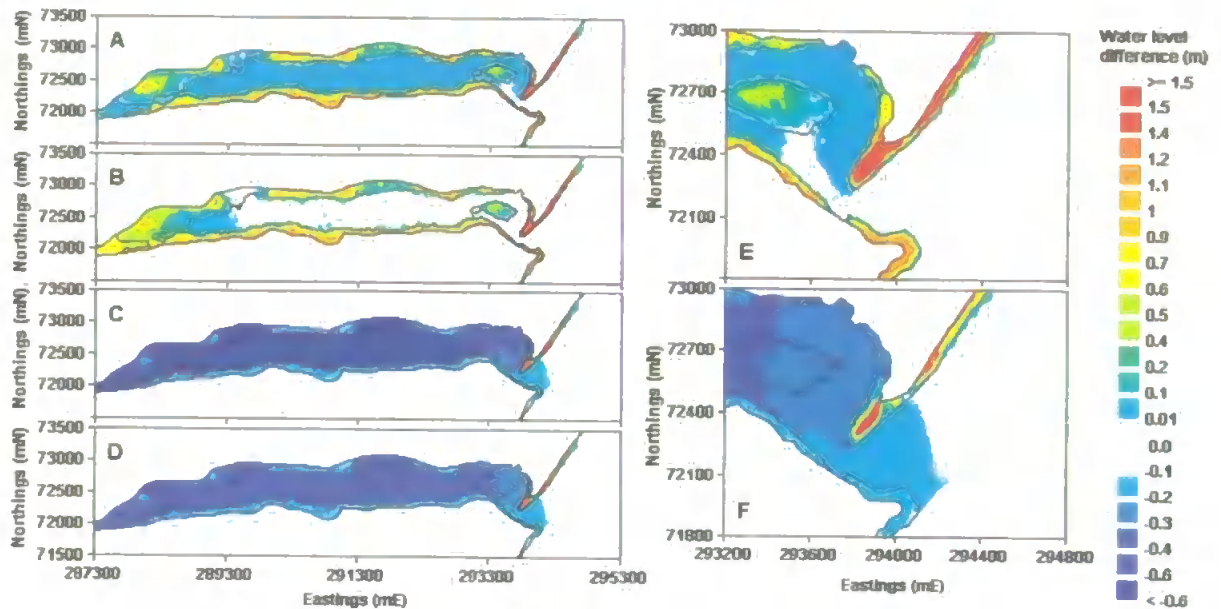


Figure 6.2: Instantaneous water level differences (relative to the pier level) during peak FLOOD currents at the estuary entrance. The following conditions are considered: 'NL' (A); 'NH' (B); 'SL' (C) and 'SH' (D). Zoomed water level differences for the cases 'NL' (E) and 'SH' (F). The 0 m (ODN) isobath is indicated as a continuous line.

The inclusion of relatively high river discharges (case 'NH'), the 'negative' balance between the estuary and the adjacent coast is suppressed, as the enhanced river discharge is responsible for forcing higher water levels at the inner estuary of about 0.04 m, in comparison to the water level at the pier. When compared to neap tides, the instantaneous water level differences (at the peak flood current) during spring tides are enhanced due to the larger tidal range (Figures 6.2.C, D and F), favouring the water level at the coastal area being higher than inside the estuary. Without freshets (case 'SL'), the inner estuary is subject to be about 0.75 m below the water level at the pier, while at the outer estuary this difference is around 0.35 m. Freshet events associated with spring tides (case 'SH', Figures 6.2.D and F) tend to reduce the water level inequalities modelled between the estuary and the adjacent coastal area, with differences at the inner (outer) estuary on the order of 0.5 m (0.3 m) lower than the pier water level. As the water level differences are larger during the ebbing tides than at the flooding phase, the resulting velocity field is expected to be ebb-dominated. This feature is assessed in further detail in the following sections.

6.2.2. Instantaneous velocities on short-term scales

During the peak ebb currents (at the estuary entrance) of the 'NL' case, under the sole effect of tidally-driven currents, the currents are expected to be around 0.9 m.s^{-1} at the channel north to the Salty (indicated by a red square in Figure 6.3.A). At the estuary mouth, the main jet-like ebb flow is confined to the main channel (Figure 6.3.E). When the effect of freshets is also included during neap tides (case 'NH'), a general increase in the velocity field is modelled, especially at the channel constraint close to head of the estuary where the peak resultant currents attain values of around 1.5 m.s^{-1} (Figure 6.3.B). In the middle reaches of the estuary, the presence of freshets cause an increase in the velocity field in excess of 50% of the magnitudes predicted for the 'NL' case.

The magnitudes of the resultant velocity vectors are roughly doubled under spring tides in comparison to the currents generated under neap tides. The most intense currents are shifted towards the offshore portion of the estuary mouth (Figures 6.3.C and D), where the ebbing flow is accommodated not only on the main channel, but also on the marginal channels at the estuary mouth (Figure 6.3.F). Modelled peak resultant velocities for the case 'SL' ('SH') is predicted to be around 3.1 m.s^{-1} (3.2 m.s^{-1}). Relatively small differences in the resultant velocity magnitudes at the outer estuary between the case 'SL' and 'SH' suggest that the tidally driven flows under spring tides are more significant than those induced by riverine currents.

Compared to the ebbing phase, the flow distribution on flood tides is characterised by a decrease in the peak resultant velocities (Figure 6.4). The areas of maximum resultant velocities are the same as described for the falling tide for the neap tides cases ('NL' and 'NH'). For spring tide conditions, maximum velocities are shifted to the landward side of the estuary mouth (Figures 6.4.C and D). For the relatively weak flooding phase under the case 'NL', the magnitude of peak resulting velocities is around 0.4 m.s^{-1} (Figures 6.3.A and E). The occurrence of freshets exacerbates the opposing directions of river-generated currents (down-estuary) and those induced by the flooding phase (up-estuary). Results for the case 'NH' show the maximum resultant velocities to be directed down-estuary (magnitudes on the order of 1.4 m.s^{-1}), indicating the prevalence of river-generated currents towards the seaward limit of the middle estuary (Figure 3.2).

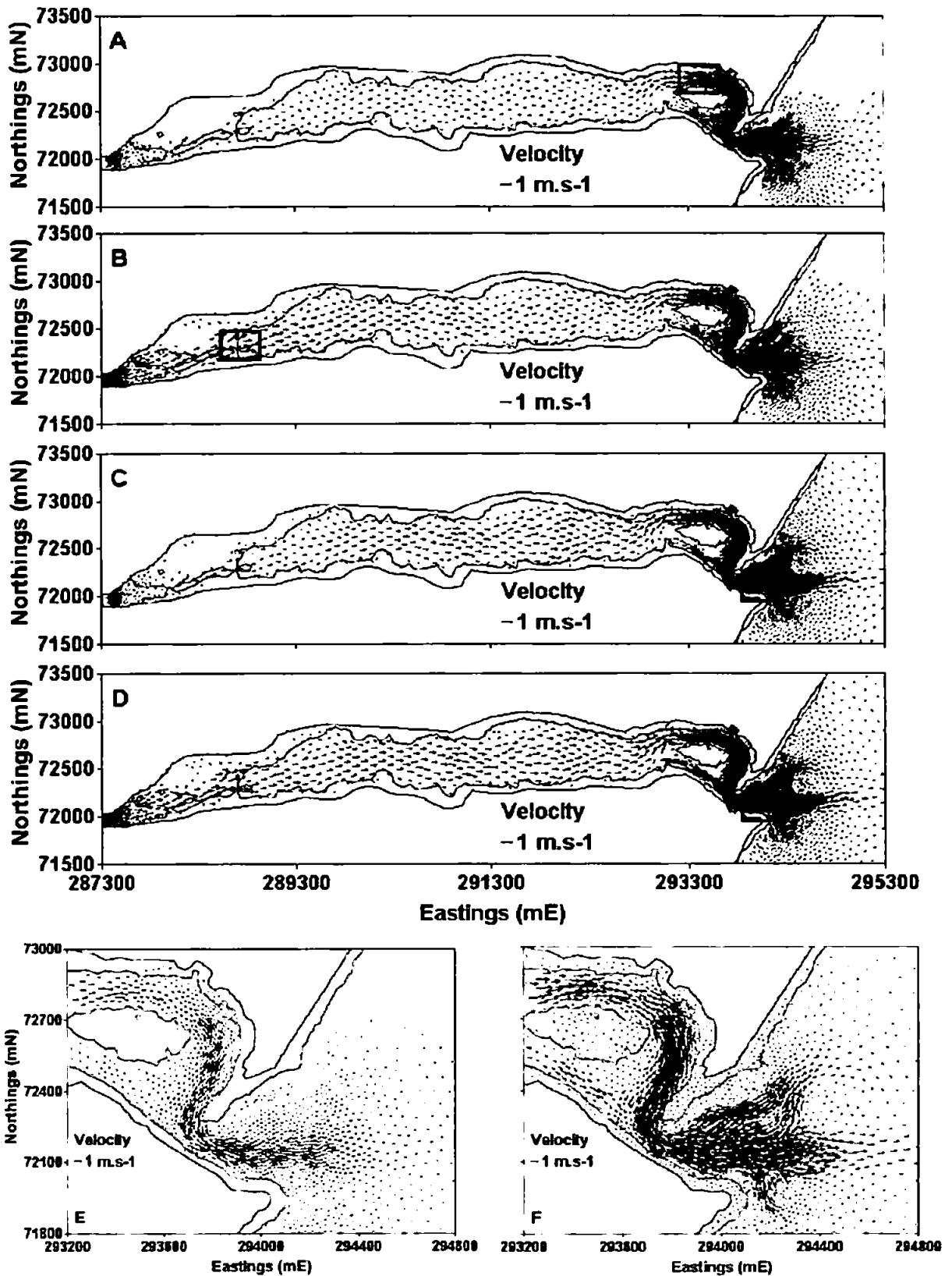


Figure 6.3: Instantaneous currents during peak EBB currents at the estuary entrance. The following conditions are considered: 'NL' (A); 'NH' (B); 'SL' (C) and 'SH' (D). Zoomed areas of cases 'NL' (E) and 'SH' (F). The 0 m (ODN) isobath is indicated by the inner continuous line. Squares indicate the areas of peak resultant current magnitudes. Vectors under 0.01 m.s^{-1} are omitted.

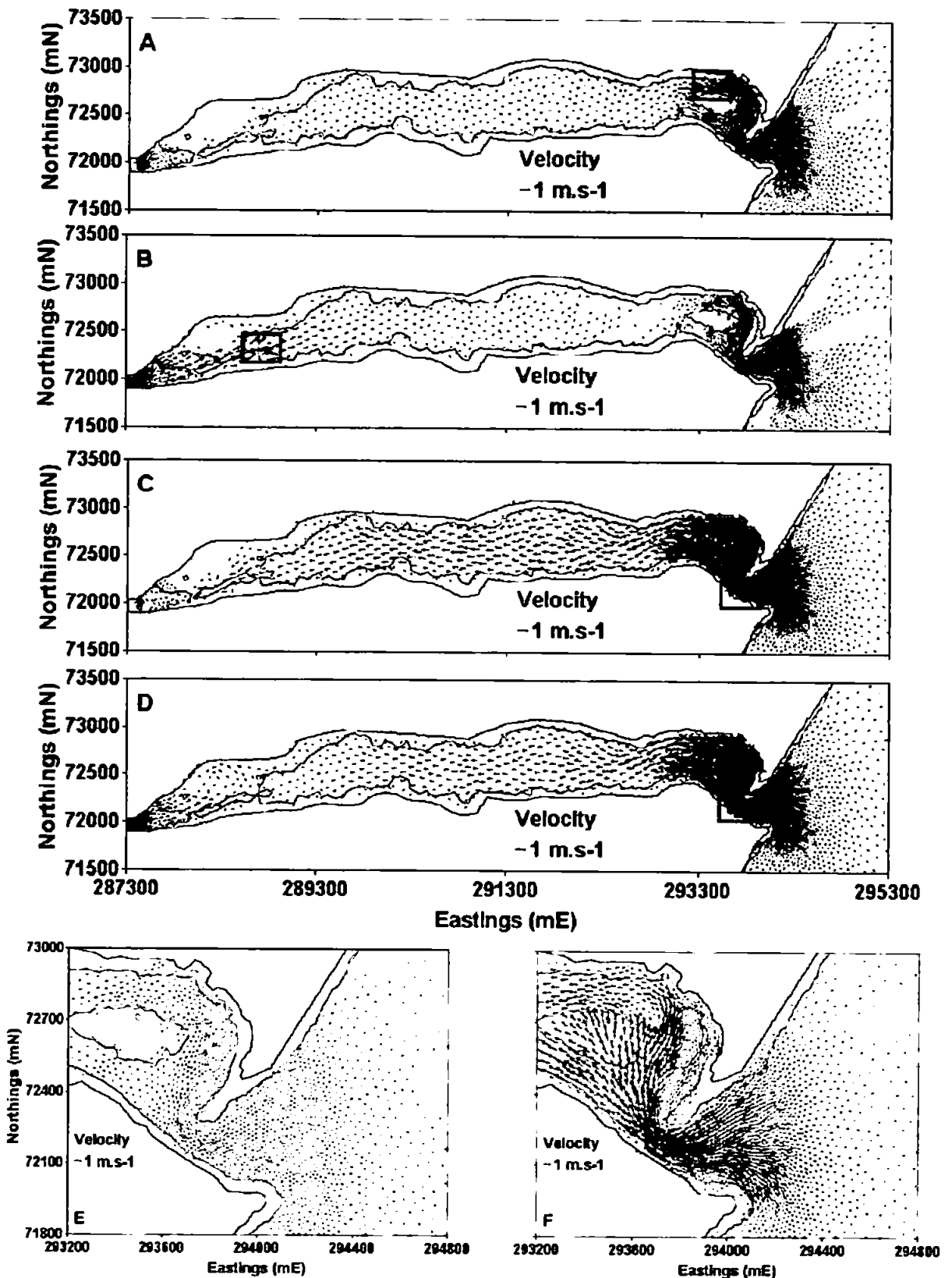


Figure 6.4: Instantaneous currents during peak FLOOD currents at the estuary entrance. The following conditions are considered: 'NL' (A); 'NH' (B); 'SL' (C) and 'SH' (D). Zoomed areas of cases 'NL' (E) and 'SH' (F). The 0 m (ODN) isobath is indicated by the inner continuous line. Squares indicate the areas of peak resultant current magnitudes. Vectors under 0.01 m.s^{-1} are omitted.

When tides dominate the estuarine hydrodynamics (i.e. for case 'SL'), modelled flooding currents can reach magnitudes of up to 0.4 m.s^{-1} at the inner estuary, whereas peak resultant velocities can be as high as 2 m.s^{-1} at the landward portion of the estuary entrance (Figure 6.3.C). However, when freshets are taken into account (case 'SH'), their down-estuary currents decrease the intensity of the peak flooding currents at the estuary mouth to about 1.8 m.s^{-1} (Figures 6.4.D and F). Contrary to the ebbing phase (Figure 6.3.F), flood currents inside the estuary would be most intense on the Salty and concentrating to the west of the main channel (Figure 6.4.F). This asymmetric pattern between ebbing and flooding velocity structure inside the estuary will have an effect on the residual morphodynamic patterns, as it will be shown from Section 6.3.

6.2.3. Morphological changes on short-term scales

The set-up parameters for the morphodynamic processes follow the parameters described in Table 4.4 (hydrodynamics) and depicted in bold in Table 4.8 (morphological module). However, unless otherwise stated, a single-grain size of 0.3 mm was considered and no wave effects were taken into account. As proposed by Villaret (2004), sediment transport rates are expressed hereafter in terms of total (bedload and suspended-load) sediment transport volume per unit width ($\text{m}^2.\text{s}^{-1}$). This unit is used in order to represent a simplified sediment transport rate, which is based on two assumptions: i) lateral homogeneity on a hypothetical cross-section of 1 m width and ii) a constant sediment density of 2665 kg.m^{-3} .

Prior to assessing the relative importance of the different sediment transport modes (i.e. bedload and suspended-load) and the overall morphodynamic evolution, it is important to highlight the limitations embedded in morphological predictions. As discussed in Section 4.4.2, no sediment transport formula is capable of representing all the grain transport conditions found in nature. Moreover, the uncertainty in the sediment transport rates can vary several orders of magnitude depending on the formulation chosen (e.g. Davies and Villaret, 2002 and Davies et al., 2002). Hence, the analysis to follow is intended as a first qualitative approach to the basic sediment transport processes in the Teign estuary.

The predicted total sediment transport is at least one order of magnitude smaller during neap tides than under spring tide conditions. Hence, only the results for the latter tides are

presented in Figure 6.5. In the absence of a freshet and under relatively weak tidal currents (case 'NL'), the spatially averaged suspended-load transport ($0.013 \times 10^{-7} \text{ m}^2 \cdot \text{s}^{-1}$) for the peak ebb velocity (at the estuary entrance and based on the formula of Bijker, 1968) is less than half of the bedload magnitude ($0.031 \times 10^{-7} \text{ m}^2 \cdot \text{s}^{-1}$). If both river discharge and tidal ranges are increased (case 'SH'), then the spatially averaged suspended-load transport ($17.8 \times 10^{-7} \text{ m}^2 \cdot \text{s}^{-1}$) at the same time as above is nearly three times more intense than the bedload transport ($6.2 \times 10^{-7} \text{ m}^2 \cdot \text{s}^{-1}$). Thus, as the main morphodynamic changes are related to events of higher energy (such as freshets and spring tides), suspended-load processes are expected to be the main mode of sediment transport of the area. Further tests must be carried out in order to investigate the behaviour of this relationship under the presence of wave-driven currents and mixed grain sizes.

When compared to measurements for the area close to the estuary entrance (Site 25 in Figure 3.6), the model predictions described in this study tend to underestimate the resulting bedload transport by at least one order of magnitude. Hoekstra et al. (2004) observed an average bedload transport of about $80 \times 10^{-7} \text{ m}^2 \cdot \text{s}^{-1}$, with peaks of up to $150 \times 10^{-7} \text{ m}^2 \cdot \text{s}^{-1}$. However, these rates were obtained under the presence of waves (with minimum wave orbital velocities of $0.3 \text{ m} \cdot \text{s}^{-1}$), which are not considered at all in the analysis carried out in this section of the thesis. If it is considered that i) the bedload estimates expected in this study are run for a different period of time and are the result of a spatially averaged area close to the estuary entrance and ii) that the predicted sediment transport rates under the joint effect of waves and currents are one order of magnitude larger than that for currents alone (Villaret, 2004), then the results modelled in this study seem to be within a reasonable level of accuracy.

Although tidally driven currents at the outer estuary tend to be relatively more important than those generated by river discharge, some differences in the sediment transport between cases 'SL' and 'SH' are modelled: i) the total sediment transport at the ebbing phase of the case 'SL' is about double that for the flooding phase (average total sediment transport of $4.1 \times 10^{-6} \text{ m}^2 \cdot \text{s}^{-1}$), whereas with the inclusion of river discharge (case 'SH') this ratio increases to three (due to enhanced total sediment transport on ebbing phase and less intense landward sediment transport on the rising tide); ii) as expected, the presence of freshets tend to cause a seaward migration of the peak sediment transport patterns.

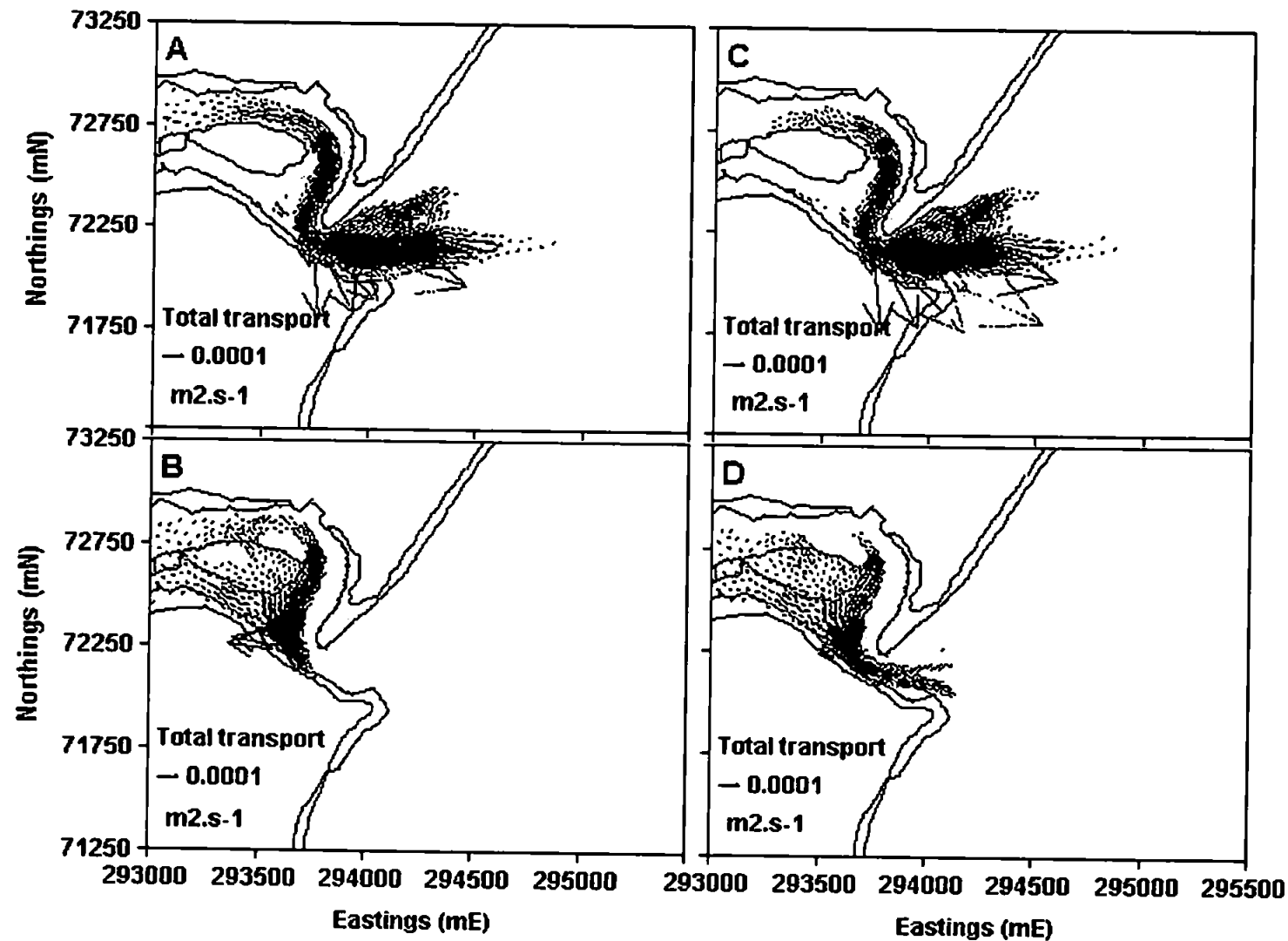


Figure 6.5: Instantaneous sediment transport during the following conditions: total sediment transport for peak EBB currents (A and C) and for peak FLOOD currents (B and D) of cases 'SL' (A and B) and 'SH' (C and D). The inner continuous lines correspond to 0 m (ODN) isobath. Vectors under $1 \times 10^{-6} \text{ m}^2 \cdot \text{s}^{-1}$ are omitted. The largest vectors emanate from the estuary entrance.

As for the instantaneous velocity distribution, the sediment transport patterns at the outer estuary tend to be accommodated in the main channel area during ebbing periods (Figures 6.5.A and C), especially between the Salty and the sandy spit. Conversely, on the flooding phase the flow is mainly concentrated closer to the eastern limit of the Salty and over this sandbank (Figures 6.5.B and D). As it will be shown in the next sections, this asymmetry between ebb- and flood-periods will influence the residual sediment transport of the outer estuary.

Results discussed so far are also assessed along the cross-section E.1 - E.2 (defined in Figure 6.1.E) in Figure 6.6. During the ebbing phase of neap tides, no considerable water level differences through the entrance of the estuary are modelled. On the other hand, on spring tides water level differences (between the outer estuary and the pier) higher than 0.5 m are predicted (Figure 6.6.A). The unrealistic 'wiggled' water level patterns are likely to be generated due to the assumption of a constant vertical turbulent coefficient (Section 4.3.2). The resultant current field during the ebbing phase of neap tides is rather smooth, with a nearly linear decrease seaward of the estuary entrance.

Figure 6.6.B shows that the presence of freshets (case 'NH') associated with neap tides caused an increase in the resultant velocity of about 20% relative to the test where tides are dominant (case 'NL'). Under spring tides, the ebbing flow is predicted to reach values in excess of 2 m.s^{-1} , with freshets causing a minor impact on the resultant flow intensities. As mentioned earlier in this section, the total sediment transport under neap tides is at least one order of magnitude smaller than that for spring tides, for which no major differences were predicted between the cases 'SL' and 'SH' (Figure 6.6.C). Peak velocity magnitudes are expected at the estuary entrance, as it tends to concentrate most of the energy in this system.

Water level differences are predicted to be much smaller during the flooding phase (Figure 6.6.D). Even under spring tides, the outer estuary is about 0.2 m lower than the water level at the pier. The resultant current flow during the flooding phase of the case 'NL' attains maximum magnitudes of about 0.3 m.s^{-1} (Figure 6.6.E), while under the opposing flow generated from the presence of a freshet the landward-directed velocities do not exceed 0.05 m.s^{-1} .

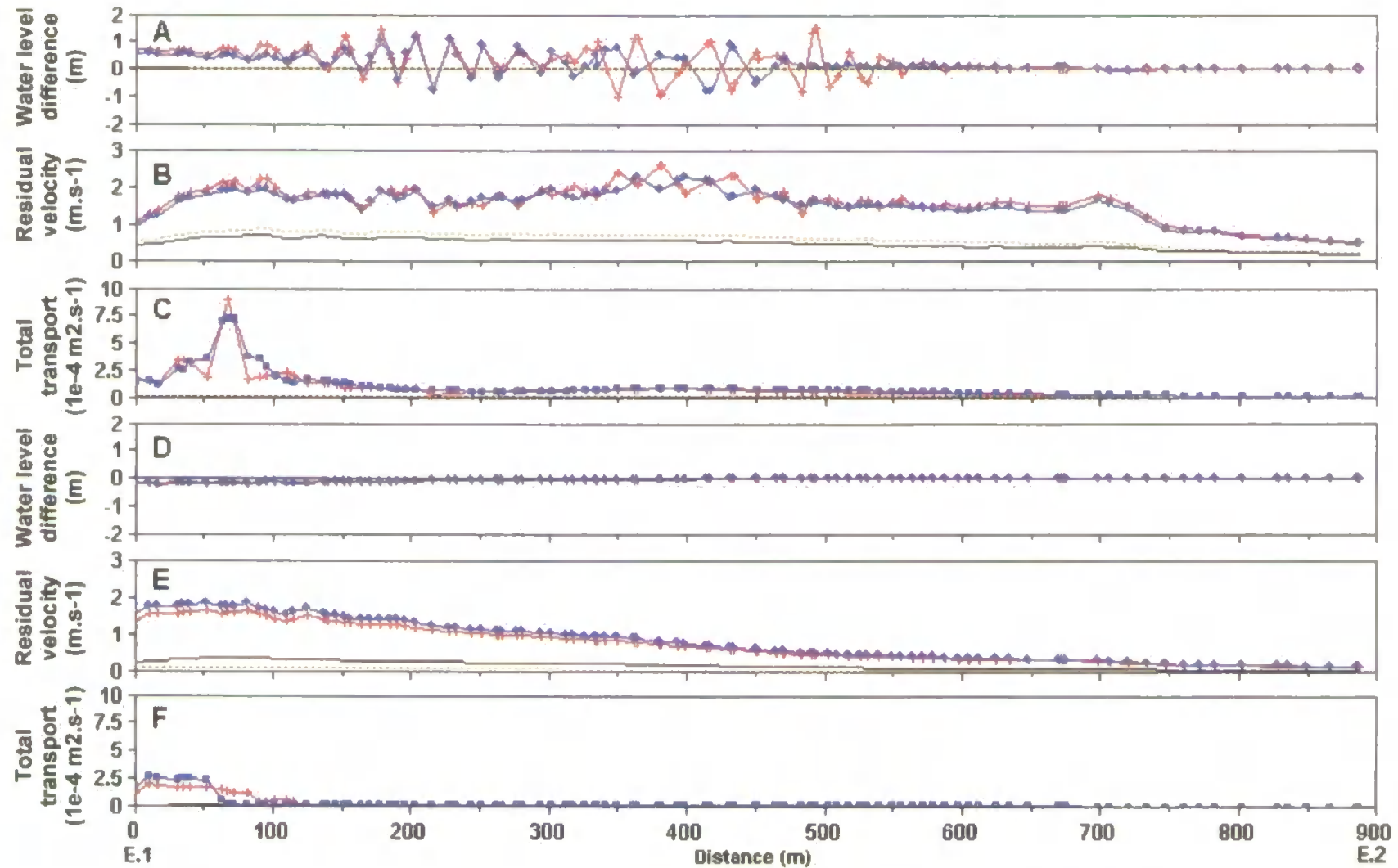


Figure 6.6: Peak resultant water level difference, current magnitudes and total sediment transport across the estuary entrance (profile E.1 to E.2, defined in Figure 6.1.E) during ebbing phase (A, B and C) and flooding phase (D, E and F): case 'NL' (continuous black line); case 'NH' (dashed orange line); case 'SL' (continuous blue line with solid squares) and 'SH' (continuous red line with crosses).

During spring tides, resultant currents tend to increase towards the estuary entrance, where predicted currents are on the order of 1.8 m.s^{-1} and 1.6 m.s^{-1} for the cases 'SL' and 'SH' (under freshet influence) respectively. Relative to ebb tides, the modelled total sediment transport for the flooding phase is around three times smaller (Figures 6.6.C and F). An up-estuary migration of the peak total sediment transport area under flood tides is also simulated.

6.3. Seasonal modulations in morphodynamic processes over the medium-term (months to years)

6.3.1. Water level distribution on medium-term scales

As pointed out by several authors (e.g. Nunny, 1980 and Wells, 2002b) and confirmed by the results in Section 6.2, the sandy spit at the Teign estuary entrance acts as a constraint to the hydrodynamics of the area. Since field data have shown the seasonal variation on the morphodynamic evolution of the area (Figure 3.11), the relative contribution of the residual water surface topography is assessed in this section. The following tests are based on the comparison of morphodynamic features modelled for two distinct periods: the winter-spring 2002/2003 (from CoastView survey 2 in December 2002 to CoastView survey 3 in May 2003) and summer-autumn 2003 (period between CoastView survey 3 and CoastView survey 4 in November 2003). The initial bathymetric conditions for the runs considered in this section are based in field surveys, where the winter-spring 2002/2003 run was initialised with CoastView survey 2 and CoastView survey 3 was used as the initial bathymetry for summer-autumn 2003. Residual properties to be discussed hereafter are calculated based on the average of several tides, where the averaging period is related to the frequency of occurrence (F_{oc}) of the tidal range of interest (as exemplified in Table 5.4).

During neap tides, virtually no differences in residual water levels between the outer estuary and the pier are predicted (Figures 6.7.A and B; 6.8.A and B) between December

2002 and November 2003. For the inner reaches of the estuary, the residual water surface behaviour under neap tides in the winter-spring 2002/2003 (Figure 6.7.A) is relatively higher than for the same tides in the summer-autumn 2003 (Figure 6.7.B) due to the less pronounced river discharge in the latter period (Figure 3.10).

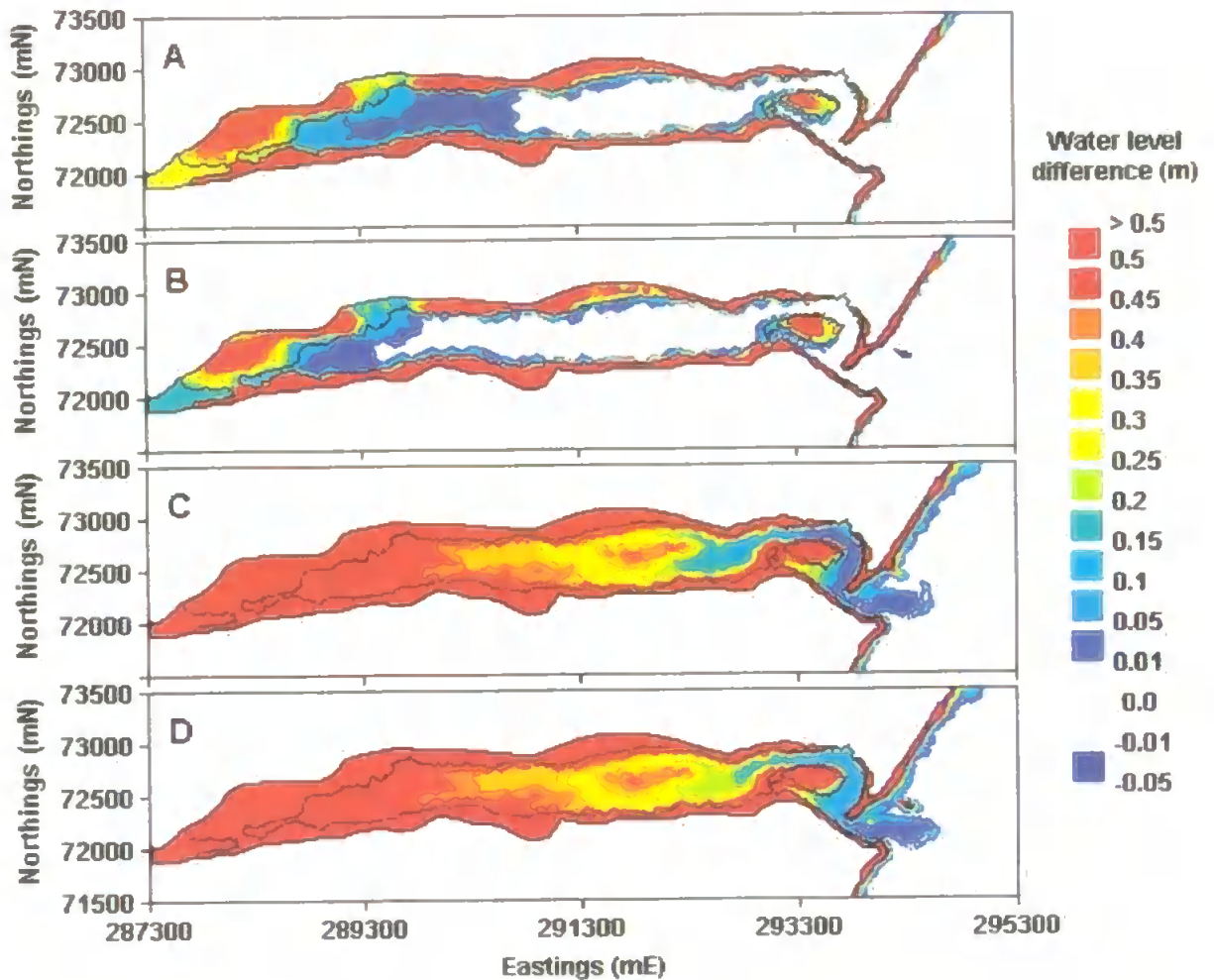


Figure 6.7: Time-averaged water level differences at the Teign estuary relative to the pier, under the following conditions: neap tides of winter-spring 2002/2003 (A) and summer-autumn 2003 (B); spring tides of winter-spring 2002/2003 (C) and summer-autumn 2003 (D). The inner continuous lines correspond to 0 m (ODN) isobath.

As discussed in Section 6.2.1, it is under spring tide periods that stronger water level differences are found. In residual terms, the outer (inner) estuary is around 0.05 m (0.6 m) higher than the water level at the pier (Figures 6.7.C and D; 6.8.C and D). Interestingly, a relatively small water level depression is modelled, with average water levels lower than the predicted for the Pier, close to the tip of the sandy spit (northern portion of the

estuarine entrance channel). As seen in Figures 6.10.C and D and 6.11.C and D, this feature will contribute to the presence of the main flood channel at the estuary entrance.

On the seasonal scale, the water level differences for spring tides were smaller during the winter-spring 2002/2003 than in summer-autumn 2003. The primary source for this variation is linked to the slightly larger average tidal ranges (not shown) for the latter period, while the river discharge influence is of minor importance due to its relatively lower values for the summer-autumn 2003 relative to the winter-spring 2002/2003 (Figure 3.10). It is also postulated that the enhanced water level differences could be linked to heightening of the bottom (i.e. sediment accumulation) observed from CoastView surveys 2 to 3 (Figures 3.11 and 3.12).

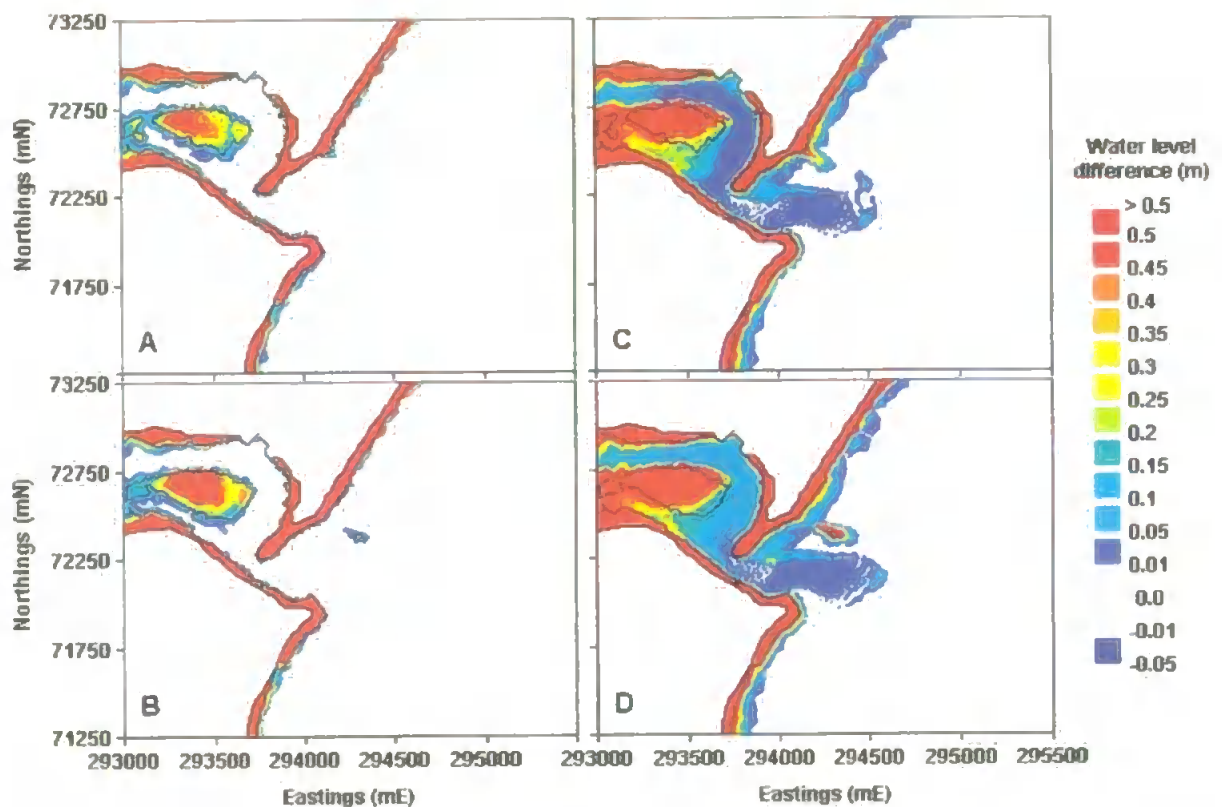


Figure 6.8: Time-averaged water level differences at the outer estuary and adjacent coast relative to the pier, under the following conditions: neap tides of winter-spring 2002/2003 (A) and summer-autumn 2003 (B); spring tides of winter-spring 2002/2003 (C) and summer-autumn 2003 (D). The inner continuous lines correspond to 0 m (ODN) isobath.

Hence, the seasonal behaviour of erosion in summer-autumn months (when tides tend to be the main forcing) and sediment deposition during winter-spring months (when the effects of waves and river discharge are more pronounced) would trigger a feedback

morphodynamic mechanism, whereby the cumulated deposition would tend to enhance the ebb-dominated currents at the outer estuary and off the estuary entrance, exporting more sediment. These feedback mechanisms illustrate the concept of dynamic equilibrium, which is also exemplified in other coastal systems by O'Brien (1969), Eysink (1990) and Dean (1991). This concept can be applied, for instance, to the sediment budget of an estuary. If the system is in dynamic equilibrium, this assumption implies that the amount of net erosion in the system is balanced by the overall sediment accretion. In the case illustrated for the Teign outer estuary, more sediment seems to be removed from the system after a winter-spring season, when sediments tend to accumulate in the area. The relatively stable net sediment budget described in Section 3.2.6 suggests that the deeper areas of the estuary are close to a condition of dynamic equilibrium in what concerns the sediment budget of this area.

6.3.2. Residual velocities on medium-term scales

During neap tides, tidally generated residual flows for these conditions are relatively weak regardless of seasonal effects (Figures 6.9.A and B to 6.11.A and B) between December 2002 and November 2003. The residual flows are the result of a time averaging of the velocity vectors throughout the period considered (e.g. $TR > 4.5$ m). At the inner and middle estuary, the residual flow is down-estuary up to the western reaches of the Salty, where most complex residual hydrodynamic features are expected. Due to relatively higher river discharge during the winter-spring 2002/2003, residual currents for this period are higher than those for the summer-autumn 2003.

At the outer estuary, a residual clockwise vortex is predicted (Figure 3.2), in line with the findings of Nunny (1980) and Wells (2002b). This recirculation cell is located between the Salty and the sandy spit. On the coastal side of the estuary entrance, the residual flow is characterised by the presence of a flood channel, which runs parallel to the sandy spit. Rippled bedforms directed towards the estuary entrance are illustrated in Figure 3.3.F. At the end of the spit, the flow turns back offshore, joining the main ebb-dominated jet. To the south of this outflow jet, a secondary flood channel is predicted. Maximum residual velocity magnitudes in the area are of the order of 0.15 m.s^{-1} and are found at the main flood channel, close to the tip of the sandy spit.

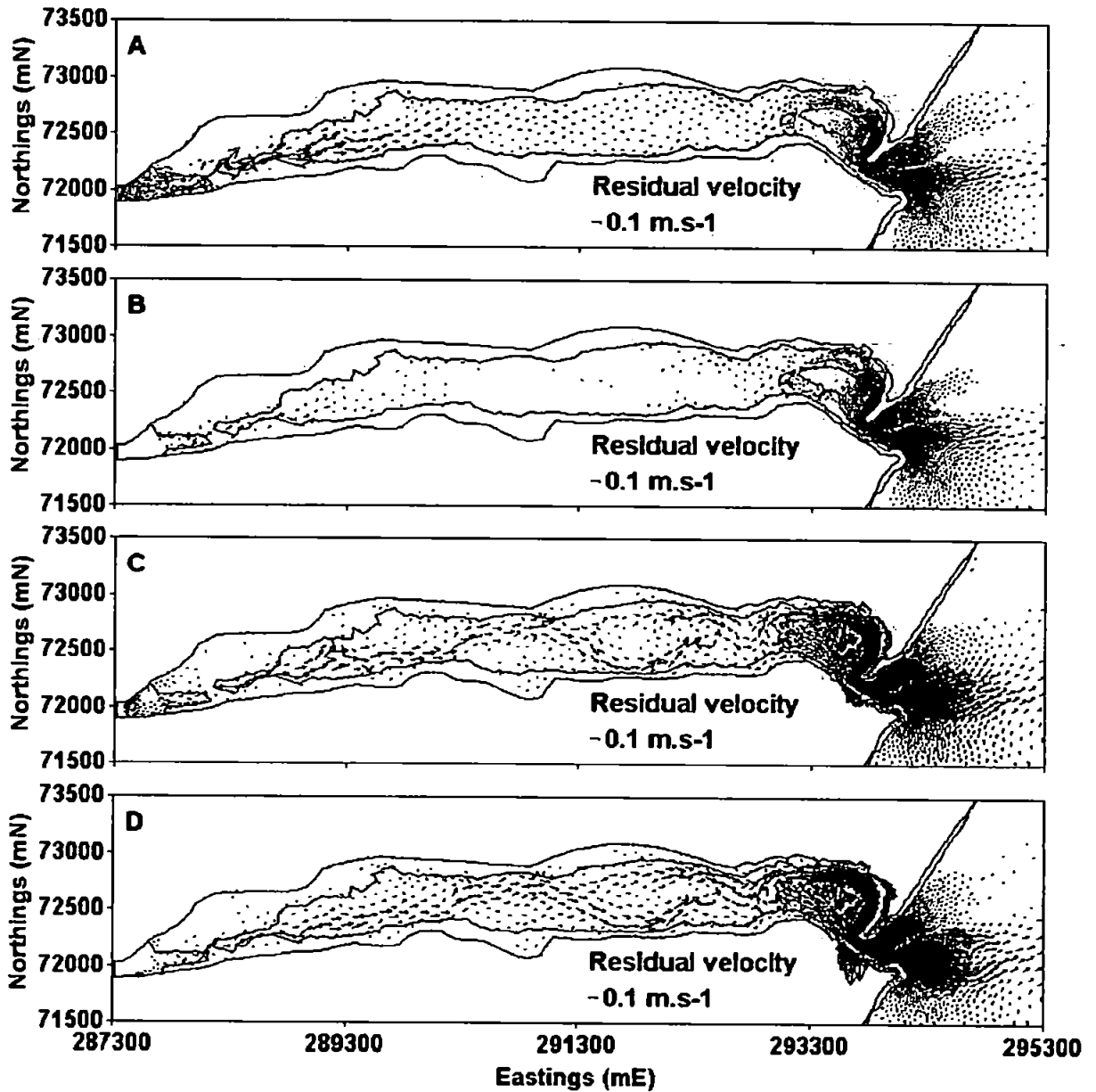


Figure 6.9: Residual currents at the Teign estuary under the following conditions: neap tides of winter-spring 2002/2003 (A) and summer-autumn 2003 (B); spring tides of winter-spring 2002/2003 (C) and summer-autumn 2003 (D). The inner continuous lines correspond to 0 m (ODN) isobath. Vectors under 0.01 m.s^{-1} are omitted.

However, it is under spring tide conditions that more dynamic conditions are expected (Figures 6.9.C and D; 6.10.G and H; 6.11.C and D; 6.12.C and D). At the inner and middle estuary, meandering ebb-dominated residual currents are modelled. During neap tides, flow reversals take place close to the western end of the Salty, reinforced by the flood-dominated currents coming from the southern parts of the Salty (Figures 6.10.D to H; 6.11.C and D).

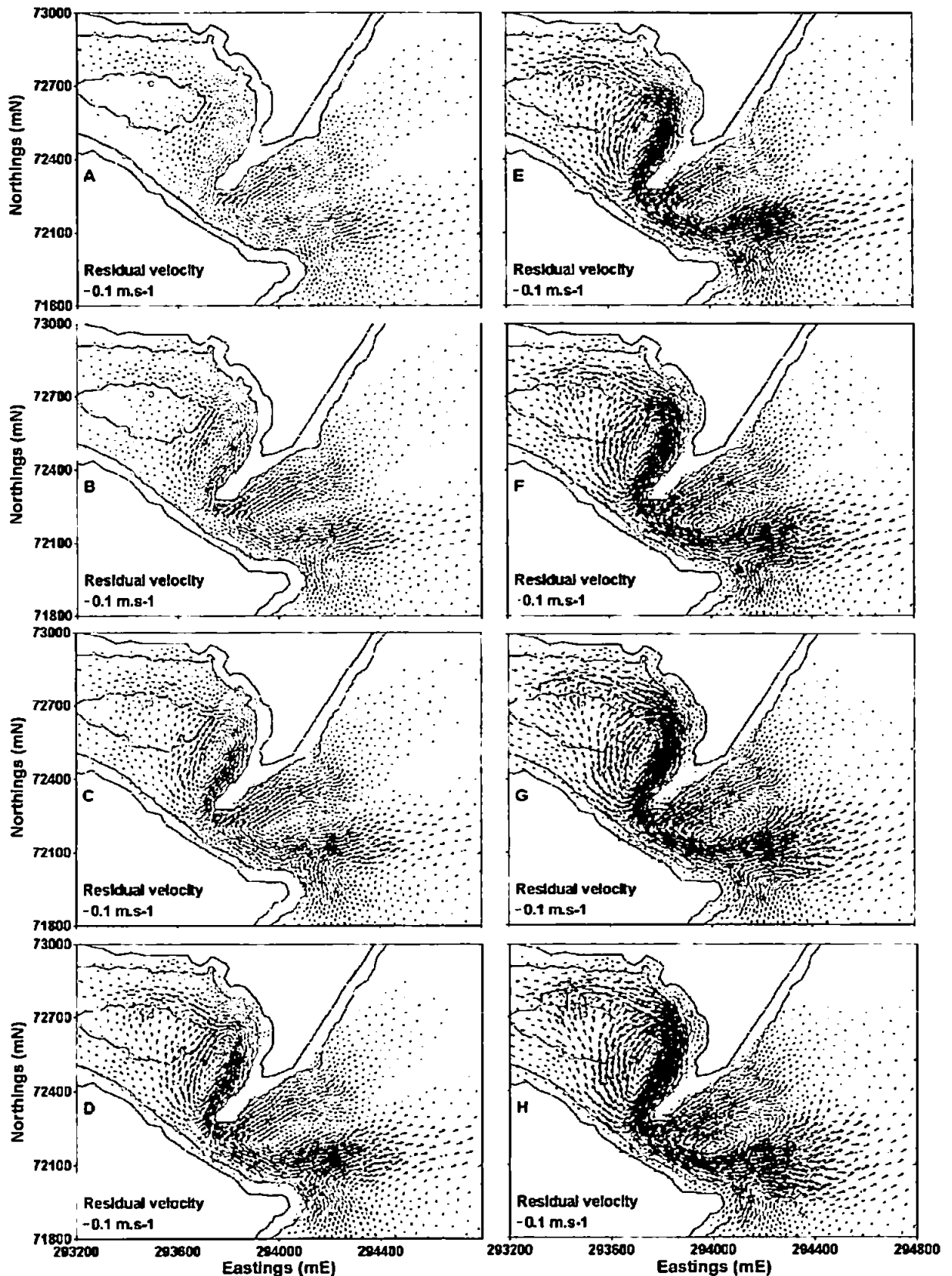


Figure 6.10: Residual velocity at outer estuary and adjacent coast associated with the tidal range for the winter-spring 2002/2003. $TR \leq 1.5$ m (A); $1.5 < TR \leq 2$ m (B); $2 < TR \leq 2.5$ m (C); $2.5 < TR \leq 3$ m (D); $3 < TR \leq 3.5$ m (E); $3.5 < TR \leq 4$ m (F); $4 < TR \leq 4.5$ m (G) and $TR > 4.5$ m (H). The inner continuous line corresponds to 0 m (ODN) isobath. Vectors under 0.01 m.s^{-1} are omitted.

In order to gain a better comprehension of the influence of the tidal range on residual currents, the distribution of this property for the winter-spring 2002-2003 period is discussed. As the tidal range increases, the residual velocity magnitude is also enhanced (Figure 6.10). Residual current patterns are rather stable regardless of the tidal range, with a three-fold enhancement of the residual current magnitudes between the smallest and the biggest tidal ranges. This finding could potentially lead to simplifications of the longer-term velocity distribution of the area, given that other forcing processes are neglected.

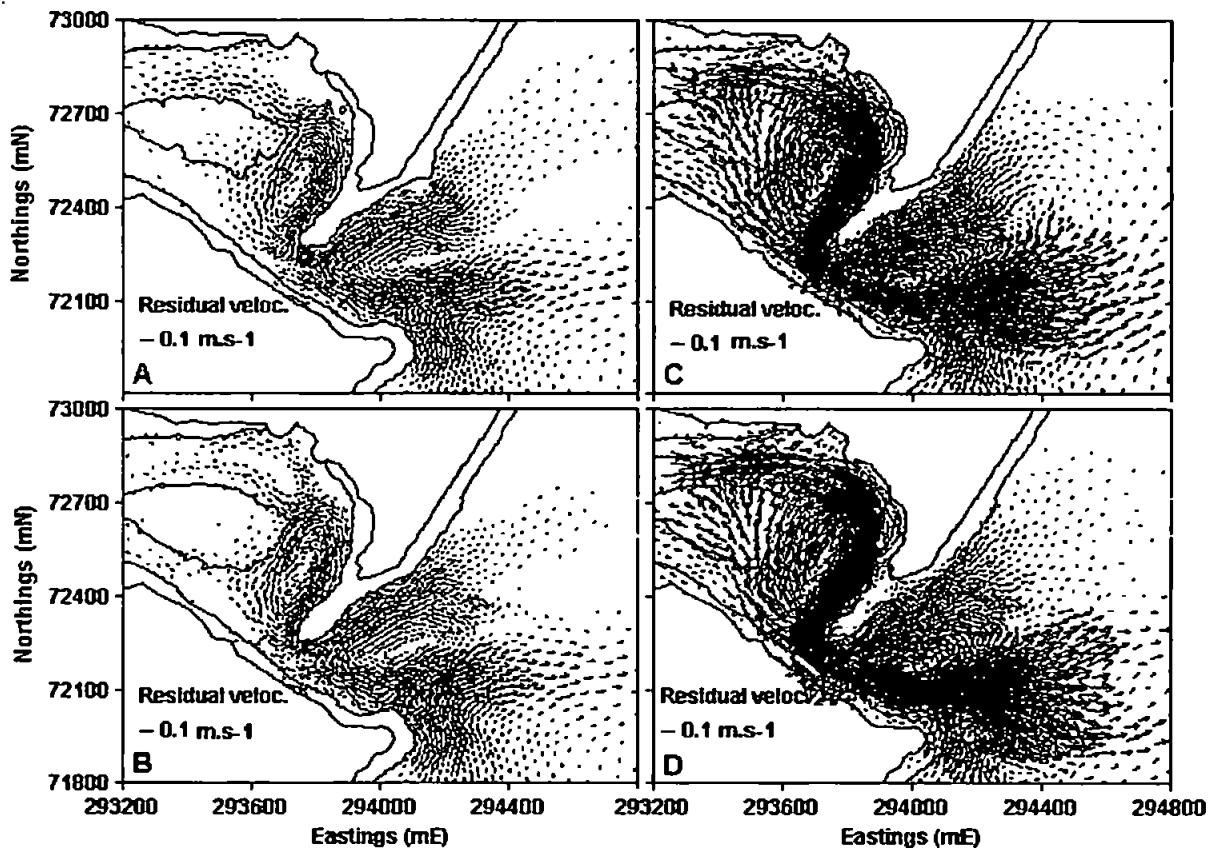


Figure 6.11: Residual currents at the outer estuary and adjacent coastal area under the following conditions: neap tides of winter-spring 2002/2003 (A) and summer-autumn 2003 (B); spring tides of winter-spring 2002/2003 (C) and summer-autumn 2003 (D). The inner continuous lines correspond to 0 m (ODN) isobath. Vectors under 0.01 m.s^{-1} are omitted.

The presence of ebb- and flood-dominated areas illustrate the complexity of the system. While the residual currents in the main channel are directed down-estuary, the following flood-dominated areas are predicted: i) at the outer estuary, affecting the Salty and the area south of it; ii) to the north of the main channel at the estuary entrance, along the sandy spit and iii) between the south of the main channel and the Ness headland. As it will be shown

in Figures 6.12.C and D, at the estuary entrance a divergence zone is formed due to the crossing of the ebb-dominated patterns in the main channel with the flooding features coming from the sandy spit towards the south of the Salty. Moreover, a zone of relative less intense currents is expected between the ebb-directed currents in the main channel and the flood-dominated area along the sandy spit (Figure 6.10).

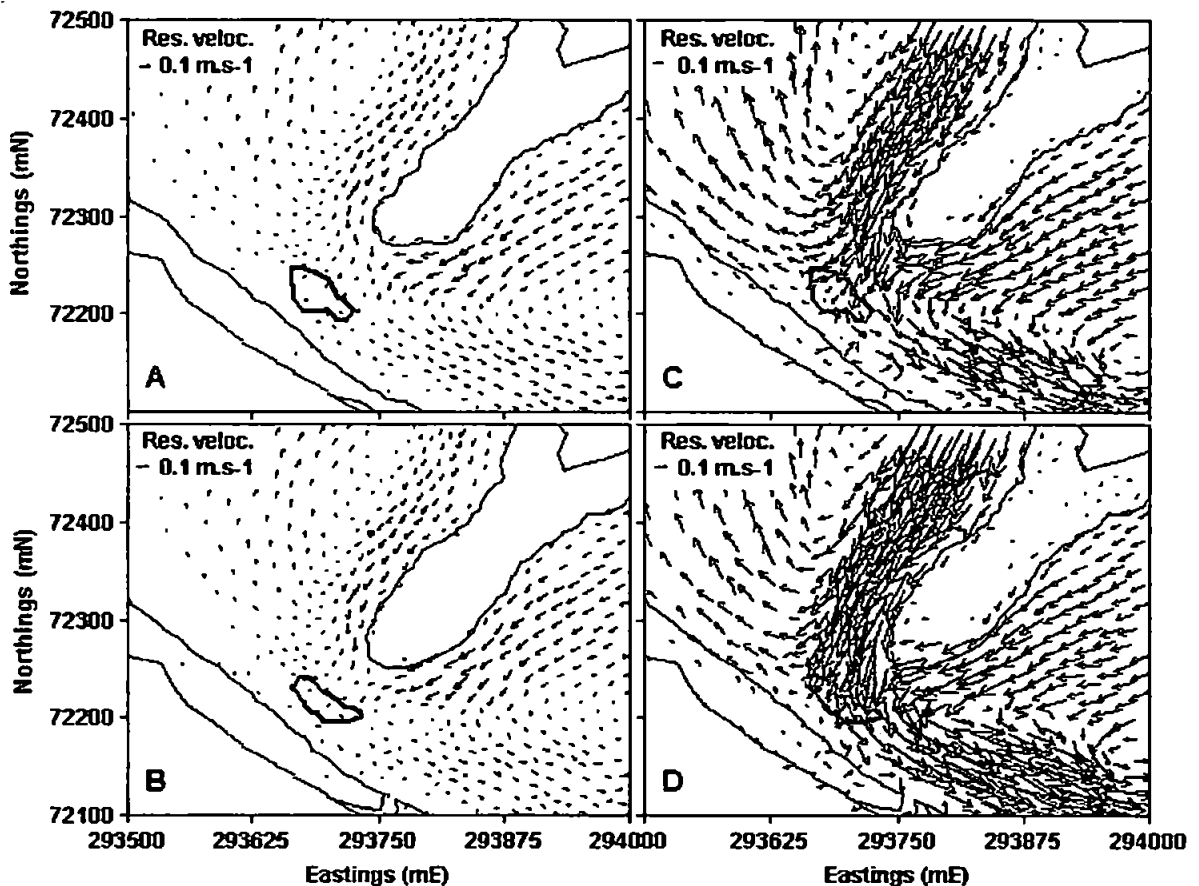


Figure 6.12: Residual currents at the estuary entrance under the following conditions: neap tides of winter-spring 2002/2003 (A) and summer-autumn 2003 (B); spring tides of winter-spring 2002/2003 (C) and summer-autumn 2003 (D). The inner continuous lines correspond to 0 m (ODN) isobath, while the red ellipsoidal element represents the -8 m (ODN) isobath. Vectors under 0.01 m.s^{-1} are omitted.

Peak residual currents are modelled at the ebb-dominated estuarine channel close to the estuary entrance. The rather irregular bottom features at the southeastern side of the Salty (Figure 3.3.D) are explained by the increase of the flood-dominated residual currents, which act on this area (Figure 6.2.B). An indirect validation of the hydrodynamic results estimated in this thesis is given by the match between the divergence area (depicted in Figures 6.12.C and D) and the position of maximum depths at the estuary entrance, where bedrock exposure is observed.

The rounded shape of the -8 m (ODN) isobath during the winter-spring 2002/2003 (Figures 6.12.A and C) could be linked to the enhanced influence of waves and river discharge upon the morphodynamic patterns in the area, as opposed to the rather elongated shape of the -8 m (ODN) isobath under the tidally-dominated summer-autumn 2003 (Figures 6.12.B and D). The predicted bi-directional (ebb-domination on the southern part of the estuary mouth and flood-dominance on the northern reaches of the channel) residual velocity field is reproduced by a photograph taken during the late stages of the ebbing phase of a spring tide and depicted in Figure 3.3.I. The presence of residual flows across the closed boundary is due to the fact that momentum is conserved along each mesh element (while the model outputs are calculated at the mesh nodes), hence if an "outward" residual vector is predicted, an "inward" current is found at the same mesh element (Baugh, pers. comm.^{6.1}).

6.3.3. Morphological changes on medium-term scales

As in section 6.2.3, a single grain size of 0.3 mm is considered, while wave effects are neglected. In the short-term scale, the sediment transport under spring tides was predicted to be at least one order of magnitude larger than during neap tides. Residual total sediment transport patterns are presented in Figures 6.13 and 6.15 for both winter-spring 2002/2003 (following parameters set up in Table 5.4) and for summer-autumn 2003 (parameters not shown). The variation of the total sediment transport according to the tidal range for the winter-spring 2002/2003 is shown in Figure 6.14.

General patterns in Figure 6.13 suggest that, under normal river discharge conditions, most of the sediment transport processes occur at the outer estuary, where the main currents are constrained by the presence of the Salty and by the sandy spit at the estuary entrance. Therefore, the outer estuary is expected to be more active than the inner portions of the estuary, especially during normal river discharge conditions. As for the previous residual properties of the estuary predicted in this study, most of the information generated by the model output still requires further validation from field data. Nevertheless, these results

^{6.1} John Baugh, HR Wallingford.

seem to be consistent with other modelling exercises carried out within the Teign estuary (e.g. Wells, 2002b).

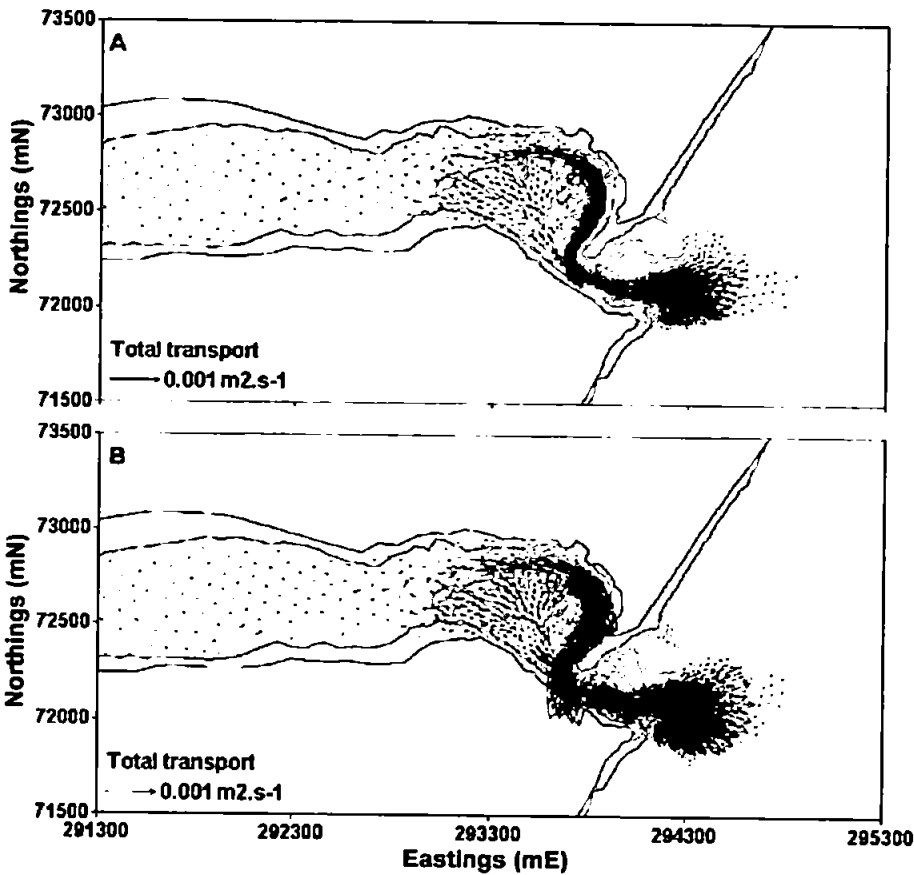


Figure 6.13: Residual total sediment transport volume per unit width at the whole estuary for spring tides of winter-spring 2002/2003 (A) and summer-autumn 2003 (B). The inner continuous line corresponds to 0 m (ODN) isobath. Vectors under $1 \times 10^{-6} \text{ m}^2 \cdot \text{s}^{-1}$ are omitted.

A monotonic increase of the residual total sediment transport is predicted as the tidal range increases (Figure 6.14). From the tidal range higher than 2.5 m and smaller than 3 m, a continuous ebb-dominated pattern emerges in the outer estuary channel, directed to the adjacent coast (Figure 6.14.D). This feature is enhanced as the tidal range increases, and is mainly restricted to the main channel area. The jet-like ebb-dominated structure at the estuary inlet widens offshore of the Ness headland. The position of the feature also seems to vary according to the tidal range.

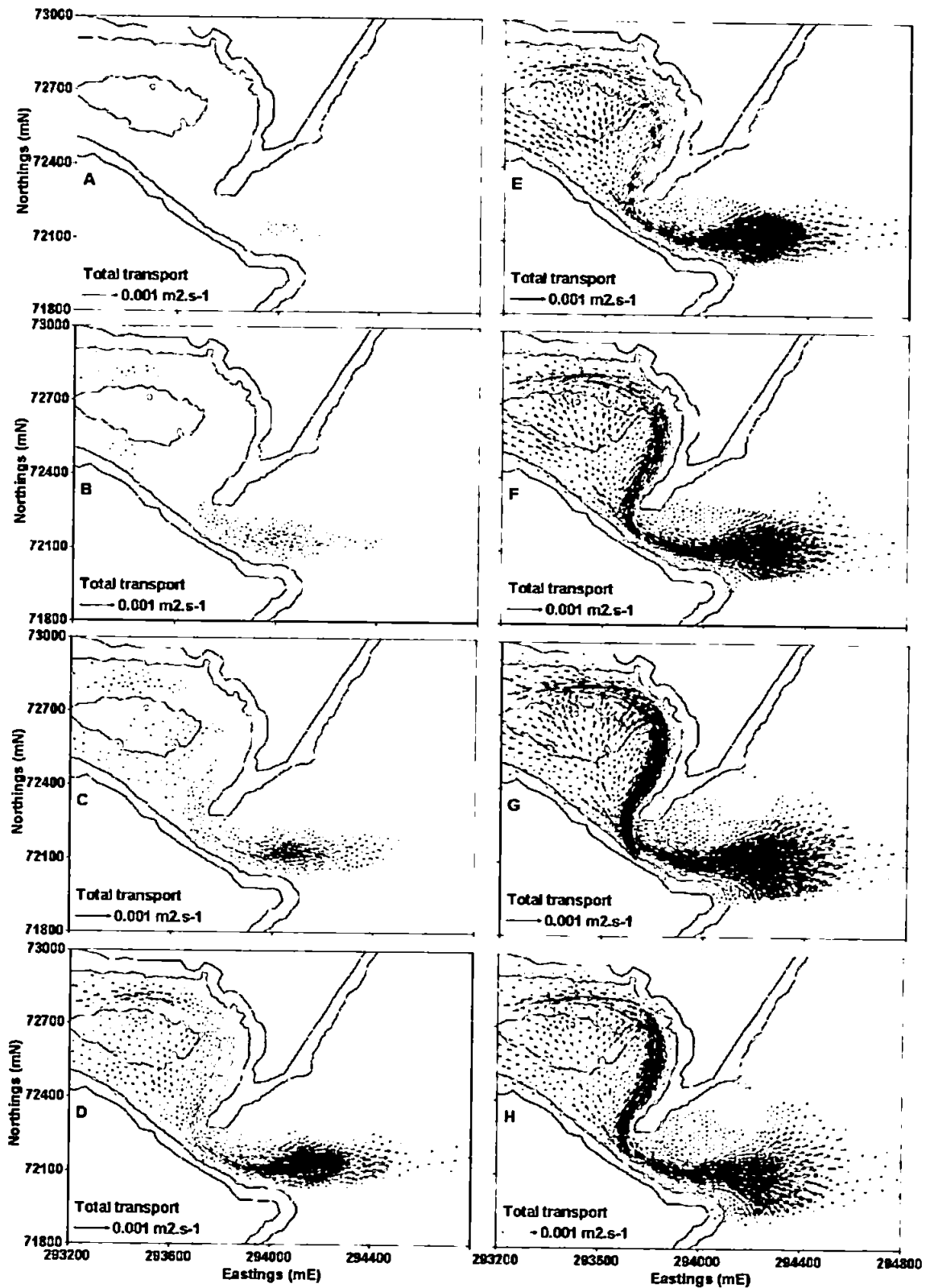


Figure 6.14: Residual total sediment transport volume per unit width at the outer estuary and adjacent coast associated with the tidal range for the winter-spring 2002/2003. $TR \leq 1.5$ m (A); $1.5 \text{ m} < TR \leq 2$ m (B); $2 \text{ m} < TR \leq 2.5$ m (C); $2.5 \text{ m} < TR \leq 3$ m (D); $3 \text{ m} < TR \leq 3.5$ m (E); $3.5 \text{ m} < TR \leq 4$ m (F); $4 \text{ m} < TR \leq 4.5$ m (G) and $TR > 4.5$ m (H). A single-grain size (0.3 mm) and the formulation of Engelund-Hansen (1967), modified by Chollet and Cunge (1979) are used. The inner continuous line corresponds to 0 m (ODN) isobath. Vectors under $1 \times 10^{-6} \text{ m}^2 \cdot \text{s}^{-1}$ are omitted.

When compared to the residual velocity structure (Figure 6.10), the sediment transport patterns are somewhat different at the outer estuary, since most of the ebb-dominated sediment transport is moved away from the sandy spit area towards the central channel. This shift is expected to have minimised the effects of the flood-dominated residual currents over the eastern limits of the Salty. Most of the flood-induced sediment transport is then predicted to take place over the Salty and on the channel south of it. Nonetheless, flood-dominated sediment transport is expected even in the absence of any wave effects (more details in Figure 6.15).

As the tidal range approaches its maximum ($TR > 4.5$ m) in the area, a slight reduction in the magnitude of the total sediment transport and thus a landward retreat of the peak sediment transport is expected. Bearing in mind that: i) the water volume in the area will increase with the tidal range and that ii) the residual velocity field does not vary significantly between $4 \text{ m} < TR = 4.5 \text{ m}$ and $TR > 4.5 \text{ m}$ (Figures 6.10.G and H), then the resulting sediment transport is expected to decrease its magnitude, as shown between Figures 6.14.G and H. Also, non-linear interactions between the water volume inside the estuary induced by the tidal range and its bathymetry (i.e. enhancement of the estuary area due to the gentler slopes of intertidal banks) may also contribute to the relative reduction of the residual sediment transport at the largest tidal range.

At a more detailed level, Figure 6.15 illustrates the ebb-dominance characteristics of the outer estuary, with most of the main outflow feeding the ebb-delta sandbanks off the estuary (Figure 3.1, items E, F and G). A rather small portion of the seaward sediment transport at the outer estuary channel is re-circulated back to the Salty area (and up-estuary) through the flooding area to the west of the estuary entrance. This pattern is also predicted by authors such as Nunny (1980) and Wells (2002a), shown in Figure 3.2. According to Stive and Wang (2003), circulation features in the residual sediment transport are common in ebb and flood dominated channels, whilst the instantaneous sediment transport is likely to be one order of magnitude higher than the overall residual patterns.

Through the application of the sediment formula proposed by Engelund-Hansen (1967) and modified by Cholley and Cunge (1979), the relatively more intense residual currents under the summer-autumn 2003 (Figures 6.8.D, 6.9.D and 6.11.D) resulted in the residual

total sediment transport being twice as big as that predicted for the winter-spring 2002/2003. However, it must be borne in mind that the magnitude of the sediment transport rates may vary significantly according to the formulation chosen, as mentioned in Section 4.1 and demonstrated by several authors such as de Vriend et al. (2003), Nicholson et al. (1997), Pechon et al. (1997), Davies et al. (1997), Walstra et al. (2001), Davies et al. (2002), Davies and Villaret (2002) and Sutherland et al. (2004).

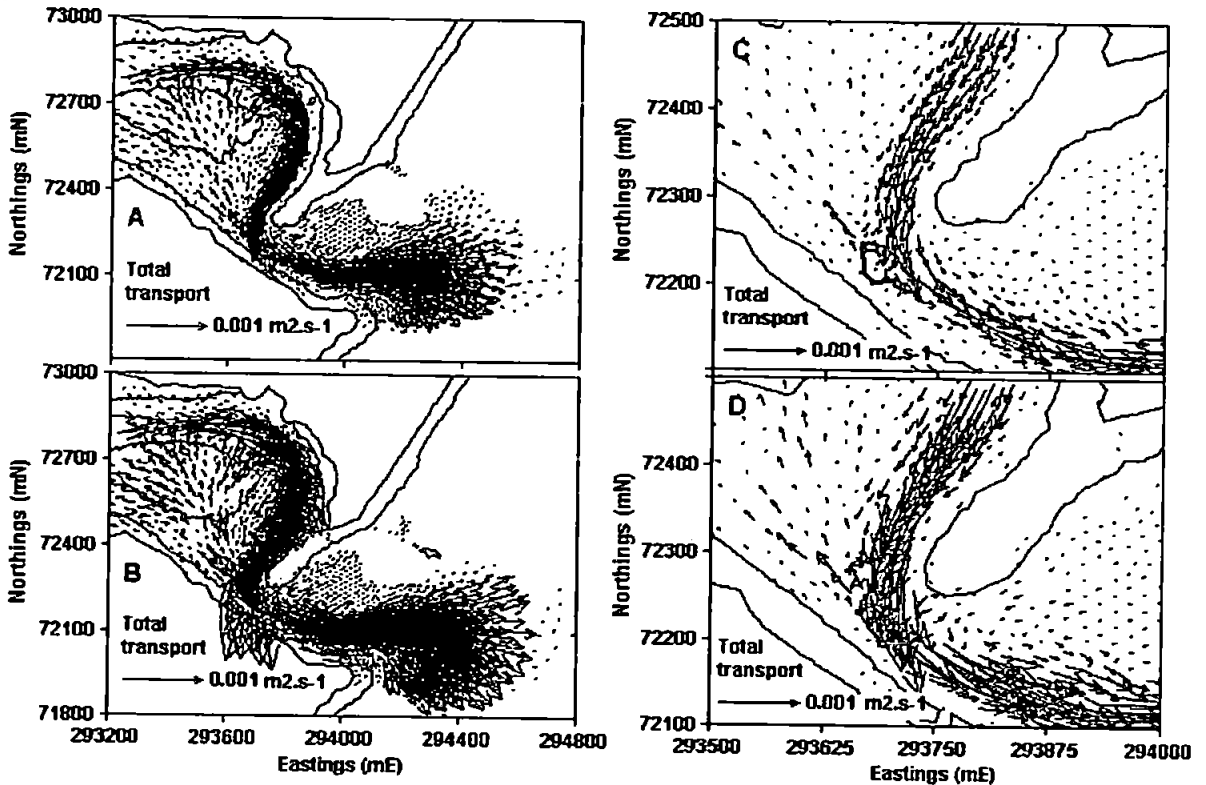


Figure 6.15: Residual total sediment transport volume per unit width at the outer estuary and adjacent coast for spring tides of winter-spring 2002/2003 (A and zoomed in C) and summer-autumn 2003 (B and zoomed in D). The inner continuous line corresponds to 0 m (ODN) isobath, while the red ellipsoidal element in plots 'C' and 'D' represents the -8 m (ODN) isobath. Vectors under $1 \times 10^{-6} \text{ m}^2 \cdot \text{s}^{-1}$ are omitted.

The morphodynamic evolution of the Teign estuary and adjacent coastal area is more complex than considered in these tests, where only tides, river discharge and a single grain size were taken into account. As a result, the comparison between predicted and observed features is very poor (Figure 6.16). The seasonal signal on the bed evolution is not reproduced by the model results, which are qualitatively very similar to each other (Figures 6.16.C and D). This finding is expected, since both runs were based on the same forcings (namely, tides and river discharge) and on the same set-up parameters. However, as these

two simulations did not represent the same periods of time, the slight differences between these two model results are likely to be due to i) different initial bathymetric conditions and ii) different observed water level and river discharge data used to force the model. The BSS for the winter-spring 2002/2003 was of -1.41 and of -2.25 for the summer-autumn 2003. The comparison between the model runs (Figures 6.16.C and D) also allows the analysis of the morphodynamic character of the model: it is shown that the enhanced residual water level differences during the summer-autumn 2003 relative to the winter-spring 2002/2003 (Figures 6.7 and 6.8) contributed to a larger and more effective bed evolution for the summer-autumn 2003 period (Figures 6.16.C and D).

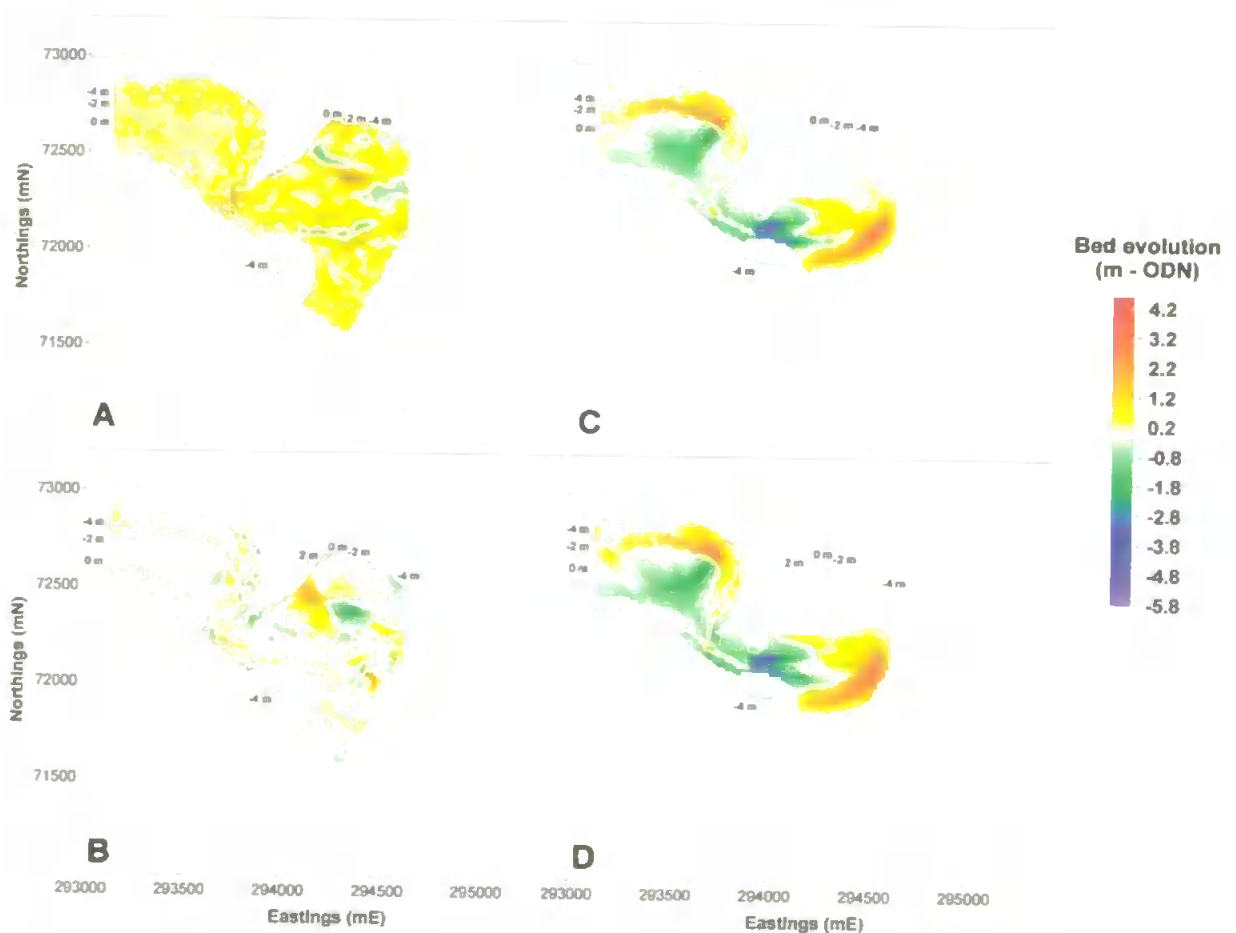


Figure 6.16: Morphological changes at the Teign estuary between December 2002 to May 2003 (A: observed data and C: model results) and May 2003 to November 2003 (B: observed data and D: model results). Erosion features are associated to green and blue areas. Yellow and red patterns correspond to sediment deposition in the period. Isobaths (m ODN) correspond to bottom properties at the beginning of the respective period.

Given that the assumptions made on the modelling exercise were not enough to satisfactory replicate field measurements (as shown in Figure 6.16), further processes seem

to be missing in the model framework. In the next section, the effects of wave stirring and of mixed grain sizes on the predicted bed evolution are assessed.

6.4. Inclusion of mixed grain sizes and wave effects on medium-term (months to years) morphodynamic processes

6.4.1. The implementation of mixed grain sizes and stirring wave effects

Recent developments in Sisyphe have allowed the introduction of variable distribution of grain sizes and the inclusion of the stirring effect of waves. Thus, the goal of this section is to address whether the consideration of such parameters in the modelling exercise would be linked to the observed sediment import (and deposition; Figure 6.16.A) at the outer estuary and adjacent coastal area for the winter-spring 2002/2003 (CoastView surveys 2 and 3). It is also important to stress that wave-generated currents are completely neglected in the following tests. As seen in previous sections, under the effects of tides and river discharge the estuary is only subject to an export of sediments through the ebb-dominated influence of tides and river discharge, whereas recirculation processes are active on the outer estuary.

Grain size properties are based on field samplings (Section 3.2.5 and Figure 3.7). Six different grain size fractions are defined: silts and clays ($D_{50}= 0.0335$ mm); very fine and fine sands ($D_{50}= 0.156$ mm); medium sands ($D_{50}= 0.375$ mm); coarse and very coarse sands ($D_{50}= 1.25$ mm); granules ($D_{50}= 3$ mm) and gravels ($D_{50}= 34$ mm). These sediment fractions are defined on a node-by-node basis, where the sum of all fractions at a given node is around 100% (i.e. the grain size composition is this given node is completely described by the six sediment fractions described above). Initial grain size distribution is shown in Figure 6.26.

Two vertical layers of sediments are considered, with no stratification between them (i.e. both layers have the same initial grain size distribution). The top layer, also called the

'active' layer (more details in Section A1.3.1) has a constant thickness of 0.05 m, while the remaining volume between the bedrock depth and the active layer will be filled by the lower layer. As the model computes the total sediment transport and bed evolution equations, then the grain size distribution on the top layer is changed accordingly. If the top layer is completely eroded at a given node, then the sediment on the layer underneath becomes available for the purposes of the sediment transport.

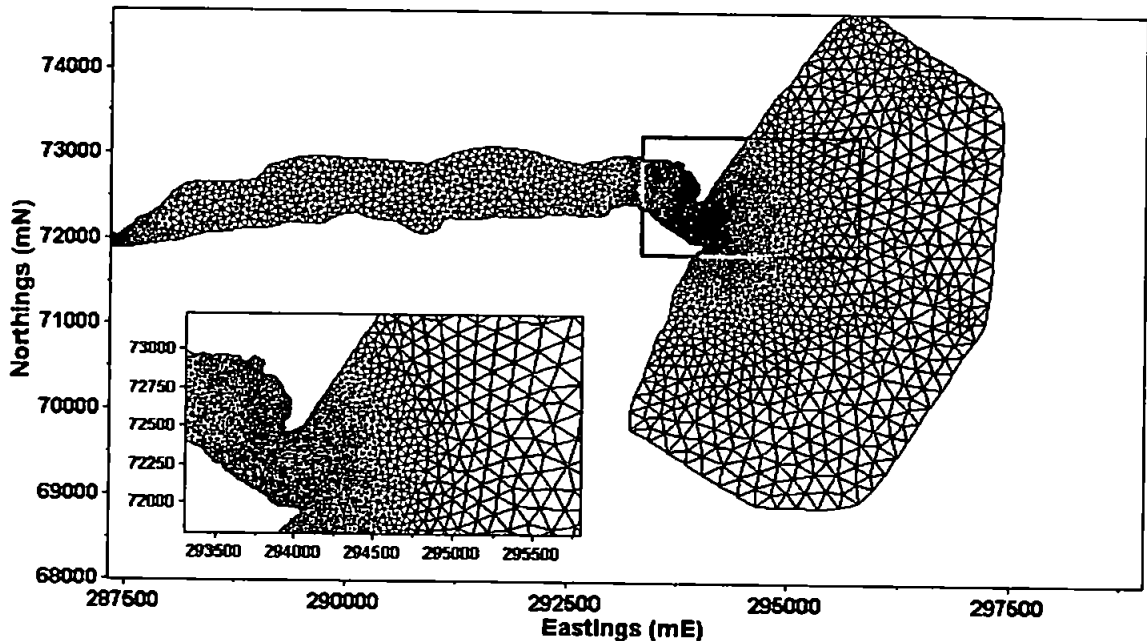


Figure 6.17: Mesh used for the simulation of mixed grain sizes and the wave-induced stirring effects (4234 nodes). The inset represents the area of further mesh refinement due to channel meandering and complex bathymetry.

Wave characteristics to be considered in the following tests are based on field data described in Sutherland et al. (2001a) in Section 3.1.2: wave heights of 0.8 m, wave period of 8 s approaching the coast from the eastern and southeastern quadrants. Wave properties vary with the local water depth, being modified according to the shallow water approximations as they reach the surf zone and the estuary entrance. Further inland, they are reduced exponentially. Given that swell waves do not penetrate into the estuary (Wells, 2002b; described in Section 3.1.2), their effects will be null landwards of the estuary entrance. As a first approach to understand the influence of waves on the morphodynamic evolution of the Teign estuary, the conditions above were assumed as time-invariant (i.e. the area is under constant high-energy wave events). More details on the calculation of the wave-induced shear stress are given in Sections A1.3.5 and A1.3.6.

The sediment transport formulation of Bijker (1968) is applied, as it allows the inclusion of some wave-related processes. The empirical factor 'b' considered in Bijker's (1968) formulation is chosen in this thesis to be equal to 2 (Appendix 1), in line with the default value proposed in Sisyphe (Villaret, 2004). Since the wave direction in this formulation is assumed to be parallel to the mean current, the offshore boundary of the selected mesh (Figure 4.2.C) is slightly shifted to replicate the origin of waves under storm periods (Figure 6.17), while the mesh generating parameters were the same as for the previous mesh.

6.4.2. Residual current patterns under the influence of mixed grain sizes and wave effects

As seen in the previous sections, under a single grain size distribution and in the absence of waves, the outer estuary would behave as a source of sediment to the adjacent ebb-tidal delta. Further results (not shown) have demonstrated that unless the mixed grain size approach and the stirring wave effects are both taken into account in the same run, a net export of sediment is predicted for the outer estuary and adjacent coast. If a single grain size of medium sand (0.3 mm) is considered to be under the influence of waves such as those described above, the resulting bed shear stress is insufficient to modify the sediment transport patterns; hence, a net export of sediment is modelled. Likewise, if mixed grain sizes are considered in the absence of waves, the net sediment transport will also follow the ebb-dominated morphodynamic behaviour described in Sections 6.3.2 and 6.3.3.

Although the initial hydrodynamic conditions were not varied from the tests described in Section 6.3, the morphodynamic processes (i.e. interactions between hydrodynamics, sediment transport and bed evolution) seem to influence the residual current patterns (Figure 6.18) as the tidal range increases, despite an overall agreement between these residual patterns. The major differences between the results shown in this section (Figure 6.18) and those discussed in Section 6.3.2 (Figure 6.10) are as follows: i) a more homogeneous current distribution in the flood-dominated areas within the outer estuary and ii) a more stable position and width of the jet-like ebb-dominated current at the estuary entrance; unlike in the previous case.

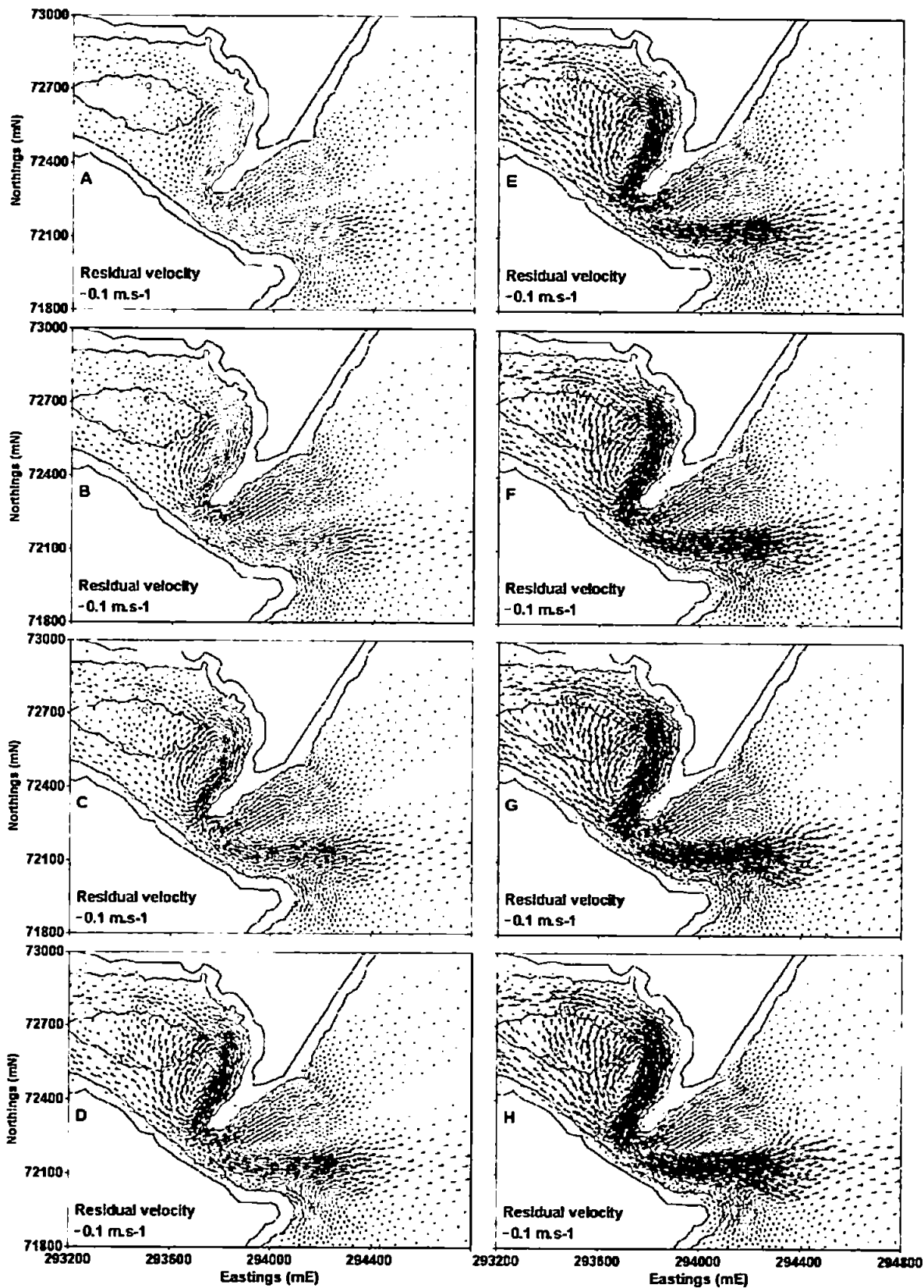


Figure 6.18: Residual velocity at outer estuary and adjacent coast for the winter-spring 2002/2003 under the joint effects of wave stirring and mixed grain sizes. $TR \leq 1.5$ m (A); $1.5 \text{ m} < TR \leq 2$ m (B); $2 \text{ m} < TR \leq 2.5$ m (C); $2.5 \text{ m} < TR \leq 3$ m (D); $3 \text{ m} < TR \leq 3.5$ m (E); $3.5 \text{ m} < TR \leq 4$ m (F); $4 \text{ m} < TR \leq 4.5$ m (G) and $TR > 4.5$ m (H). The inner continuous line corresponds to 0 m (ODN) isobath. Vectors under 0.01 m.s^{-1} are omitted.

The complexity and variety of phenomena included in this process-based morphodynamic model pose a limitation in pinpointing the exact causes of the differences described above, as also pointed out by Hibma et al. (2003). However, the presence of mixed grain sizes, the increase in the sediment transport dynamics due to the wave stirring effects and the difference in the sediment transport formulation between the tests described in Section 6.3.2 (Engelund-Hansen, 1967, modified by Cholley and Cunge, 1979) and the one selected in this section (Bijker, 1968) illustrate how the processes prescribed in the morphological module are capable of influencing the residual hydrodynamic patterns. This is another example of the inherent morphodynamic essence of this modelling exercise.

6.4.3. Residual total sediment transport patterns under the influence of mixed grain sizes and wave effects

The consequences of the inclusion of mixed grain sizes and the stirring effects of waves are considerable: while the residual hydrodynamic patterns are still ebb-dominated, the respective sediment transport is shifted to a flood-oriented behaviour (Figure 6.19). In other words, the estuary tends to import sediments under the presence of wave-generated storms approaching from the eastern and southeastern quadrants. As illustrated by de Vriend (1993) and shown in Table 2.1, the residual sediment transport can be in an opposite direction to the tidally-driven residual currents as long as the bed shear stress resulting from the joint effect of flood tidal currents and the stirring generated by approaching waves is larger than the bed shear stress induced by the ebbing currents.

For the simulations carried out in this section, the net sediment infilling process described above seems to be most efficient during the smallest and the highest tidal ranges. During 'average' tidal ranges the capacity of sediment import would be reduced. The import of sediment under the smallest tidal range ($TR = 1.5$ m; Figure 6.19.A) is predominantly originated at the flood channel to the south of the estuary entrance. Once inside the estuary, the flood channel to the south of the Salty is predicted to be the main pathway.

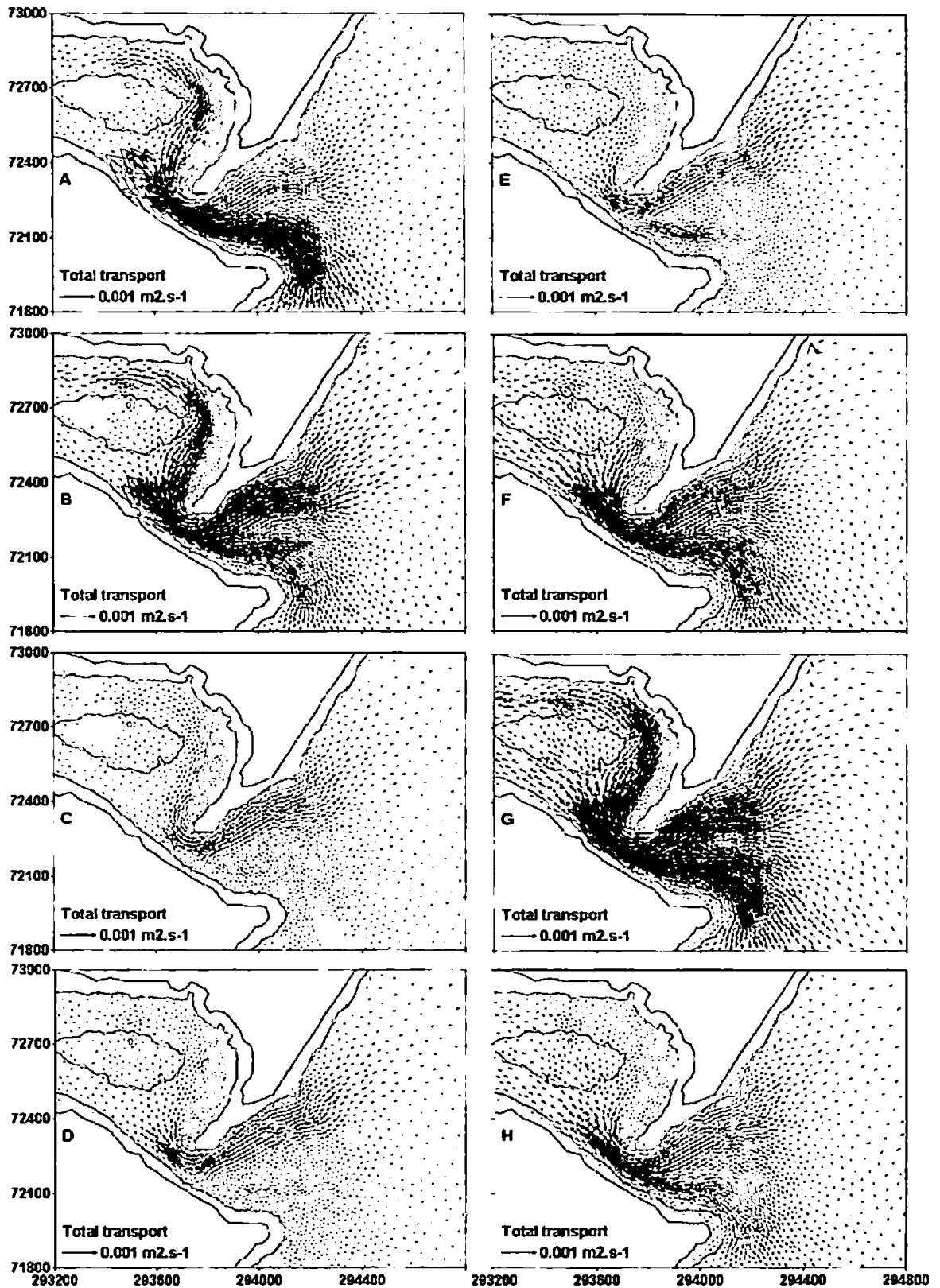


Figure 6.19: Residual total sediment transport volume per unit width at outer estuary and adjacent coast for the winter-spring 2002/2003 2003 under the joint effects of wave stirring and mixed grain sizes. $TR \leq 1.5$ m (A); $1.5 \text{ m} < TR \leq 2$ m (B); $2 \text{ m} < TR \leq 2.5$ m (C); $2.5 \text{ m} < TR \leq 3$ m (D); $3 \text{ m} < TR \leq 3.5$ m (E); $3.5 \text{ m} < TR \leq 4$ m (F); $4 \text{ m} < TR \leq 4.5$ m (G) and $TR > 4.5$ m (H). The inner continuous line corresponds to 0 m (ODN) isobath. Vectors under $1 \times 10^{-6} \text{ m}^2 \cdot \text{s}^{-1}$ are omitted.

Alternatively, the main channel at the outer estuary can also be used for the import of these very fine grains. As a result of the tidal ebb-dominated currents on the eastern side of the main channel (Figures 6.10 and 6.18), the import of sediment transport is confined to the western portion of the channel, closer to the edge of the Salty (Figures 6.19.A and B). From the $1.5 \text{ m} < TR = 2 \text{ m}$, with the increase in the water depth, the relatively shallow flood channel along the sandy spit also becomes an important pathway for the import of sediments, resulting in an overall enhancement of the sediment transport magnitude (Figure 6.19.B).

The net infilling mechanism is then reduced by the enhanced ebb-dominated tidal currents, up to a point where an export of sediment is predicted off the estuary entrance (Figure 6.19.E). The net sediment transport then approaches a condition of dynamic equilibrium. From the $3.5 \text{ m} < TR = 4 \text{ m}$ onwards (Figure 6.19.F), it is important to make an analogy between the sediment transport patterns described in this section with those under a single grain size in the absence of stirring wave effects (Figure 6.14). For the latter conditions, it is seen that as the tidal range increases, not only the magnitude of the sediment transport is increased, but also the position of the bulk sediment transport processes is shifted seawards, off the Ness headland (Figures 6.14.E to H). Although the sediment transport formulae used in these two simulations are different, a qualitative agreement between the different formulae (not shown) allows some comparisons between these results.

If the tidally-driven residual patterns resemble those shown in Figure 6.14, it is proposed that the seaward migration of the peak sediment transport area under tidal influence would eventually take place offshore of the Ness headland, favouring the enhancement of flood-dominated patterns on either sides of the main channel. In Section 6.3.3, it is also proposed that non-linear interactions between the water volume inside the estuary induced by the tidal range and its bathymetry (i.e. enhancement of the estuary area due to the gentler slopes of intertidal banks) may also contribute to the relative reduction of the residual sediment transport at the largest tidal range. The decrease in the residual sediment import for the highest tidal range (Figure 6.19.H) would be linked to the relative decrease in the magnitude of the respective residual currents, thus causing a retreat of the ebb-dominated sediment transport towards the estuary entrance.

Despite the description of the residual sediment transport patterns given above, further investigation must be pursued in order to determine the causes of the asymmetric net sediment transport, where the import of sediments is predicted to be more effective during either the lowest or the highest tidal ranges. Hence, a breakdown of the sediment transport patterns for each of the six grain size fractions is discussed below.

In order to gain some insight into the morphodynamic behaviour of the different grain sizes observed in the Teign estuary, Figures 6.20 to 6.23 show the residual total sediment transport for each of the six grain size fractions under four different tidal ranges: $TR = 1.5$ m (Figure 6.20); $2 \text{ m} < TR = 2.5$ m (Figure 6.21); $3 \text{ m} < TR = 3.5$ m (Figure 6.22) and $4 \text{ m} < TR = 4.5$ m (Figure 6.23). These results confirm that the sediment transport processes of silt and clay fraction dominate the overall behaviour, being at least one order of magnitude larger than that of the remaining grain sizes (note the scale variation in Figures 6.20 to 6.23). It is important to stress that although cohesive sediments are not formally modelled by Sisyphe - as they are considered as passive tracers, cohesionless and responding instantaneously to the flow (more details in Sections 4.1) - the results to be discussed below serve as a preliminary indication of the behaviour of these grain fractions.

Although the direction component is missed in this analysis, the shape and the magnitude of the partitioned (i.e. for each grain fraction) total sediment transport help the understanding of the main morphodynamic processes governing the evolution of this area. At the smallest tidal range (Figure 6.20), the import of silts and clays is predicted, as demonstrated in Figures 6.19.A and 6.20.A, potentially reaching the inner estuary (not shown). Despite the relatively small magnitude of the residual tidal currents under such tidal ranges, silts and clays up to the inner areas of the estuary are expected to be remobilised as suspended-load. These results reinforce the findings of Nunny (1980) and Wells (2002a) shown in Table 3.1, whereby marine muds would accumulate in the inner estuary. It is only in this thesis, however, that a direct link is established between the wave stirring effects - which enhance the availability of sediment at the adjacent coastal area - and the accumulation of silts and clays as far as the inner estuary.

At this stage, very fine and fine sands, along with coarse sands are prevented from entering the estuary. The smaller magnitude of the sediment transport for medium sands fraction (Figure 6.20.C) is explained by the relatively low concentration of this grain size fraction

at the beginning of the simulation in the estuary entrance (Figure 6.20.C). Due to the insufficient energy conditions associated, granules and gravels are expected to be mainly immobile under the smaller tidal ranges (Figures 6.20.E and F).

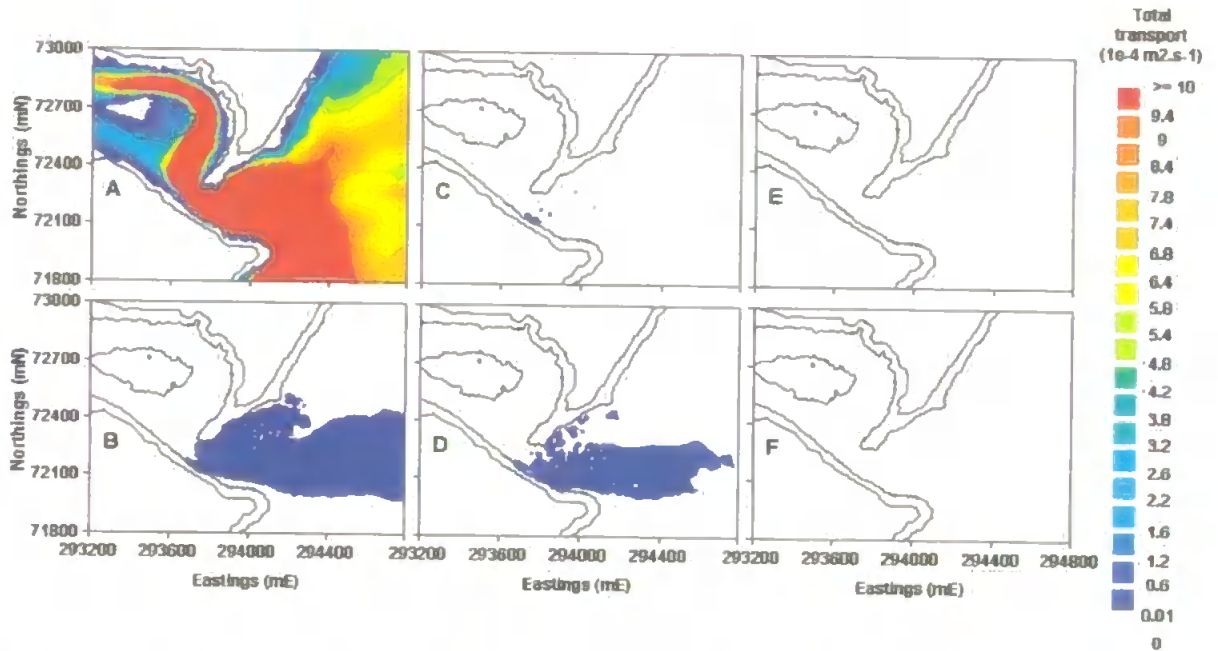


Figure 6.20: Partitioned total sediment transport for $TR \leq 1.5$ m. Silt and clay fraction (A); Very fine and fine sands (B); medium sands (C); coarse and very coarse sands (D); granules (E) and gravels (F). The inner line corresponds to 0 m (ODN) isobath.

As the tidal range increases, tidally-induced processes will also enhance the ebb-dominance and the export of sediments, although a portion of these sediments will be trapped into the estuary due to the recirculation processes acting on the outer estuary. Hence, the net sediment transport tends towards a condition of equilibrium, as illustrated in Figures 6.19.C to E, reflected in the reduction of the import of silt and clay fractions shown in Figure 6.21.A. The 'T' shape shown in this figure illustrates the bi-directional character of the sediment transport processes acting on the silt and clay fraction, which is mainly fed by the flood channel along the sandy spit at the estuary entrance. Despite this relative reduction in the import capacity of silts and clays, the transport of these grain fractions is extended up-estuary close to the estuary head (not shown).

During these conditions, very fine and fine sands can be potentially brought into the estuary, with exception of the ebb-dominated eastern side of the main channel (closer to the sandy spit) or can be flushed out of the estuary entrance by tidally-induced net currents

(Figure 6.21.B) Although of a smaller magnitude, a similar tendency is predicted for medium sands (Figure 6.21.C). Interestingly, coarse and very coarse sands (Figure 6.21.D) are distributed more effectively by the residual processes than medium sands, being possibly carried into the estuary. Meanwhile, granules are carried seawards (Figure 6.21.E), while gravel fraction is generally immobile under this tidal range.

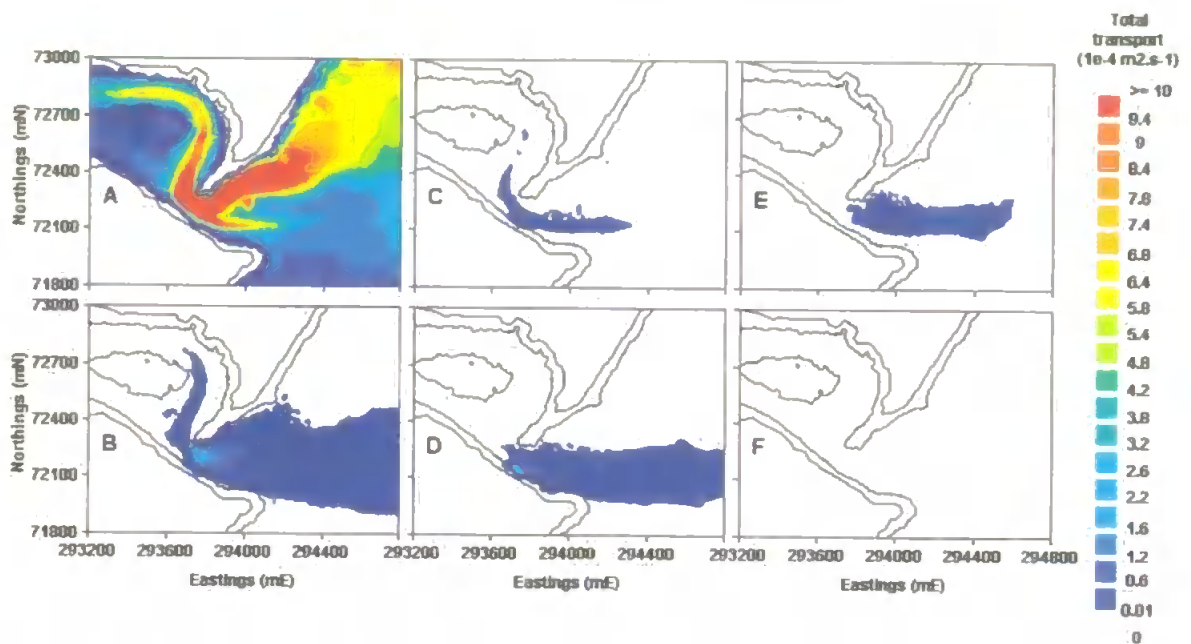


Figure 6.21: Partitioned total sediment transport for $2 \text{ m} < \text{TR} \leq 2.5 \text{ m}$. Silt and clay fraction (A); Very fine and fine sands (B); medium sands (C); coarse and very coarse sands (D); granules (E) and gravels (F). The inner line corresponds to 0 m (ODN) isobath.

When the tidal range is about average conditions, the import of silts and clays due to the joint effect of wave stirring effects and the flood-induced residual currents is reduced even further; while seaward of the estuary entrance the capacity for exporting this sediment fraction is enhanced (Figure 6.22.A), due to the ebb-dominated sediment transport shown in Figure 6.19.E. The morphodynamic conditions predicted for this tidal range would be enough to cause the remobilisation of sandy material present as far as the reaches of the middle estuary.

It is important to stress that it is from this sort of tidal range (i.e. $3 \text{ m} < \text{TR} \leq 3.5 \text{ m}$) that other grain size fractions can potentially be taken into the estuary either by the recirculating residual cell into the outer estuary and/or by the flood channels to the south of the Salty (Figures 6.22.B to D). However, the location of the peak sediment transport

values suggest that coarser grains are more likely to be exported from the estuary entrance. Although the transport of granules is mainly expected in the main channel seaward of the estuary entrance, it is also seen from Figure 6.21.E that granules could also be remobilised on the flood channel along the sandy spit. This suggests that this grain fraction could be potentially taken into the estuary under more energetic conditions, as demonstrated in Figure 6.22.E.

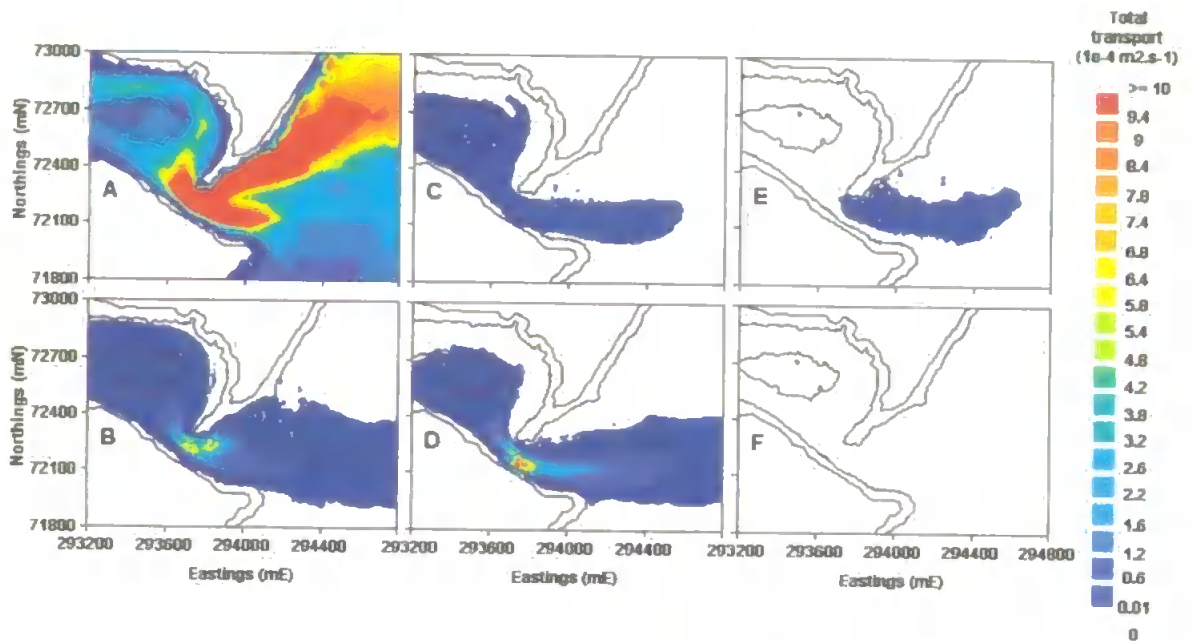


Figure 6.22: Partitioned total sediment transport for $3 \text{ m} < \text{TR} \leq 3.5 \text{ m}$. Silt and clay fraction (A); Very fine and fine sands (B); medium sands (C); coarse and very coarse sands (D); granules (E) and gravels (F). The inner line corresponds to 0 m (ODN) isobath.

Finally, at the second largest tidal range ($4 \text{ m} < \text{TR} \leq 4.5 \text{ m}$), all sediment fractions are reworked in some way. Apart from gravels, all the other sediment fractions could potentially be imported into the estuary (Figures 6.23.A to E). Very fine and fine sands would also be imported into the estuary through the flood channel along the sandy spit. In combination with silt and clays, the resulting total sediment transport would be sufficient to modify the sediment composition all the way up to the inner estuary, while medium and coarse sands up to the middle estuary could be influenced (not shown). Under these energy conditions, granules would be expected to be found up to the Shaldon bridge area (Figure 6.23.E).

Based on the calculation of the residual sediment transport for each of the grain fractions, it is concluded that: i) the asymmetric response of the residual transport (Figure 6.19) is

mainly dominated by the dynamics of silts and clays, since the mobility of this sediment fraction is at least one order of magnitude larger than that of the remaining fractions; ii) as the tidal range increases, coarser grain sizes as big as granules will eventually be imported into the estuary. Unlike the dynamics of silts and clays, model results suggest that the remobilisation of coarser grains is expected to be proportional to the tidal range. The comparison between observed and predicted bed evolutions is improved when compared to the results based on a single grain size in the absence of wave stirring effects (Figure 6.16). More details are given later in this chapter (Figure 6.28).

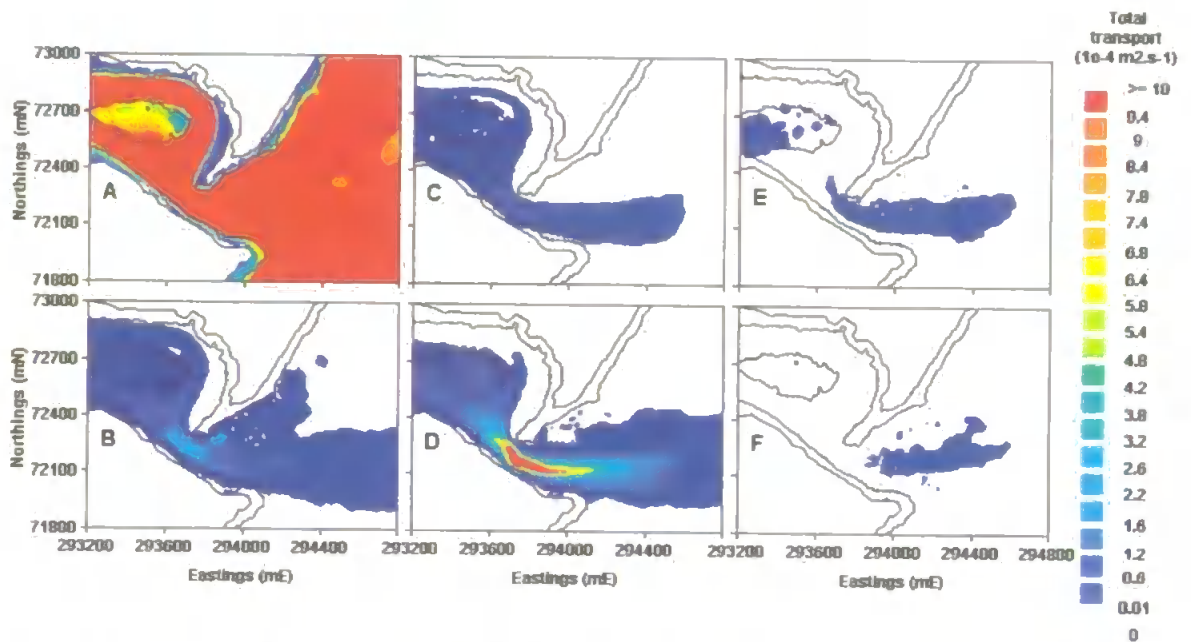


Figure 6.23: Partitioned total sediment transport for $4 \text{ m} < \text{TR} \leq 4.5 \text{ m}$. Silt and clay fraction (A); Very fine and fine sands (B); medium sands (C); coarse and very coarse sands (D); granules (E) and gravels (F). The inner black line corresponds to 0 m (ODN) isobath.

In order to provide further understanding of the differences between the sediment transport patterns without wave effects and a single grain size (Figure 6.14) against the tests which include the wave stirring effect and multiple grain sizes (Figure 6.19), two schematic diagrams are respectively proposed (Figures 6.24 and 6.25).

In the absence of wave stirring effects, the residual tidal currents will drive the ebb-dominated sediment transport (Figure 6.24). Thus, the export of sediment will be proportional to the tidal range. However, a relatively small fraction of this sediment could be prevented from leaving the estuary as it could be trapped in the recirculation process,

which is induced by the flood-dominated residual tidal currents acting on the Salty and on the flood channel to the south of the sandbank.

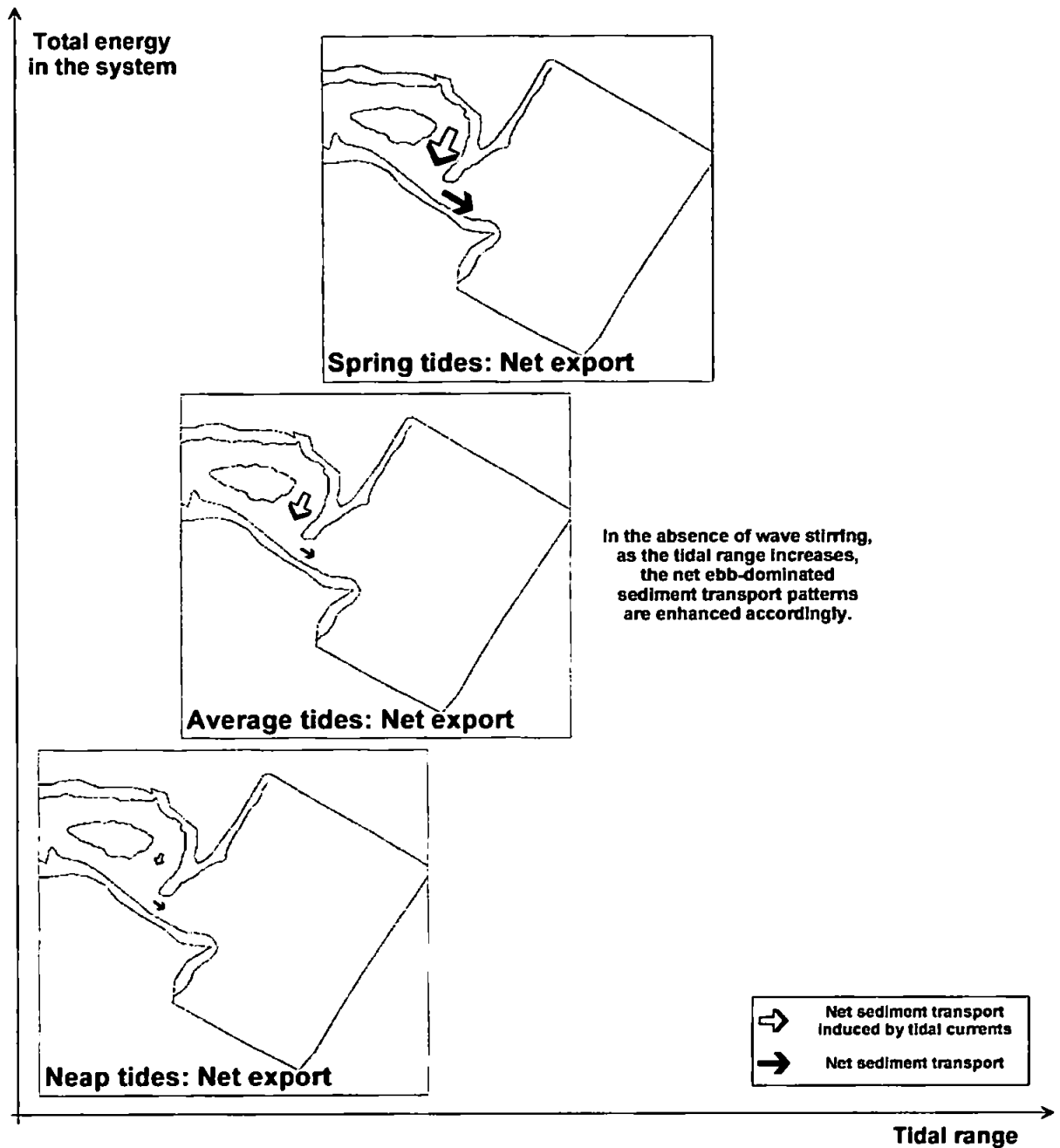


Figure 6.24: Schematic residual sediment transport patterns for the silt and clay fraction under tides, river discharge and a single grain size. Normal river discharge conditions (under $15 \text{ m}^3 \cdot \text{s}^{-1}$) are considered throughout. Tidally-induced residual sediment transport is indicated by red shaded arrows; thinner blue arrows are related to the net sediment transport.

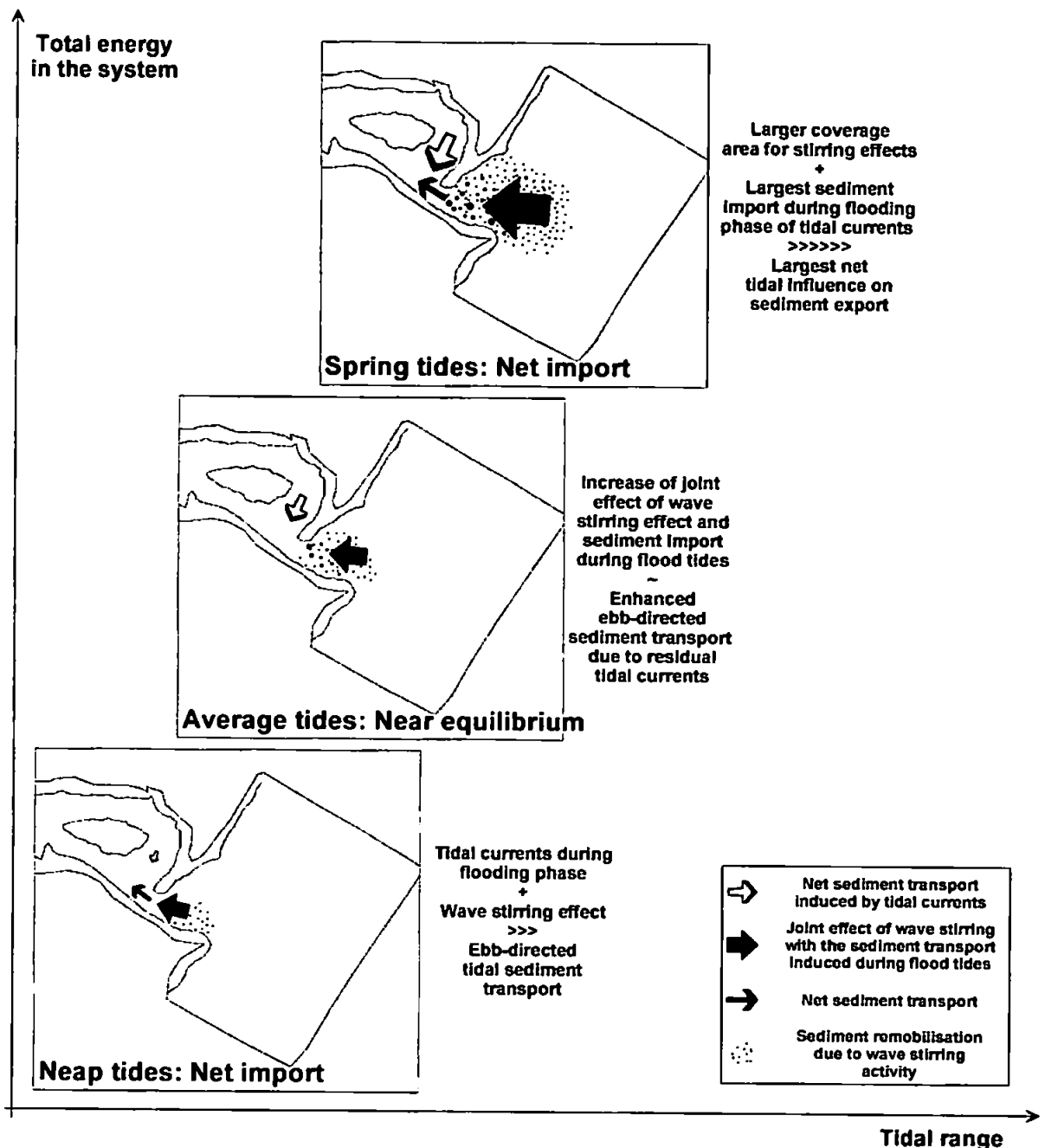


Figure 6.25: Schematic residual sediment transport patterns for the silt and clay fraction under mixed grain sizes and considering the wave stirring effect. Normal river discharge conditions (under $15 \text{ m}^3 \cdot \text{s}^{-1}$) are considered throughout. Tidally-induced residual sediment transport is indicated by red shaded arrows; the net effect of the wave stirring is given by black arrows and thinner blue arrows are related to the net sediment transport. The sediment availability as a function of the wave stirring is represented by black dots.

With the inclusion of multiple grain sizes and wave stirring effect, the monotonic distribution of the residual sediment transport is significantly changed. At the smallest tidal ranges (i.e. around neap tides), the residual tidal currents are relatively low (Figures 6.18.A and B). Hence, the sediment remobilised by the wave stirring effect and transported into

the estuary during the flood tides is enough to overcome the incipient ebb-directed sediment transport. A net import of finer sediments - especially of silts and clays - is modelled, while the export of sands from the estuary entrance seawards is initiated (Figure 6.20).

As the tidal range approaches average conditions, the net sediment transport patterns are increased accordingly at the outer estuary and on the adjacent coastal area. Despite the fact that the wave properties (i.e. H_s and T_s) remain unchanged at the boundary, larger tidal ranges will contribute to a more efficient wave stirring closer to the shore. The most likely factors to contribute to the enhancement of the wave stirring are the following: i) as the tidal range increases, the surf zone will tend to broaden on the flatter low tide terrace, thus potentially contributing to an increase in the area affected by wave stirring; ii) a wider influence of waves would be also linked to the remobilisation of the sediments on the various shallow shoals and sandbanks present in the coastal area. As these shallower areas are typically composed of coarser grains (Figure 6.26), the wave stirring effects on larger tidal ranges will also favour the sediment transport of coarser grains.

During average tides, if the sediment transport resulting from the sum of all sediment fractions is taken into account (Figure 6.22), it is seen that the sediment transport of silts and clays is only prevalent over the remaining grain fractions at the flood channel along the sandy spit and at either sides of the estuary entrance. As discussed in Section 6.4.3, this 'T' shape in the residual transport of silts and clays implicitly suggests that a dynamic equilibrium between the ebb-dominated tidal currents and the import of sediments related to the larger wave stirring is approached (Figure 6.25).

At spring tides, the residual tidal currents and the respective sediment transport reach their largest magnitudes. In the meantime, all sediment fractions are expected to be mobile under such dynamic conditions, especially silts and clays (Figure 6.23). Despite the fact that ebb-domination induced by residual tides approaches its largest values, it is overcome by a much more effective sediment import due to the combined wave stirring (now also acting over an even larger area) with the enhanced flood tides.

Summarising, the asymmetric sediment transport patterns described in Figures 6.19 and 6.25 are associated mainly with silts and clays, which would be mainly transported as suspended-load. This mode of transport is expected to be relatively enhanced due to extra

mixing provided by the inclusion of the wave stirring effects, resulting in an increase of the sediment availability in the system as a whole. Due to the absence of lag effects in the modelling framework (i.e. resulting in an instantaneous response of the sediment to the driving hydrodynamic process), both the remobilisation and settling processes of finer grains are likely to be overestimated when compared against their natural behaviour in the environment.

On the other hand, it is proposed that the behaviour of heavier grains, such as sandy material, granules and gravels will tend to increase proportionally with the tidal range in a more symmetric mode (Figures 6.20 to 6.23, more like the behaviour illustrated in Figure 6.24). Therefore, if there is sediment available (in this case, mainly driven by wave stirring at the adjacent coastal area) the import of silts and clays into the estuary would be enhanced during the smallest and largest tidal ranges, whilst coarser grains would tend to be imported with more efficiency as the tidal ranges increases, mainly through an enhancement of the bedload processes.

6.4.4. The fate of sediment fractions under the influence of mixed grain sizes and wave effects

In this section, the fate of the different grain size fraction inside the estuary and at the adjacent coastal area is discussed. The main goal of this analysis is to determine whether the model is capable of emulating realistic grain sorting processes in the Teign estuary. As the initial conditions, the model is fed with the grain size distribution shown in Figure 6.26. As the simulation progresses, the grains will be subject to being moved within the model domain. The relative variation in the grain size distribution is then calculated as the difference between the grain size concentration at a given time minus the initial concentration of that sediment fraction at the beginning of the simulation. This difference is called the 'grain size variation factor', expressed in terms of percentage. For example, if the initial concentration of medium sands at a certain node was 40% and at the end of the simulation it was 100%, then the resulting grain size variation factor will be 60%. In general terms, the initial conditions already embed some grain sorting, since finer sediments tend to be in the inner reaches of the estuary, whereas coarser grain sizes predominate towards the estuary entrance (Figure 6.26). The estuary is also seen to be nearly depleted of granules and gravels.

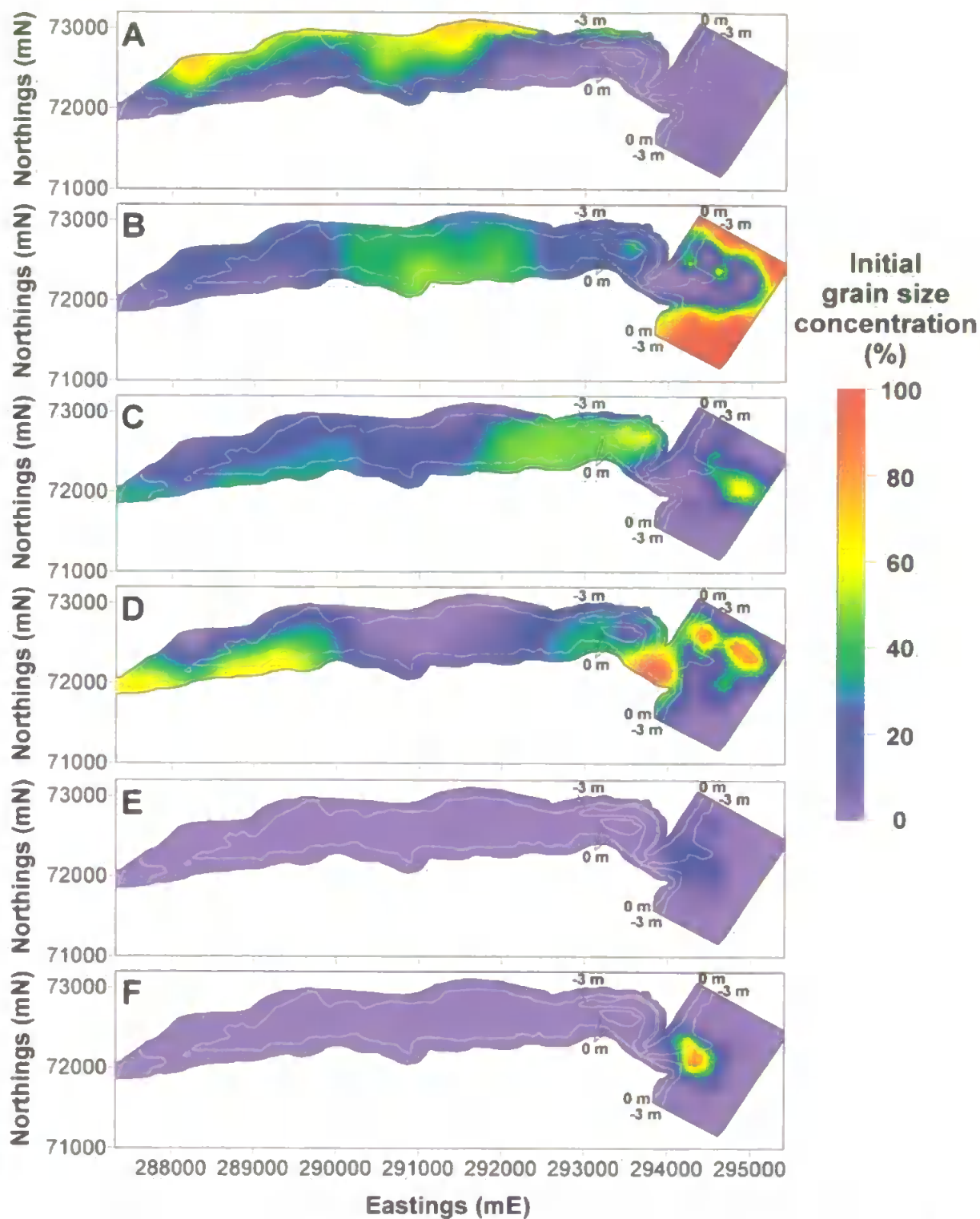


Figure 6.26: Initial grain size concentration for the tests with mixed sediments. Red and yellow patterns are associated with concentrations higher than 50%, while the areas with purple and blue colours are related to grain concentrations smaller than around 30%. Silt and clay fraction (A); Very fine and fine sands (B); medium sands (C); coarse and very coarse sands (D); granules (E) and gravels (F).

After the simulation of the winter-spring 2002/2003 period, the overall result of the interactions between the different forcing conditions and the multiple grain sizes is shown in Figure 6.27. In general terms, an improvement of the grain sorting is predicted inside the estuary, with finer sediments being deposited on its upper and inner reaches, while a sediment coarsening is simulated towards the estuary entrance.

On the seasonal scale, it is shown that the joint effect of wave stirring (associated with higher wave activity) and residual tidal currents are expected to increase the concentration of silts and clays in the Teign estuary and adjacent coastal area (Figure 6.27.A). Since only these sediment fractions are predicted to have a widespread distribution throughout the outer estuary and adjacent coast at the end of the simulation, it is postulated that the bulk of the sediment deposition observed during CoastView surveys (Figures 3.11.A and C) is composed of silts and clays. If wave-driven currents were to be considered, a wider range of finer sediments would also be expected to be deposited in the area. The concentration of silts and clays was also predicted to increase on the intertidal areas within the estuary, especially at the southern intertidal areas and at the head of the estuary (Figure 6.26.A). This relative difference between the northern and the southern intertidal banks is due to the prescription of the initial grain size distribution (Figure 6.26.A), where silts and clays were mostly present in the northern limits of the estuary.

In the absence of nearshore processes, such as wave-driven and longshore currents, silts and clays are also expected to be deposited on the beaches along the coastline. Seawards, it is seen that with exception of the estuary gorge and a restricted area of the ebb-delta, the concentration of silts and clays tend to increase under the conditions considered in this section. Since the boundary conditions for the morphological model are able to supply sediments to the domain if required, the overall enhancement of silts and clays at the end of the simulation period is likely to mimic an import of finer sediments from the Lyme Bay area during higher wave energy events.

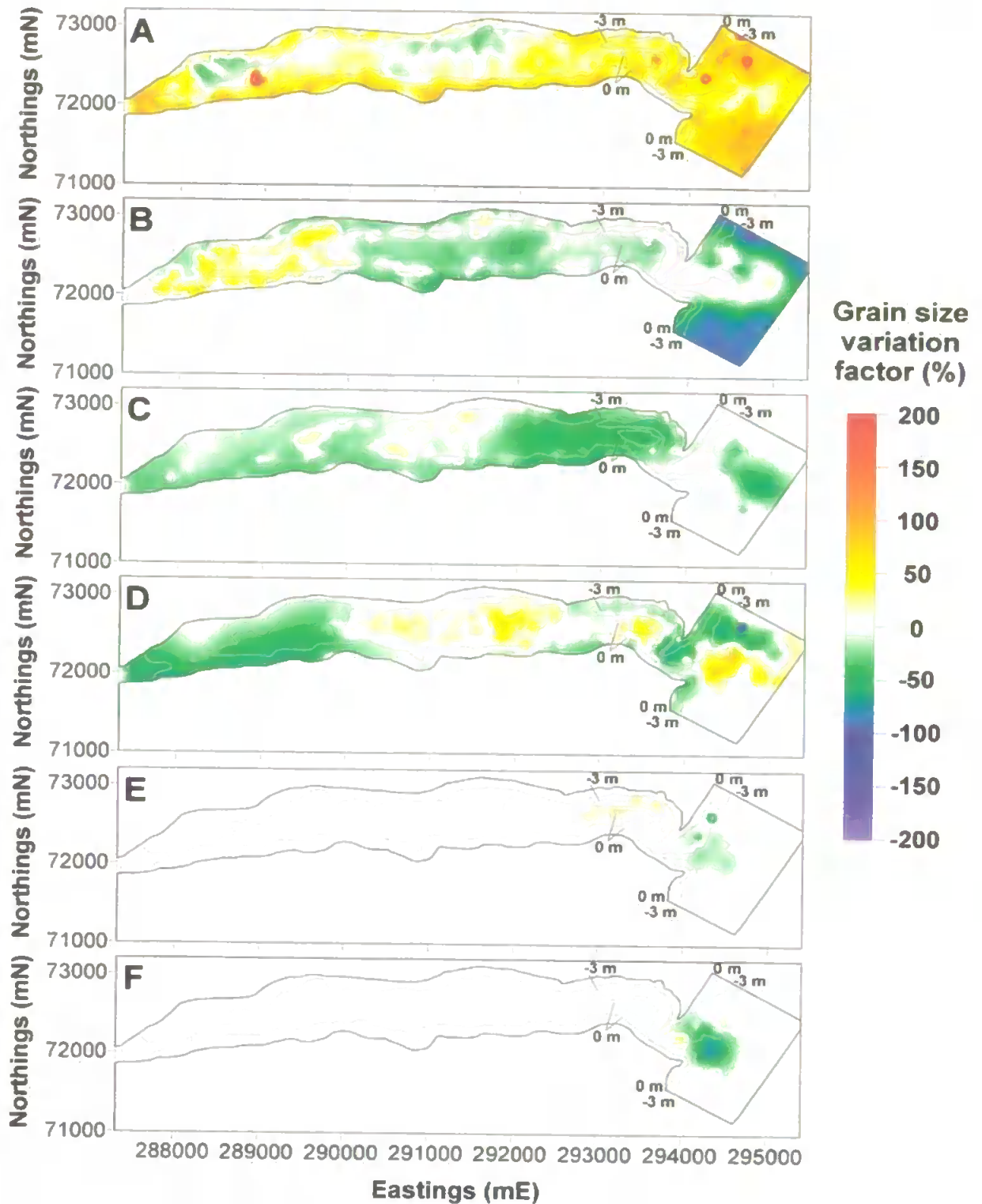


Figure 6.27: Differences in the grain size concentration at the end of simulation of the winter-spring 2002/2003 period relative to the initial conditions. Red and yellow patterns are associated with the accumulation of sediments, while the reduction of a given grain fraction is shown in green and blue tones. Silt and clay fraction (A); Very fine and fine sands (B); medium sands (C); coarse and very coarse sands (D); granules (E) and gravels (F).

The concentration of very fine and fine sands was enhanced in the inner estuary, while their distribution along the 0 m (ODN) isobath and close to the estuary entrance remained generally unchanged, which indicates that this sediment fraction may be in equilibrium at that depth (Figure 6.27.B). At the outer estuary and adjacent coast, the initial concentration of very fine and fine sands - which was close to zero - remains largely stable on the main channel area as this type of sediment is not expected to be deposited in areas of enhanced morphodynamic activity. Meanwhile, outside of the limits of the main channel, on the Salty and on the flood channel areas, a net decrease in the contents of these sediments is expected.

Medium sands were consistently remobilised from the intertidal areas and from the outer estuary, while the most likely areas to find these sediments were expected to be in the middle reaches of the estuary (Figure 6.27.C). The ebb-delta is also predicted to experience a decrease in the concentration of medium sands. As a whole, medium sands appear to be either flushed out of the estuary or being transported further inland.

Coarse and very coarse sands were transferred from the inner estuary to the middle portions of the system (Figure 6.27.D). At the outer estuary, these sediment fractions were mainly removed from the sandy spit and, in a smaller proportion, from the intertidal areas. The deposition sites were either the Salty sandbank or on the ebb-delta banks off the estuary entrance along the -4 m (ODN) isobath. The concentration of granules are predicted to be enhanced on the main channel to the north and to the west of the Salty, predominantly in the outer estuary (Figure 6.27.E). Along with gravels, the coarsest grain sizes on the ebb-delta shoals are expected to have their concentrations reduced (Figure 6.27.F). As predicted in Section 6.4.3 (and illustrated by Figures 6.20 to 6.23), grain sizes as large as granules are shown to be imported to the estuary. The enhancement of the granules concentration from nearly a complete absence inside the estuary to an enhancement of about 30% demonstrates the effectiveness of the joint effects of the wave stirring effects and the flood tides in transporting sediment into the estuary.

The inclusion of the wave stirring effects and of mixed grain sizes is found to play a key role in the import of sediments into the estuary under wave-generated storm conditions (Figure 6.28.B). However, other processes may play a role in the morphodynamic evolution of estuaries like the Teign, namely wave-driven currents, longshore flows and

lag effects. Hence, a future inclusion of wave-induced currents is expected to enhance the morphodynamic evolution of the area by supplying more sediments to it, as observed by Hoekstra et al. (2004). Longshore currents may also act as another source of sediments to the adjacent coastal area (and ultimately to the estuary), as they seem to contribute to maintaining the sandy spit on the northern limit of the estuary entrance. On the other hand, by taking into account non-equilibrium conditions (i.e. lag effects) the dispersion of the sediments in the area would be possibly more effective, mimicking the smoother widespread deposition patterns observed in the field (Figure 6.28.A). It is also important to stress that periods of high river discharge can potentially favour conditions for the remobilisation of sediments deposited within the estuary, contributing to the seasonal deposition/erosion patterns observed during CoastView surveys.

While the observed volume change for the area covered by CoastView surveys between December 2002 and May 2003 was of around 358,300 m³ (Table 3.6), the modelled sediment input to the same area was of about 76,620 m³. Hence, the net sediment transport induced by wave stirring effects and tidal currents under mixed grain sizes seems to be insufficient to explain the observed bed evolution features. This seems to reinforce the role of wave-driven flows, since it has been observed by Hoekstra et al. (2004) that enhanced sediment accretion takes place at the adjacent coastal area under stormy periods.

Apart from the import of sediment to the estuary, the model was able to predict the observed sediment accumulation on the tip of the sandy spit, although most of this deposition was modelled to be on the estuary gorge. Through the comparison between Figures 6.27 and 6.28, it is concluded that silts and clays contribute to the deposition patterns on the shallower areas, while the sediment accretion on the main channel is linked to coarse sands, very coarse sands and granules.

Unlike the negative BSS obtained for the tests with a single grain size in the absence of any wave effects (Section 6.3.3), the results shown in Figure 6.28.B are very close to the assumption of no change in the morphological features at the end of the simulation period, as the BSS= -0.003. This result illustrates the rigour of the BSS, despite the qualitative match between observations and model results with regard to the sediment infilling in the main channel of the outer estuary.

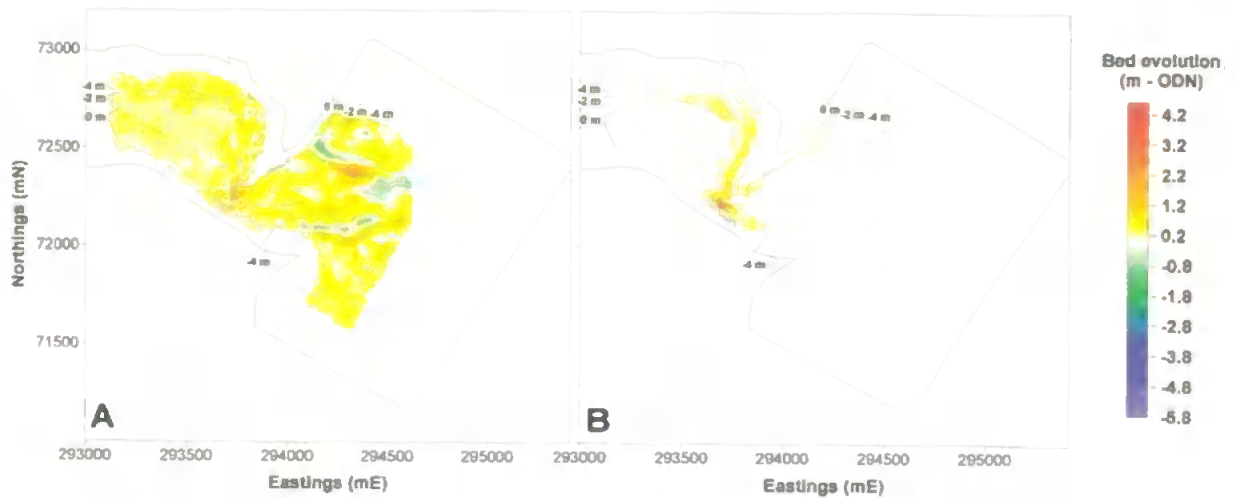


Figure 6.28: Morphological changes at the Teign estuary between December 2002 to May 2003: observed data (A) and model results (B). Erosion features are associated to green and blue areas. Yellow and red patterns correspond to sediment deposition in the period. Isobaths (m ODN) correspond to bottom properties at the beginning of the respective period.

6.4.5. The effects of isotropy on the sediment distribution patterns

In order to investigate the ability of the model in reproducing the observed grain size distribution, the test described in Section 6.4.4 is repeated with one difference: the initial grain size distribution is based on an isotropic field. Apart from the gravel fraction (with a relative concentration of 12.5%), the remaining grain size fractions have the same initial concentration everywhere at the beginning of the simulation (17.5 %). When summed up, the total grain size distribution at each node equals 100%. The main temporal and spatial scales in the transport of mixed grain sizes can then be assessed through this exercise.

After the simulation of the first tide ($TR \leq 1.5$ m, Table 5.4), the grain size distribution is already modified from the initial conditions (Figure 6.29), suggesting that morphodynamic processes within the Teign estuary can be rather active if the system is in any way in disequilibrium (i.e. the unlikely isotropic grain size distribution). Despite the findings of Wells (2002a; described in Section 3.1.2) that swell waves would not be able to penetrate into the estuary entrance, the results derived from the isotropic distribution imply that the estuarine morphodynamics would be coupled to the presence of wave-generated storms in the adjacent coastal area. This influence is likely to be increased if wave-driven currents were to be taken into account, since they are expected to enhance the sediment availability to be imported from the coast.

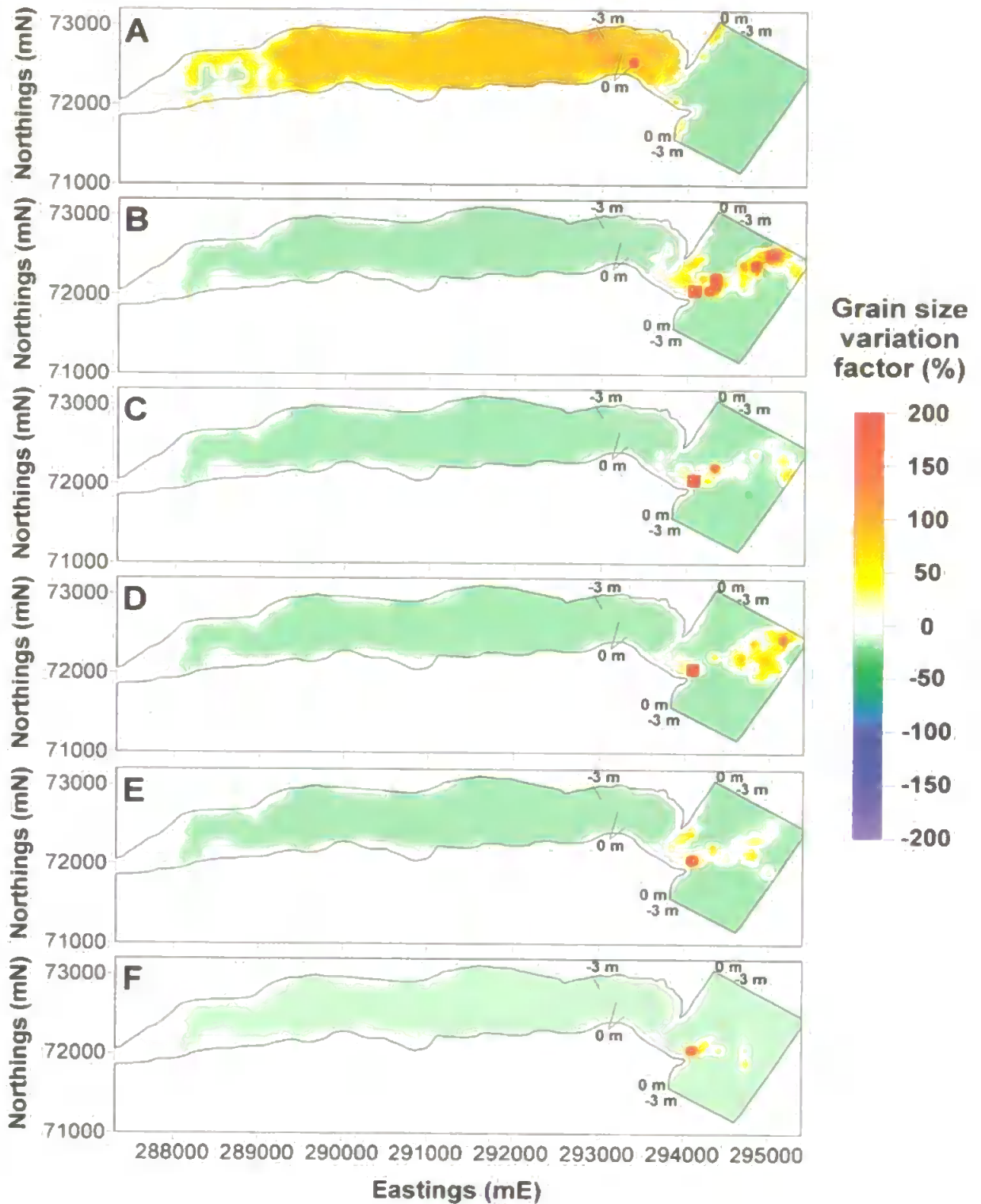


Figure 6.29: Differences in the grain size concentration at the end of the first tide ($TR \leq 1.5$ m) for the winter-spring 2002/2003 period relative to an isotropic initial distribution. Red and yellow patterns are associated with the accumulation of sediments, while the reduction of a given grain fraction is shown in green and blue tones. Silt and clay fraction (A); Very fine and fine sands (B); medium sands (C); coarse and very coarse sands (D); granules (E) and gravels (F).

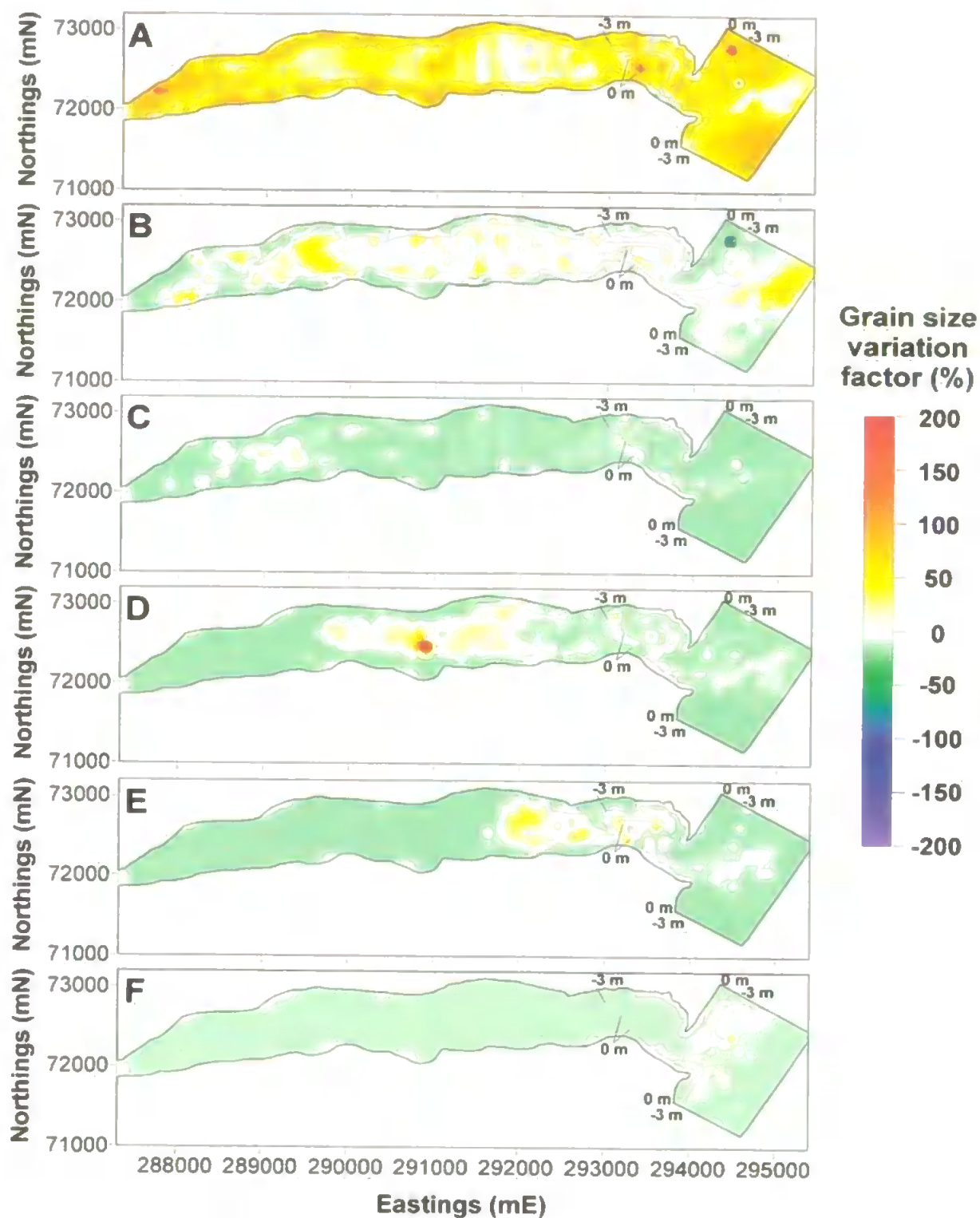


Figure 6.30: Differences in the grain size concentration at the end of simulation of the winter-spring 2002/2003 period relative to an isotropic initial distribution. Red and yellow patterns are associated with the accumulation of sediments, while the reduction of a given grain fraction is shown in green and blue tones. Silt and clay fraction (A); Very fine and fine sands (B); medium sands (C); coarse and very coarse sands (D); granules (E) and gravels (F).

Although there is a limited influence of the tidal currents into the inner areas of the estuary during the smallest tidal range, the general pattern of import of finer sediments (in this example, silts and clays) and export of coarser grains is noted at the end of the first tidal range. This process is predicted through the enrichment of silts and clays inside the estuary and on the beaches (in the absence of nearshore processes, as discussed earlier in Section 6.4.4; Figure 6.29.A) and the subtle transport of coarser grains seawards (Figures 6.29.B to F).

After six months of simulation, the results based on the isotropic distribution suggest a grading process, like the one predicted in Section 6.4.4. There is a general enhancement of the concentration of silts and clays throughout the system (enrichment of around 60% to 70%); some stability on their relative concentration around the Salty and off the ebb-delta sandbank and a localised decrease of their concentration on the southern (Shaldon) side of the estuary entrance (Figure 6.29.A). Within the estuary, intertidal banks, the head of the estuary and the Salty would be mostly enriched in their contents of silts and clays at the end of the six-month simulation period. Despite the model limitations in the modelling of cohesive sediments, these results confirm the model ability in replicating the basic behaviour of such sediments.

As the average grain size is increased, the sediment mobility of sands and coarser grain sizes is enhanced accordingly. As a result, the concentrations of these sediments are progressively enhanced inside the estuary. The relative concentration of very fine and fine sands seemed to be fairly stable, especially at the channel portions in the middle and outer estuary, and at the estuary entrance (Figure 6.30.B). The estuarine intertidal areas may have been the most likely source for the very fine and fine sands deposited in the channel reaches. Apart from the sandy spit, most of the intertidal areas at the outer estuary experience a relative stability in the grain size contents (Figures 6.30.B to F). The model predicts that medium sand concentrations are likely to be smaller for most of the estuary than the one prescribed at the beginning of the simulations (17.5%; Figure 6.30.C). The areas which are expected to contain the initial relative concentration are found at the inner estuary (channel funneling area); along the 0 m (ODN) isobath and close to the estuary entrance.

It is seen that coarse and very coarse sands will correspond to more than half of the sediments expected to be found at the deeper areas (below 0 m-ODN) of the middle estuary (Figure 6.30.D). Likewise, granules would be the most common grain fraction further seawards (Figure 6.30.E). Towards the estuary entrance, the presence of granules is increased between the middle and the outer estuary, with some enhancement around the Salty (Figure 6.30.E). The presence of gravels inside the estuary is also decreased, despite the smaller magnitude of the changes, due to the more energetic morphodynamic conditions required to transport this type of sediment. Although the areas subject to a relative enrichment of gravels is quite limited, the white areas in Figure 6.30.F suggest that the coastal zone between 0 m and -4 m (ODN) has a concentration of gravels between 10% to 15%.

Based on the application of the coupling between Telemac-2D and Sisyphe, short- to medium-term morphodynamic processes in the Teign estuary were assessed. The inclusion of mixed grain sizes and the wave stirring effects represent a step forward towards a thorough understanding of the future evolution of this area. The limitations highlighted in this thesis are likely to be minimised in the future, as within the frame of the Telemac system (Sisyphe 5.5), non-equilibrium conditions are already accounted for. Once the coupling between the wave-driven flow module and the morphodynamic system represented by Telemac-2D and Sisyphe is implemented, further understanding can be gained from the use of such process-based models in the medium-term - and ultimately in longer-term - evolution of estuaries.

6.5. Conclusions

In this chapter, the main model results showed that the water level differences between the estuary and the adjacent coastal area is sufficiently strong to play an important role in both the instantaneous and residual current fields.

The presence of the sandy spit at the estuary entrance seems to act as an important feature in the build up of such a gradient. The asymmetric character of the tidal wave propagation inside the estuary seems to be linked to the predictions, in residual terms, of higher water levels inside the estuary relative to the adjacent coast. This process influences the ebb-

dominated hydrodynamic patterns in most of the estuary entrance. In the absence of wave effects, this ebb-domination is also extended to the morphodynamic evolution in the form of a net export of sediments from the estuary.

The estuarine morphodynamic processes are modulated by the spring-neap cycle. The magnitudes of the resultant velocity vectors are roughly doubled under spring tides in comparison to the currents generated under neap tides. The predicted total sediment transport is at least one order of magnitude smaller during neap tides than under spring tide conditions. It must be stressed that this result only considers a single-grain size and neglects the effects of the wave stirring effects. Unless otherwise stated, the following findings only take into account the joint effects of tidal currents and normal ($< 15 \text{ m}^3 \cdot \text{s}^{-1}$) conditions of river discharge.

In the absence of freshets and under tidal ranges below average conditions, suspended-load transport at the estuary entrance is expected to be less than half of the bedload magnitude. Given that wave-driven flows were not modelled in this thesis, the predicted bedload transport rates compare reasonably well with the measurements described in Hoekstra et al. (2004). If both river discharge and tidal ranges are increased, then the average suspended-load transport is nearly three times larger than the bedload one. Thus, suspended-load processes are expected to be the main mode of sediment transport, as the most energetic morphodynamic conditions are expected under freshets and higher tidal ranges. In order to assess these findings in more detail further tests under the presence of wave-driven currents and mixed grain sizes must be carried out.

While there is a qualitative agreement between the residual currents of varying tidal ranges, a three-fold enhancement of the residual current magnitudes between the smallest and the biggest tidal ranges is expected. The most dynamic residual sediment transport patterns are found in the outer estuary and in the adjacent coastal area. Under the effects of river discharge and tidal currents, a net export of sediments is predicted, although some sediment can be trapped inside the estuary due to the recirculating patterns modelled even in the absence of any wave effects.

Along with the sediment import provided by the flooding phase of the tidal currents, the modelling of mixed grain sizes and the inclusion of wave stirring effects have proven to be key processes in the import of sediments under wave-generated storms. Some insight into

the main sediment transport pathways can be gained by the analysis of the interactions between the sediment export mainly induced by residual tidal currents and the import of sediments driven by the joint effects of wave stirring and the tidal flood phases.

Despite not being assessed in this thesis (since normal river discharge conditions are assumed) spates of river discharge are also likely to contribute to the sedimentary budget of the Teign estuary and adjacent coastal area. However, as demonstrated in this chapter the enrichment of sediments inside the estuary by tidal currents and by the wave presence at the adjacent coast are large enough to influence the sediment distribution throughout the Teign estuary.

The sediment transport of silts and clays is expected to largely dominate the total sediment transport behaviour under the residual effects of the following processes: tidal currents, normal river discharge and a hypothetical presence of high-energy wave events ($H_s = 0.8$ m and $T_p = 8$ s). The asymmetric sediment transport patterns described in Figures 6.19 and 6.25 are associated mainly with silts and clays, which would be mainly transported as suspended-load. This mode of transport is expected to be relatively enhanced due to extra mixing provided by the inclusion of the wave stirring effects, resulting in an increase of the sediment availability in the system as a whole.

On the other hand, it is proposed that the behaviour of heavier grains, such as sandy material, granules and gravels will tend to increase proportionally with the tidal range in a more symmetric mode (Figures 6.20 to 6.23, like the behaviour illustrated in Figure 6.24). Therefore, if there is sediment available (in this case, mainly driven by wave stirring at the adjacent coastal area) the import of silts and clays into the estuary would be enhanced during the smallest and largest tidal ranges, while coarser grains would tend to be imported with more efficiency as the tidal ranges increases, mainly through an enhancement of the importance of bedload processes.

It has been demonstrated that the morphodynamics of the Teign estuary and adjacent coastal area is also modulated on a seasonal time scale. During summer periods, the frequency of wave-generated storms tends to be smaller, while the freshwater influence is generally around average. Thus, a net export of sediments is expected from the estuary to the adjacent coast due primarily to tidal dominance, which results in erosion patterns observed during CoastView surveys. During winter periods, the more frequent presence of

storms and higher river discharge tend to add more energy to the system. In this case, wave-derived processes will tend to import mainly finer grains, although predictions suggested that sediment fractions as big as granules could be transported into the estuary.

At the end of the six-month simulation, a grain sorting is predicted. Inside the estuary, a coarsening of the sediment grains is expected from the inner and upper reaches of the estuary towards its deeper and outer areas, a finding consistent with observations. Although *Sisyphe* does not formally model the dynamics of cohesive sediments (i.e. treated as passive, cohesionless tracers, where lag effects are totally neglected), the predominance of silts and clays on the inner and upper reaches of the estuary indicates an overall model skill in predicting the dynamics of such fine sediments.

Compared to the observed volume variation for the winter-spring 2002/2003 period, the modelled sediment accumulation for the outer estuary and adjacent coastal area during the same period was around 80% smaller. This seems to reinforce the role of wave-driven flows, since it has been observed by Hoekstra et al. (2004) that enhanced sediment accretion takes place at the adjacent coastal area under stormy periods. Through the comparison between Figures 6.27 and 6.28, it is concluded that silts and clays contribute to the deposition patterns on the shallower areas, while the sediment accretion on the main channel is linked to coarse sands, very coarse sands and granules. Unlike the negative BSS obtained for the tests with a single grain size in the absence of any wave effects (Section 6.3.3), the inclusion of wave stirring effects and mixed grain sizes induced a nearly null BSS, implying that the baseline bathymetric condition has not been significantly changed at the end of the simulation. This result illustrated the rigour of the BSS, despite the qualitative match between observations and model results with regard to the sediment infilling in the main channel of the outer estuary.

The simulation of an isotropic grain size distribution showed the model ability in generating a grain size sorting, which was similar to the model results for the case based on field grain size distribution. Thus, finer grain sizes are expected to be found in the upper and inner areas of the estuary, while coarser grains seawards. Since wave-driven currents are not included in the modelling exercise, these results suggest that even if swell waves do not penetrate into the estuary entrance - as claimed by Wells (2002a) and described in Section 3.1.2 - they are expected to increase the sediment availability in the coastal area adjacent to the Teign estuary.

Chapter 7 - General Conclusions and Further Research

7.1. General conclusions

This thesis has provided a substantial contribution to the medium-term (months to years) morphodynamic modelling of estuaries. An input reduction technique has been successfully implemented, resulting in a considerable reduction of run time whilst ensuring accurate predictions when compared to the model output of a complete simulation. Moreover, this study has enhanced the current knowledge on the mechanisms associated with the import of sediments into estuaries.

The principal morphodynamic mechanisms of an active and complex system, the Teign estuary (UK), were assessed through the application of a morphodynamic, process-based (bottom-up) model. The coupling between Telemac-2D (hydrodynamic module) and Sisyphe (morphological module; both modules in version 5.3) has been shown to successfully represent the contribution of tides, wave stirring and multiple grain sizes to the morphodynamic evolution of the area.

The use of extensive field data sets (Chapter 3) to calibrate and validate the model (Chapter 4) has also proven to be a key aspect in providing accuracy to the modelling exercise. The dynamic behaviour of the outer portions of the Teign estuary and of the adjacent coastal area was illustrated by strong bathymetric seasonal changes measured by the surveys carried out in the CoastView^{7.1} project. During the 2-year period (December 2002 to November 2004), the results suggested a net deposition during winter-spring periods and an overall erosion during summer-autumn months (Figure 3.11). Longer-term (order of years) trends derived from the seabed volume time-series indicated that the area has undergone a net sediment infilling over the past 2 years, with an average deposition rate of about 20 cm.year⁻¹ (Table 3.6 and Figure 3.12). Such a rate is unlikely to be sustained in longer-time scales. Within the concept of a morphodynamic equilibrium,

^{7.1} For further details, visit: <http://www.thecoastviewproject.org>

processes such as tidal currents and the intermittence of freshets would enhance the export of sediment, pushing the estuary back to its equilibrium conditions.

In line with the specific objectives laid out in Chapter 1, the main conclusions of this thesis are as follows:

- Implement, calibrate and validate a hydrodynamic model based on Telemac-2D for the Teign estuary and adjacent coastal area

The performance of the model was assessed through visual comparison and by the application of robust statistical methods. For the hydrodynamic results, the following tools were used: Relative Mean Absolute Error - RMAE and Adjusted Relative Mean Absolute Error - ARMAE, proposed by Sutherland et al. (2001); van Rijn et al. (2003) and Sutherland et al. (2004). According to the classification system of the statistical methods applied, the overall accuracy of the hydrodynamic calibration and validation of Telemac-2D was objectively described as 'reasonable'. However, when measurement-related errors are removed from the statistical analysis, the model results are consistently improved towards the estuary entrance, achieving a 'good' to 'excellent' classification. Despite being based on simplified boundary conditions and on a more efficient mesh gridding (i.e. finite element approach), the model results presented in this thesis showed a similar skill to other models (Sutherland et al., 2001b and Siegle, pers. comm.) applied to the Teignmouth area (Section 4.3).

- Enhance the current knowledge of morphodynamic processes in coastal systems through the implementation of a morphodynamic model to the Teign estuary and adjacent coastal area

Given that morphodynamic models are not yet sophisticated enough to accurately predict morphological changes in coastal systems, the results described in this thesis provide important insights into the complex feedback mechanisms between tides, river discharge, waves and multiple grain sizes. Even in the absence of wave-driven currents - which were neglected due to operational model limitations - observed seasonal sediment deposition

during winter months and net erosion during summer periods were qualitatively reproduced by the model. Along with residual tidal currents, wave stirring effects and the presence of multiple grain sizes were shown to be directly associated with the seasonal import/export patterns observed at the outer estuary and at the adjacent coastal area. The use of the Brier Skill Score (BSS), first adapted to coastal morphodynamic studies by Brady and Sutherland (2001) and Sutherland et al. (2001) to objectively assess the accuracy of the morphodynamic prediction, proved to be a very robust technique. Its use in the analysis of coastal processes is therefore encouraged. The model skill in predicting medium-term (order of months to years) morphologic changes in such a dynamic and active area was shown to be relatively improved.

- Develop and validate an accurate and computationally efficient method for longer-term morphodynamic simulations

The prediction of longer-term morphodynamic processes carried out with process-based models such as the one used in this thesis is very time consuming due to the frequent iterations required between the hydrodynamic and the morphological modules. Based on the work of Latteux (1995), the so-called ensemble technique was proposed and successfully applied to tidal and riverine data, where a time efficient performance and accurate results - when comparing the model outcomes based on the ensemble technique against those of a reference model run - were ensured. Moreover, the technique has the added benefit of a potential applicability to any process-based numerical model capable of simulating medium-term morphodynamic processes (Chapter 5).

When comparing the bed evolution of the ensemble technique against the outcome of complete simulation (reference run), 'excellent' values of the BSS (around 0.91; Figure 5.6) were found, according to the classification system proposed by van Rijn et al. (2003). Not only the accuracy of the results was ensured, as the simulation time was significantly reduced. This reduction is shown to be proportional to the number of average tides (N_{TIDES}) used. The simulation time was reduced to about 85% of the original time. The ensemble technique encompasses several steps, which are described below:

- All average tides, based on classes of different tidal ranges, must be included in the modelling process as a continuous record. For the Teign estuary a single representative tide was found not to satisfactorily encapsulate the morphodynamic evolution of the reference run;
 - A cumulative bed evolution change must be ensured by the use of the bed evolution of a given average tide to be used as initial conditions for the modelling of the next average tide;
 - As suggested by Latteux (pers. comm.), a scaling factor (S_C) can be used in the sediment transport formula to ensure simultaneously a time- and quality-effective result;
 - For the tests with a spring-neap cycle, a chronology effect was observed to play a role in the bed evolution predicted for the ensemble technique runs. For the longer-term simulation of tides, the chronology of the tidal events is expected to be less important due to their cyclical behaviour.
- Identify the main mechanisms and their interactions responsible for the short-term (order of hours to days) morphodynamic evolution of the area

The water level differences found between the Teign estuary and the adjacent coastal area are the main driving mechanism responsible for the short-term circulation in the area (Section 6.2). This finding is corroborated by the accurate reproduction of observed velocity magnitudes closer to the estuary entrance (Tables 4.5 and 4.6).

The estuarine morphodynamic processes are modulated by the spring-neap cycle. Relative to neap tides, velocity magnitudes are roughly doubled under spring periods. The predicted total sediment transport is at least one order of magnitude smaller during neap tides than under spring tide conditions.

During low-energy conditions (i.e. neap tides in the absence of freshets), suspended-load transport is about less than half of the bedload magnitude. Given that wave-driven flows were not modelled in this thesis, the predicted bedload transport rates compare reasonably well with the measurements described in Hoekstra et al. (2004; Section 6.2.3). Suspended-

load processes will be more important in the presence of waves, through the remobilisation of more sediment in the area. If both river discharge and tidal ranges are increased, then the average suspended-load transport will also be enhanced, being predicted to be nearly three times larger than bedload. Thus, suspended-load processes are expected to be the main mode of sediment transport in the Teign estuary, given that the most energetic morphodynamic conditions are expected under freshets, higher tidal ranges and in the presence of waves.

- Understand the effects of residual patterns on the seasonal morphodynamic evolution of the area

Residual water level differences for spring tides were smaller during the winter-spring of 2002/2003 than in summer-autumn period of 2003. The primary source for this variation was linked to the slightly higher average tidal ranges for the latter period, since the river discharge influence was found to be of minor importance in the summer-autumn 2003 (Figure 3.10). Model results were shown to replicate the more energetic conditions during the summer-autumn 2003 relative to the winter-spring 2002/2003, illustrated in both residual currents (Figures 6.9 and 6.11) and in the resulting morphological changes (Figure 6.16).

While there was a qualitative agreement between the residual currents of varying tidal ranges, a three-fold enhancement of the residual current magnitudes between the smallest and the biggest tidal ranges was predicted (Section 6.3). In the absence of wave stirring effects and based on a single-grain size ($D_{50}=0.3$ mm), residual tidal currents will tend to increase monotonically with the tidal range (Figure 6.10). Under these conditions, an ebb-dominated trend is expected to prevail in the inner reaches of the estuary, being reinforced under freshet periods. Between the middle and the outer estuary, flood-dominated areas were expected, where a zone of null residual currents was expected around this area.

Seawards, complex residual patterns are simulated, including: i) an ebb-dominated channel; ii) lateral flood-oriented channels along the seaward side of the sandy spit close to the estuary entrance and iii) a relatively less intense pattern between the ebb-directed jet off the estuary entrance and the Ness headland (Figure 6.10). Inside the estuary, a flood-

dominated channel contributes to the hydrodynamic recirculation patterns, which are formed by the ebb-dominated channel and the residual flooding features to the south and across the Salty sandbank. At the estuary entrance, a divergence zone is found along the main channel (Figure 6.12).

The most dynamic residual sediment transport patterns are found in the outer estuary and in the adjacent coastal area, while the inner areas of the estuary are dominated by tidal and eventually river-related processes (Figure 6.13). Under the effects of 'normal' river discharge ($< 15 \text{ m}^3 \cdot \text{s}^{-1}$; Table 3.1) and of average tidal currents, the estuary will tend to a net export of sediments. However, even in the absence of waves, some sediment can be trapped at the outer estuary due to the recirculating patterns induced by the presence of a residual vortex, as discussed by Nunny (1980) and Wells (2002b). The match between the observed position of the bedrock exposure at the estuary entrance with the divergence zone associated with the modelled sediment transport patterns is an indirect validation of the model performance in the area (Figure 6.15).

- Explore the role of waves and multiple grain sizes on the evolution of the area and assess the main sediment transport pathways on medium-term scales.

If waves are completely neglected and a single grain size is considered, the Teign estuary is shown to act as an exporter of sediments to the adjacent coastal area (Figure 6.14). This net pattern is shown to be reversed under the inclusion of wave stirring effects and multiple grain sizes (Section 6.4). The extra sediment remobilised by the wave stirring effect at the adjacent coastal area is mainly taken into the estuary as suspended-load during flood tides, being consequently deposited into the estuary. Although residual tidal currents will tend to flush these sediments out of the estuary through bedload, this export process is not sufficient to overcome the import of sediments. Hence, with the exception of gravels, a net sediment accretion is predicted (Figures 6.27 and 6.30).

The increase of the tidal range will have various effects on the sediment transport patterns of the Teign estuary. As the tidal range approaches spring tides, the net ebb-dominated sediment transport will be enhanced accordingly. Despite the fact that the wave properties (i.e. H_s and T_s) remain unchanged, larger tidal ranges will contribute to a more efficient

wave stirring closer to the shore. The most likely factors to contribute to the enhancement of the wave stirring are the following: i) as the tidal range increases, the surf zone will tend to broaden on the flatter low tide terrace, thus potentially contributing to an increase in the area affected by wave stirring; ii) a wider influence of waves would be also linked to the remobilisation of the sediments on the various shallow shoals and sandbanks present in the coastal area. As these shallower areas are typically composed of coarser grains (Figure 6.26), the wave stirring effects on larger tidal ranges will also favour the sediment transport of coarser grains.

This thesis has highlighted the role of the combined effects of wave stirring and mixed grain sizes on the import of sediments in estuarine environments. The sediment transport of silts and clays is expected to largely dominate the total sediment transport behaviour under the residual effects of the following processes: tidal currents, normal river discharge and higher wave-energy events ($H_s = 0.8$ m and $T_p = 8$ s). Silts and clays are expected to be more efficiently imported into the estuary during neap and spring tides (Figures 6.19 to 6.25). During the smallest and largest tidal ranges, the increase of sediment availability due to the wave stirring at the adjacent coast (and taken into the estuary by the flood tides) is relatively larger than the net ebb-dominated residual sediment transport due to tidal currents. During average tidal ranges (between $2.5 \text{ m} < \text{TR} = 3.5 \text{ m}$), the overall import of silts and clays is reduced, due to the establishment of near-equilibrium conditions between the import and export of sediments. Meanwhile, the net import of coarser (and heavier) grain sizes is expected to be proportional to the tidal range, given that the wave stirring effects will tend to be less efficient in remobilising coarser grain sizes.

At the end of the simulations, which replicated the higher energy events typical of winter periods, a grain sorting is predicted throughout the estuary and over the shallower areas of the modelling domain. Inside the estuary, a coarsening of the sediment grains is expected from the inner and upper reaches of the estuary towards its deeper and outer areas (Figure 6.27), consistent with observations. Since only silts and clays are predicted to have a widespread distribution throughout the outer estuary and adjacent coast at the end of the simulation, it is postulated that the bulk of the sediment deposition observed during CoastView surveys (Figures 3.11.A and C) is composed of these grain fractions.

The modelled volume variation for the winter-spring 2002/2003 period was around 80% smaller than that estimated from the CoastView field surveys. This seems to reinforce the role of wave-driven flows, since it has been observed by Hoekstra et al. (2004) that enhanced sediment accretion takes place at the adjacent coastal area under stormy periods. Unlike the negative BSS obtained for the tests with a single grain size in the absence of any wave effects (Section 6.3.3), the inclusion of wave stirring effects and mixed grain sizes induced a nearly null BSS, implying that the baseline bathymetric condition has not been significantly changed at the end of the simulation (Figure 6.28). This result illustrated the rigour of the BSS, despite the qualitative match between observations and model results with regard to the sediment infilling in the main channel of the outer estuary.

The simulation of an isotropic grain size distribution showed the model ability in generating a grain size sorting, as modelled for the case based on field grain size distribution (Figure 6.30). Thus, finer grain sizes are expected to be found in the upper and inner areas of the estuary, while coarser grains are predicted to be more common seawards. Since wave-driven currents are not included in the modelling exercise, these results suggest that although swell waves do not penetrate into the estuary entrance (Wells, 2002a; Section 3.1.2), they are expected to increase the sediment availability in the coastal area adjacent to the Teign estuary.

While there is room for improvements on the morphodynamic model used in this study, the principles associated with the import of sediments into the Teign estuary are likely to be applicable to other estuarine systems. The concept that flood currents acting jointly with wave-related processes (such as wave stirring and wave-driven currents) induce the accretion of sediments in estuaries may be useful as part of a broader comprehension of the morphodynamic evolution of estuaries in longer-term scales.

7.2. Further research

The findings described in this thesis represent another step forward in the comprehension of the medium-term modelling of morphodynamic processes. Nevertheless, many different

aspects related to the evolution of this and other estuarine systems have still to be considered. Further advances in this area must necessarily go through consistent and continuous data sampling in the field.

Regarding the processes which still require attention, future research into the morphodynamics of the Teign estuary should include the modelling of wave-driven currents, as it has been predicted in this thesis that waves on the adjacent coastal area can play an important role in the stirring and supply of sediments to the estuary.

The effects of freshets and extreme river discharge conditions on the morphodynamic processes is also likely to be important for the input of terrigenous sediments to the system. In order to study these events and the stratification processes associated, the application of three-dimensional models is required.

Due to the grain size heterogeneity in the area, further modelling of mixed grain sizes inside the estuary must also give preference to models capable of dealing with both cohesive and non-cohesive sediment fractions. Additionally, the modelling of lag effects is strongly encouraged, since they are expected to play a fundamental role in the dispersion and diffusion of finer grain sizes during higher energy events.

In order to investigate the relative influence of marine and river-related processes to the net sediment budget in the Teign estuary, special attention should be given to the measurement of the sediment fluxes at the estuary entrance and at the head of the estuary.

Keeping the seasonal bathymetric and topographic surveys in the outer estuary and in the adjacent coastal area should be a priority for future research projects at the Teign estuary, as it could provide valuable information on the system response in face of the shallowing longer-term patterns observed during CoastView surveys. If possible, it is also desirable to extend the coverage of such surveys towards the inner reaches of the system. Considering that five surveys (coverage of 2 years) have been carried out in the area within the frame of the CoastView project, the extension of such database may provide very useful information on the morphodynamic evolution of estuaries in general, given the uniqueness of such information.

Finally, the combination of a morphodynamic model such as the one used in this work with some type of long-term model (top-down) is likely to provide further information on the longer-term evolution behaviour of the Teign estuary and adjacent coastal area.

Appendix 1 - Model Description

A1.1. Introduction

As described in Chapter 4, the numerical model applied in this work was Telemac-2D, developed by Laboratoire National d'Hydraulique -LNH and Electricité de France - EDF/DER. As part of the TELEMAC system, Telemac-2D is intended for maritime, coastal and river hydraulics applications through the application of depth-averaged free surface flow Saint-Venant equations. The system is modular, written in Fortran-90 and based on finite elements techniques (although finite volumes methods are also available for the estimation of some processes). Several processes can be modelled, like the propagation of long waves (including non-linear effects), bed friction, rotation effects, atmospheric pressure and winds, turbulence, supercritical and subcritical flows, wetting and drying processes, etc (EDF-DER, 1998). The version used in this work and described hereafter is the 5.3.

The pre-processing structure is also modular: bathymetric data are digitised through a software called Sinusx. Based on these data, the mesh generation and definition of boundary conditions is carried out in Matisse. Once these steps are completed, the derived data is then fed into the flow models, Telemac-2D or Telemac-3D, with the possibility of linking these results to wave, sediment transport, water quality and other modules. Post-processing can be done through several packages, like Rubens (default software for Telemac-2D or Postel-3D for Telemac-3D), EnSim (developed by the Canadian Hydraulic Center) and other gridding approaches (e.g. Surfer or Matlab), given that TELEMAC-derived output files are compatible and/or readable from these softwares.

The process-based morphodynamic approach is completed by the inclusion of the accompanying module Sisyphe, which estimates the sediment transport rates and the corresponding bed evolution. In this appendix, a general overview of the main characteristics of the model is given, based on the manuals issued by the developers of the model, especially EDF-DER (1998) for Telemac-2D and Villaret (2004) for the description of Sisyphe.

A1.2. Telemac-2D

A1.2.1. Overview

From the full Navier-Stokes equations, several assumptions are made in order to simplify these equations into depth-averaged conditions: i) hydrostatic pressure; ii) negligible vertical velocities and iii) impermeability of the surface and of the bottom. Thus, the following equations are solved simultaneously by Telemac-2D:

Continuity:

$$\frac{\partial h}{\partial t} + \vec{u} \cdot \vec{\nabla}(h) + h \operatorname{div}(\vec{u}) = S_h \quad (\text{A1.1})$$

Momentum along the x axis:

$$\frac{\partial u}{\partial t} + \vec{u} \cdot \vec{\nabla}(u) = -g \frac{\partial Z}{\partial x} + S_x + \frac{1}{h} \operatorname{div}(h \nu_t \vec{\nabla} u) \quad (\text{A1.2})$$

Momentum along the y axis:

$$\frac{\partial v}{\partial t} + \vec{u} \cdot \vec{\nabla}(v) = -g \frac{\partial Z}{\partial y} + S_y + \frac{1}{h} \operatorname{div}(h \nu_t \vec{\nabla} v) \quad (\text{A1.3})$$

Tracer conservation:

$$\frac{\partial T}{\partial t} + \vec{u} \cdot \vec{\nabla}(T) = S_T + \frac{1}{h} \operatorname{div}(h \nu_T \vec{\nabla} T) \quad (\text{A1.4})$$

where:

h (m) corresponds to water depth; u and v (m.s^{-1}) are the velocity components; T (g.l^{-1} or $^{\circ}\text{C}$) is a non-buoyant tracer; g (m.s^{-2}) is the gravity acceleration; ν_t and ν_T (both in $\text{m}^2.\text{s}^{-1}$) are the momentum and tracer diffusion coefficients respectively; Z (m) is the free surface elevation; t (s) is time; x and y (both in m) are the horizontal space coordinates; S_h (m.s^{-1})

corresponds to source or sink of fluid; S_x and S_y (both in m.s^{-2}) are source or sink terms in dynamic equations (e.g. wind, Coriolis force, bottom friction) and S_T ($\text{g.l}^{-1}.\text{s}^{-1}$) corresponds to the source or sink of tracer.

The equations are given in Cartesian coordinates (reference system applied in this work), but can be used in terms of spherical ones. The depth of water and the depth-averaged velocity components are calculated at each node of the computational mesh. Two methods are available for the spatial discretisation: linear triangle and quasi-bubble triangle, with the former being applied in this work for the computation of the unknown variables (h , u , v and T). The default solver, based on conjugate gradient on normal equation, is applied in this work.

A1.2.2. Numerical methods of Telemac-2D

The different terms of these equations are processed in one or more steps, through the Operator-Splitting method (Marchuk, 1975 and Zienkiewicz and Ortiz, 1995) or fractional step technique, which is based on a separate treatment of the hyperbolic and parabolic parts of Navier-Stokes equations in order to maximise the numerical performance and accuracy. Therefore, the solution is solved in two steps: i) advection of h , u , v and T and ii) propagation, diffusion and source terms of the dynamic equations (and, if necessary, diffusion and source terms of the tracer transport equation).

The numerical discretisation is formulated within Telemac-2D through different options: method of characteristics (trajectories); centred semi implicit scheme with the streamline upwind Petrov-Galerkin (SUPG) scheme; conservative scheme with SUPG; PSI scheme and N scheme. As recommended by the manual, in order to avoid long simulation times and to ensure stability under conditions of steep bathymetries and tidal flats, the velocity field is advected in this work through the method of characteristics (with a fractional step), whereas the water depths are advected by a conservative scheme with SUPG method.

➤ *Advection step*

The method of characteristics used in the model is based on a method of Runge-Kutta of order 1 and the interpolation at the foot of the characteristic follows the type of finite element chosen for the "propagation-diffusion-source terms" stage. Runge-Kutta method of order 2 has also been tested, without significant improvements and with higher computational time (EDF-DER, 1998). The SUPG method has been applied to solve the advection of h (Brookes and Hughes, 1982), being implemented in Telemac-2D to ensure mass conservation and an oscillation-free solution without excessive mesh refinement or the addition of artificial diffusivity (Bates et al., 1998). Extended to a Petrov-Galerkin formulation, the standard Galerkin weighting functions are modified by adding a streamline upwind perturbation. The modified weighting function is applied to all terms in the equation, resulting in a consistent weighted residual formulation (EDF-DER, 1998).

➤ *Propagation, diffusion and source terms step*

The propagation, diffusion and source terms are solved by the finite element method, where an implicit time discretisation allows the calculation of the non-linearities in the equations. Variational formulations and space discretisation transform the continuous equations into a linear discrete system where the values of h , u and v at the nodes are the unknown variables. This system is solved by an iterative conjugate gradient method (Hervouet and van Haren, 1994). Telemac-2D makes significant savings in both computational time and storage requirements through the use of an element-by-element solution technique, where the matrices in the linear system are stored in their elementary form without recourse to full assembly (Bates et al., 1997).

A1.2.3. Bottom friction of Telemac-2D

As shown in Chapter 4, model results tend to be very sensitive to the choice of bed roughness. In Telemac-2D the bed shear stress $\bar{\tau}$ ($\text{kg.m}^{-1}.\text{s}^{-2}$) is represented as a quadratic function of velocity:

$$\bar{\tau} = \frac{1}{2} \rho C_d |U| \bar{U} \quad (\text{A1.5})$$

where ρ is the water density (kg.m^{-3}); C_d is the dimensionless friction coefficient and U is the depth-averaged velocity of the flow (m.s^{-1}).

The friction coefficient (C_d) can be parameterised either in terms of the Chézy (C , in $\text{m}^{1/2}.\text{s}^{-1}$), Manning (m , in $\text{m}^{1/3}.\text{s}^{-1}$) or Nikuradse (k_s in mm) friction coefficients. The Chézy law, which was established for a uniform flow but is applied to all types of flow, is expressed in the following terms:

$$F_x = - \frac{1}{\cos(\alpha_b)} \frac{g}{hC^2} u \sqrt{u^2 + v^2} \quad (\text{A1.6})$$

$$F_y = - \frac{1}{\cos(\alpha_b)} \frac{g}{hC^2} v \sqrt{u^2 + v^2} \quad (\text{A1.7})$$

where F_x and F_y are the source terms of the momentum equations in u and v , respectively; α_b is the slope angle of the bottom and C is the Chézy friction coefficient ($C_d = g/C^2$).

When the Manning law of bottom friction is applied, the friction coefficient is substituted by:

$$C_d = \frac{gm^2}{h^{1/3}} \quad (\text{A1.8})$$

When the Nikuradse law is considered, then the friction coefficient is changed to:

$$C_d = \frac{1}{32 \left\{ \log \left(\frac{14.8h}{k_s} \right) \right\}^2} \quad (\text{A1.9})$$

Moreover, the bottom friction is treated in a totally implicit way, avoiding instability problems associated with explicit schemes: the inversion of velocity for large values of friction or time step (EDF-DER, 1998).

A1.2.4. Boundary conditions of Telemac-2D

In Telemac-2D code, a distinction is made between "physical" (which are divided into solid and liquid) and "technical" boundary conditions: the latter are algorithmic representations of the former. At solid boundaries, the assumptions are the following: i) the flow normal to the boundary is null; ii) a free slip condition at the wall for all vectors tangent to the wall is assumed; iii) the friction coefficient at the bed is written as $\left[\frac{\partial(\vec{u} \cdot \vec{t})}{\partial n} = C_d(\vec{u} \cdot \vec{t}) \right]$; iv) no transfer of water takes place either through the bottom or from the surface and v) the water surface height is free and the surface boundary condition is a stress calculated from the wind speed and coefficient of wind speed.

The treatment of liquid boundaries is, however, rather more complex, because it supposes the existence of a fluid domain which is not part of the calculation domain, but which could have a crucial effect on the model outcome. Based on four types of situations (torrential inflow; tranquil inflow; torrential outflow and tranquil outflow), the number of boundary conditions will change accordingly. Added complexity is expected when prescribing oscillatory flows at liquid boundaries, such as the "inflow" and "outflow" character of tides. Wave reflections are minimised from the model domain as long as their direction is normal to the liquid boundary. In this thesis (Section 4.2.3.), the river discharge was prescribed at the head of the estuary, while a free velocity and prescribed elevation were assigned to the offshore boundary.

A1.2.5. Turbulence modelling

When solving equations A1.1 to A1.4, Telemac-2D employs a mean flow concept to treat turbulent flows, reducing instantaneous velocities to average values in order to estimate the

mean motion (Reynolds averaging). In this formulation, an additional term - the Reynolds stress - is added to the governing equations to represent the increased internal shear stress on mean flow induced by velocity fluctuations (Hervouet and van Haren, 1996).

In order to overcome the problem posed by the fact that the resulting equations are not closed (i.e. there are more unknowns than equations to solve the problem posed), the estimation of turbulence is done through the so-called closure models. Hervouet and van Haren (1996) suggested two ways of obtaining a closure to the Reynolds equations: the more elaborate method consists of developing explicit equations for the Reynolds stress tensor; the alternative approach would be to apply the Boussinesq eddy-viscosity concept (not to be confused with the Boussinesq approximation), which expresses the Reynolds stress tensor in terms of the local velocity gradient and introduces a turbulent viscosity. Telemac-2D uses the Boussinesq eddy-viscosity concept and offers the following possibilities: a constant viscosity; the Elder model; the Smagorinski approach or by solving directly the transport equations for the kinetic energy and its rate of dissipation through the k - ϵ model.

A1.2.6. Wetting and drying modelling

The treatment of wetting and drying processes in Telemac-2D is given by two methods: i) correction of the gradient of the free surface (Figure A1.1, approach selected in this work) or removing from the calculations all the elements which are not entirely wet. If the correction of the gradient of the free surface is the method selected, then semi wet elements will be characterised by a discontinuity in the gradient, from a value close to zero where there is water to a value close to the local bottom gradient at dry areas. As no unknowns are added and only the momentum equation is modified, mass conservation properties are not affected (Bates et al., 1997). By applying the equation of conservation of momentum to dry elements, then surface gradient term is likely to be balanced by the bed friction.

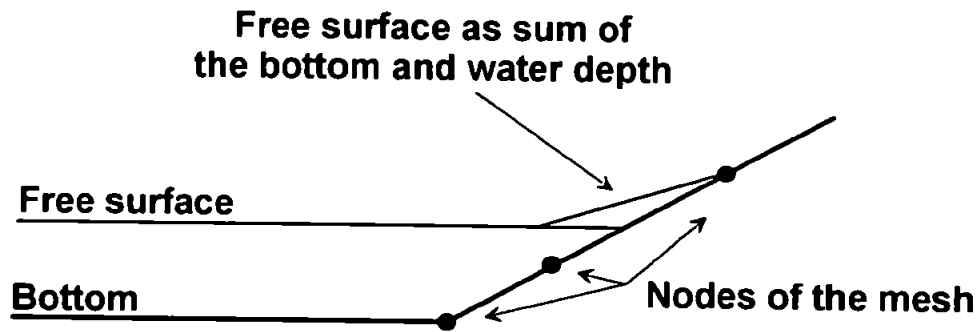


Figure A1.1: Correction of the free surface gradient in Telemac-2D (after Hervouet and van Haren, 1996).

A1.2.7. Global parameters of Telemac-2D

Table A1.1: Set-up parameters used in Telemac-2D. Default values are marked with an *.

<i>Parameters</i>		<i>Values</i>
Version		5.3
Mesh resolution		
Simulations up to Section 6.3.3		4355 nodes
Section 6.4 onwards		4234 nodes
Time step		Constant: 5 seconds
Coupling period with Sisyphe	36 (data transmission to Sisyphe every 3 minutes)	
Forcings considered		Tides and river discharge
Initial conditions		Constant elevation
		Depth-dependent (m-ODN)
		Chézy ($\text{m}^{1/2} \cdot \text{s}^{-1}$)
Bed friction		$H < -3 = 68$ $-3 < H < -1 = 64$ $-1 < H < 1 = 62$ $H > 1 = 60$
Wind effect		None
Treatment of tidal flats		Correction of free gradient surface (option 1 *)
Water density		$1020 \text{ kg} \cdot \text{m}^{-3}$
Mean temperature		20°C (*)
Eddy viscosity		Constant: $0.5 \text{ m}^2 \cdot \text{s}^{-1}$
Turbulence model for solid boundaries		Smooth wall (option 1 *)
Advection of u and v		Method of characteristics
Advection of h		Conservative scheme with SUPG
Option for the diffusion of velocities		Diffusion term is written as $\text{div}[\overline{v \text{grad}(U)}]$

Continued

	(option 1 - *)
SUPG option	Upwinding is equal to the Courant number (option 2 *)
Upwind coefficients	1 (*)
Hybrid scheme option	Normal hybrid scheme with characteristics+SUPG (option 1 *)
Implication for depth	0.6
Implication for velocity	0.99
Maximum number of iterations for solver	200
Preconditioning	Diagonal preconditioning (option 2 *)
C-U preconditioning	Enabled (option 1 *)
Discretisations in space	Binary triangle (option 11 *)
Solver	2
Matrix storage	Classic method (option 1 - default value)
Matrix-vector product	Non assembled matrix product (option 1 *)
Treatment of the linear system	Coupled method (option 1 *)
Option for liquid boundaries	River boundary
	Prescribed flowrate (option 1 *)
	Oceanic boundary
	Prescribed water level
Cost function	Thompson method
	Computed with h , u and v (option 1 *)
Finite volume scheme	Kinetic order 1
H clipping	Unabled (option 1 *)

A1.3. Sisyphe

A1.3.1. Overview

Sisyphe is part of the TELEMAC system, being used for estimating the bed-load or total-load) sediment transport rate, depending on the choice of sediment transport formula. The bottom evolution equation is also solved by the application of either a finite element method or a finite volume one (Villaret, 2004). The bottom evolution and the solid transport rate are calculated at each node of the computational domain. In the version used in this thesis, Sisyphe is only capable of estimating the transport of non-cohesive sediments. The inclusion of multiple grain sizes; consideration of vertical stratification of

the bed; the effects of bottom slopes and the consideration of rigid beds are some of the most recent features included in the configuration of this module. The pre and post-processing tools, as the treatment of tidal flats, are the same as described for Telemac-2D in Section A1.1 and A1.2.6, respectively.

Sisyphe can only compute rather simplified flow conditions. For more complex situations, hydrodynamic results (Telemac-2D, Telemac-3D or the waves module, Tomawac) must be fed into Sisyphe. This can be done in two ways: i) by the "chaining method", where the hydrodynamic modules are run first and then the results serve as inputs for Sisyphe or ii) through the coupling between one of the hydrodynamic modules and Sisyphe. Hence, if the joint effects of tides and waves are to be considered, then only the "chaining method" is available.

The first method is applicable to relatively simple flows, since the flow rate is assumed to be constant. On the other hand, the coupling between one of the hydrodynamic modules with Sisyphe is more realistic, given the more frequent update of the flow conditions. For both methods, the run is stopped if a given threshold (i.e. ratio between the bed evolution at a given node and the local water depth) defined by the user is achieved.

The following sediment formulae are available in Sisyphe: for bed-load transport (Meyer-Peter and Muller, 1948; Einstein, 1950; Engelund and Hansen, 1967) or total transport (Bijker, 1968; van Rijn, 1984a,b, adapted by Soulsby, 1997; Bailard, 1981; Dibajnia and Watanabe, 1992) induced by current-borne and by wave-borne flows. Like in Telemac-2D, boundary conditions in Sisyphe can be prescribed in different ways: i) solid boundary, i.e. total-load transport is null; ii) imposed evolution rate of the bed elevation and iii) free evolution rate. Regarding Sisyphe, the open boundaries are set as time-independent of a free evolution-type in this thesis.

A1.3.2. Bed evolution

The following bottom evolution equation is solved by Sisyphe:

$$(1 - n_b) \frac{\partial Z_f}{\partial t} + \text{div}(\bar{Q}_s) = 0 \quad (\text{A1.10})$$

where: n_b is the bed porosity; Z_f is the bottom elevation and \bar{Q}_s ($\text{m}^2 \cdot \text{s}^{-1}$) is the solid volume transport per unit width.

According to the formulation above, the variation of sediment thickness is derived from a mass balance. It is only valid for equilibrium conditions between the bed-load transport and the turbulent flow (although it can be extended to total-load), i.e. it is assumed that sand concentration has reached its equilibrium concentration, corresponding to saturation conditions (Villaret, 2004). In order to represent non-equilibrium conditions, equation A1.10 is coupled to a transport-diffusion equation for suspended sand concentration. However, the inclusion of non-equilibrium conditions was not possible in this thesis due to time constraint.

A1.3.3. Bed-load and suspended-load

The total sediment transport rate (given in terms of volume/volume) is divided into bed-load (Q_{bed}) and suspended-load (Q_{susp}). The bed-load takes place very close to the bed. The thickness of the layer depends on either the maximum grain size or the bed roughness. Thus, this mode of sediment transport responds rapidly to changes in flow conditions, making the equilibrium conditions generally valid. The bed-load transport can then be estimated through the application of one of the several formulations available.

The character of the suspended-load transport is broader and more dependent on inertial processes, since it takes place on most of the water column. The suspended-load is defined as a depth-integrated mean flux of sediment concentration from the top of bed-load transport layer to the free surface. In the water column, the sediment concentration can be

regarded as a passive scalar, being transported in the water column by the local flow under a transport-diffusion equation. If advection terms can be neglected, then equilibrium conditions can be achieved for quasi-uniform and steady flow conditions.

A1.3.4. Bottom friction of Sisyphe

The influence of the flow conditions on the bottom friction is of paramount importance in the sediment transport. In Sisyphe, the bed shear stress τ_0 is calculated at each time step, based on the depth-averaged mean flow velocity U and on the quadratic friction coefficient given in Equation A1.5. In order to ensure consistency in results, the laws of bottom friction in Sisyphe are the same as those programmed for Telemac-2D.

A1.3.5. Wave effects

Sediment transport rates under the combined effects of waves and tidal currents are generally one order of magnitude larger than in the case of tidal currents alone. In Sisyphe version 5.3, only the stirring effect of waves under equilibrium conditions is considered. Hence, other relevant processes associated to the presence of waves, such as the increase in the near-bed flows and the generation of wave-derived ripples are neglected.

As mentioned in Section 6.4, steady wave conditions (H_s significant height and T_p peak period) are assumed throughout the simulations. Since the sediment transport formula used in this thesis was Bijker's, the wave direction (θ_w) is assumed to be parallel to the main current direction. The wave orbital velocity U_w is calculated in Sisyphe by the application of linear wave theory:

$$U_w = \frac{H_s \omega}{2 \sinh(kh)} \quad (\text{A1.11})$$

where $\omega=2\pi/T_p$ is the wave frequency and $k=2\pi/L$ is the wave number (and L is the wave length). The wave number is given by:

$$\omega^2 = gk \tanh(kh) \quad (\text{A1.12})$$

The maximum stress due to waves is calculated at each time step as a function of the wave orbital velocity, expressed in a quadratic friction coefficient f_w due to waves:

$$\tau_w = \frac{1}{2} \rho f_w U_w^2 \quad (\text{A1.13})$$

The wave friction is then estimated as a function of relative density $f_w = f_w(A_w/r)$; where A_w is the wave orbital amplitude on the bed ($A_w = U_w/\omega$) and r is the bed roughness. In Sisyphe, the formula of de Swart (1976) is implemented:

$$\begin{cases} f_w = \exp\left[-6 + 5.2\left(\frac{A_w}{r}\right)^{-0.19}\right] & \text{if } \left(\frac{A_w}{r}\right) > 1.57 \\ f_w = 0.3 & \text{if } \left(\frac{A_w}{r}\right) \leq 1.57 \end{cases} \quad (\text{A1.14})$$

There are several models implemented in Sisyphe to calculate the combined shear stress due to the effects of waves and currents (τ_{cw}), but they are not described in this appendix. For the model of Bijker, the formulation of τ_{cw} is given in Equation A1.25.

A1.3.6. Sediment transport formulae

Many semi-empirical formulae to estimate sediment transport can be found in the literature. These formulae will be a function of hydrodynamic properties (e.g. water depth, flow velocity, bottom friction, waves, etc.) and sediment-related parameters (D_{50} , D_{90} , relative density, etc.) and are generally based on similar principles:

$$\theta = \frac{\tau_0}{(\rho_s - \rho)gD} \quad (\text{A1.15})$$

$$\Phi_s = \frac{Q_s}{\sqrt{g(s-1)D^3}} \quad (\text{A1.16})$$

where: θ is the dimensionless bottom friction or Shields parameter (0.047); τ_0 is the bed shear stress; ρ_s is the sediment density (2665 kg.m⁻³ by default); D is the sand grain diameter ($D=D_{50}$ for uniform grains); Φ_s is the non-dimensional current-induced transport rate and s is the relative density (ρ_s/ρ , being 2.65 by default).

➤ *Meyer-Peter and Muller (1948) formula*

This classical bed-load formula was validated for coarse sediments ($D > 2$ mm). It is based on the concept of initial entrainment:

$$\begin{cases} \Phi_b = 0 & \text{if } \mu\theta < \theta_c \\ \Phi_b = 8(\mu\theta - \theta_c)^{3/2} & \end{cases} \quad (\text{A1.17})$$

where θ_c is the critical Shields parameter and μ is the correction factor for skin friction, i.e. as a ripple correction factor ($\mu < 1$).

A Chézy coefficient due to skin friction is introduced and denoted as C_{hp} . The ripple correction factor is calculated by:

$$\mu = \left(\frac{C_h}{C_{hp}} \right)^{3/2} \quad (\text{A1.18})$$

and

$$C_{hp} = 18 \log_{10} \left(\frac{12h}{3D_{50}} \right) \quad (\text{A1.19})$$

Equation A1.15 is also approximately equivalent to:

$$C_{hp} = \sqrt{\frac{g}{k}} \log\left(\frac{30h}{ek_{sp}}\right) \quad (\text{A1.20})$$

where C_h is the Chézy coefficient associated to total friction (given by $C_h = \sqrt{\frac{2g}{C_d}}$); k is the von Karman constant (0.4) and k_{sp} is the skin friction roughness.

➤ *Einstein-Brown (1950) formula*

This bed-load is recommended for coarse sand ($0.4 \text{ mm} < D_{50} < 2.9 \text{ mm}$) and large bed shear stress $\theta > \theta_c$, being expressed as

$$\Phi_b = F(D_*)f(\theta) \quad (\text{A1.21})$$

$$F(D_*) = \left(\frac{2}{3} + \frac{36}{D_*}\right)^{1/2} - \left(\frac{36}{D_*}\right)^{1/2} \quad (\text{A1.22})$$

$$\begin{cases} f(\theta) = 2.15 \exp^{(-0.391/\theta)} & \text{if } \theta \leq 0.2 \\ f(\theta) = 40\theta^3 & \text{if } \theta > 0.2 \end{cases} \quad (\text{A1.23})$$

where D_* is the non-dimensional grain diameter defined by:

$$D_* = \left[\frac{g(s-1)}{v_w^2} \right]^{1/3} \cdot D \quad (\text{A1.24})$$

where v_w is the water viscosity ($1.10^{-6} \text{ m}^2 \cdot \text{s}^{-1}$ by default).

➤ *Engelund-Hansen (1967) formula*

The Engelund-Hansen formula predicts the total-load sediment transport. It is recommended for fine sediments (from $0.2 \text{ mm} < D_{50} < 1 \text{ mm}$), being described in general terms as:

$$\Phi_s = 0.05(\mu\theta)^{5/2} \quad (\text{A1.25})$$

$$\mu = \left(\frac{1}{C_d} \right)^{2/5} \quad (\text{A1.26})$$

In Sisyphe, the version of this formula modified by Chollet and Cunge (1979) is also available, accounting for the effects of sand dunes formation. Relative to the original formulation, Villaret (2004) estimated that the adapted one would overestimate the sand transport rates by a factor of 2 or more. This modified version was tested in Section 4.4. Its dimensionless shear stress θ is calculated as a function of the dimensionless skin friction θ_p :

$$\begin{cases} \theta = 0 & \text{if } \theta_p < 0.06 \text{ (flat bed regime - no transport)} \\ \theta = \sqrt{2.5(\theta_p - 0.06)} & \text{if } 0.06 < \theta_p < 0.384 \text{ (dune regime)} \\ \theta = 1.065\theta_p^{0.176} & \text{if } 0.384 < \theta_p < 1.08 \text{ (transition regime)} \\ \theta = \theta_p & \text{if } \theta_p > 1.08 \text{ (flat bed regime - upper regime)} \end{cases} \quad (\text{A1.27})$$

➤ *Bijker (1968) formula*

From the formulation of Bijker onwards, the effect of waves are also accounted for. However in Sisyphe the solid transport is assumed to be oriented in the direction of the mean current, with the possible deviation induced by waves being neglected. The total-load sediment transport formula is estimated based on calculating the bed-load and the suspended-load separately. The development is made on the scalar variables, since Bijker's formula is an extension of a steady flow formula to account for the effect of the wave enhanced shear stress. The suspended-load transport is treated in a simplified approach: the concentration profile is assumed to be continuously in equilibrium, i.e. lag effects are neglected. In addition, no exchange takes place with the bed-load layer; only the continuity of concentration is ensured in that case (Villaret, 2004).

Bijker extended the steady bed-load formula proposed by Frijlink (1952) by adding the stirring effects of waves into it. In non-dimensional variables, the bed-load transport rate is given by:

$$\Phi_b = b\theta_c^{0.5} \exp\left(-0.27 \frac{1}{\mu\theta_{cw}}\right) \quad (\text{A1.28})$$

where b is an empirical value ($b=5$ in the original formulation, but it is suggested that $b=2$ gives better results, thus being used in this thesis) and θ_{cw} is the non-dimensional shear stress due to wave-current interaction. The ripple correction factor μ is calculated in the same way as in the Meyer-Peter formula. The shear stress under combined wave and current (τ_{cw}) is given by the following equation:

$$\tau_{cw} = \tau_c + \frac{1}{2} \tau_w \quad (\text{A1.25})$$

where τ_c is the bed shear stress induced by currents and τ_w is the wave-derived shear stress.

The suspended-load fraction is obtained by vertically integrating the product of the volume concentration by the mean horizontal velocity, using as a reference level the corresponding thickness of the bed-load layer. After depth-integration and assuming: i) a Rouse profile for the concentration and ii) a logarithmic velocity profile for the mean velocity, the suspended-load is written as:

$$Q_{susp} = Q_{bed} I \quad (\text{A1.29})$$

where Einstein's integral is given by:

$$I = 1.83 \times 0.216 \frac{B^{A-1}}{(1-B)^A} \int_B^1 \left(\frac{1-y}{y}\right)^A \ln\left(\frac{33y}{B}\right) dy \quad (\text{A1.30})$$

$$\begin{cases} A = \frac{w_s}{ku_{*cw}} \\ B = \frac{k_s}{h} \end{cases} \quad (\text{A1.31})$$

$$u_{*cw} = \sqrt{\frac{\tau_{cw}}{\rho}} \quad (\text{A1.32})$$

where w_s is the grain settling velocity (m.s^{-1}) and u_{*cw} is the friction velocity derived from the wave-current interaction (m.s^{-1}).

➤ *Soulsby-van Rijn formula (van Rijn, 1984a,b adapted by Soulsby, 1997)*

This formula can be applied to estimate both components of the total-load sand transport rate, being also suitable for rippled beds (validated by the assumption of a rippled bed roughness r of 0.18 m). The validity range of this formula is as follows: $h = 1$ to 20 m; $U = 0.5$ to 5 m.s^{-1} ; $D_{50} = 0.1$ to 2 mm and water temperature at 15 °C. The transport rate due to the combined action of waves and currents is provided by the following equation:

$$Q_s = A_s U \left[\left(U^2 + 2 \frac{0.018}{C_d} U_w^2 \right)^{0.5} - U_{cr} \right]^{2.4} \quad (\text{A1.33})$$

$$A_{bed} = \frac{0.005h(D_{50}/h)^{0.5}}{[(s-1)gD_{50}]^{0.5}} \quad (\text{A1.34})$$

$$A_{susp} = \frac{0.012D_{50}D_*^{-0.6}}{[(s-1)gD_{50}]^{0.5}} \quad (\text{A1.35})$$

where A_s is the total-load coefficient ($A_s = A_{bed} + A_{susp}$); C_d is the quadratic drag coefficient (Equation A1.5) due to currents alone; U_{cr} is the critical entrainment velocity (m.s^{-1}), which is defined as:

$$\begin{cases} U_{cr} = 0.19D_{50}^{0.1} \log_{10} \left(\frac{4h}{D_{90}} \right) & \text{if } 0.1 \text{ mm} \leq D_{50} \leq 0.5 \text{ mm} \\ U_{cr} = 8.5D_{50}^{0.6} \log_{10} \left(\frac{4h}{D_{90}} \right) & \text{if } 0.5 \text{ mm} \leq D_{50} \leq 2 \text{ mm} \end{cases} \quad (\text{A1.36})$$

➤ *Bailard (1981) formula*

This formula is based on the 'energetics approach'. The bed-load and the suspended-load components of the sand transport rate are expressed respectively as the third- and fourth-order momentum of the near-bed time-varying velocity field $\overline{U(t)}$.

$$Q_{bed} = \frac{f_{cw}}{g(s-1)} \frac{\varepsilon_c}{\tan \varphi} \left\langle |\vec{U}|^2 \vec{U} \right\rangle \quad (A1.37)$$

$$Q_{susp} = \frac{f_{cw}}{g(s-1)} \frac{\varepsilon_s}{w_s} \left\langle |\vec{U}|^3 \vec{U} \right\rangle \quad (A1.38)$$

where ε_c and ε_s are empirical factors ($\varepsilon_c=0.1$ and $\varepsilon_s=0.02$); φ is the sediment friction angle ($\tan \varphi=0.63$) and $\langle \rangle$ represents a time-average over a wave period.

➤ *Dibajnia and Watanabe (1992) formula*

This formula accounts for unsteady flows, taking into account inertial effects. The sand transport rate is given by:

$$\frac{\overline{Q_s}}{w_s D_{50}} = \alpha \frac{\bar{\Gamma}}{|\Gamma|^{1-\beta}} \quad (A1.39)$$

where α and β are empirical factors ($\alpha=0.0001$ and $\beta=0.55$); $\bar{\Gamma}$ represents the difference between the amount of sediments transported onshore and offshore. This formula is used to estimate the intensity of the solid transport rate, as the direction is assumed to follow the mean current direction.

A1.3.7. Treatment of non-erodable areas

The effects of rigid beds are to reduce the sand transport rate and to let the incoming sediment to pass over the bed. Although conceptually simple, numerically it poses some

difficulties. In Sisyphe, there are several methods to treat this process: i) the sand transport rate is reduced when the non-erodable bed is reached, although Hervouet et al. (2003) found that erosion was predicted underneath the rigid bed; ii) mass-conservative methods (either based on finite elements or finite volumes techniques) that avoid the erosion of rigid beds without spurious signals. In this thesis, the mass-conservative method based on finite volumes is chosen to estimate the rigid beds.

A1.3.8. Multiple grain sizes, bed stratification and hiding effects

From the version 5.3 (the one applied in this thesis), multiple grain sizes can be accounted for in sediment transport rates modelled by Sisyphe. The granulometry distribution can be discretised in up to 10 classes. Each class of sediment is defined by its mean diameter and volume fraction in the mixture at every node. By assuming equilibrium conditions, then the total-load transport rates are computed separately for each class. These N transport rates will correspond to N bed evolution, thus allowing for the determination of the global evolution and also to be used to compute the new composition of sediment mixture.

The bed can also be vertically stratified in a maximum of 8 layers, with composition of the sediment mixture being defined not only at every node, but also at every layer. A thin, upper layer (so-called active layer) is used to exchange sediment with the fluid above. This active layer is assumed to have a constant thickness, being fed or transmitting extra sediment to an underneath layer, called 'active stratum'.

Due to the difference in grain sizes, a hiding/exposure factor is applied, since smaller grains tend to be protected between coarser grains. Thus, the classical sediment transport formulae, which were originally defined for uniform grain sizes, have to be corrected for the 'hiding effect'. Based on the sediment transport formulations used in this thesis, the method proposed by Karim and Kennedy (1982), which directly modifies the transport rate, is used to account for the hiding factor. At each node, it is expressed as:

$$Q_{s,i} = \zeta_i \cdot Q_{s,i}^* \quad (\text{A1.40})$$

$$\zeta_i = \left(\frac{D_i}{D_m} \right)^{0.85} \quad (\text{A1.41})$$

where: $Q_{s,i}$ is the corrected sediment transport rate for the i -th sediment fraction; ζ_i is the hiding factor for the i -th sediment fraction; $Q_{s,i}^*$ is the uncorrected sediment transport rate for the i -th sediment fraction; D_i is the average grain size of the i -th sediment fraction (mm) and D_m is the average grain size of all sediments found in the active layer (mm).

A1.3.9. Numerical methods of Sisyphe

As for Telemac-2D, the computational domain is also based on the finite element technique. Sisyphe uses the same mesh as that being used for the hydrodynamic simulations. The various functions are expressed as:

$$f = \sum_{i=1}^n f_i \Psi_i \quad (\text{A1.42})$$

where: n is the number of discretisation points (nodes); f_i is the value of function f at point i and Ψ_i is the point-related basic function. It is 1 at that point and 0 at all the remaining nodes. The functions are only evaluated at the discretisation points. If the value of a function is required within a given element, a basic interpolation method is carried out.

In order to speed up the calculation performance, a mass-lumping technique is applied. It consists of adding all terms of each line of the mass-matrix onto the diagonal term in order to create a diagonal matrix. This operation is possible due to the formulation of the finite element technique. The solution, however, is smoothed.

A1.3.10. Numerical solution of the bed evolution equation

The bed evolution equation (A1.10) is solved using a predictor-corrector scheme, which can be split up into three steps:

➤ *Prediction step*

This step is solved through a finite element method (conjugated gradient methods or mass-lumping concept, the latter one was used in this thesis), leading to the following system:

$$M\tilde{Z}_f^{n+1} = M\tilde{Z}_f^n - \Delta t \cdot \int_{\Omega} \text{div}(\bar{Q}_s^n) \cdot \Psi_i \cdot d\Omega \quad (\text{A1.43})$$

where Z_f^n is the bottom depth at the time $n\Delta t$; Δt is the time step; \tilde{Z}_f^{n+1} is the assessment of the bottom depth at time $(n+1)\Delta t$ and M is the mass-matrix.

➤ *Correction step*

The sediment transport can be computed from \tilde{Z}_f^{n+1} , the first assessment of bottom elevation at the time $(n+1)\Delta t$ with a θ scheme:

$$\bar{Q}_s^{n+\theta} = \theta \tilde{\bar{Q}}_s^{n+1} + (1 - \theta) \bar{Q}_s^n \quad (\text{A1.44})$$

where $\tilde{\bar{Q}}_s^{n+1} = \bar{Q}_s(\tilde{Z}_f^{n+1})$ and \bar{Q}_s^n are explicitly computed at the time Δt . The default value of the empirical factor θ (zero) was applied in this thesis.

➤ *Final step*

The following equation is solved in the final step:

$$(1 - n) \frac{\partial Z_f}{\partial t} = -\text{div}(\bar{Q}_s^{n+\theta}) \quad (\text{A1.45})$$

A1.3.11. Global parameters of Sisyphe

Table A1.2: Set-up parameters used in Sisyphe. Default values are marked with an *.

<i>Parameters</i>	<i>Values</i>
Version	5.3
Mesh resolution	4355 nodes
Simulations up to Section 6.3.3	
Section 6.4 onwards	4234 nodes
Time step	Constant: 120 seconds
Coupling period with Sisyphe	24 (data transmission to Telemac-2D every 24 minutes)
Computation method	Complete (option 5 *)
Bed-load transport formula	
Simulations in Chapter 5 and in Section 6.3.3	Engelund-Hansen (1967), modified by Cholley and Cunge (1979)
Remaining tests	Bijker (1968; $b=2$ *)
	NB: Both formulae are multiplied by the scaling factor S_t when required
Bed friction	Same as in Telemac-2D
Treatment of tidal flats	Same as in Telemac-2D
Minimum value of water depth	0.1 m
Critical evolution ratio	1
Number of size classes of bed material	6
Mean diameters of the size classes	0.0335; 0.1565; 0.375; 1.25; 3; 34 (mm)
	0.175; 0.175; 0.175; 0.175; 0.175; 0.125
Initial fraction for particular size class	NB: Only for isotropic case, since in the remaining cases the field distribution (Figure 3.7) on a node-by-node basis
Hiding factor formula	Karim and Kennedy (1982), option 4
Treatment of non-erodable beds	Conservative method based on finite volumes (option 4)
Shields parameter	0.047 (*)
Coefficient function of porosity (P_c)	1.6
Slope effect (β)	1.6
Active layer thickness	0.05 m
Stratum thickness	100 m
Water viscosity	$10^{-6} \text{ m}^2 \cdot \text{s}^{-1}$ (*)
Water density	$1000 \text{ kg} \cdot \text{m}^{-3}$ (*)
Sediment density	$2665 \text{ kg} \cdot \text{m}^{-3}$
Mass-lumping	Enabled (*)
Implication coefficient (θ)	0.5
Preconditioning	Diagonal preconditioning (option 2 *)
Solver	Conjugated gradient on the normal equation (option 3 *)
Solver accuracy	10^{-4}
Maximum number of iterations for solver	60 (*)

References

- Andersen, O.H.; Hedegaard, I.B.; Deigaard, R.; de Girolamo, P. and Madsen, P. (1988). Model for morphological changes under waves and current. *Proceedings IAHR Symposium on Mathematical Modelling of Sediment Transport in the Coastal Zone*. Copenhagen, DHI, Horsholm: 310-319.
- Andersen, O.H.; Hedegaard, I.B.; Ronberg, J.K.; Deigaard, R. and Madsen, P. (1991). Model for morphological changes in the coastal zone. *Preprints IAHR Symposium on Suspended Sediment Transport*. Florence: 327-338.
- Anderson, F.E. (1983). The northern muddy intertidal: A seasonally changing source of suspended sediments to estuarine waters - A review. *Canadian Journal of Fisheries and Aquatic Sciences*, 40 (Supplement 1): 143-159.
- Babovic, V. and Keijzer, M. (2000). Genetic programming as a model induction engine. *Journal of Hydroinformatics* 2(1): 35-60.
- Bailard, J. (1981). An energetics total load transport model for a plane sloping beach. *Journal of Geophysical Research* 86(C11): 10938-10954.
- Bastos, A.; Collins, M. and Kenyon, N. (2003). Water and sediment movement around a coastal headland: Portland Bill, southern UK. *Ocean Dynamics* 53(3): 309-321.
- Bates, P.D.; Anderson, M.G.; Hervouet, J.-M. and Hawkes, J.C. (1997). Investigating the behaviour of two-dimensional finite element models of compound channel flow. *Earth Surface Processes and Landforms* 22: 3-17.
- Bates, P.D.; Horrit, M. and Hervouet, J.-M. (1998). Investigating two-dimensional, finite element predictions of floodplain inundation using fractal generated topography. *Hydrological Processes* 12: 1257-1277.
- Bijker, E.W. (1968). Mechanics of sediment transport by the combination of waves and current. In: *Design and Reliability of Coastal Structures. 23rd Int. Conf. on Coastal Engineering*: 147-173.
- Black, K.P. (1987). A numerical sediment transport model for application to natural estuaries, harbours and rivers. In: Noye, J. (Ed.), *Numerical Modelling Applications to Marine Systems*, 145, North Holland/Elsevier, Amsterdam: 77-105.
- Black, K.P.; Healy, T.R. and Hunter, M.G. (1989). Sediment dynamics in the lower section of a mixed sand and shell-lagged tidal estuary. *Journal of Coastal Research* 5(3): 503-521.

- Boothroyd, J.C. (1978). Mesotidal inlets and estuaries. In: Davis, R. A. (Ed.) *Coastal Sedimentary Environments*. Springer, New York: 287-360.
- Brady, A.J. and Sutherland, J. (2001). COSMOS Modelling of COAST3D Egmond Main Experiment. Wallingford, HR Wallingford: 36.
- Brooks, A.N. and Hughes, T.J.R. (1982). Streamline Upwind/Petrov-Galerkin formulations for convection dominated flows with particular emphasis on the incompressible Navier-Stokes Equations. *Computer Methods in Applied Mechanics and Engineering* 32: 199-259.
- Camenen, B. and Larroude, P. (2003). Comparison of sediment transport formulae for the coastal environment. *Coastal Engineering* 48: 111-132.
- Cameron, W.M. and Pritchard, D.W. (1963). Estuaries. In: Hill, M. N (Ed.) *The Sea* . Vol. 2, Wiley, New York: 306-324.
- Carter, D. and Bray, M. (2003). SCOPAC sediment transport study: Volume 5 Start Point to Portland Bill. Report to SCOPAC. University of Portsmouth.
- Cayocca, F. (2001). Long-term morphological modelling of a tidal inlet: the Arcachon Basin, France. *Coastal Engineering* 42: 115-142.
- Cheng, R.T.; Burau, J.R. and Gartner, J. W. (1991). Interfacing data analysis and numerical modeling for tidal hydrodynamic phenomena. *Tidal Hydrodynamics*. B. B. Parker. Rockville, Maryland, John Wiley & Sons: 201-219.
- Chesher, T.J. and Miles, G.V. (1992). The concept of a single representative wave for use in numerical models of long term sediment transport predictions. *Second International Conference on Hydraulic and Environmental Modelling of Coastal, Estuarine and River Waters*, Bradford, UK, Ashgate: 371-380.
- Chollet, J.P. and Cunge, J.A. (1979). New interpretation of some head loss - flow velocity relationships for deformable movable beds. *Journal of Hydraulic Research* 17(1): 1-13.
- Coco, G.; Huntley, D.A. and O'Hare, T.J. (2000). Investigation of a self-organization model for beach cusp formation and development. *Journal of Geophysical Research* 105: 21991-22002.
- Cowell, P.J. and Thom, B.G. (1995). Morphodynamics of coastal evolution. *Coastal Evolution: Late Quaternary Shoreline Morphodynamics*. Carter, R.G.W. and Woodroffe, C.D. (Eds.). Cambridge, Cambridge University Press: 33-86.
- Dalrymple, R.W.; Zaitlin, B.A. and Boyd, R. (1992). A conceptual model of estuarine sedimentation. *Journal of Sedimentary Petrology* 62: 1130-1146.

- Davidson M.A.; Aarninkhof, S.G.J.; Van Koningsveld M. and Holman. R.A. (submitted). Developing Coastal Video Monitoring Systems In Support of Coastal Zone Management. *Journal of Coastal Research* SI 39. ICS 2004, Brazil.
- Davies, J.H. (1964). A morphogenetic approach to world shorelines. *Z. Geomorphol.* 8: 127-142.
- Davies, A.G.; Ribberink, J.S.; Temperville, A. and Zyserman, J.A. (1997). Comparisons between sediment transport models and observations made in wave and current flows above plane beds. *Coastal Engineering* 31: 163-198.
- Davies, A.G.; van Rijn, L.C.; Damgaard, J.S.; van de Graaff, J. and Ribberink, J.S. (2002). Intercomparison of research and practical sand transport models. *Coastal Engineering* 46: 1-23.
- Davies, A.G. and Villaret, C. (2002). Prediction of sand transport rates by waves and currents in the coastal zone. *Continental Shelf Research* 22: 2725-2737.
- Davis, R.E. (1976). Predictability of sea surface temperature and sea level pressure anomalies over the North Pacific Ocean. *Journal of Physical Oceanography* 6: 249-266.
- Dean, R.G. (1991). Equilibrium beach profiles: Characteristics and applications. *Journal of Coastal Research* 7: 53-84.
- de Swart, H.E. (1976). Offshore sediment transport and equilibrium beach profiles. *Delft Hydraulics Report 131*. Delft University, Delft.
- de Vriend, H.J. (1981). Steady flow in shallow channel bends. Delft, Netherlands. Hydraulic Department of Civil Engineering, Delft University of Technology.
- de Vriend, H.J. (1991). Mathematical modelling and large-scale coastal behaviour, Part 1: physical processes. *Journal of Hydraulic Research* 29: 727-740.
- de Vriend, H.J. (1993). Two-dimensional horizontal and weakly three-dimensional models of sediment transport due to waves and currents. In: Abbott, M.B. and Price, W.A. (Eds.) *Coastal, Estuarial and Harbour Engineer's Reference Book*. London, Chapman & Hall: 215-238.
- de Vriend, H.J.; Zyserman, J.; Nicholson, J.; Roelvink, J.A.; Pechon, P. and Southgate, H.N. (1993). Medium-term 2DH coastal area modelling. *Coastal Engineering* 21: 193-224.
- de Vriend, H.J.; Capobianco, M.; Chesher, T.; de Swart, H.E.; Latteux, B. and Stive, M.J.F. (1993). Approaches to long-term modelling of coastal morphology: a review. *Coastal Engineering* 21: 225-269.

- de Vriend, H.J.; Bakker, W.T. and Bilse, D.P. (1994). A morphological behaviour model for the outer delta of mixed-energy tidal inlets. *Coastal Engineering* 23: 305-327.
- de Vriend, H.J. (1996). Mathematical modelling of coastal morphodynamics. *Advanced Series on Ocean Engineering*. World Scientific. Singapore.
- de Vriend, H.J. and Ribberink, J.S. (1996). Mathematical modeling of meso-tidal barrier island coasts. Part II: process-based simulation models. In: Liu, P.L.-F. (Ed.) *Advances in Coastal and Ocean Engineering*. Ithaca, NY, World Scientific Publishing, 2: 151-197.
- Dibajnia, M. and Watanabe, A. (1992). Sheet flow under non-linear waves and currents. *Proceedings of the International Conference on Coastal Engineering*: 2015-2029.
- Di Silvio, G. (1989). Modelling the morphological evolution of tidal lagoons and their equilibrium configuration. *Proceeding of the 23rd IAHR Congress*, Ottawa: C.169-175.
- Di Silvio, G. (1991). Averaging operations in sediment transport modelling: short-step versus long-step morphological simulations. *Preprints of the International Symposium on Transport of Suspended Sediment Modelling*, Florence: 723-739.
- Dyer, K.R. (1994). Estuarine sediment transport and deposition. In: Pye, K. (Ed.). *Sediment Transport and Depositional Processes*. Oxford, Blackwell Scientific Publications: 193-218.
- Dyer, K.R. (1997). *Estuaries: A Physical Introduction*. 2nd Edition. John Wiley and Sons. Chichester, UK. 195 p.
- Dyer, K.R. and Huntley, D.A. (1999). The origin, classification and modelling of sand banks and ridges. *Continental Shelf Research* 19(10): 1285-1330.
- Dyer, K.R. (2002) FutureCoast Estuary Assessment. On: *FutureCoast CD-ROM*, Halcrow, Swindon, UK.
- Dyke, P.P.G. (2001). Coastal and Shelf Sea Modelling. Boston, Kluwer Academic Publishers: 257.
- EDF-DER (1998). "TELEMAC-2D software Version 4.0: User Manual." EDF-DER, Chatou, 72.
- Einstein, H.A. (1950). The bed load function for sediment transportation in open channel flow. US Dep. of Agriculture, Tech. Bull. No 126.
- EMPHASYS (2000). A Guide to Prediction of Morphological Change within Estuarine Systems: Version 1B. *EMPHASYS Consortium for MAFF Project FD1401*. Report TR 114. HR Wallingford, Wallingford.
- Engelund, F. and Hansen, E. (1967). A monograph on sediment transport in alluvial

- streams. 3rd Edition Techn. Univers. of Denmark. Copenhagen.
- Environmental Resources Ltd. (2002). Teign Estuary Regional Sewage Disposal Scheme: Environmental Statement. *Report for South West Water Ltd.*
- EUROSION (2004). Living with coastal erosion in Europe: Sediment and Space for Sustainability. PART I - Major findings and Policy Recommendations of the EUROSION project. Brussels, Directorate General Environment - European Commission: 25 (www.euroSION.org).
- Eysink, W.D. (1990). Morphological response of tidal basins to changes. *Proceedings 22nd International Conference on Coastal Engineering*, ASCE: 1948-1961.
- Fernandes, E.H. (2001). Modelling the Hydrodynamics of the Patos Lagoon, Brazil. PhD Thesis. Institute of Marine Studies. University of Plymouth, Plymouth: 198.
- Fernandes, E.H.L.; Dyer, K.R.; Moller, O.O. and Niencheski, L.F.H. (2002). The Patos Lagoon hydrodynamics during an El Nino event (1998). *Continental Shelf Research* 22(11-13): 1699-1713.
- Fernandes, E.H.L.; Marino-Tapia, I.; Dyer, K.R. and Moller, O.O. (2004). The attenuation of tidal and subtidal oscillations in the Patos Lagoon estuary. *Ocean Dynamics* 54(3-4): 348-359.
- Finkl, C.W. (2004). Coastal Classification: Systematic Approaches to Consider in the Development of a Comprehensive Scheme. *Journal of Coastal Research* 20(1): 166-213.
- Fokkink, R. (1992). Fundamental Considerations on Morphodynamic Modelling in Tidal Regions, Part II: A semi-analytical method for tidal basins. Report Z331-2, Rotterdam, Delft Hydraulics: 36 pp.
- Fortunato, A.B. and Oliveira, A., 2002. Towards a Modeling System for Long-Term Morphodynamics. *Extended Abstracts of 11th International Biennial Conference on Physics of Estuaries and Coastal Seas (PECS)*. Hamburg, Germany: 296-300.
- Frijlink, H. (1952). Discussion des formules de debit solide de Kalinske, Einstein et Meyer-Peter and Muller compte tenue des mesures recentes de transport dans les rivières neerlandaises. 2nd *Journal Hydraulique, Societe Hydraulique de France*: 98-103.
- Golden Software (1995). SURFER for Windows Manual. Golden, Colorado. Golden Software Inc.
- Green, M.O.; Black, K.P. and Amos, C.L. (1997). Control of estuarine sediment dynamics by interactions between currents and waves at several scales. *Marine Geology* 144: 97-

116.

- Green, M.O. and MacDonald, I.T. (2001). Processes driving estuary infilling by marine sands on an embayed coast. *Marine Geology* 178: 11-37.
- Hanson, H.; Aarninkhof, S.; Capobianco, M.; Jimenez, J.A.; Larson, M.; Nicholls, R.J.; Plant, N.G.; Southgate, H.N.; Steetzel, H.J.; Stive, M.J.F. and de Vriend, H.J. (2003). Modelling of Coastal Evolution on Yearly to Decadal Time Scales. *Journal of Coastal Research* 19(4): 790-811.
- Hayes, M.O. (1975). Morphology of sand accumulation in estuaries: an introduction to the symposium. In: Cronin, L. E. (Ed.). *Estuarine Research*, Academic Press, New York. Vol. 2: 3-22.
- Hervouet, J.-M. (1994). Computation of 2D Free Surface Flows: The State of the Art in the TELEMAC System. *Hydroinformatics 94*. Balkema.
- Hervouet, J.-M. and van Haren, L. (1994). TELEMAC-2D Principle Note. Electricité de France. Report HE-43/94/051/B.
- Hervouet, J.-M.; Hubert, J.-L.; Janin, J.-M.; Lepeintre, F. and Peltier, E. (1994). The computation of free surface flows with TELEMAC: an example of evolution towards hydroinformatics. *Journal of Hydraulic Research* 32(Extra issue): 45-64.
- Hervouet, J.-M.; Janin, J.-M and Barros, E. (1995). Refined flow modelling in coastal areas. Brebbia, C.A.; Traversoni, L. and Wrobel, L.C. (Eds.). *Computer modelling of seas and coastal regions II*. Computational Mechanics Publications, Southampton: 3-10.
- Hervouet, J.-M. and van Haren, L. (1996). Recent advances in numerical methods for fluid flows. In: Anderson, M.G.; Walling, D.E. and Bates, P.D. (Eds.) *Floodplain Processes*: 183-214.
- Hervouet, J.-M.; Machet, C. and Villaret, C. (2003). Dealing with rigid beds in saturated bed load transport equations *Proceedings of Coastal Engineering '03, the Sixth International Conference on Computer Modelling and Experimental Measurements of Seas and Coastal Regions*. Cadiz.
- Hibma, A.; Schuttelaars, H.M. and Wang, Z.B. (2003a). Comparison of longitudinal equilibrium profiles of estuaries in idealized and process-based models. *Ocean Dynamics* 53 (3): 252-269.
- Hibma, A.; de Vriend, H.J. and Stive, M.J.F. (2003b). Numerical modelling of shoal pattern formation in well-mixed elongated estuaries. *Estuarine, Coastal and Shelf Science* 57 (5/6): 981-991.

- Hibma, A.; Schuttelaars, H.M. and de Vriend, H.J. (2004a). Initial formation and long-term evolution of channel-shoal patterns. *Continental Shelf Research* 24: 1637-1650.
- Hibma, A.; Stive, M.J.F. and Wang, Z.B. (2004b). Estuarine morphodynamics. *Coastal Engineering* 51: 765-778.
- Hoekstra, P.; Bell, P.; van Santen, P.; Roode, N.; Levoy, F. and Whitehouse, R. (2004). Bedform migration and bedload transport on an intertidal shoal. *Continental Shelf Research* 24(SI): 1249-1269.
- Holman, R.A. (1994). The ARGUS Program. *Bulletin of the Coastal Imaging Lab*. Oregon State University, Corvallis, OR 97331.
- Huang, W. and Murray, C. (2003). Application of an Artificial Neural Network to Predict Tidal Currents in an Inlet. Vicksburg, MS, *U.S. Army Engineer Research and Development Center*: 18.
- Huthnance, J.M. (1982). On the formation of sand banks of finite extent. *Estuarine, Coastal and Shelf Science* 15: 277-299.
- Idier, D. and Astruc, D. (2003). Analytical and numerical modeling of sandbank dynamics. *Journal of Geophysical Research* 108 (C3) 3060, 15 p.
- Karim, M.F. and Kennedy, J.F. (1982). IALLUVIAL: A computer-based flow and sediment-routing model for alluvial streams and its application to the Missouri River. *IHR Report No. 250*, Iowa Institute of Hydraulic Research, The University of Iowa, Iowa City.
- Koch, F.G. and Flokstra, C. (1981). Bed level computations for curved alluvial channels. *19th Congress of the International Association for Hydraulic Research*. New Delhi, India.
- Komar, P.D. (1996). Tidal-Inlet Processes and Morphology Related to the Transport of Sediments. *Journal of Coastal Research* 23(SI): 23-45.
- Kragtwijk, N.G.; Zitman, T.J.; Stive, M.J.F. and Wang, Z.B. (2004). Morphological response of tidal basins to human interventions. *Coastal Engineering* 51: 207-221.
- Krol, M.S. (1990). The method of averaging in partial differential equations. PhD thesis, University of Utrecht, Utrecht, 81 pp.
- Lanzoni, S. and Seminara, G. (2002). Long-term evolution and morphodynamic equilibrium of tidal channels. *Journal of Geophysical Research* 107(C1): 1-13.
- Latteux, B. (1987). Modelisation du transport solide - methodologie de simulation a long terme de l'evolution des fonds. Chatou, Electricité de France: 85.
- Latteux, B. (1990a). Synthesis of work carried out at LNH on tidal averaging of sediment

- transport. Chatou, Electricité de France: 21.
- Latteux, B. (1990b). Synthesis of work carried out at LNH on input filtering for morphodynamic computation under tidal action. Chatou, Electricité de France: 16.
- Latteux, B. (1993). Long-Term Morphological Modelling in Tidal Areas. Chatou, Electricité de France: 72.
- Latteux, B. (1995). Techniques for long-term morphological simulation under tidal action. *Marine Geology* 126: 129-141.
- Lesser, G.R.; Roelvink, J.A.; van Kester, J.A.T.M. and Stelling, G.S. (2004). Development and validation of a three-dimensional morphological model. *Coastal Engineering* 51: 883-915.
- Livezey, R.E.; Masutani, M. and Ming, J. (1996). SST-forced seasonal simulation and prediction skill versions of the NCEP/MRF model. *Bulletin of the American Meteorological Society* 77(3): 507-517.
- Malcherek, A. (2000). Application of TELEMAC-2D in a Narrow Estuarine Tributary. *Hydrological Processes* 14 (13): 2293-2300.
- Marchuk, G.I. (1975). *Methods of Numerical Mathematics*, Springer-Verlag.
- Marcos, F. and Benoit, M. (1999). A Steady-State Shallow-Water Spectral Wave Model Based on Unstructured Spatial Meshing. *Proceedings of the Ninth International Offshore and Polar Engineering Conference*. Volume 3: 126-131.
- Mason, D.C. and Garg, P.K. (2001). Morphodynamic Modelling of Intertidal Sediment Transport in Morecambe Bay. *Estuarine, Coastal and Shelf Science* 53: 73-92.
- Masselink, G. and Hughes, M.G. (2003). *Introduction to Coastal Processes & Geomorphology*. Arnold Publishers, London: 354 p.
- Masson, A. and Machet, C. (2002). Sisyphe Release 5.2: User Manual. Laboratoire National d'Hydraulique et Environnement. EDF, Chatou, France. Report HP-75/02/023/A, 53 p.
- Meyer-Peter, E. and Muller, R. (1948). Formulas for bed-load transport. *Sect. Int. IAHR Congress*, Stockholm, Sweden.
- Miles, J.R., Russell, P.E. and Huntley, D.A. (1997). Introduction to COAST3D field study site at Teignmouth. Plymouth, University of Plymouth. *COAST3D Kick-off Workshop Report*. EC MAST Project No. MAS3-CT97-0086.
- Mulligan, M. and Wainwright, J. (2004). Modelling and Model Building. In: Wainwright, J. and Mulligan, M. (Eds.) *Environmental Modelling*. Chichester, UK, John Wiley and Sons: 430.

- Murphy, A.H. and Epstein, E.S. (1989). Skill Scores and Correlation Coefficients in Model Verification. *Monthly Weather Review* 117: 572-581.
- Negen, E.H. (1994). Morphological study with 2DH numerical models near Eierland (Texel). Delft Hydraulics/Delft University, *Technical Report H1887/H460.68*.
- Nichols, M.M. and Biggs, R.B. (1985). Estuaries. In: Davis, R. A (Ed.) *Coastal Sedimentary Environments*, Springer-Verlag, New York: 77-186.
- Nicholson, J.; Broker, I.; Roelvink, J.A.; Price, D.; Tanguy, J.M. and Moreno, L. (1997). Intercomparison of coastal area morphodynamic models. *Coastal Engineering* 31: 97-123.
- Nunny, R.S. (1980). A study of sediment dynamics in a shallow estuary: River Teign, Devonshire. *Faculty of Geography*. Unpublished PhD Thesis, Exeter, University of Exeter: 364.
- O'Brien, M.P. (1969). Equilibrium flow areas of inlets on sandy coasts. *Journal of Waterways, Harbours and Coastal Engineering Division* (ASCE 95-WWI) 15: 43-52.
- O'Connor, B.A.; Nicholson, J. and Rayner, R. (1990). Estuary geometry as a function of tidal range. *Proceedings of the 22nd ICCE*, Delft: 3050-3062.
- Oertel, G.F. (1972). Sediment transport of estuary entrance shoals and the formation of swash platforms. *Journal of Sedimentary Petrology*, 42: 837-863.
- Oldman, J.; Green M.O. and Senior, A. (2002). Spatial variability of waves in estuaries and relationship with bed sediments. *Proceedings of the 28th International Conference on Coastal Engineering*, Cardiff: 3078-3090.
- Pan, S.; Nicholson, J. and O'Connor, B. (2001). 2DH modelling of the Teignmouth site. *COAST3D, Final Volume of Summary Papers*. HR Wallingford, Wallingford, Report TR121.
- Péchon, P.; Rivero, F.; Johnson, H.; Cheshier, T.; O'Connor, B.; Tanguy, J.-M.; Karambas, T.; Mory, M. and Hamm, L. (1997). Intercomparison of wave-driven current models. *Coastal Engineering* 31: 199-215.
- Pritchard, D.W. (1952). Salinity distribution and circulation in the Chesapeake Bay Estuaries system. *Journal of Marine Research* 11: 106-123.
- Pritchard, D.W. (1955). Estuarine circulation patterns. *Proceedings of the American Society of Civil Engineers*, 81, No. 717.
- Robinson, A.H.W. (1975). Cyclical Changes in Shoreline Development at the Entrance to Teignmouth Harbour, Devon, England. In: Hails, J. and Carr, A. (Eds.) *Nearshore Sediment Dynamics and Sedimentation*. London, John Wiley & Sons: 181-198.

- Roelvink, J.A. and Broker, I. (1993). Cross-shore profile models. *Coastal Engineering* 21: 163-191.
- Roelvink, J.A.; Jeuken, M.C.J.L.; van Holland, G.; Aarninkhof, S.G.J. and Stam, J.M.T. (2001). Long-term, process-based modelling of complex areas. *Proceedings of Coastal Dynamics '01*, Lund, Sweden, ASCE: 383-392.
- Sauvaget, P.; David, E. and Guedes Soares, C. (2000). Modelling tidal currents on the coast of Portugal. *Coastal Engineering* 40(4): 393-409.
- Schramkowski, G.P.; Schuttelaars, H.M. and de Swart, H.E. (2002). The effect of geometry and bottom friction on local bed forms in a tidal embayment. *Continental Shelf Research* 22: 1821-1833.
- Schramkowski, G.P.; Schuttelaars, H.M. and de Swart, H. E. (2004). Non-linear channel-shoal dynamics in long tidal embayments. *Ocean Dynamics* 54 (3-4): 399-406.
- Schuttelaars, H.M. and de Swart, H.E. (1999). Initial formation of channels and shoals in a short tidal embayment. *Journal of Fluid Mechanics* 386: 15-42.
- Seminara, G. and Tubino, M. (2001). Sand bars in tidal channels, Part 1: Free bars. *Journal of Fluid Mechanics* 440: 49-74.
- Sha, L.P. (1989). Sand transport patterns in the ebb-tidal delta off Texel inlet, Wadden Sea, the Netherlands. *Marine Geology* 86: 137-154.
- Shimizu, T.; Nodani, H. and Kondo, K. (1990). Practical application of the three-dimensional beach evolution model. *Proceedings 22nd ICCE*, Delft, Netherlands: 2481-2494.
- Siegle, E. (2003). Sediment Transport and Morphodynamics at an Estuary Mouth: a Study using Coupled Remote Sensing and Numerical Modelling. *School of Earth, Ocean and Environmental Sciences*. PhD Thesis, Plymouth, University of Plymouth: 257.
- Siegle, E.; Huntley, D.A. and Davidson, M.A. (2004). Physical controls on the dynamics of inlet sandbar systems. *Ocean Dynamics* 54: 360-373.
- Sierra, J.P.; Sanchez-Arcilla, A. and Mosso, C. (2001). Teignmouth modelling using LIMOS model. *COAST3D, Final Volume of Summary Papers*. HR Wallingford, Wallingford, Report TR121.
- Soulsby, R.L. (1997). Dynamics of Marine Sands. A Manual for Practical Applications. Wallingford, HR Wallingford: 142.
- Soulsby, R.L. (1998). Coastal sediment transport: the COAST3D project. *Proceedings of the 26th International Conference on Coastal Engineering*, ASCE. Copenhagen, Denmark: 2548 - 2558.

- Soulsby, R.L. (2001). Sediment transport and morphodynamics on complex coastlines - the COAST3D project. *Proceedings of Coastal Dynamics '01*, Lund, Sweden, ASCE: 92 - 101.
- Southgate, H.N. (1995). The effects of wave chronology on medium and long term coastal morphology. *Coastal Engineering* 26: 251-270.
- Spratt, T. (1856). An investigation of the movements of Teignmouth Bar. John Weale, London: 36.
- Steijn, R.C. (1989). Schematization of the natural conditions in multi-dimensional numerical models of coastal morphology. Delft, Delft Hydraulics. *Report H 526-1*.
- Steijn, R.C. (1992). Input filtering techniques for complex morphological models. Delft, Delft Hydraulics. *Report H 824.53*.
- Steijn, R.C. and Hartsuiker, G. (1992). Morphodynamic response of a tidal inlet after a reduction in basin area. Delft Hydraulics, *Coastal Genesis Report H840.00*, 75 p.
- Steijn, R.C.; Louters, T.; van der Spek, A.J.F. and de Vriend H.J. (1992). Numerical model hindcast of the ebb-tidal delta evolution in front of the deltaworks. *International Conference of Hydraulic and Environmental Modelling of Coastal, Estuarine and River Waters*, Bradford, UK, Gower Technical: 255-264.
- Stive, M.J.F.; Capobianco, M.; Wang, Z.B.; Ruol, P. and Buijsman, M.C. (1998). Morphodynamics of a tidal lagoon and the adjacent coast. In: Dronkers, J., Scheffers, M. (Eds.), *Physics of Estuaries and Coastal Seas*. Balkema, Rotterdam: 397-407.
- Stive, M.J.F. and Wang, Z.B. (2003). Morphodynamic Modeling of Tidal Basins and Coastal Inlets. In: Lakhan, V.C. (Ed.). *Advances in Coastal Modeling*. Amsterdam, Elsevier Science. 67: 367-392.
- Sutherland, J.; Waters, C.B. and Whitehouse, R.J.S. (2001a). Continuous Monitoring of Tides, Waves and Currents at Teignmouth, UK (1998-1999). Wallingford, HR Wallingford. Report TR 116.
- Sutherland, J.; Hall, L.J. and Chesher, T.J. (2001b). Evaluation of the coastal area model PISCES at Teignmouth (UK). Wallingford, HR Wallingford. Report TR 125: 28.
- Sutherland, J. and Soulsby, R.L. (2003). The use of model performance statistics in modelling coastal morphodynamics. *Coastal Sediments '03*, ASCE. Clearwater Beach, Florida. CD-ROM.
- Sutherland, J.; Walstra, D.J.R.; Chesher, T.J.; van Rijn, L.C. and Southgate, H.N. (2004a). Evaluation of coastal area modelling systems at an estuary mouth. *Coastal Engineering* 51: 119-142.

- Sutherland, J.; Peet, A.H. and Soulsby, R.L. (2004b). Evaluating the performance of morphological models. *Coastal Engineering* 51: 917-939.
- Townend, I.H. (1995). Estuaries from a users perspective. In: *Estuary Management Workshop*, Institute of Estuarine and Coastal Studies, University of Hull, Hull, UK.
- Townend, I.H. (1997). Industry: an overview of some of the port issues. In: *European Workshop on the Implementation of the Habitats Directive*, IEEP, London.
- Tyrrell, D. (in prep.). Modelling the Water Quality of the Patos Lagoon, Brazil. PhD Thesis. *School of Earth, Ocean and Environmental Sciences, University of Plymouth*, Plymouth.
- van de Kreeke, J. (1996). Morphological Changes on a Decadal Time Scale in Tidal Inlets: Modeling Approaches. *Journal of Coastal Research* 23(SI): 73-81.
- van Lancker, V.; Lanckneus, J.; Hearn, S.; Hoekstra, P.; Levoy, F.; Miles, J.; Moerkerke, G.; Monfort, O. and Whitehouse, R. (2004). Coastal and nearshore morphology, bedforms and sediment transport pathways at Teignmouth (UK). *Continental Shelf Research* 24(SI): 1171-1202.
- van Leeuwen, S.M. and de Swart, H.E. (2002). Intermediate modelling of tidal inlet systems: spatial asymmetries in flow and mean sediment transport. *Continental Shelf Research* 22: 1795-1810.
- van Overeem, J.; Steijn, R.C. and van Banning, G.K.F.M. (1992). Simulation of morphodynamics of tidal inlet in the Wadden Sea. In: Sterr, H., Hofstede, J. and Plag, H. -P. (Eds.). *Proceedings of the International Coastal Congress*, Kiel. Peter Lang Verlag, Frankfurt am Main: 351-364.
- van Rijn, L.C. (1984a). Sediment Transport, Part I: Bed Load Transport. *Journal of Hydraulic Engineering* 110(10): 1431-1456.
- van Rijn, L.C. (1984b). Sediment Transport, Part II: Suspended Load Transport. *Journal of Hydraulic Engineering* 110(11): 1613-1641.
- van Rijn, L.C.; Grasmeijer, B.T. and Ruessink, B.G. (2000). Measurement errors of instruments for velocity, wave height, sand concentration and bed levels in field conditions. Delft, Holland, University of Utrecht and WL / Delft Hydraulics: 47.
- van Rijn, L.C.; Ruessink, B.G. and Mulder, J.P.M. (2002). COAST3D-Egmond, the behaviour of straight sandy coast on the time scale of storms and seasons. Amsterdam, Aqua Publications.
- van Rijn, L.C.; Walstra, D.J.R.; Grasmeijer, B.; Sutherland, J. ; Pan, S. and Sierra, J.P. (2003). The predictability of cross-shore bed evolution of sandy beaches at the time

- scale of storms and seasons using process-based profile models. *Coastal Engineering* 47: 295-327.
- Villaret, C. and Latteux, B. (1992). Long-Term Simulation of Cohesive Sediment Bed Erosion and Deposition by Tidal Currents. *International Conference on Computer Modelling of Seas and Coastal Regions and Boundary Elements and Fluid Dynamics*. Partridge, P. W. (Ed.), Southampton, UK, Boston Publications: 363-378.
- Villaret, C. (2004). Sisyphe Release 5.4: User Manual. Paris, R&D, Electricité de France: 69.
- Walker, D.J.; Dong, P. and Anastasiou, K. (1991). Sediment transport near groynes in the nearshore zone. *Journal of Coastal Research* 7(4): 1003-1010.
- Walstra, D.J.R.; Reniers, A.J.H.M.; Roelvink, J.A.; Wang, Z.B.; Steetzel, H.J.; Aarninkhof, S.G.J.; van Holland, G. and Stive, M.J.F. (1997). Maasvlakte-2. Morfologische effecten op de Nederlandse kust van Zeeuws-Vlaanderen tot Den Helder over een periode van een 300 jaar. WL / Delft Hydraulics Report Z2255 (in Dutch).
- Walstra, D.J.R.; Sutherland, J.; Hall, L.; Blogg, H. and van Ormondt, M. (2001). Verification and comparison of two hydrodynamic area models for an inlet system. *Coastal Dynamics '01*, Lund, Sweden, ASCE: 433-442.
- Walton, T.L.Jr. (2002). Tidal velocity asymmetry at inlets. *ERDC/CHL CHETN IV-47*. U.S. Army Engineer Research and Development Center, Vicksburg, MS. <http://chl.wes.army.mil/library/publications/chetn>
- Wang, Z.B. (1991). Morphodynamic Modelling for a tidal inlet in the Wadden Sea. Rotterdam, Delft Hydraulics: 1-37.
- Wang, Z.B.; Louters, T. and de Vriend, H.J. (1995). Morphodynamic modelling for a tidal inlet in the Wadden Sea. *Marine Geology* 126: 289-300.
- Watanabe, A.; Shimizu, T. and Kondo, K. (1991). Field application of a numerical model of beach topography change. In: Kraus, N. C., Gingerich, K. J. and Kriebel, D. L. (Eds.). *Proceedings of Coastal Sediments '91 Conference*, Seattle, WA. ASCE, New York: 1814-1828.
- Wells, T.J. (2002a). Teignmouth Quay Development Environmental Statement. Southampton, ABP Marine Environmental Research Ltd. *Report R.984a*: 119.
- Wells, T.J. (2002b). Teignmouth Quay Development Environmental Statement: Changes to Physical Processes. Southampton, ABP Marine Environmental Research Ltd. *Report R.984c*: 140.

- Wentworth, C.K. (1922). A scale of grade and class terms for clastic sediments. *Journal of Geology* 30: 377-392.
- Westra, M.R.; van Vledder, G.P.; van Banning, G.K.F.M. and Hurdle, D.P. (2002). Predicting water levels using artificial neural networks. *Proceedings of the 28th International Conference on Coastal Engineering*, Cardiff.
- Whitehouse, R.J.S. and Sutherland, J. (2001). COAST3D data report - 3D experiment, Teignmouth, UK. HR Wallingford, Wallingford, *Report TR119*.
- Whitehouse, R.J.S. (2004). Teignmouth special issue: Editorial. *Continental Shelf Research* 24(11): 1165-1169.
- Wright, L.D. and Thom, B.G. (1977). Coastal depositional landforms: a morphodynamic approach. *Progress in Physical Geography*, 1: 412-459.
- Wu, B.; Molinas, A. and Julien, P.Y. (2004). Bed-Material Load Computations for Nonuniform Sediments. *Journal of Hydraulic Engineering* 130(10): 1002-1012.
- Wu, W. (2004). Depth-Averaged Two-Dimensional Numerical Modeling of Unsteady Flow and Nonuniform Sediment Transport in Open Channels. *Journal of Hydraulic Engineering* 130(10): 1013-1024.
- Zienkiewicz, O.C. and Ortiz, P. (1995). A split-characteristic based finite element model for the shallow water equations. *International Journal for Numerical Methods in Fluids* 20: 1061-1080.